JAERI-M
82-027

ANNUAL REPORT OF THE FUSION RESEARCH AND DEVELOPMENT CENTER FOR THE PERIOD OF APRIL 1, 1980 TO MARCH 31, 1981

March 1982

Fusion Research and Development Center

日本原子力研究所
Japan Atomic Energy Research Institute

JAERI-Mレポートは，日本原子力研究所が不定期に公刊している研究報告書です。
入手の問合わせは，日本原子力研究所技術情報部情報資料課（〒319-11茨城県那珂郡東海村）あて，お申しこしください。なお，このほかに財団法人原子力弘済会資料センター（〒319-11 茨城県那珂郡東海村日本原子力研究所内）で複写による実費頒布をおこなっております。

JAERI-M reports are issued irregularly.
Inquiries about availability of the reports should be addressed to Information Section, Division of Technical Information, Japan Atomic Energy Research Institute, Tokai-mura, Naka-gun, Ibaraki-ken 319-11, Japan.

編集兼発行　日本原子力研究所
印　　刷　いばらき印刷㈱

JAERI-M 82-027

Annual Report

of

the Fusion Research and Development Center

for the period of April 1, 1980 to March 31, 1981

Fusion Research and Development Center

Tokai Research Establishment, JAERI

(Received March 4, 1982)

Research and development activities of the Fusion Research and Development Center (Division of Thermonuclear Fusion Research and Division of Large Tokamak Development) from April 1980 to 1981 are described.

In plasma physics research, 1.5 MW NBI heating experiments were successfully made on JFT-2 to yield an average beta value of 2.5 % without any deleterious effect on plasma confinement. Joint JAERI-US/DOE ECRH experiments revealed detailed physics of plasma heating. Installation of a 1 MW ICRF system was completed. In the Doublet-III experiment, a JAERI-US/DOE cooperation program, extensive studies were made on Joule heated dee-shaped Plasmas. In theory and computation emphasis was placed on beta optimization of tokamaks.

Construction of JT-60 was continued as planned. Manufacturing of the major components and facilities was advanced well, e.g. 14 out of the 19 toroidal field coils were completed. Construction of the buildings was continued at the Naka site.

In plasma heating technology, construction of the JT-60 prototype NBI unit was in progress, and development works on ion sources and beam line components as well. Trial fabrication of high power klystrons for JT-60 RF heating was started.

In superconducting magnet technology, cool-down tests of cluster coils were successfully made. Manufacturing of the Japanese coil for the Large Coil Task under the auspiece of IEA, and of a Nb_3Sn test module coil was continued. A test facility for the LCT coil was completed.

Basic studies on key processes of tritium technology were continued using hydrogen and deuterium. Design of the Tritium Process Laboratory was continued.

Development of first wall materials for JT-60 was advanced. Extensive tests were made on a number of low-Z coatings.

Design studies of INTOR, a cooperative work in IAEA, were continued. In addition, design of the Fusion Experimental Reactor was started on a conventional type tokamak reactor and swimming pool type one.

Keywords: Annual Report, Plasma Confinement, Plasma Physics, JFT-2 Tokamak, JFT-2M Tokamak, Diagnostics, Neutral Beam Injector, RF Heating, Surface Study, Superconducting Magnet, Reactor Design, JT-60 Tokamak, Doublet-III, Tritium Technology, Fusion Experimental Reactor, INTOR。

JAERI－M 82－027

核融合研究開発推進センター年報（昭和55年度）

日本原子力研究所　東海研究所
核融合研究開発推進センター

（1982年3月4日受理）

核融合研究開発推進センター（核融合研究部および大型トカマク開発部）における1980年4月から1981年3月までの研究開発の現状とその成果をとりまとめた。* 概要は次のとおりである。

プラズマ物理研究の分野では，JFT－2における1.5MW中性粒子入射加熱実験を行ない，プラズマ閉じ込めに対して何らの悪影響を及ぼすことなく平均ベータ値2.5％の達成に成功した。

一方，日米協力による電子サイクロトロン共鳴加熱実験（ECRH）では，プラズマ加熱の物理機構が詳細に解明された。1MWイオンサイクロトロン共鳴加熱装置も，その据付を終了した。日米核融合研究協力計画として進められているダブレットⅢによる非円形断面トカマクの実験研究では，ジュール加熱によるD型断面プラズマの挙動について広範囲な研究が行なわれた。理論解析の分野では，トカマク・プラズマのベータ値最適化の研究が精力的に進められた。

JT－60の建設は計画どおり進行している。主要機器，及び主要設備の製作も順調に進み，19個のトロイダルコイルのうち，14個までが完成した。茨城県那珂町での建設整備も順調に工事が続けられている。

加熱工学の分野では，JT－60のための中性粒子入射加熱用原型ユニットの建設，イオン源，ビームライン用各機器の開発研究が進行中である。JT－60高周波加熱装置のための大電力クライストロンの試作も開始された。

超電導磁石の研究開発においては，2回のクラスター・テスト・コイル冷却通電試験に成功した。国際エネルギー機関による大型コイル事業のためのLCTコイルの製作，ニオブ・スズ化合物導体を使用するテスト・モジュール・コイルの製作も進行中である。LCTコイル国内試験装置は，56年6月に完成した。

トリチウム技術の開発では，水素，重水素を用いた各種の基礎研究を行なうかたわら，トリチウムプロセス研究棟の建設準備が引き続き行なわれた。

真空壁の表面現象の研究では，JT－60第一壁材料の開発が進められ，第一壁の低Z（原子番号）コーティングに関する実験が種々の材料を用いて実施された。

国際原子力機関による国際次期トカマク炉（INTOR）の設計検討が引き続き行なわれた。さらに，核融合炉設計研究の分野では，国内次期装置の設計に着手し，在来型，及びスィミングプール型の2型式について概念検討が実施された。

---

* 既刊されている年報は，昭和45年以降それぞれJAERI－M 4654, 5029, 5564, 5888, 6359, 6926, 7479, 8059, 8661及び9421である。

Contents

目　　次

PREFACE

A blief summary of activities in the Fusion Research and Development Center during the fiscal year 1980 is as follows:

JT-60:

Almost all equipments are under fabrication, in particular main components such as TF coils and supporting structures are almost completed at the factory. Construction of the main buildings are underway.

JFT-2:

Experiments are focussed on heating experiments. Current drive experiment has continued with lower hybrid wave and has shown promising data so far. Combined heating with ICRF and NBI offered successful results as well as ECRH experiment on the US-Japan collabolation basis. Preparation for replacing JFT-2 by a new version JFT-2M is underway, aiming at advanced tokamak experiments, such as non-circular high-β, simplified divertor, ICRF and LHR heating and current drive.

Doublet-III:

Joule heating experiment with Dee-shaped plasma in Doublet-III was completed and the machine was shut down for the installation of NBIs. Its main results are control of stable plasma of a highly elongated Dee shape, low-q operation without a conducting shell, studies of a divertor configuration and so on.

Plasma Heating Technology:

The NBI prototype for JT-60 was fabricated and are ready for installation at Naka. 2 GHz, 1 MW klystrons have been developed for JT-60 LHR heating.

Surface Science and Vacuum Technology:

Activities are focussed on the development of low-Z first wall materials for JT-60. TiC coating on Molybdenum base appears to be a possible candidate. Vacuum technology experiments are underway by using JVX facilities.

Superconducting Magnet Technology:

CTF (Cluster Test Facility) was completed and tested. 1.5 mϕ NbTi coils are cooled down to 4 °K and achieved the maximum field of 7 Tesla. The LCT coil was fabricated and its domestic test facility was completed at Naka.

Tritium Technology:

The Tritium Process Laboratory is under design and ready for construction. Simulation studies of key processes with H and D are continuing.

Reactor Design:

Contribution to the cooperative work of INTOR design study is continuing. The design work for the Japanese fusion experimental reactor started, with an emphasis on ignition and tritium breeding.

(Yasuhiko Iso)

I. PLASMA THEORY AND COMPUTATION

1. Introduction

The important objective of the researches at Plasma Theory Laboratory is to understand a tokamak plasma comprehensively from the theoretical viewpoints in relation with the experimental program. This is accomplished by taking various kinds of approaches, namely, computations or simulations by using a fluid and particle models and analytical methods, especially, the kinetic theroretical ones. The main research items in an intermediate-term schedule are beta optimization with respect to MHD instabilities and understanding and controlling of nonlinear MHD phenomena in a tokamak plasma. From the previous years on, large parts of efforts are put into the computational studies based on a fluid model, i.e. the project TRITON.

For example, ERATO and BOREAS codes, which are low-n and high-n linear MHD stability codes, are tuned up for efficient and accurate analyses and various kinds of analyses, especially, of the INTOR plasma are carried out. In relation with it equilibria in the second stability region of the high-n ballooning mode is also studied by using a 1-1/2D tokamak code APOLLO of the code system TRITON.

Relating problems were also studied in the framework of the kinetic theoretical approach. For example, comparison of the kinetic instability growth rates between MHD-stable and unstable regions suggests that rather easy path to the second stability region of the ballooning mode may be found. Ballooning instability of equilibria with anisotropic pressure distribution is also analyzed in this framework, which is a very important problem of a tokamak plasma subject to an additional

heating. These results confirm that comprehensive studies over wide range of parameters, i.e., from a fluid region to a kinetic region, bring qualitatively new informations on a tokamak plasma and these studies are indispensable, especially, in the coming tokamak research program. In addition to these, development of nonlinear MHD codes and analyses of experimentally oberved nonlinear phenomena are intensively carried out as for the project TRITON. Concerning the kinetic theory, kink-like instabilities, collisional drift-tering instabilities, radio frequency flux control, and so on are investigated.

Computer simulations based on a particle-like numerical model are minly applied to the problem relating to the divertor. These analyses are considered very important not only in relation with design of large tokamak devices but also in relation with the present tokamak experiments.

Consolidation of the code system TRITON is also progressing. Many kinds of the TRITON codes are being developed and checked. Supporting codes, such as graphic I/O subsystem, numerical analysis code, supervisor code for the system and so on are also developed and utilized very effectively.

2. Kinetic study of instability and transport

2.1 Introduction

When we want to analyze the stability of a tokamak plasma, it is important to take into consideration toroidicity and kinetic effects. They often change stability properties considerably. Previous MHD models, usually, lack the kinetic effects and the kinetic studies were often carried out for the cases of simplified configuration, such as, without toroidicity.

The main works in this period concening the kinetic approach are devoted to examine the stability of a tokamak plasma in more practical models such as for the case with the toroidicity. Toroidal effects on the drift wave in a sheared magnetic field and electrostatic ballooning mode, which is unstable in a low beta limit, are investigated. Kinetic effects on MHD ballooning mode and drift tearing mode are investigated. As described in the previous section, these studies are carried out in close connection with the MHD computations.

2.2 Toroidal drift wave[1)]

Toroidal effects on the electrostatic drift wave in a sheared magnetic field are investigated by using not only a strong coupling method but also a variational method. The conditions of wave damping due to the magnetic shear are shown. It is found that, in usual tokamak plasmas, unstable fluctuation have same localization width both in radial and poloidal directions.

2.3 Electrostatic ballooning mode[2)]

Numerical solution of high-n electrostatic ballooning mode is obtained without approximations. We keep correct forms of electron and ion responses to the wave. We find instabilities which arise due to toroidal effects. The dependences on the aspect ratio, magnetic shear, and wave length are also studied. The growth rate γ is large and statisfies the relation $\omega < \gamma - \omega_*$. Depending on the parameters the real frequency ω changes its sign. The drift mode, which has been found stable in a slab plasma, persists in the toroidal plasma remaining almost always stable.

The density fluctuations in tokamaks, which have been observed by use of the microwave scattering method, can be qualitatively explained by the theory of the electrostatic ballooning mode.

2.4 Kinetic theory of nonlocal high-n ballooning mode[3)]

Kinetic theory of high-n (n: toroidal mode number) electromagnetic ballooning mode is presented with consistent inclusion of plasma β-value, ion gyroradius, kinetic parallel conductivity and magnetic shear effects. We found a new unstable branch of nonlocal eigenmodes in a collisionless toroidal plasmas. The growth rate of kinetic high-n ballooning modes are much smaller than the ones predicted by fluid theory. Electron temperature gradient effect is also discussed.

2.5 Ballooning instability in a tokamak with anisotropic ion temperature[4)]

The stability of high-mode-number ballooning modes in a tokamak plasma with anisotropic ion pressure is investigated, taking into account the finite ion gyroradius effect. The stability condition is derived as

$$\frac{8\pi n_0 (T_e + T_{i\perp})}{B^2} \leqq \beta_c$$

where β_c is the critical β value for the case of isotropic pressure.

2.6 Kinetic theory of kink-like instabilities[5)]

Kinetic theory of drift-tearing mode in a finite-β, collisionless inhomogeneous cylindrical tokamak is investigated. We find that

1) When the density is low, kinetic drift-tearing modes are unstable, while they become stabilized as the density increases; 2) The medium m (poloidal mode number) modes have smaller growth rate; 3) The electron temperature gradient further stabilizes them. Due to the magnetic shear and finite-β value, out-going drift wave is associated with the tearing mode and hence the ion Landau damping stabilizes the mode when β increases. The local current density is found to be crucial for the instability. We note that the stability criterion of MHD tearing mode, $\Delta' > 0$ (Δ': jump of the logarithmic derivative of $\tilde{B}_r$ across the mode rational surface), is no longer valid for kinetic tearing mode.

For future tokamak parameters, low and medium m ($2 \leq m \lesssim 50$) kinetic drift-tearing modes are found to be stable in a cylindrical geometry.

2.7 Kinetic theory of collisional drift-tearing instability[6)]

Kinetic theory of collisional drift-tearing instability in a finite-β cylindrical tokamak is investigated using the BGK collision operator in the absence of a temperature gradient. The drift-tearing mode, which is stabilized by the coupling to the out-going drift mode, is further stabilized by the electron collision.

2.8 Improvement of plasma confinement by radio frequency flux control[7)]

A method to control cross field plasma fluxes by use of RF waves (RFFC) is presented. An RF field of $\omega > \omega_*$, with a momentum density in the direction of the electron diamagnetic drift can reduce plasma losses when the wave is efficiently absorbed by electrons.

We show the accessibility of this RFFC scheme by applying it to shear Alfvén mode in a cylindrical tokamak, and by solving the propagation equation. The induced inward fluxes are calculated and an appreciable reduction of anomalous losses is found to be achieved by application of an RF power of the order of ohmic power.

We also analyze the steady-state operation with inclusion of rf current drive and heating as well as RFFC, and demonstrate the considerable improvement of plasma parameters. For a reactor plasma, we evaluated the reduction of critical $n\tau$ value for the break-even condition.

Reference

1) T. Tuda, K. Itoh and S.I. Itoh, JAERI-M 9263 (Dec. 1980) in Japanese.

2) T. Tuda, K. Itoh and S.I. Itoh, JAERI-M 9456 (Apr. 1981)

3) K. Itoh, S.I. Itoh and T. Tuda, J. Phys. Soc. Japan 50 (1980) 655.

4) K. Itoh, S. Inoue and T. Tuda, JAERI-M 9067 (Sep. 1980) in Japanese.

5) S.I. Itoh and K. Itoh, Nuclear Fusion 21 (1981) 3.

6) K. Itoh and S.I. Itoh, Phys. Letters 82A (1981) 85.

7) S. Inoue and K. Itoh, Proceedings of the 8th International Conference of Plasmas Physics and Controlled Nuclear Fusion Research, Brussels 1-10 July 1980, IAEA CN-38/Z2.

3. Computation and project TRITON

3.1 Introduction

Problems which are urgently tackled within the project TRITON are studies of optimized equilibria with sufficiently high beta value and

studies of nonlinear MHD phenomena to understand and control disruptive instabilities. These physics problems correspond to the planned TRITON codes and development of them will surely brings about answers to these problems from the theoretical viewpoints. Among them the linear ideal MHD stability analysis code ERATO is most intensively studied. Properties of the code is investigated minutely and a new interfacing module between the equilibrium and stability codes is developed. In relation with it a new accurate inverse equilibrium solver SELENE50 was developed on the basis of the finite element method with bicubic basic functions. Scaling laws of optimized beta value versus various parameters are investigated for an elliptic and circular cross-sectional plasmas by using a high-n ballooning mode analysis code BOREAS. Equilibria in a second stability region of the ballooning instability are found out.

As for the nonlinear MHD phenomena two important studies are being progressed. One is the study of an m=1 resistive internal mode which is a plausible cause of phenomena of the suppression of internal disruption and appearance of large amplitude stationary m=1 oscillation observed in the JFT-2 experiment. In connection with it spectral analyses of a resistive plasma are also carried out. The other is three dimensional computation aiming at understanding of disruptive instabilities.

Particle-like simulations are applied to the problem relating to divertors. Neutral gas cooling near the divertor plate is being investigated self-consistently.

New numerical methods, such as a determinant calculation to solve a complicated eigenvalue problem appearing in the kinetic approach, are also intensively studied and applied to practical problems. To develop and run the above described physics codes efficiently, supporting

codes of the code system TRITON are especially helpful. These codes are ARGUS (a graphic I/O subsystem), HARMONIA (a supervising code of the code system TRITON), PLUTO (a code analyzer), EOS (a preprocessor to facilitate running a code), and HERA (a code for data aquisition and editing of results of computations). Studies of code optimization and extensive runs of the TRITON codes (ERATO, AEOLUS-R1, AEOLUS-II, and AEOLUS-RT) on a vector processing computer, FACOM 230-75 APU are also indispensable to get a large amount of computational results within a short period.

3.2 Ballooning mode analyses

3.2.1 High-n ballooning mode analysis code BOREAS

A new ballooning code BOREAS is developed, which solves the CHT equaiton on the basis of the finite element method. The functional for the finite element method is given by

$$L = \int_{-\infty}^{\infty} \{-B_1 (\frac{\partial F}{\partial s})^2 + p' \cdot \hat{B}_2 F^2 + \omega^2 B_3 F^2\} ds, \qquad (1)$$

where

$$B_1 = \frac{1}{RB_\chi^2} + \frac{R^2 B_\chi^2}{B^2} Z^2,$$

$$B_2 = p' \hat{B}_2 = \frac{2p'}{B^2 B_\chi^2} \frac{\partial}{\partial \psi} (p + \frac{B^2}{2}) - \frac{2p'I}{B^4} Z \frac{\partial}{\partial s} (\frac{B^2}{2}),$$

$$B_3 = \frac{1}{R^2 B_\chi^3} + \frac{R^2 B_\chi}{B^2} Z^2.$$

When one would like to perform a beta-optimization of a toroidal equilibrium one should search for a marginally stable equilibrium with respect to the ballooning mode. But it is often difficult to calculate null-eigenvalue state and in this case comparatively large error is often contained in the solution. The difficulty is avoided if one solves Eq.(1) as an eigenvalue problem of pressure gradient p' instea of the squared frequency ω^2 by letting $\omega^2=0$.

In this way we obtain two kinds of eigenvalue problems from the variation of Eq.(1). One ia an eigenvalue problem with respect to ω^2 and from this formulation detailed structure of spectra and eigenvectors of the ballooning modes are analyzed. The other is an eigenvalue problem with respect to the pressure gradient and by this formulation one can quickly and rather accurately determine a marginally stable equilibrium for the ballooning modes if one can prepare a well-guessed initial equilibrium which is almost marginally stable to the ballooning mode.

3.2.2 Beta optimization and beta scaling

It is desirable from the economic viewpoint that a tokamak fusion reactor is operated in the high beta state. The possible beta value, the ratio of the plasma pressure to the magnetic pressure, may be restricted by MHD instabilities, especially by unstable high-n ballooning modes. So we study in detail about the dependencies of this value on the safety factor at the plasma surface q_s, the aspect ratio A, and the ellipticity ε.

We start the computation from a very low beta equilibrium with the safety factor at the magnetic axis is unity. This plasma is heated up to higher beta by the pressure source with the profile $(1-\psi^2)^2$,

where ψ is the poloidal magnetic flux normalized as $\psi_{axis} = 0$ and $\psi_s = 1$. After the plasma becomes unstable locally, the pressure profile near the unstable region is changed by the anomalous diffusion. The beta value still continues to increase by changing the pressure profile. Finally, the whole plasma region becomes marginally stable and the beta value saturates. It must be noted that the final beta value and pressure profile are independent of the source profile.

The critical value is mainly dependent on the plasma shape and the q profile. Figure I.3-1 shows the critical beta value as functions of q_s, A and ε. The critical beta decreases with increasing q_s and A (Figs.I.3-1 a, b, and c). The beta value depends almost linearly on the ellipticity in the range $0.8 < \varepsilon < 2.0$ (Fig.I.3-1 d). From these results, we get the functional dependence of β on q_s, A and ε as

$$\beta(\%) \simeq 7.8 q_s^{-0.54} (A-1)^{-0.76} \varepsilon^{1+0.14(q_s-1)}$$

Above relation is much different from the well-known one, $\beta \sim 1/q_s^2 A$. This is caused mainly by the effect of the shear.

3.2.3 The second stability region of ballooning modes[1)]

In the analysis of the critical beta value in the previous subsection, the unstable ballooning modes produce the infinitely large thermal conductivity. However, if we take into account the finite-n correction and finite larmor effect, the $k_\perp \rho_i$ for the most unstable modes is around the order of unity and we can expect the effect of finite thermal conductivity for these modes. In this case if the plasma is heated up faster than thermal loss due to unstable ballooning modes, then it can go into the second stable region.

In order to study this sequence, we solved the 1-1/2D tokamak code combined with the ballooning mode analysis code. In this calculation we assume that the flux is conserved during all the sequence and the thermal conductivity is zero during the heating phase and becomes finite after the heating is turned off. Figure I.3-2 shows the ballooning unstable region against the beta value during the heating phase. When beta becomes higher than 10 %, the second stability region appears in the middle of the plasma column. The equilibrium with beta of 14 % is shown in Fig.I.3-3, where $dp/d\psi|_{crit}$ is the critical pressure gradient and the ballooning modes are unstable in the region of $dp/d\psi > dp/d\psi|_{crit}$. After the heating is turned off at this beta value, the anomalous heat transport by the unstable ballooning modes relaxes pressure gradient in the unstable region and finally establishes the equilibrium which is stable against the ballooning modes over the whole plasma column. Figure I.3-4 shows the stable equilibrium with beta of about 12%, which was relaxed from the equilibrium shown in Fig.I 3-3. This simulation shows that the high beta ballooning stable equilibria are accessible, if the plasma is heated up faster than the anomalous thermal conductivity due to unstable modes. The required heating power depends on the anomalous value, which will be clarified by the kinetic studies on the ballooning instability.

3.3 Analyses by the code ERATO

3.3.1 Convergence property of the ERATO solution[2)]

The effects of the finite hybrid element (FHE) on linear MHD stability calculations were investigated in the cylindrical approximation. The use of the FHE in the θ direction changes the poloidal mode number

m to $\bar{m} = m \tan(\frac{\pi m}{2N_\theta})/(\frac{\pi m}{2N_\theta})$ where N_θ is the number of equidistance meshes in the θ direction ($0 \leq \theta \leq \pi$), and results the following effects on the eigenvalue Γ^2;

(a) There appears N dependence as well as N_r dependence in the computed growth rate of the internal mode (N_r is the number of meshes in the radial direction). For the case of the uniform q profile, Γ^2 is written as

$$\Gamma^2 = C_0 \left(1 + \frac{A_1}{N_r^2}\right)^{-1}\left(1 + \frac{B_1}{N_\theta^2}\right)^{-1} - \left(\frac{\bar{m}}{q} - n\right)^2 \quad .$$

(b) The change of the poloidal mode number shifts the peak of Γ^2 in the nq space. In order to eliminate this shift, the toroidal mode number n is to be corrected as

$$\bar{n} = n \tan(\frac{\pi nq}{2N})/(\frac{\pi nq}{2N}) \simeq n\,(1 - 0.8825(\frac{nq}{N_\theta})^2 - 0.1353(\frac{nq}{N_\theta})^4)^{-1}.$$

This correction is almost the same as that employed in the code ERATO.

(c) The correction n yields additional source term $d\bar{n}^2/dr \simeq 3.29\, n^2 \frac{n^2 q}{N_\theta}\frac{dq}{dr}$ in the MHD equation. Then FHE calculation gives a pessimistic solution for $dq/dr > 0$ as a tokamak plasma, and an optimistic solution for $dq/dr < 0$ as a reversed field pinch plasma.

For the case of toroidal plasma, we studied the N_ψ, N_θ dependences on the growth rate, eigensolution and potential energy computed by the code ERATO[3]. The equilibrium used in ERATO calculations is that of INTOR plasma with $\beta = 8.4$ %. We mainly studied the convergence property for the n = 5 internal mode. The results give the best fitting expression of the growth rate:

$$\Gamma^2 = \Gamma_0^2 + \Gamma_1^2 \left(1 + \frac{A_1}{N_\psi^2}\right)\left(1 + \frac{B_1}{N_\chi^2} + \frac{B_2}{N_\chi^4}\right) \quad .$$

The eigenvalue and eigensolution strongly depend on N_χ. It is found that the numerical source term $d\bar{n}^2/dr$ plays important roles in the high n and/or high shear case. This term can change the eigensolution drastically from the converged one when N_χ is not large enough.

3.3.2 Interfacing between the equilibrium and stability code

When we analyze linear MHD stability of tokamak plasmas by using the code ERATO, we must compute metric quantities on the natural coordinate system (ψ, χ)[4]. Poloidal magnetic flux $\psi(R, Z)$ is obtained by solving Grad Shafranov equation in the (R, Z) plane. We developed a new version of an interfacing module (ERATO-1) to calculate metrics from $\psi(R, Z)$ by means of two dimensional B-spline. In this method, equi-ψ lines are drawn by solving the differential equation for them. The new method has the following features;

(a) It does not use any finite difference approximation to calculate derivatives which appear in metrics.

(b) It does not need to perform the least square fitting of $\psi(R,Z)$ near the magnetic axix as the old version does.

(c) The metrics obtained by the new method have accuracy independent of the number of (ψ, χ) mesh. Thus we can reduce the error in the computed eigenvalue due to interfacing.

Fig.I.3-5 shows examples of the convergence curves of the eigenvalues of n = 1 internal mode. The old version (128 × 64 equilibrium mesh) cannot give a convergence curve, and, there appears 'resonance-like phenomena'[5] in the curve obtained from old version (512 × 256 equilibrium mesh). On the other hand, the new version (128 × 64 equilibrium mesh) gives a smooth convergence curve without resonance-like phenomena and we can extrapolate the eigenvalue because the curve is quadratic for $N \geq 30$.

3.3.3 MHD equilibrium code SELENE50

An inverse equilibrium solver SELENE50 is developed, in which computational meshes are constructed on the basis of the magnetic surfaces and the positions (R, Z) of nodal points of the meshes are computed as a function of (ψ, χ). This kind of equilibrium solver is especially useful for internal mode stability analyses by the code ERATO and high-n ballooning mode analyses of a high-beta tokamak, such as with a second stable equilibrium. In the inverse equilibrium solver described here, the finite element method is used and the Grad-Shafranov equilibrium equation is solved iteratively by reconstructing the meshes so that the edges of the meshes are aligned along the ψ, χ directions. Usually, isoparametric linear basis functions are adopted for the finite element calculation of this kind. In the code SELENE50 bicubic functions are used so that the ψ and $\nabla\psi$ values are continuous at the nodal points of the meshes.

3.4 Analyses of nonlinear MHD phenomena

3.4.1 Saturation of the m = 1 magnetic island due to a resistive internal mode

The recent high power neutral beam injection experiments of the JFT-2 tokamak[6] showed the suppression of the internal disruption and the appearance of the m = 1 stationary oscillation with large amplitude. One of the possible explanations of this new phenomenon is the stability of the m = 1 internal mode. As was predicted by Bussac et al.[7], the internal mode becomes unstable in a toroidal plasma, when the poloidal beta value exceeds a certain critical value. Although the saturation level of this mode is quite low due to the development

of the skin current at the q = 1 surface, as pointed out by Rosenbluth et al.[8], the finite resistivity η can relax this skin current and cause the large magnetic island. From this point of view, we studied the linear stability and nonlinear evolution of the resistive internal mode[9]. We developed the new reduced set of MHD equations in a cylindrical plasma under the assumption of the incompressible fluid motion $\nabla\cdot\vec{v} = 0$. This new set of equations is reduced to the conventional one when the longitudinal wave number k_z goes to infinity with keeping $k_z B_z$ constant. This set of equations has been solved by expanding variables into Fourier components and using the predictor-corrector explicit time integration scheme. Figure I.3-6 shows the temporal change of the position of the magnetic axis r_a due to the resistive mode, the resistive internal mode, and the internal mode. The safety factor and the pressure profiles are chosen as $q(r) = 0.8(1+r^2)$ and $p(r) = 2(1-r^2)$, respectively, and the magnetic fields B_θ and B_z are given by solving the equilibrium equation under the condition of $B_\theta = 1$ at $r = 0.5$. When $k_z = 0$ and $\eta = 10^{-4}$, the internal mode is marginally stable and the magnetic axis shifts to the cooler region exponentially in time due to the resistive mode, and the internal disruption occurs when the magnetic axis touched the critical surface $r = r_c$, as predicted by Kadomtsev. When $k_z = 1.3$ and $\eta = 0$, the internal mode shifts the magnetic axis, but this shift saturates at low level, which is consistent with the analysis by Rosenbluth et al. When we take into account the finite resistivity $\eta = 10^{-4}$, then the magnetic axis shifts beyond this level due to the magnetic island formation, as the resistive mode, but the shift saturates before touching the critical surface. This saturation of the magnetic shift is caused by the island formation of the B_z field, which is constant in time for the resistive

mode. Figure I.3-7 shows the magnetic flux surface at the saturation level.

3.4.2 AEOLUS-RT code

MHD activities, such as tearing mode or resistive ballooning mode, have a clucial role in plasma confinement by tokamak. We develope a three dimensional code "AEOLUS-RT" written in a reduced set of equations to study these phenomena precisely. In this reduced set of equations, we have made following assumptions: a standard tokamak ordering; $a/R_0 \ll 1.$, where a and R_0 are minor and major radii, respectively, and a plasma is incompresible and low beta. Using this code we are now studying nonlinear tearing mode of different helicities, which is considered to be one of the candidates of the major disruption.[10-12)]

We choose q profile in this calculation as follows;

$$q(r) = 1.38(1. + (r/r_0)^8)^{1/4}$$

and q at plasma surface becomes 3.84.

Figure I.3-8 shows the time evolution of magnetic islands of each helicity. In contrast with the two dimensional calculation of single helicity (dashed line), the results of multi helicity (solid line) show rapid destabilization of 3/2 mode by the nonlinear interaction of different helicity from the time when the magnetic islands of 2/1 and 3/2 modes are overlapping. Furthermore from that time some of the magnetic field lines become stochastic and at the end of the calculation the stochastic magnetic field lines extend almost the plasma column. (Fig.I.3-9).

This stochasticity of magnetic field lines may lead to temperature flattening due to pararell heat conduction. In the last stage,

the negative voltage spike observed in experiments also occurs in our calculation.[12] Detailed investigation is now being carried out.

3.4.3 Spectrum of resistive mode

We calculate the spectrum of tearing mode using the same, linearrized, reduced set of equations as the previous subsection with toroidal and finite beta effects, these effects can easily be applied to the above nonlinear three dimensional calculation. In this linear case, we solve the equations as an eigenvalue problem.

The q profile in this calculation is chosen as,

$$q(r) = 0.95(1. + (r/r_0)^4)^{1/2}$$

whre r_0 is determined so as to q(0.7) = 1..

The first eigenvalues and eigenfunctions are shown in Fig.I.3-10. These results reveal two features: one is that the cylindrical m = 1 mode remains unchanged in toroidal calculation, which is well-known result, and the other is that m = 2 mode excites a "toroidal" m = 1 mode by toroidal coupling. This excited "toroidal" m = 1 mode is further increased by finite beta effect, and the maximum amplitude of eigenfunctin of "toroidal" m = 1 mode is greater than that of cylindrical m = 2 mode in the case of $\varepsilon = 0.1$ and $\beta_p = 0.5$, where ε is inverse aspect ratio and β_p is poloidal beta. This latter result is consistent with Bussac's analytical treatment.[13]

3.5 Neutral gas cooling

The divertor in a tokamak is expected to sweep out impurities, reduce impurity back-flow, exhaust ash, and so on. The reduction of

the plasma temperature near the divertor plate is also expected to suppress plasma-wall interactions such as sputtering. When the ionization mean-free-path ℓ_i of re-injected hydrogen neutrals from the divertor plate once becomes shorter than the thickness d of the scrape-off layer near the plate, i.e., $n_p > n_{crit}$ and $T_e > T_{crit} \simeq 10$ eV, both the plasma density n_p and neutral density are continuously increased untill the electron temperature T_e is decreased to T_{crit}. This is because the ratio ℓ_i/d becomes small as n_p becomes large and the recycling of low energy neutral/charged hydrogens effectively takes place near the plate. The H radiation power in the divertor region may become several 10% of the power coming from the main plasma. Thus the plasma is cooled and plasma-wall interactions are suppressed.

In the above consideration, however, we assume that the plasma flow from the main plasma to the divertor region is not changed by the increment of plasma density near the divertor plate. In order to study characteristics of the scrape-off layer plasma for that case, we have developed a one-dimensional electrostatic particle code. The effects of ionization, charge-exchange, radiation, and Coulomb collisions are simulated as well as the self-consistent electrostatic field. The detailed investigation is under progress.

3.6 Matrix method for kinetic ballooning mode

The difference-differential equation which describes high-n kinetic ballooning mode was solved by means of finite difference approximation,[14] so that mode coupling effect and the full electron and ion responses are kept in correct forms. The finite difference approximation reduces the eigenvalue problem of the original equation to that

of a matrix equation, $A\bar{x} = 0$. The eigenvalue ω is given by the solution $D(\omega) \equiv \det(A) = 0.1$. It is solved by Newton's method with the help of contour map. Matrix renumering saves CPU time and core memory. We investigated performance, convergence property and accuracy of the method in detail. Fig.I.3-11 shows an example of convergence curve of electrostatic high-n ballooning mode in the fluid limit. The convergence is quadratic with positive gradient for $Re(\omega)$ (solid line) and negative for $\gamma = Im(\omega)$ (dot linet). The extrapolated values of them accord with those for shooting method with very high accuracy.

3.7 TRITON system and the supporting codes

As described previously various kind of numerical codes relating to the MHD problems in a tokamak plasma have been developed and used to solve the problems. These codes are put in order and rechecked for easiness to use in the future. Several codes in the code system TRITON are used together to understand behaviour of a tokamak plasma comprehensively. For this purpose standardization and modular structure of codes are desirable. However, it is often the case that rules for standardization and modular structure are neglected in order to quickly write a code and quickly obtain physics results. Therefore, in the code system TRITON we do not rely on strict rules during development of a code but the physics codes are put in order by using a supervizing code HARMONIA after they are completed. Formal structure of any Fortran code is analyzed by using the code analyzer PLUTO, and some numerical codes are run by using a preprocessor EOS, which considerably save time when one would like to run a certain code over a wide range of parameter values. Preliminary version of above supporting codes were

already developed in the previous fiscal year. In this fiscal year several improvements were carried out and these codes were used extensively to gain high efficiency in development, maintenance, and use of various physics codes. In addition to these supporting codes, an automatic data aquisition and editing code for computations and simulations, HERA (High level Editor of Results of numerical Anayses) is newly developed.

References

1) Tuda, T. et al., "Ballooning stable high beta tokamak equilibria" JAERI-M 9427 (April 1981).

2) Takizuka, T. et al., Computer Phys. Commun. 23 (1981) 19.

3) Takizuka, T. et al., "Computational studies of tokamak plasmas" JAERI-M 9354 (February 1981).

4) Gruber, R. et al., Computer Phys. Commun. 21 (1981) 323.

5) Tsunematsu, T. et al., Computer Phys. Commun. 19 (1980) 179.

6) Yamamoto, S. et al., "Magnetohydrodynamic activities in JFT-2 tokamak with high power neutral beam injection heating" submitted to Nucl. Fusion.

7) Bussac, M.N. et al., Phys. Rev. Letters 35 (1975) 1638.

8) Rosenbluth, M.N. et al., Phys. Fluids 16 (1973) 1894.

9) Coppi, B. et al., "Resistive internal modes", MATT-1271 (1976).

10) Waddell, B.V. et al., Phys. Rev. Letters 13 (1978) 1386.

11) Carreras, B. et al., Phys. Fluids 23 (1980) 1811.

12) Carreras, B. et al., Phys. Fluids 24 (1981) 66.

13) Bussac, M.N., private communication.

14) Tuda, T. et al., "Electrostatic ballooning mode", JAERI-M 9456 (April 1981).

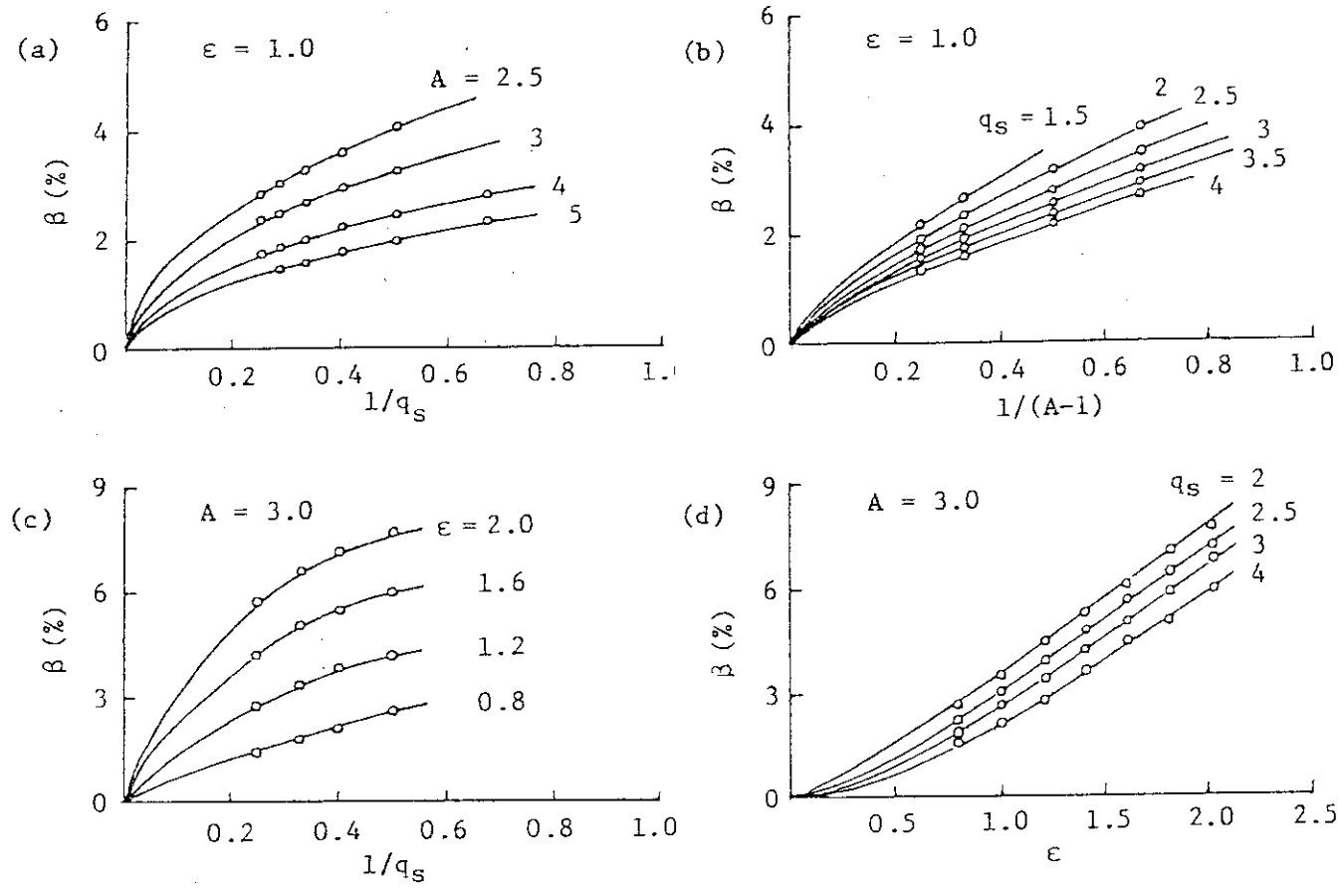

Fig.I.3-1 Critical beta values β(%) as functions of (a) the safety factor at the plasma surface q_s for the aspect ratio A = 2.5, 3, 4, 5 and the ellipticity ε = 1, (b) A for q_s = 1.5, 2, 2.5, 3, 3.5, 4 and ε = 1, (c) q_s for A = 3 and ε = 0.8, 1.2, 1.6, 2 and (d) ε for A = 3 and q_s = 2, 2.5, 3, 4. The safety factor at the axis is chosen to be q_a = 1.

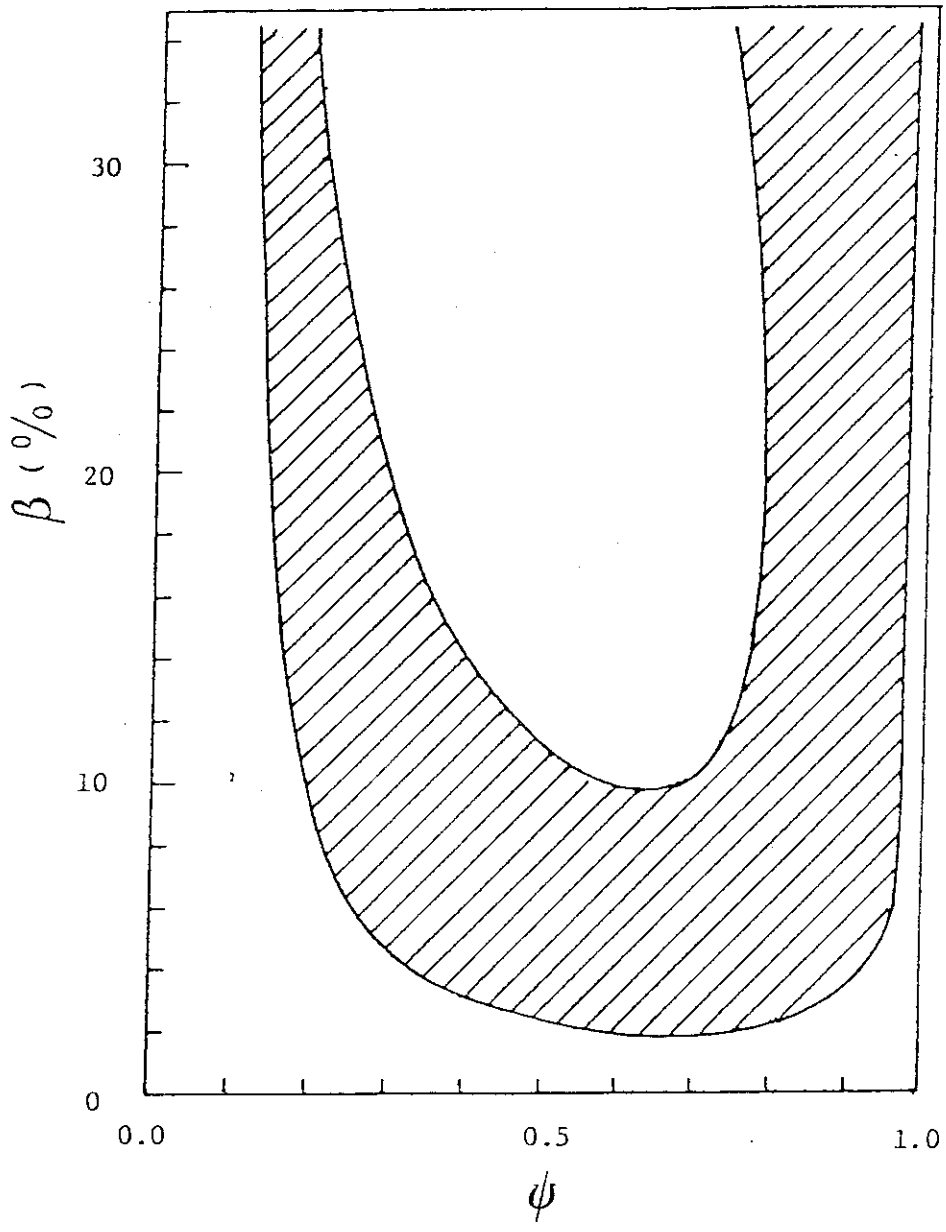

Fig.I.3-2 Ballooning unstable region in the ψ - β plane of the plasma, which is heated up with pressure source $S(\psi) = (1 - \psi^2)^2$ from the force-free equilibrium.

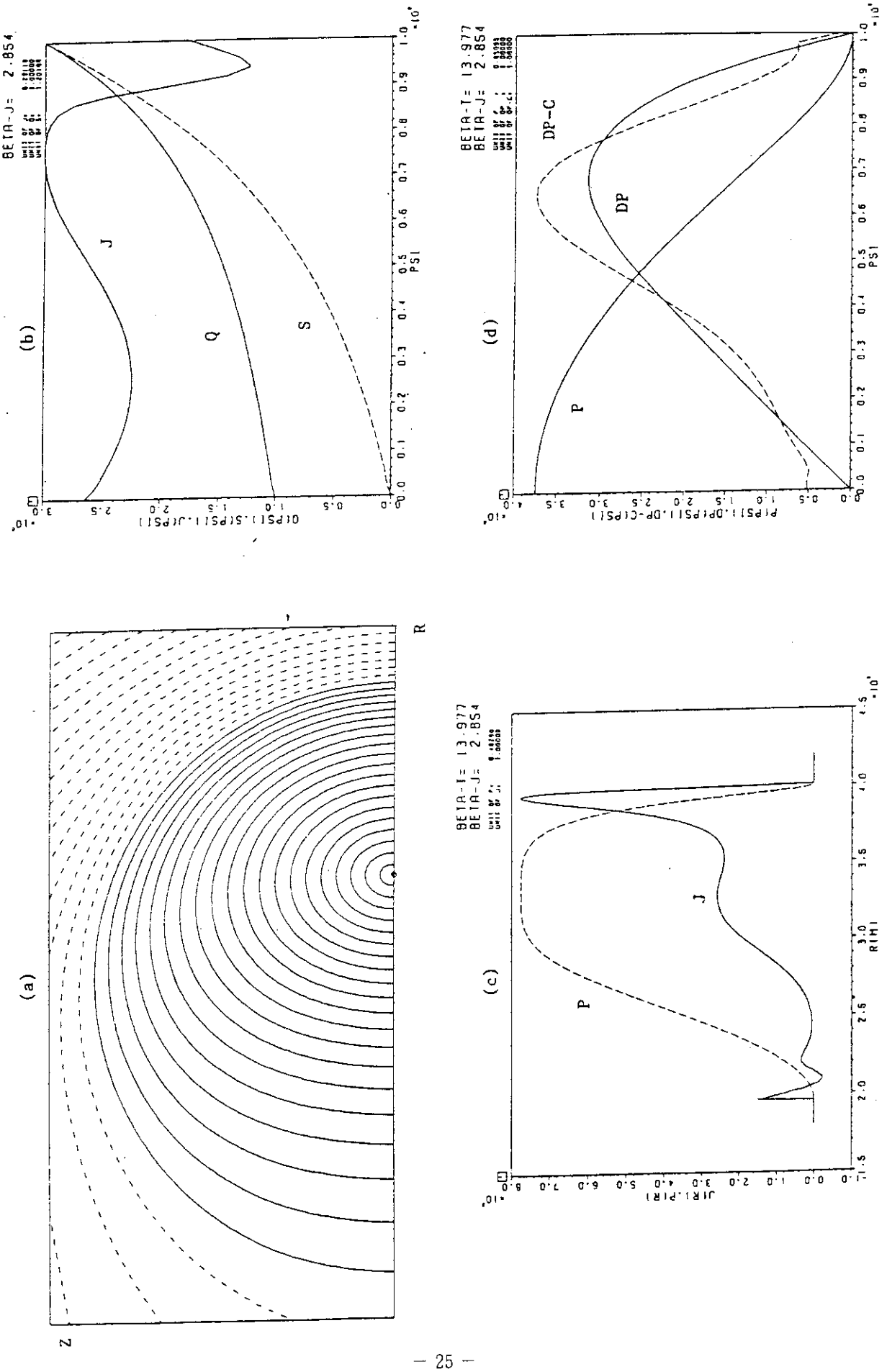

Fig.I.3-3 FCT equilibrium with β = 13%.

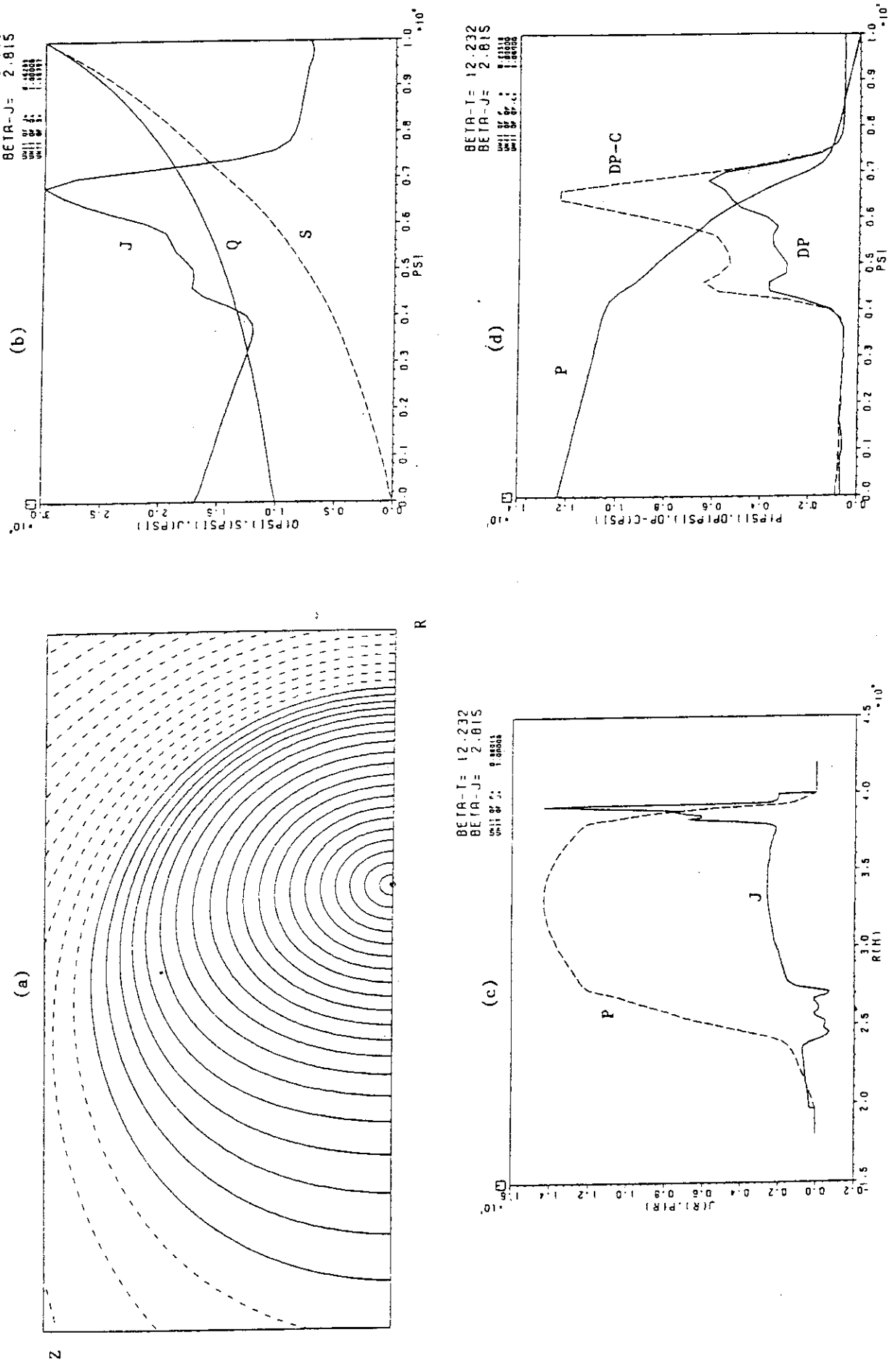

Fig.I.3-4 Equilibrium with β = 12% stable against ballooning modes in a whole plasma region.

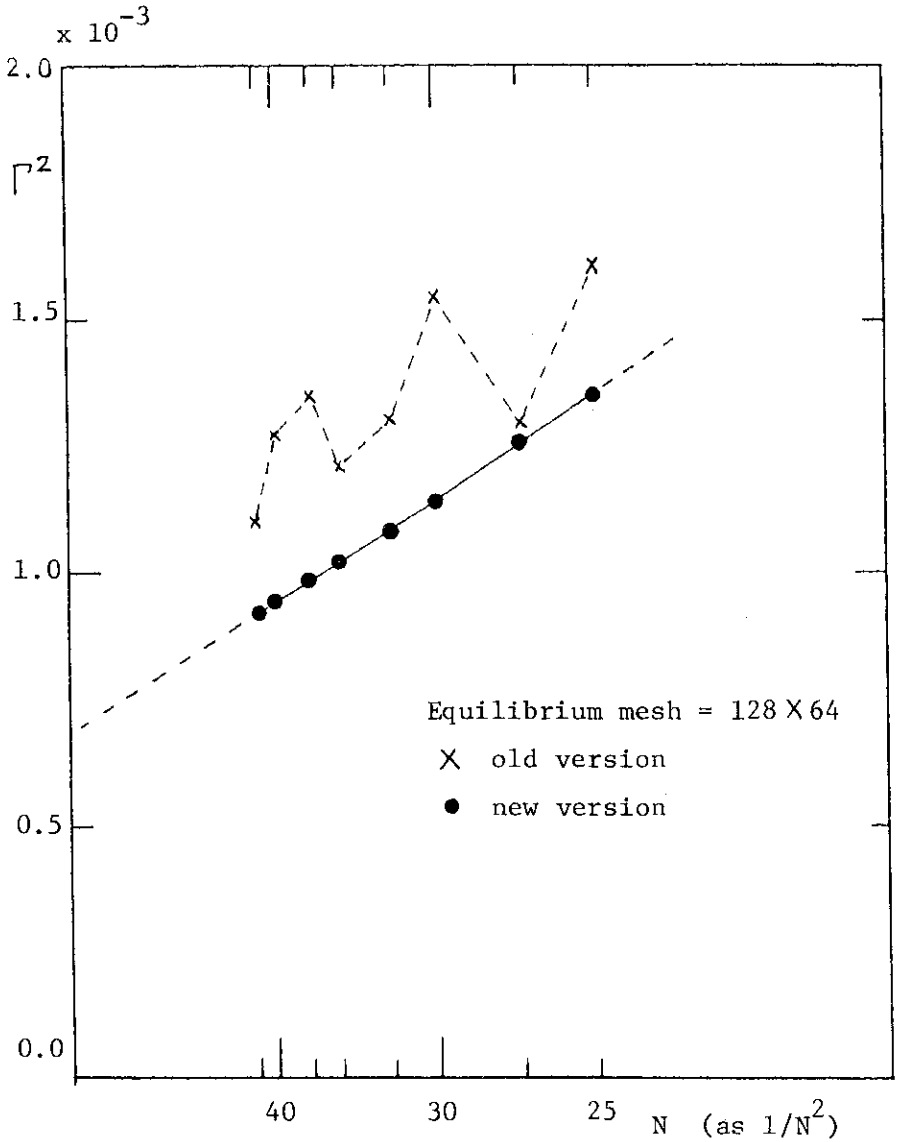

Fig. I.3-5(a) Example of convergence curve of n = 1 internal mode for 128×64 equilibrium mesh. ×: old version, ●: new version.

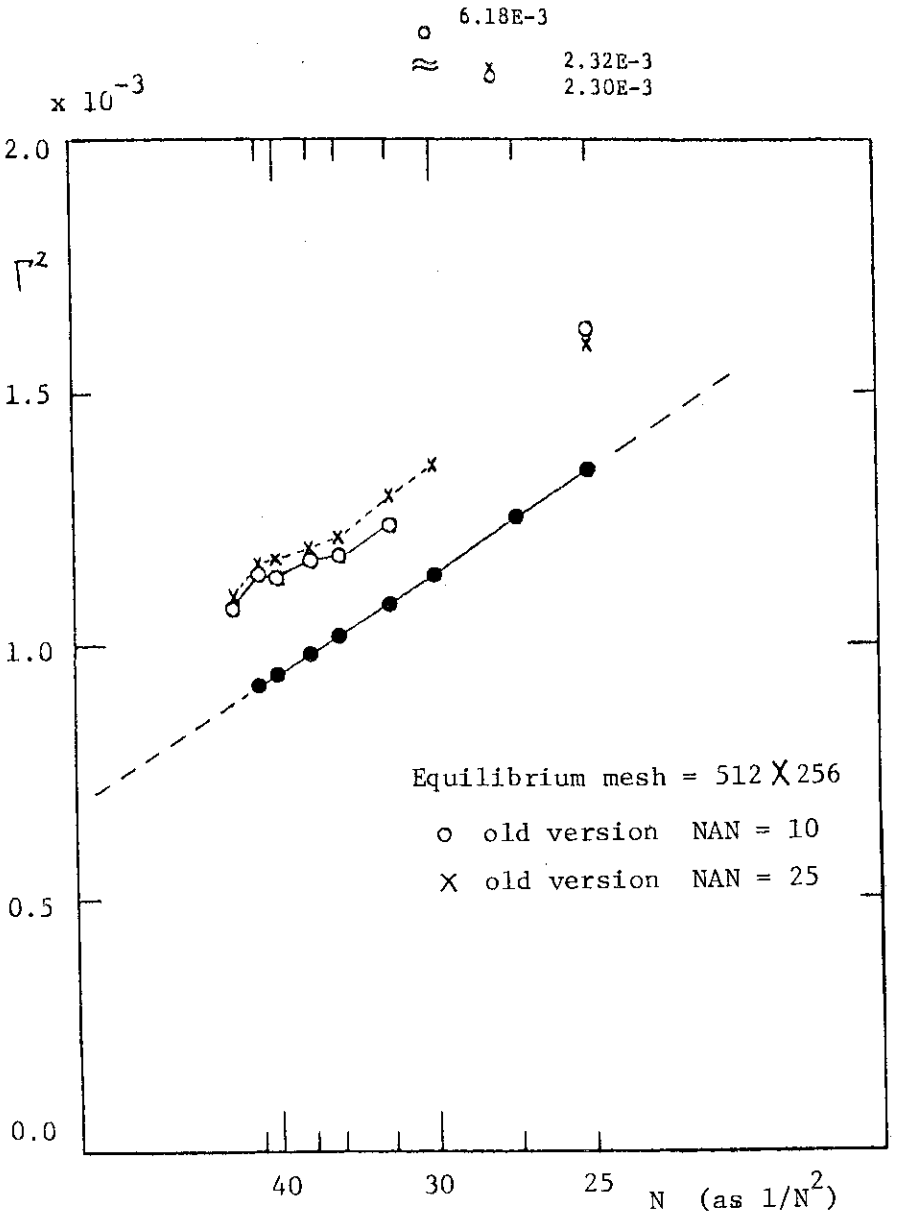

Fig. I.3-5(b) The convergence curves of r 512×256 equilibrium mesh (old version). The least square fitting region is NAN = 10 (o) and NAN = 25 (×).

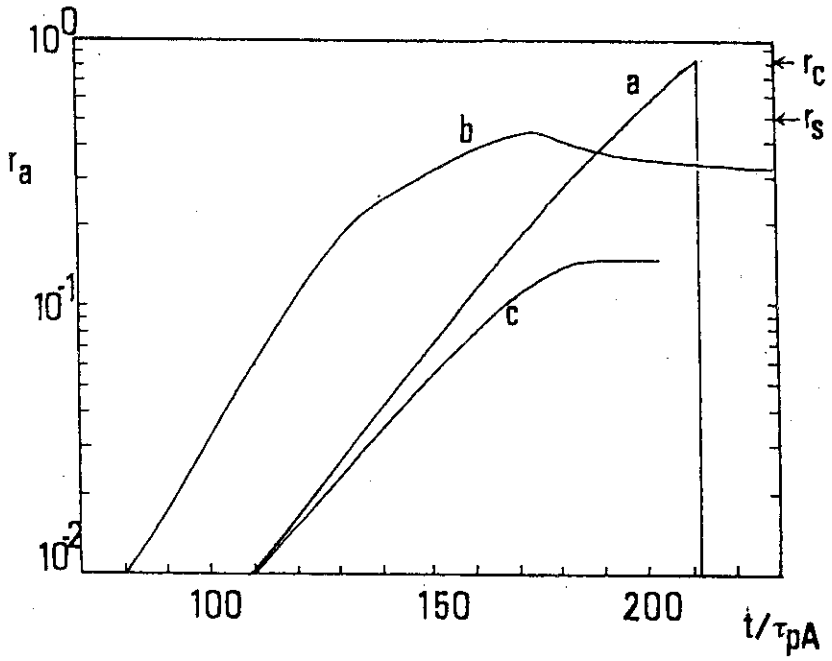

Fig.I.3-6 Temporal change of the position of the magnetic axis r_a due to the resistive mode (a), resistive internal mode (b), and internal mode (c).

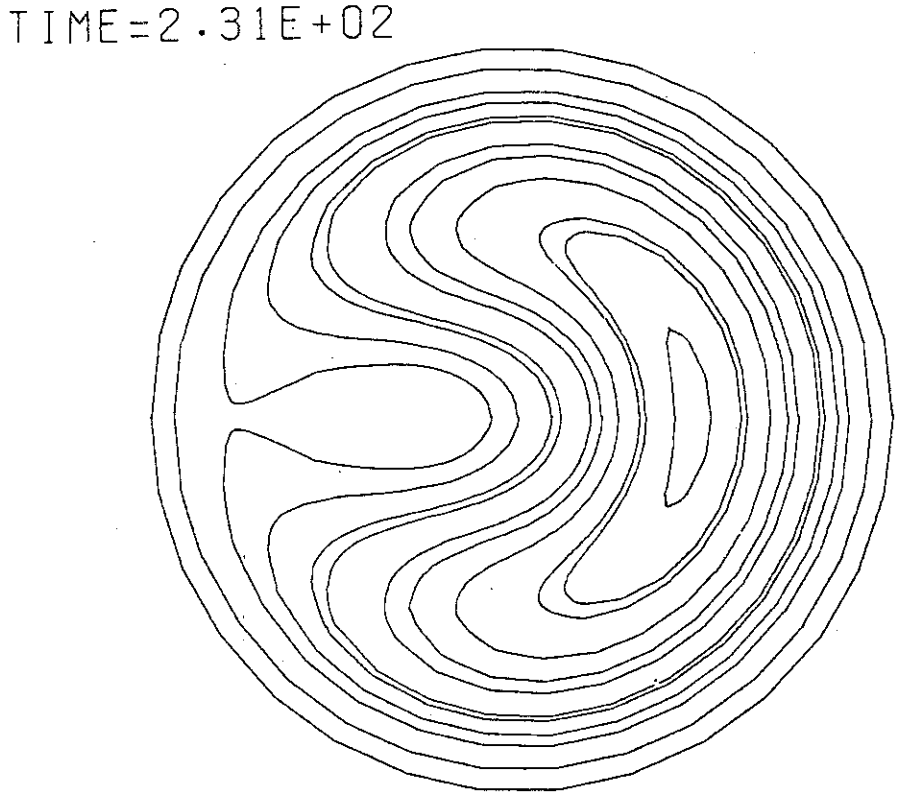

Fig.I.3-7 Magnetic flux surfaces at the saturation level of the resistive internal mode.

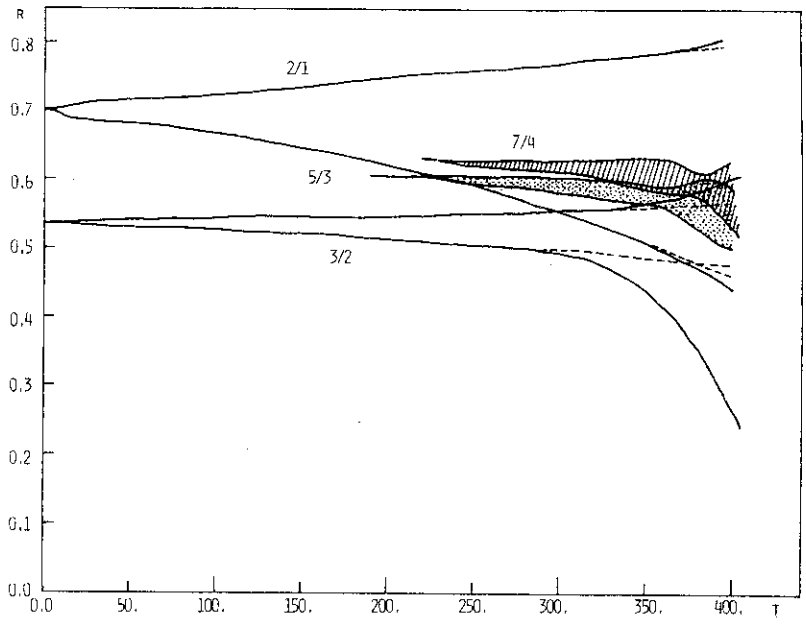

Fig.I.3-8 Time evolution of magnetic island width and their position for the 2/1, 3/2, 5/3, and 7/4 modes. Dashed and solid lines represent results of single and multi-helicities, respectively.

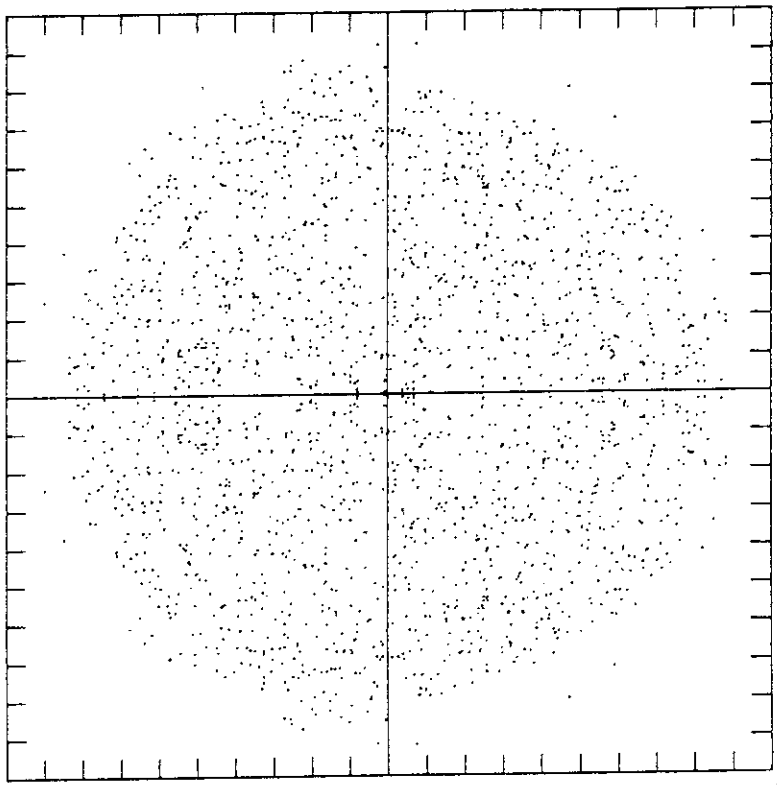

Fig.I.3-9 Intersection of a single magnetic field line with a poloidal plane, z = 0, in the last stage of the calculation. The initial position of the field line tracing is r = 0.5, θ = 0, and z = 0.

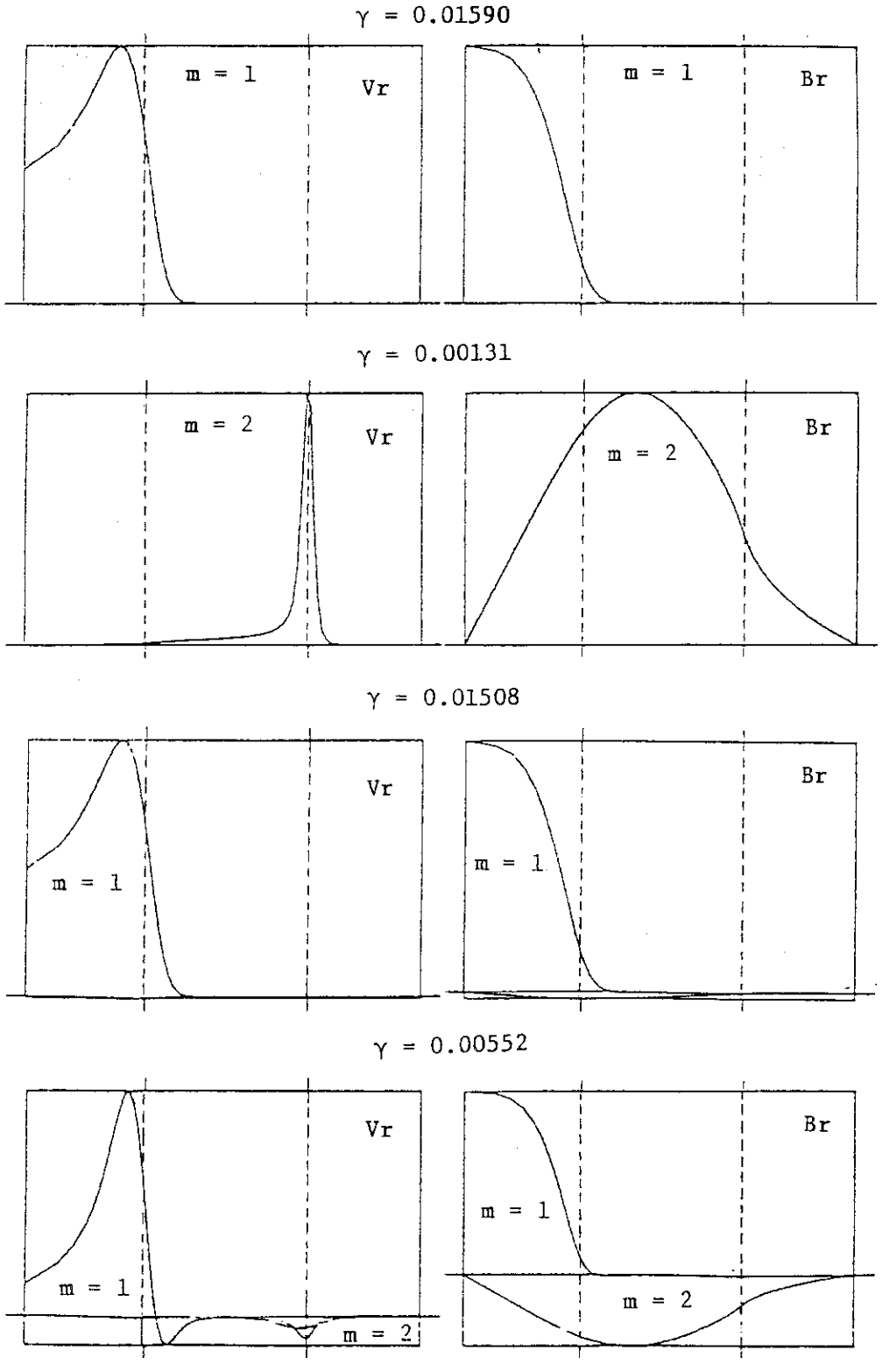

Fig.I.3-10 Eigenvalues and their eigenfunctions of V^r and B^r, radial components of velocity and magnetic field in respective order, in the case of (a) $\varepsilon = 0$, $\beta_p = 0$, (b) $\varepsilon = 0.1$, $\beta_p = 0.5$, where ε and β_p are inverse aspect ratio and poloidal beta, respectively. Dashed lines represent the singular surfaces of m = 1 and m = 2 modes.

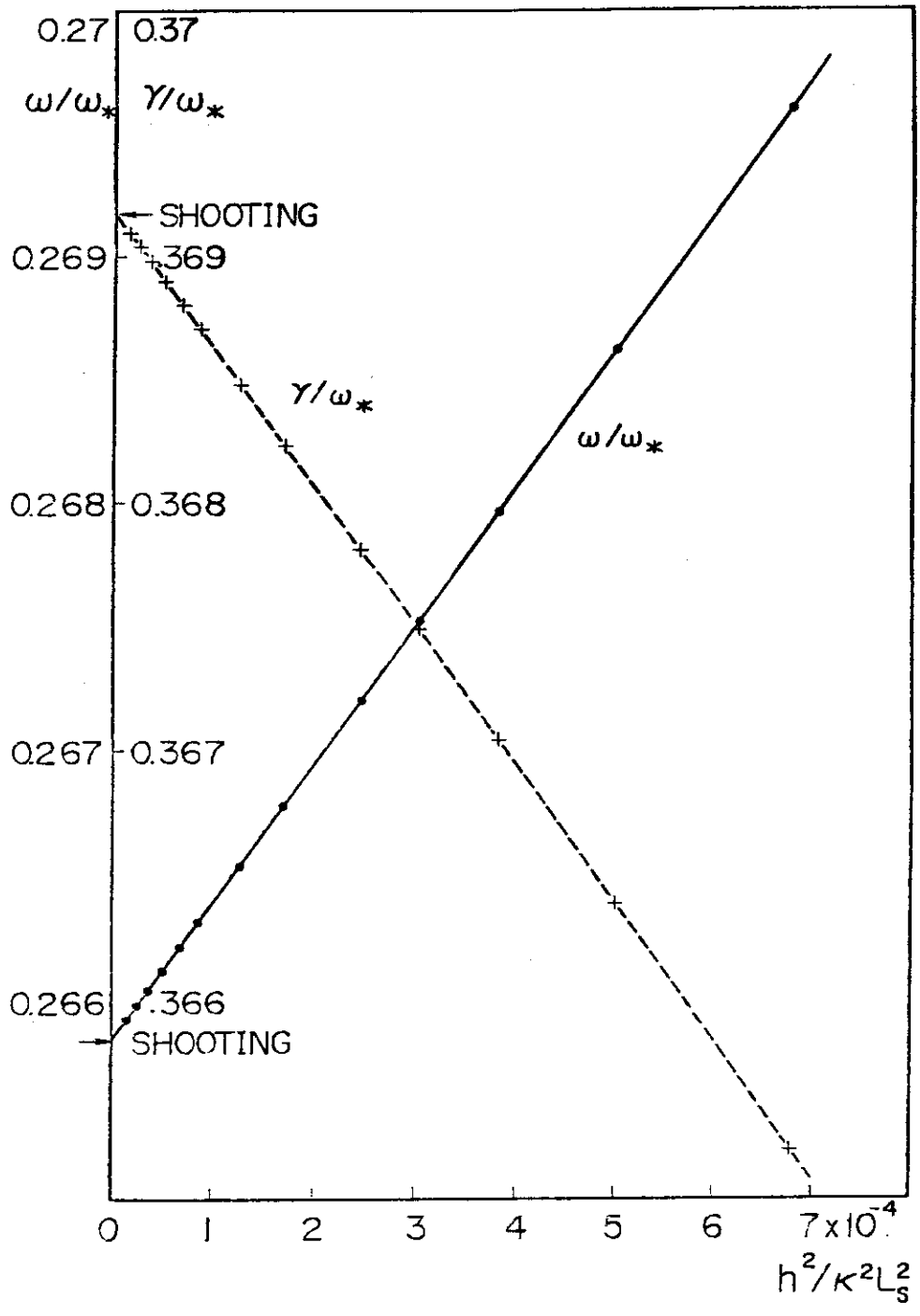

Fig.I.3-11 Example of convergence curve of the matrix equation which approximates the electrostatic high-n ballooning mode in the fluid limit. Solid line denotes Re(ω) and dot line $\gamma = \mathrm{Im}(\omega)$.

II. TOROIDAL CONFINEMENT EXPERIMENT

1. Introduction

The JFT-2 experiment placed much importance in the high-power neutral beam heating, current drive by the lower hybrid wave and electron cyclotron heating during the present reporting period.

The high-power beam injection into JFT-2 was commenced after the installation of the injection system in the end of the previous period, and characteristics of high-beta plasma with a circular cross-section were investigated. The observed maximum β-value at the axis reached up to 7 % due to the thermal component. The density clamping and MHD activity during the neutral beam injection were also studied in detail.

Succeeding the first promising result of current drive by the lower hybrid wave in 1979, the soft-X ray energy spectra were examined to demonstrate a plateau in an electron velocity distribution induced by the irradiated rf wave. The observed distortion of the electron distribution function indicated the current generation of 15 A/cm^2 at the plasma center for the net rf power of 150 kW.

The electron cyclotron heating using a 28 GHz, 200 kW gyratron was successfully performed and completed in February 1981 under the US-Japan Cooperation on Fusion Research Program. The experiment in JFT-2 emphasized good results on the electron heating with the heating rate of 5 ~ 7 eV/kW and the heating efficiency of 80 %.

A 1 MW-class heating experiment on ion cyclotron range of frequency starts from March in 1981. A 20-MHz powerful oscillator was installed in February 1981, and the antenna design was also completed.

The design of JFT-2M (a medium-sized noncircular tokamak) was completed, and the construction of toroidal field coils is now in progress. By the end

of 1982, the JFT-2M tokamak will be installed at the area occupied by the JFT-2 tokamak shortly after the disassembly of JFT-2. JFT-2M is a flexible, easily modified facility in mid 1980s for studies relevant to the improved advance concepts of the tokamak reactor.

2. JFT-2

2.1 High-power neutral beam injection heating experiment[1,2,3)]

Characteristics of high-β tokamak plasmas of a circular cross-section are investigated experimentally and numerically with q_a = 2-4, R/a = 3.5-4.75 and NBI of 0.8-1.2 MW. The observed maximum β value at the axis is 7 % due to the thermal component and 10 % including the beam component, and the volume average β is 2.6 % and 3 %, respectively. The observed β values including the beam component are much higher than the critical β values obtained from the ballooning analysis and the β values only due to the thermal component are slightly higher than the critical values. The mhd activities and impurity behavior are modified by NBI but the observed modifications are not due to a high-β effect. Ion and electron confinement characteristics are very similar to those in a low-β tokamak.
Concluding the result, no new behavior is observed in the high-β tokamak plasma.

2.1.1 β-value

Neutral beam injection heating[4)] of 0.8 ÷ 1.2 MW was applied to an ohmically heated plasma (Fig.II.2-1). Typical time behaviors of plasma characteristics in a low q discharge of $q_a \sim 2$ with neutral injection power P_{inj} of about 1.2 MW are shown in Fig.II.2-2. Oscillograms of PIN diode signal along the horizontal central chord S.X.① and pick-up loop signal

$\tilde{\dot{B}}_\theta$ are shown over the full time of the discharge (Fig.II.2-2-(d)). Those expanded oscillograms during the ohmic heating phase and during the beam heating phase are shown in Fig.II.2-2-(e) and -(f), respectively. The other plasma parameters are on an expanded time scale starting at 70 ms. After the start of neutral beam injection heating, the loop voltage decreases, the ion and electron temperatures increase and also the plasma density increases because of intense gas puffing (Fig.II.2-2-(c)). The line radiation from metallic ions increases during the first 25 ms and falls after that. The radiation loss power is mainly due to oxygen and is about 20 % of the total input power during NBI heating. The central beta value β_0 increases up to 7.6 % due to the thermal component and up to 10 % including the calculated beam components of the pressure. Plasma profiles at 25 ms after starting NBI are shown in Fig.II.2-3-(a) and the volume average β-values $<\beta>$ is 2.6 % due to the thermal component and 3 % including the beam component. An optimized pressure profile at the critical β value obtained from the ballooning analysis[5] is compared with the experimental data in Figs.II.2-3-(b) and -(c). Figures II.2-4-(a) and -(b) show the measured central beta β_0 and the volume averaged beta $<\beta>$ versus aspect ratio R/a and versus safety factor q_a, respectively. The open points indicate the thermal contribution to beta and the solid points indicate the thermal and fast-ion beam contributions. The striped bands show the critical peaked beta values and volume averaged beta values from the high n ballooning mode analysis. The lower lines of each bands indicate the critical values for $q_0 = 1$ and the upper lines for $q_0 = 0.9$, respectively. The total beta values including the beam component are higher than the calculated critical beta values in many discharges. However, it must be noted that the maximum thermal beta values are only slightly higher than the theoretical values. The stability analysis of high n ballooning modes in

a tokamak plasma with anisotropic ion pressure, taking into account the finite ion gyroradius effects, suggest that having the parallel temperature greater than the perpendicular temperature does not contribute to the ballooning mode instability[6]. Since in the experiment only total beata values significantly exceed the critical values and this excess is comparable to the anisotropic fast-ion contribution, the beta measurements seems consistent with the stability analysis. The parameter dependence of the observed β-values on the safety factor q_a seems similar to those of theoretical values (Fig.II.2-4-(b)). This parameter dependence, however, is due to the characteristics, i.e. a higher-β plasma is easily obtained in a lower-q plasma. Therefore it is necessary to increase the heating power in order to obtain a real critical β value.

2.1.2 Transport

The slowing-down process of fast ions produced by the neutral beam injection into the JFT-2 plasma has been studied by a simulation code using Monte-Carlo techniques. The energy transfer from the beams to the plasma and the loss of fast ions due to charge exchange and drifting motion are investigated. An example of calculation results is shown in Fig.II.2-5. In a low density case, the power losses due to charge exchange neutrals and shine-through beams are very large. Otherwise, in a high density case, the energy transfers to the electrons and ions are so large that the effective plasma heating can be expected.

The observed temperature and β-value are analyzed by using a tokamak code including NBI heating, neutral particle transport and the sawtooth effect[7,8]. The density and temperature profiles and the parameter dependence on plasma density and toroidal magnetic field B_t are well explained by the tokamak code with the same heat conductivities as in ohmic plasmas;

$\chi_e = 2.0 \times 10^{17}/n_e$ $cm^2 s^{-1}$ and $\chi_i = 1.5\ \chi_{neo}$ where n_e is plasma density in cm^{-3} and χ_{neo} the neoclassical value.

The density clamp as observed in ISX-B with the NBI heating[9] and in JFT-2 with the LHR heating[3] is also observed in this experiment. To clarify the cause of density clamping, particle confinement time and the recycling rate was directly measured during NBI experiment.

Simple particle balance equation is written as followingly,

$$dN_e/dt = -N_e/\tau_p + RN_e/\tau_p + S = -(1-R)N_e/\tau_p + S \quad ,$$

where τ_p: particle confinement time, R: recycling rate, S: gas influx. Gross particle confinement time τ_p, is defined as $F = N_e/\tau_p$ where F is the total particle loss flux to the first wall and the limiter. From the measurement of the wall and limiter efflux, τ_p and also trapping efficiency of the particle at the limiter and wall defined by $T = 1 - R = (S-N_e)/(F_L+F_W)$ where R: recycling rate, S: gas influx, F_L: limiter flux, F_W: wall flux, were obtained.

Figure II.2-7 shows the results of the typical measurements. Neutral beams were injected at density ramping phase. Although hydrogen gas was continuously puffed in, density was clamped by the injection (Fig.II.2-7-(a)). The limiter flux and the wall flux increase with the injection. electron boundary temperature also increases (Fig.II-2.7-(b)). With the injection particle confinement time τ_p decreases about 25 % and the trapping efficiency becomes almost doubled (Fig.II.2-7-(c)).

τ_p and trapping efficiency 1-R were measured under various conditions. Results of particle confinement time are summarized in Fig.II.2-8. Since scaling of τ_p is not well understood, τ_p is plotted against the normalized plasma density assuming τ_E like scaling, $\propto \overline{na}^2$. From this, it was shown that τ_p with injection slightly levels off compared with OH case.

And maximum decrement during a single shot is 20 to 30 per cent with the injection, and no difference was found between counter injection and co-injection as for reduction of τ_p.

Figure II.2-9 shows the relation of the trapping efficiency to the electron temperature near the limiter. Trapping efficiency tends to increase with the rise of the electron edge temperature by the injection. During the injection sheath potential of the limiter and the wall surface increase with the rise of the temperature. Then, protons would impinge on the limiter and the wall surface at higher energies than those of ohmic heating phase. Therefore it is possible that trapping efficiency increases during the injection.

From these measurement it was made clear that for the observed change of dN/dt, contribution of the enhanced trapping efficiency is much larger that the contribution of decreased particle confinement time. Therefore enhancement of the trapping efficiency during the injection is the dominant cause of the density clamping. This density clamping is easily suppressed by intense gas puffing, and this does not set the upper limit of the plasma density. Densities achieved during the neutral beam injection experiments are shown in Fig.II.2-10. Maximum density expressed in a form of $\overline{n_e}$ $(10^{13}\ cm^{-3})/[B_T(T)/R_0(m)]$ reaches around 8.

2.1.3 Impurities

In usual cases, the metal impurities such as Ti, Fe and Mo increase with a high-power heating. This increment can be suppressed by an intense gas puffing. The edge cooling is observed with the intense gas puffing. And the metal impurities decrease during the NBI heating phase in the optimized condition as shown in Fig.II.2-11. Therefore, it is reasonable to consider that this reduction of metal impurities during the NBI phase is

due to the reduction of influx rather than the change of transport.

Arcing is not observed during the NBI heating as in a stable ohmic plasma[10]. In a helium operation, the increment of the metal impurities are higher than those in a hydrogen operation. These results show that the ion sputtering is also the dominant cause of metal impurity release as in an ohmic plasma[11].

2.1.4 MHD activity

The MHD activities are modified by the NBI heating. The PIN diode signal shown in Fig.II.2-2 is the case of the enhanced sawtooth oscillations. The sawtooth repetition time and the amplitude of enhanced sawtooth oscillations in the NBI heating phase are longer and larger than those of classical sawtooth oscillations with ohmic heating. The magnetic fluctuation level is low except during sawtooth disruption. As the sawtooth disruption phase is approached, the $m = 2/n = 1$ poloidal fluctuations grow and abruptly increase at the disruption phase. The same phenomena are observed in the case with only ohmic heating. However, the amplitude of the $m = 2/n = 1$ poloidal fluctuations are larger ($\delta B_\theta/B_\theta \sim 0.6$ %) than those ($\delta B_\theta/B_\theta < 0.1$ %) in the ohmic heating phase. The experimental results suggest that the change of electron temperature profile or current profile during the sawtooth disruption phase in the case of neutral beam injection heating is larger than that in the case of ohmic heating, and that the energy loss due to enhanced sawtooth oscillation is larger than that due to classical sawtooth oscillation.

In order to simulate beam induced sawtooth oscillation on the diffusion time scale, a model for the sawtooth oscillation is established in a similar manner to Jahns et al's work[12], and the model is incorporated into a one-dimensional tokamak transport code[7], including Fokker-Planck code for NBI

heating. These simulations show that enhanced sawtooth oscillations can be explained by Kadomtsev's theory[13].

Even under nearly the same discharge conditions with nearly the same injection power, different types of MHD behavior were sometimes observed in the higher q_a discharge of $q_a \sim 4$. Figures II.2-12-(a) and -(b) show oscillograms of PIN diode signals and pick-up loop signals in the case of $q_a = 4.2$ and $P_{inj} = 1.2$ MW. In the case shown in Fig.II.2-12-(a), sawtooth oscillations continued during neutral beam injection heating. On the other hand, in the case shown in Fig.II.2-12-(b), (of which more detail oscillograms are shown in Fig.II.2-13), the sawtooth oscillations are strongly deformed and completely disappear after sawtooth oscillations lasting only a few cycles, and again sawtooth oscillations appear after one injector is shut off.

Figure II.2-13-(a) and -(c) show expanded PIN diode signals and pick-up loop signals during the time of high frequency oscillations of m=1/n=1 modes without sawtooth oscillations shown in Fig.II.2-12-(b). The m=1/n=1 poloidal magnetic fluctuation level is very high ($\delta B_\theta / B_\theta \sim 1.2$ %).
The amplitude of frequency doubling on the PIN diode signals at the central chord gradually increases as the round sawtooth oscillations smoothly change into high frequency oscillations without sawtooth oscillations.
The frequency doubling of the m=1 mode on the central chord corresponds to the fact that the magnetic axis, slightly displaced by the growing island, is seen twice for each rotation by the central detector[14].

In the following, we consider the mechanism of the suppresion of the internal disruptions and appearance of the m=1 stationary oscillations with large shift of the magnetic axis. One of the possible cause is due to m=1 internal mode. As was predicted by Bussac et al[15], the internal mode becomes unstable in a toroidal plasma, when the poloidal beta value exceeds

a certain critical values. Although the saturation level of this mode is quite low due to the development of the skin current at the q=1 surface, (as pointed out by Rosenbluth et al[16]), the finite resistivity η can relax this current and cause the large magnetic island. Thus, resistive internal mode has a possibility for the explanation of the m=1 stationary oscillations with large amplitude.

REFERENCES

1) SHIMOMURA, Y., SUZUKI, N., YAMAMOTO, S., MAENO, M., OHASA, K., et al., "High-β Study in JFT-2", JAERI-M 9065 (1980).

2) YAMAMOTO, S., MAENO, M., SUZUKI, N., AZUMI, M., TOKUDA, S., et al., "Magnetohydrodynamic Activity in the JFT-2 Tokamak with High Power Neutral Beam Injection Heating", Nucl. Fusion 21 (1981) 993.

3) SUZUKI, N., IMAI, T., FUJISAWA, N., MAENO, M., YAMAMOTO, T., et al., in Plasma Physics and Controlled Nuclear Fusion Research (Proc. 8th Int. Conf. Brussels, 1980), Vol.1, IAEA, Vienna (1981) 525.

4) Annual Report of the Fusion Research and Development Centor for the Period of April 1, 1979 to March 31, 1980, p.88.

5) AZUMI, M., TSUNEMATSU, T., ITOH, K., TUDA, T., KURITA, G., et al., in Plasma Physics and Controlled Nuclear Fusion Research (Proc. 8th Int. Conf. Brussels, 1980), Vol.1, IAEA, Vienna (1981) 293.

6) ITOH, K., INOUE, S., TUDA, T., Japan Atomic Energy Research Institute Report JAERI-M 9067.

7) AMANO, T., OKAMOTO, M., Japan Atomic Energy Research Institute Report, JAERI-M 8420 (1979).

8) TANI, K., KISHIMOTO, H., TAMURA, S., in Plasma Physics and Controlled Nuclear Fusion Research (Proc. 8th Int. conf. Brussels, 1980), Vol.1, IAEA, Vienna (1981) 631.

9) MURAKAMI, M., SWAIN, D.W., BATES, S.C., BUSH, C.E., CHARLTON, L.A., et al., in Plasma Physics and Controlled Nuclear Fusion Research (Proc. 8th Int. Conf. Brussels, 1980), Vol.1, IAEA, Vienna (1981) 377.

10) YAMAMOTO, S., SHIMOMURA, Y., OHASA, K., KIMURA, H., SENGOKU, S., J. Phys. Soc. Jpn. 48 (1980) 1053.

11) OHASA, K., MAEDA, H., YAMAMOTO, S., NAGAMI, M., OHTSUKA, H., Nucl. Fusion 18 (1978) 872.

12) JAHNS, G.L., SOLER, M., WADDELL, B.V., CALLEN, J.D., HICKS, H.R., Nucl. Fusion 18 (1978) 609.

13) KADOMTSEV, B.B., Fiz. Plazmy 1 (1975) 710.

14) DUBOIS, M.A., MARTY, D.A., POCHELON, A., Nucl. Fusion 20 (1980) 1355.

15) BUSSAC, M.N., PELLAT, R., EDERY, D., SOULE, J.L., Phys. Rev. Lett. 35 (1975) 1638.

16) ROSENBLUTH, M.N., DAGAZIAN, R.Y., RUTHERFORD, P.H., Phys. of Fluids 16 (1973) 1894.

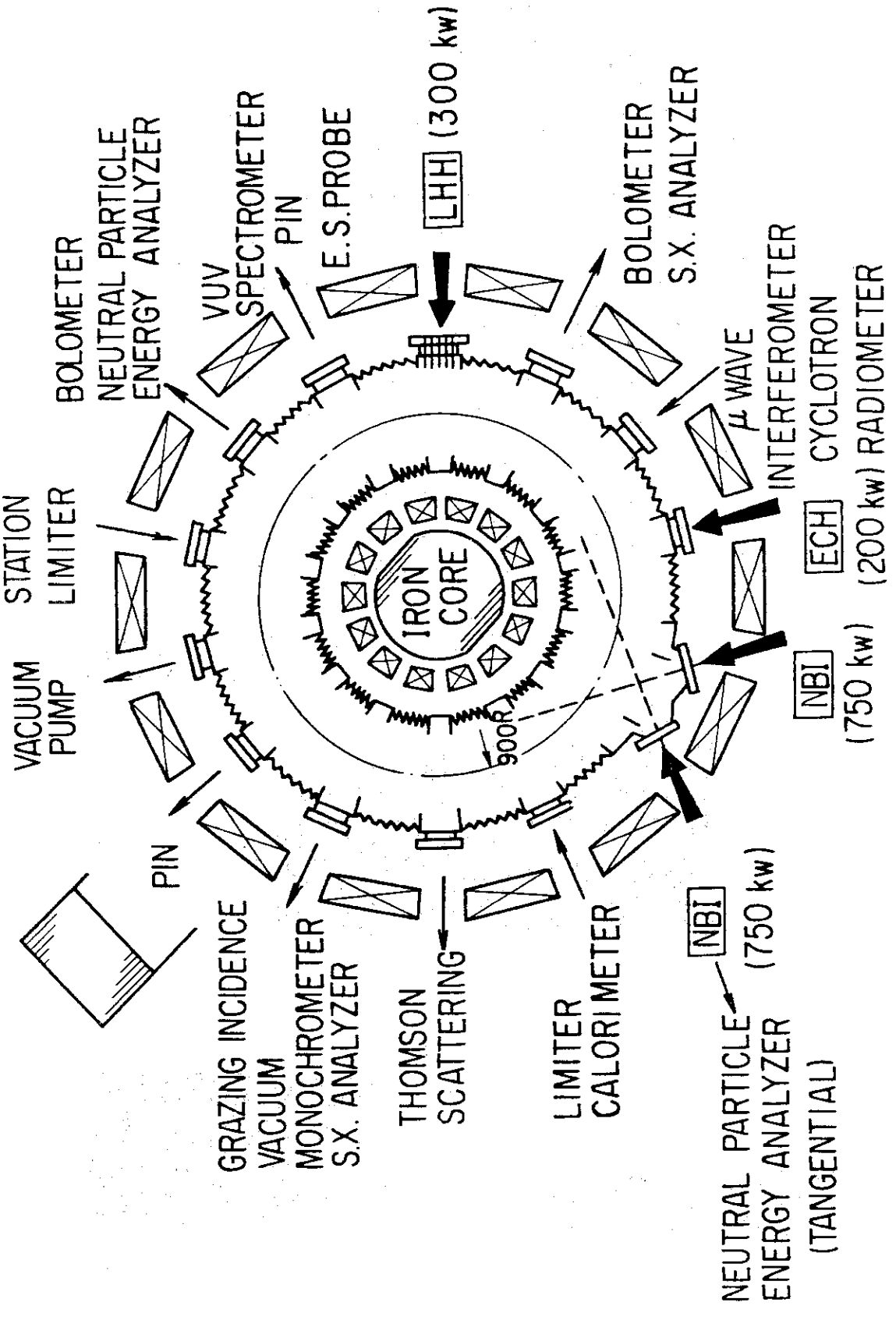

Fig.II.2-1. Configuration of the NBI system and the diagonostic system in the modified JFT-2 tokamak.

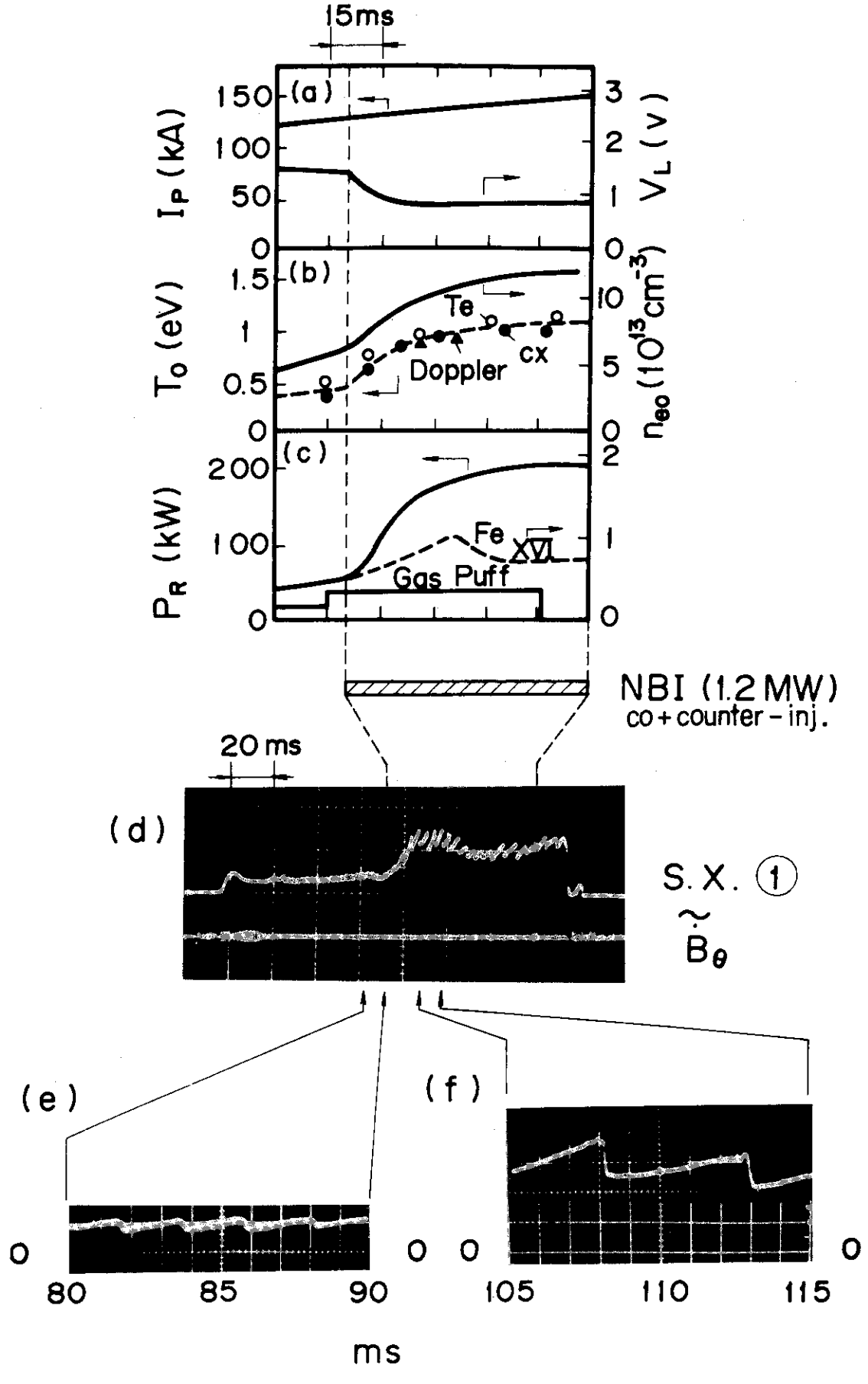
15ms
(a)
150
100
50
0
I_P (kA)
3
2
1
0
V_L (V)
(b)
1.5
1
0.5
0
T_0 (eV)
Te
cx
Doppler
10
5
0
n_{e0} (10^{13}cm^{-3})
(c)
200
100
0
P_R (kW)
Fe XVI
Gas Puff
2
1
0
NBI (1.2 MW)
co + counter - inj.
20 ms
(d)
S.X. ①
$\tilde{B}_\theta$
(e)
(f)
0
0
0
0
80
85
90
105
110
115
ms

Fig.II.2-2. Typical time behavior of plasma parameters. Time bahavior of plasma current I_p, loop voltage V_L, central density n_{eo}, ion temperature T_{io}, electron temperature T_{eo}, radiation loss power P_R, line intensity of F_e XVI 361.0 Å and gas influx are on an expanded scale starting at 70 ms.

: Ion temperature measured by a charge exchange (C.X.) neutral particle energy analysis.

: Ion temperature measured by doppler broadening of titanium emitted from a central part of the plasma column.

: Electron temperature measured by Thomson scattering (relativistic effect is not included) and measured by soft-X-ray energy analysis.

The volume averaged beta $<\beta>$ is 2.6 % due to thermal compoment and 3.0 % including beam component and the central beta β_0 is 7 % and 10 %, respectively. Oscillograms of PIN diode signals, S.X. 1 along the central chord and pick-up loop signal, $\dot{\tilde{B}}$ are shown over full time discharge and these expanded oscillograms during the ohmic heating phase and during the neutral beam injection phase are also shown. $B_T = 1.1$ T and $q_a = 2.0$. $P_{inj} = 1.2$ MW (co+counter injection)

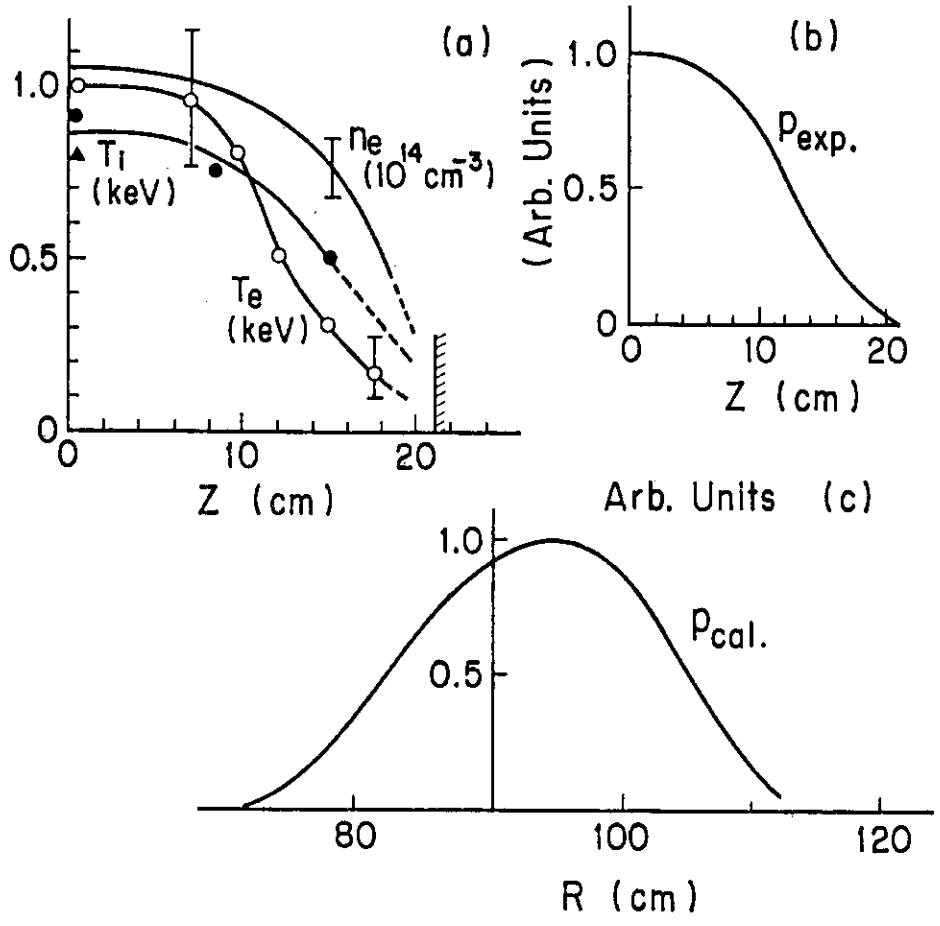

Fig.II.2-3. Plasma profile.

(a) Density and temperature profiles. (b) Thermal pressure profile in experiment. (c) Pressure profile in ballooning mode analysis.

The discharge conditions are shown in Fig.II.2-2. The volume averaged beta $<\beta>$ is 2.6 % due to thermal component and 3 % including beam component.

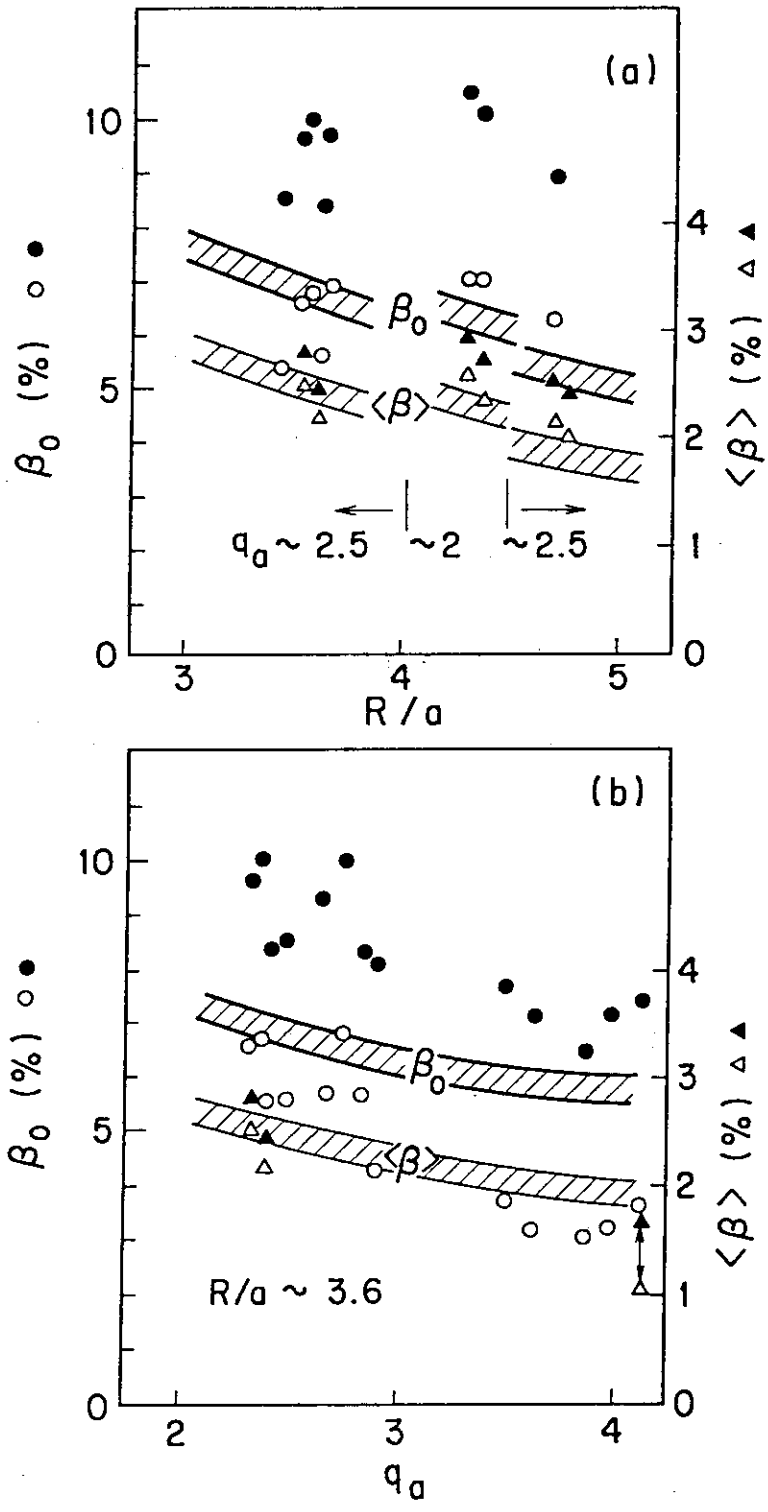

Fig.II.2-4. Critical β values obtained from the ballooning analysis and measured β values. R/a: aspect ratio, q_a: safety factor, β_0: peak β and $<\beta>$: average β. ○△ due to thermal component and ●▲ : including the beam component in experiment. ////// : critical peak β value from the analysis and ////// : critical average β value. The lower lines of each bands indicate the critical values for $q_0 = 1$ and the upper lines for $q_0 = 0.9$.

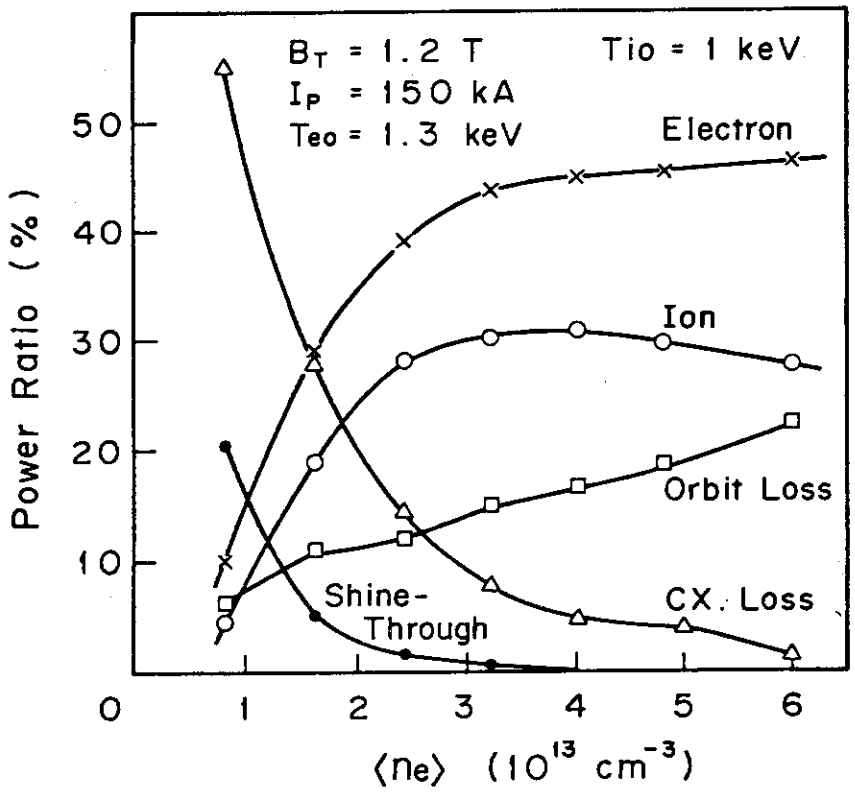

Fig.II.2-5. The energy transfer from fast ions to both electrons and ions and the energy losses due to charge exchange, drifting motion and shine-through vs. electron densities.

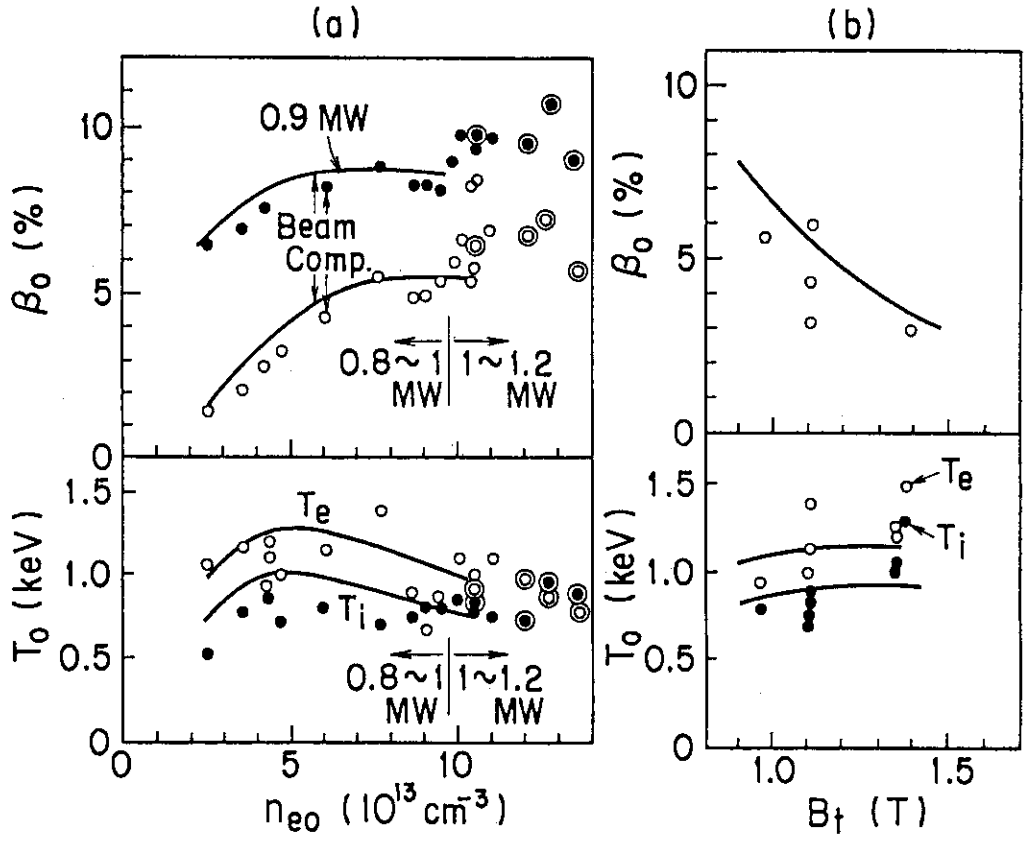

Fig.II.2-6(a) The peak β values and the peak temperatures. Solid lines indicate numerical results with $\chi_e = 2 \times 10^{17}/n_e(\mathrm{cm}^{-3})$ $\mathrm{cm}^2\mathrm{s}^{-1}$, $\chi_i = 1.5\ \chi_{ne0}$, $D_e = 8 \times 10^{16}/n_{e0}(\mathrm{cm}^{-3})$ $\mathrm{cm}^2\mathrm{s}^{-1}$, $a = 25$ cm, $I_p = 130$ kA, $B_t = 1.1$ T. Experiment is done with $B_t = 1.1$ T, $I_p = 120 \sim 150$ kA, and $a \simeq 25$ cm (○●) and $a \simeq 21$ cm (◎ ◉).

(b) The thermal peak β values and temperatures. Solid lines indicate the numerical result. Numerical and experimental conditions are the same in Fig.II.2-6-(a) except B_t, $a \simeq 25$ cm and $n_{e0} \simeq (5 \div 7) \times 10^{13}$ cm^{-3}.

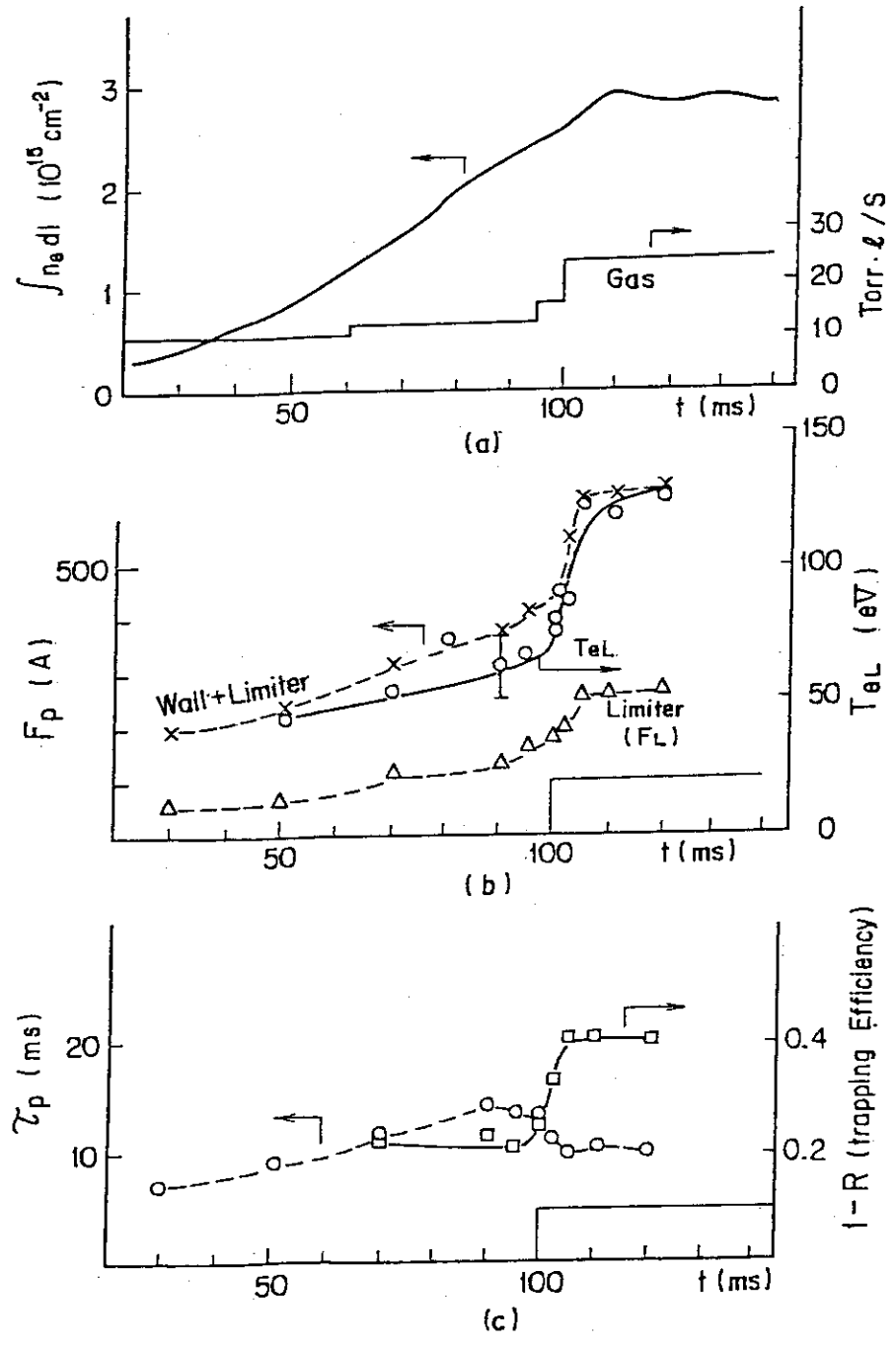

Fig.II.2-7. Discharge evolution for typical NBI experiment in JFT-2 (NBI starts from 100 ms). (a) Electron line density and gas influx. (b) Electron temperature at the limiter edge, limiter flux, and the total efflux to the limiters and the wall. (c) Particle confinement time and trapping efficiency 1-R.

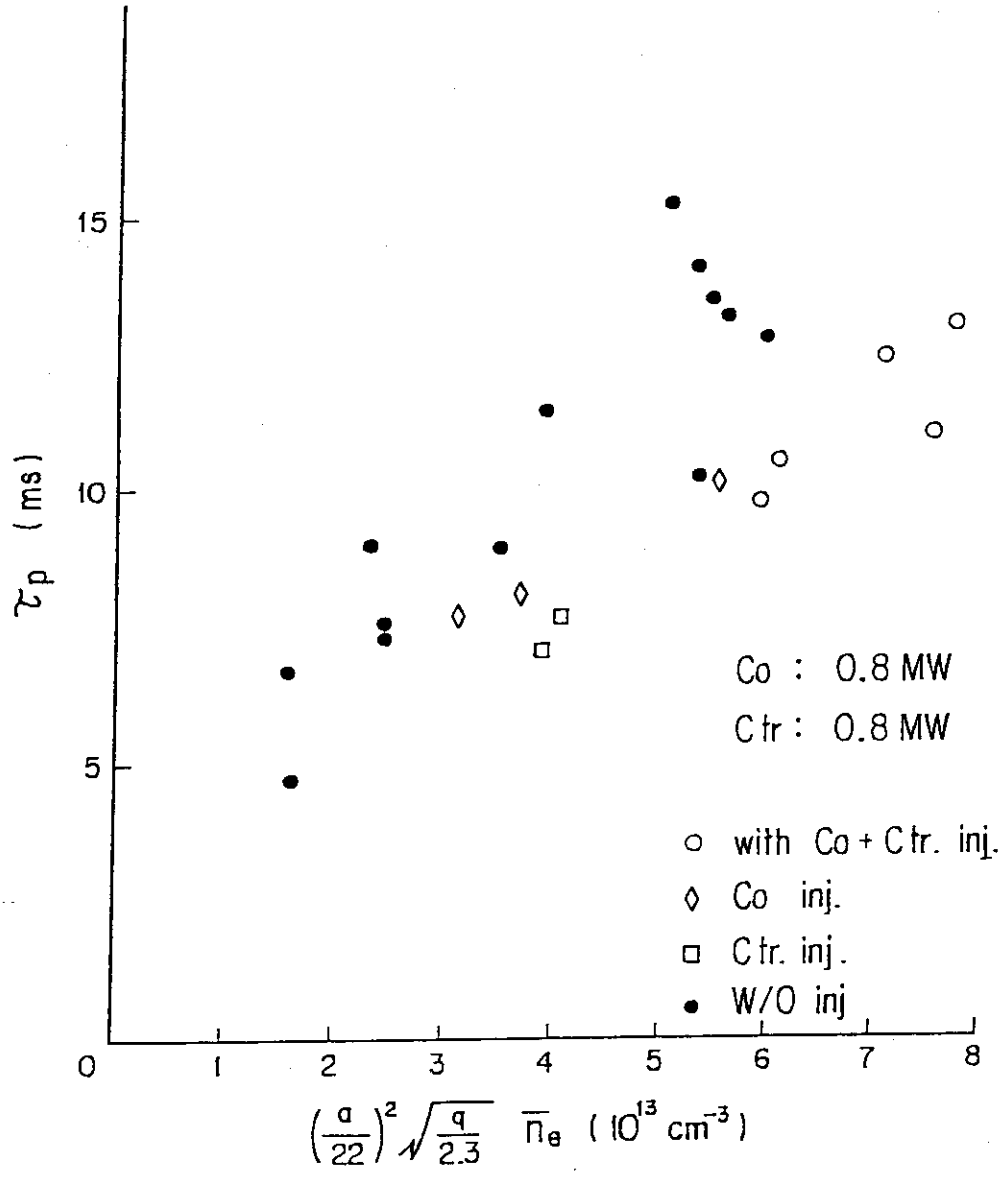

Fig.II.2-8. Particle confinement time versus normalized density $(a/22)^2\sqrt{q/2.3}\ \bar{n}_e$.

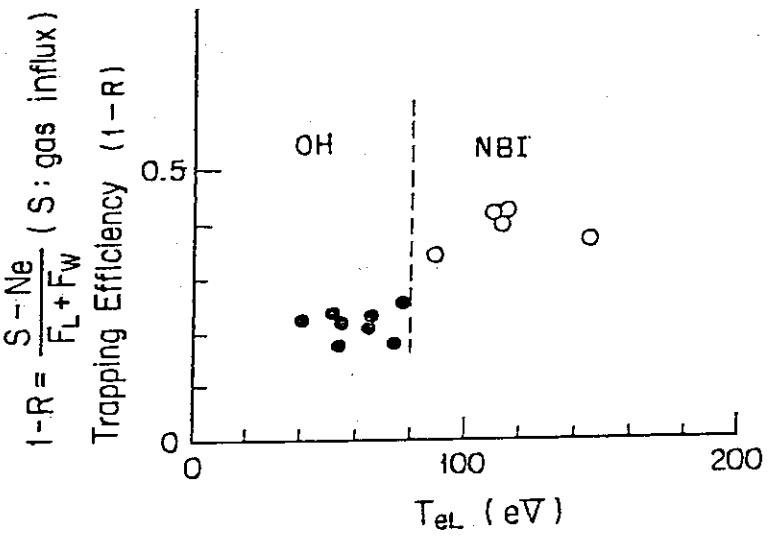

Fig.II.2-9. Trapping efficiency versus electron temperature at the limiter edge. Open circles represent data during the injection and dots denote data in ohmic heating phase.

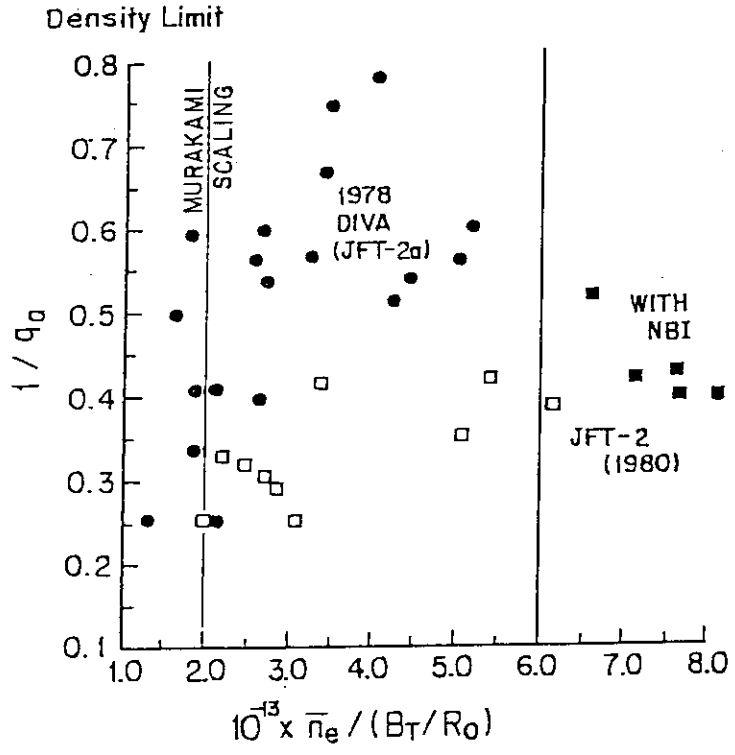

Fig.II.2-10. Line averaged electron density versus $1/q_a$. □ represent data in ohmic heating phase and ■ represent data with NBI. ● denote reference data of JFT-2a joule plasma.

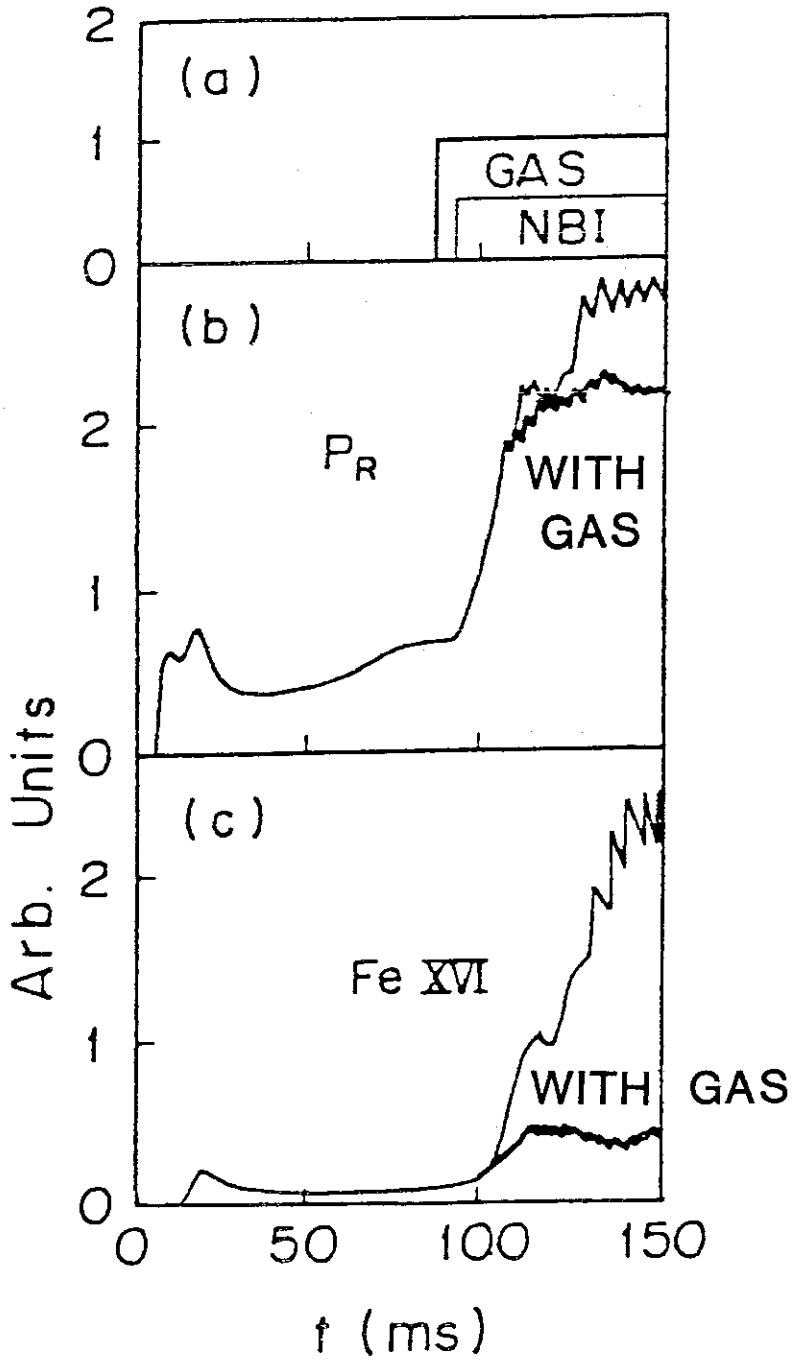

Fig.II.2-11. High-z impurity influx during NBI heating. The NBI heating induces a large influx because of enhanced ion sputtering due to a higher edge temperature. The influx is strongly reduced by cooling the edge plasma with an intense gas puffing.

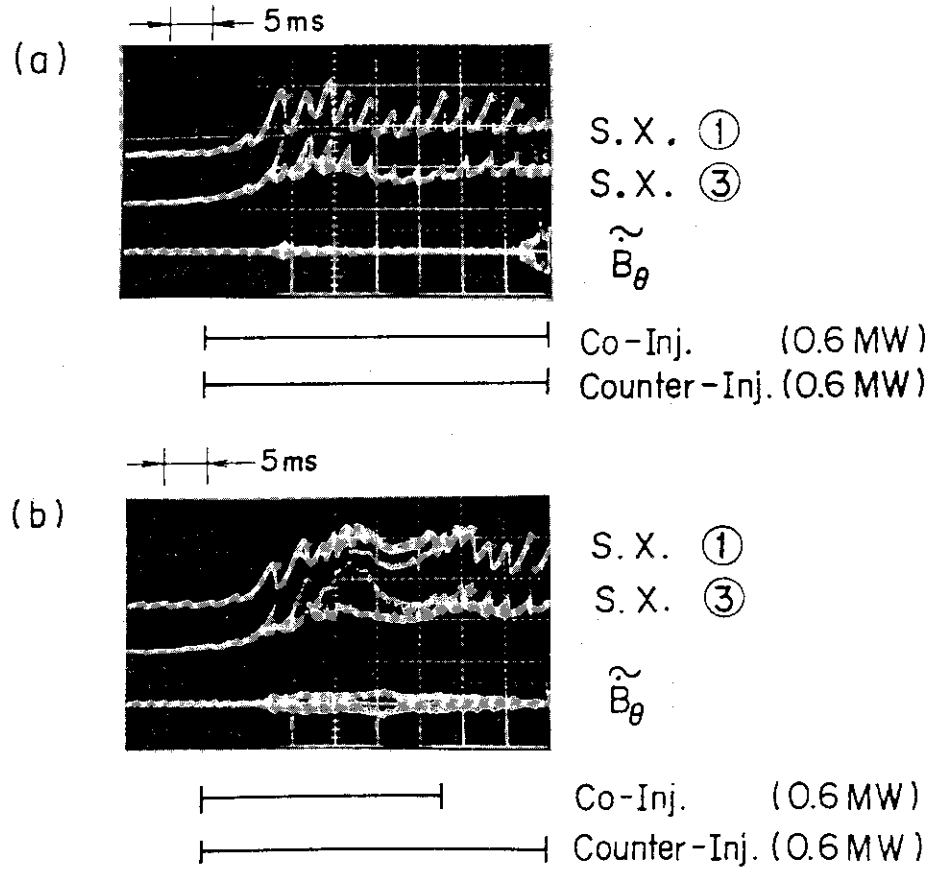

Fig.II.2-12. Two different types of MHD behavior with the nearly the same plasma parameters and neutral beam injection power. $B_T = 1.4$ T, $L_p = 140$ kA, $n_{e0} = 5.7 \times 10^{13}$ cm^{-3}, $q_a = 4.2$ and $P_{inj} = 1.2$ MW (co+counter injection).
(a) Sawtooth oscillations case.
(b) High frequency oscillations case.
Expanded signals of high frequency oscillation case are shown in Fig.13. Symbols, S.X.① and S.X.② denote PIN diode signals from along the central chord and near the central chord, respectively. S.X.③ and S.X.④ denote signals from along the off-central chord.
Especially S.X.④ denotes those from the region outside $q = 1$ magnetic surface.

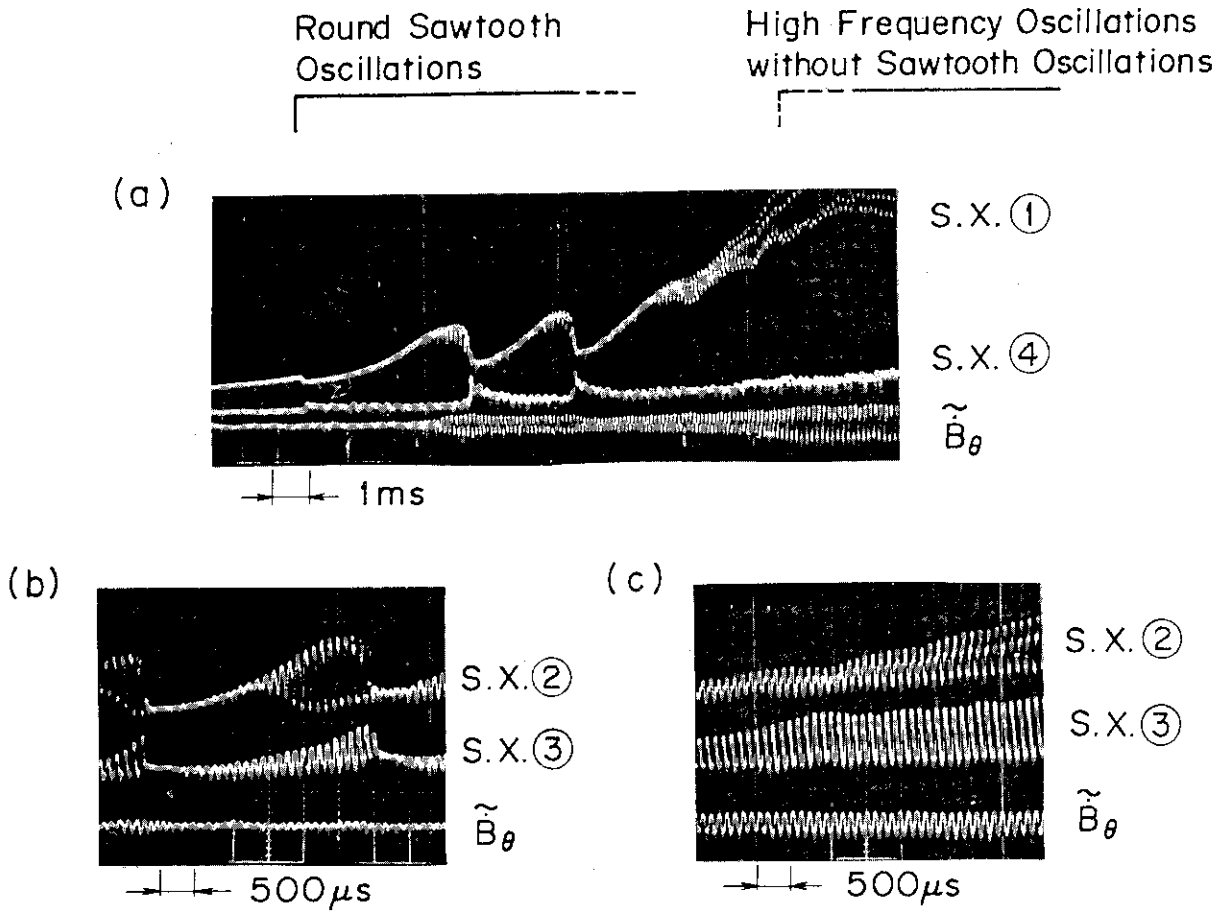

Fig.II.2-13. Expanded signals of high frequency oscillations case.

(a) Line-integrated emissivity at different horizontal chords and pick-up loop signals $\tilde{\dot{B}}_\theta$. Enahnced sawtooth oscillations change into round sawtooth oscillations, and then change into high frequency oscillations during neutral beam injection heating.

(b) Round sawtooth oscillations phase.

(c) High frequency oscillations without sawtooth oscillations phase.

$B_T = 1.4$ T, $I_p = 140$ kA, $n_{e0} = 5.1 \times 10^{13}$ cm^{-3}, $q_a = 3.5$ and $P_{inj} = 1.1$ MW (co+counter injection).

2.2 Study of the rf-driven current by lower hybrid waves

It is well known that the interaction between the lower hybrid waves and electrons via Landau damping leads to the rf-driven current in a tokamak[1,2]. This interaction is described by the coupled quasi-linear Fokker-Planck equation for the electron velocity distribution function. Linearizing the Fokker-Planck operator by taking the scattering distribution to be Maxwellian and introducing the assumption that perpendicular distribution is Maxwellian with a bulk electron temperature, we obtain the quasi-steady state distribution function integrated over the perpendicular velocity as[3]

$$F(w) = C \exp\int^{w} \frac{-w\,dw}{1 + w^3 D(w)} \quad , \tag{1}$$

where C is a normalization factor, w is the parallel electron velocity normalized by the thermal velocity v_{te} and D(w) is the quasi-linear diffusion coefficient normalized by $v_{te}^2 \nu_0$ with the collision frequency ν_0. Then, the generated current density is given by

$$j = -e n_e v_{te} \int_{-\infty}^{\infty} w F(w)\, dw \quad , \tag{2}$$

where e is electron charge and n_e and T_e are the electron density and temperature. So the measurement of the electron distribution function becomes important for studying the coupling between the lower hybrid waves and electrons. The electron distribution function in a high temperature plasma can be estimated from the soft X-ray energy spectrum of Bremssranlung radiation. In this section, we describe an experimental study of the rf-driven current in the JFT-2 tokamak using the soft X-ray diagnostic method. The experiments were carried out under the conditions of no existence of lower hybrid resonance inside the plasma and minor effects of parametric

processes.

The experiment, with a 750 MHz and 320 kW rf source, was performed in the JFT-2 tokamak which was converted to a circular shell-less tokamak with an active control system of the plasma position. The experimental setup and the discharges in the converted JFT-2 tokamak were reported in detail elsewhere[4], and hence will be described only briefly here. In the present experiment, the following discharge was used as a magnetohydrodynamically stable operation; toroidal magnetic field $B_t = 10$ kG, plasma current $I_p = 60$-70 kA, mean line-of-sight electron density $\overline{n_e} = 0.4$-1.4×10^{13} cm^{-3}, central electron temperature $T_{e0} = 500$-700 eV with the joule heating and effective ionic charge $Z_{eff} = 1.5$-2. The working gas was deuterium. A phased array of four rectangular waveguides was employed as a wave launcher and each waveguide has inner dimension of 1.4 cm by 29 cm. The phase difference between adjacent waveguides, $\Delta\phi$, is adjustable by a remote phase shifter. The energy of waves launched with $\Delta\phi = 90°$ is directed downstream of electrons and then is in favour of the current drive. Calculated power spectrum of the slow waves excited with respect to the refractive index, n_z, shows the gentle peak near $n_z = 5$ with the full-half width of $\Delta n_z = 7$.

Data from a typical plasma experiment on the current drive are shown in Fig.II.2-14. The dotted curves in the figure correspond to no rf condition. The loop voltage V_l is seen to fall smoothly and to reach a quasi-steady state level 10 msec after the rf turned on. The incremental increase of $\Delta I_p \simeq 3$ kA in the plasma current is also found in Fig.II.2-14-(a). Figure II.2-14-(b) shows the central electron temperatures obtained from Thomson scattering and soft X-ray measurements. The soft X-ray energy spectrum emitted along a line of sight through the major axis of the plasma was measured by a pulse-hight analysis system with an intrinsic germenium

detector covering a wide energy range up to 200 keV. The measured spectrum with no rf pulse showed a bi-Maxwellian electron distribution indicating runaway electrons. However, during the rf pulse the runaway electrons were suppressed and the soft X-ray emission in the energy range of 3-15 keV has enhanced remarkably. Also no increase of electron temperatures estimated from the laser scattering and the soft X-ray emission were observed. These results confirm that the relative drop in the loop voltage, $\Delta V_l/V_l$ due to the application of the rf pulse results from no excitation of the runaway electrons but the rf-induced current. Then, the rf-induced current of $I_{rf} = 20$ kA can be estimated from the relation of $I_{rf} = I_p(\Delta V_l/V_l)$. At same time a significant density build-up and remarkable decrease in the second harmonic cyclotron radiation were observed. The decrease of the cyclotron radiation is consistent with the disappearance of the runaway electrons. Figure II.2-15 shows the soft X-ray energy spectrum during the rf pulse under the same conditions as Fig.II.2-14. The solid circles indicate the experimental values superposed for 50 identical shots. The solid curve shows calculated spectrum from the electron distribution function (shown by the dotted line) which is adjusted for the calculated spectrum to best-fit the measured one. In these calculation, the cross section for Bremsstralung was taken from ref.5 and the observed and calculated values were fitted at the energy of 2 keV. It is found that the distribution function shows the quasi-linear plateau in the energy range of 3-18 keV corresponding to $n_z = 8.5$-3.7. This range of the coupling agrees well with the wave spectrum calculated from the Grill theory. The modification of the distribution function yields the plasma current and an rf-driven current density of $j(0) = 15$ A/cm^2 is estimated from eq.(2). Assuming the radial profile of the rf driven current to be $j(r)/j(0) = (1-(r/a)^2)n_j$, the estimated current density at the center and the total

rf induced current of 20 kA give $n_j = 0.4$ which indicated the current profile peaked at the plasma center not at plasma periphery.

In conclusion, we have obtained the followings.

(1) For lower density of $\overline{n_e} \lesssim 6 \times 10^{12}$ cm^{-3}, a substaintial drop of the loop voltage indicating 20 kA of the totally generated current was observed with $P_{rf} \simeq 150$ kW and $\Delta\phi = 90°$.

(2) The measured soft X-ray energy spectrum showed the formation of a velocity-space plateau on the electron distribution function in the velocity range nearly equal to the phase velocity of the waves predicted from the Grill theory.

(3) The observed distortion of the distribution function indicated an rf driven current of 15 A/cm^2 at the center of plasma, which gave a broad radial profile of the rf driven current peaked at the center of the plasma.

REFERENCES

1) Fisch, N.J.: Phys. Rev. Lett. 41 (1978) 873.

2) Yamamoto, T. et al.: Phys. Rev. Lett. 45 (1980) 716.

3) Karney, C.F.F. and Fisch, J.J.: Phys. Fluids 22 (1979) 1817.

4) Sizuki, N. et al.: 8th International conference on plasma physics and controlled unclear fusion research Brussels, (1980) IAEA-CN-38/T-2-3.

5) Gluckstern, R.L. and Hull, H.H. Jr.: Phys. Rev. 90 (1953) 1030.

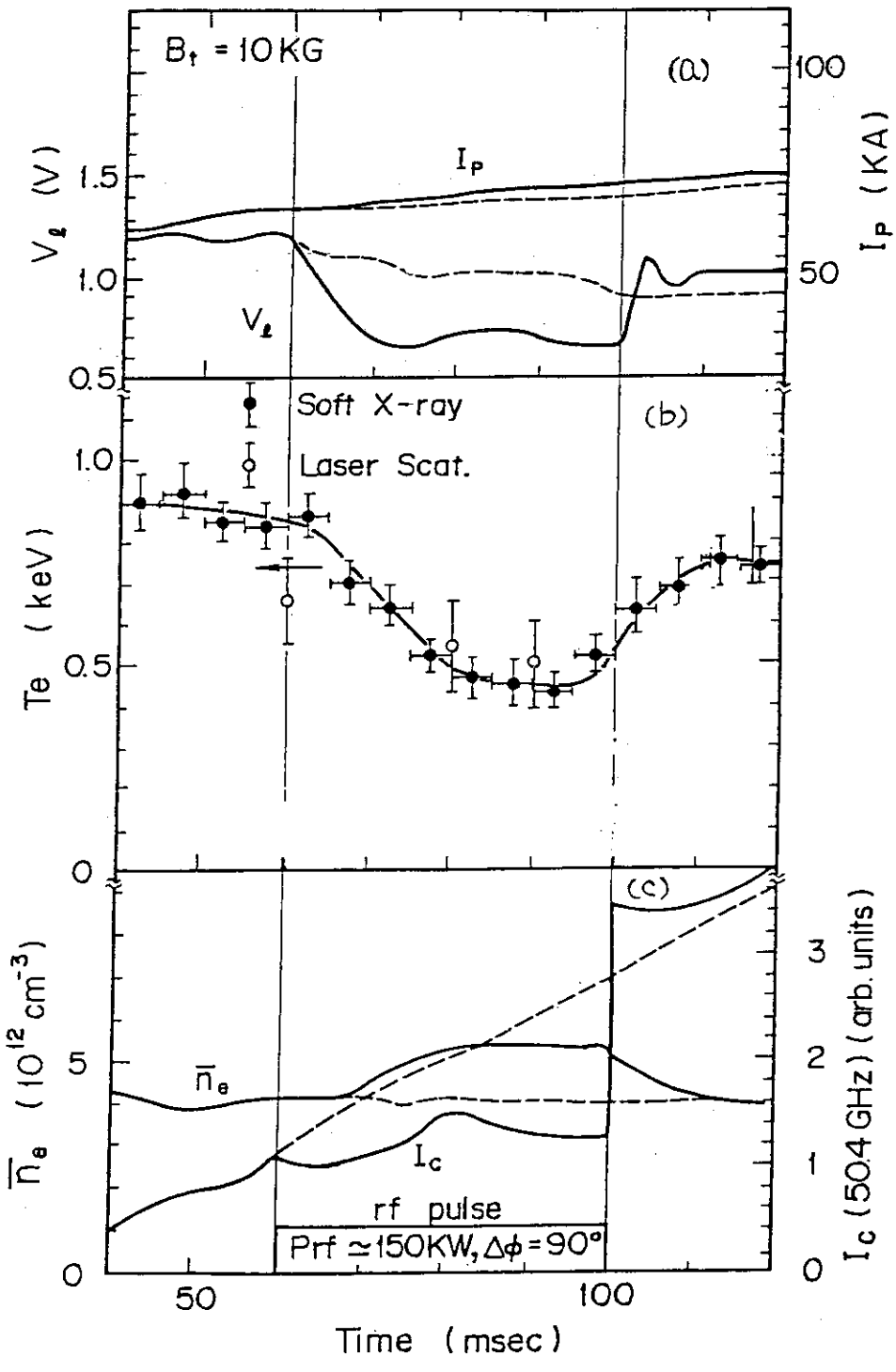

Fig.II.2-14. The time evolution of plasma current I_p, loop voltage V_l, central electron temperature $T_e(0)$, mean electron density $\bar{n}_e$ and second harmonic cyclotron radiation I_c. The solid dotted lines are with and without the rf pulse, respectively.

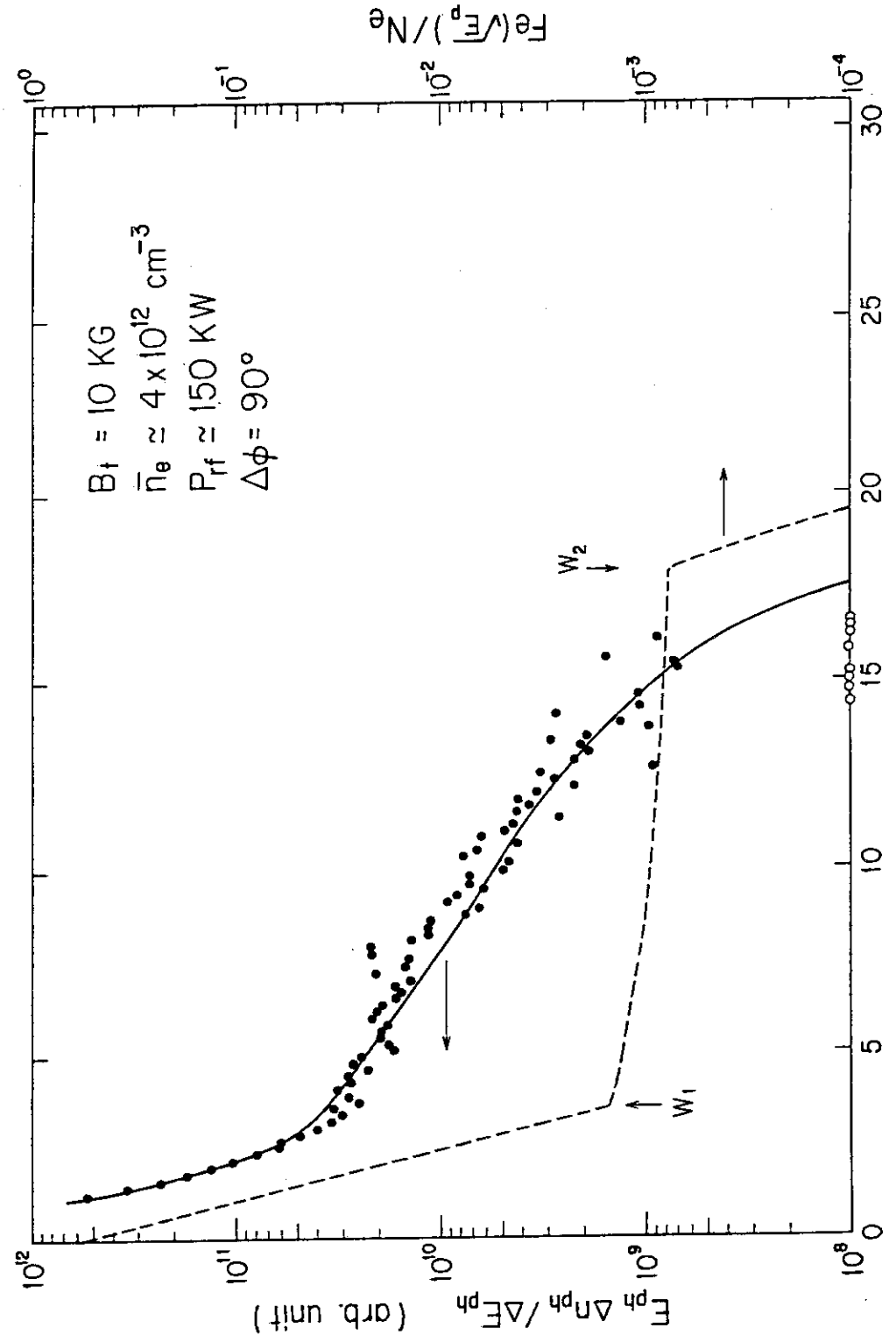

Fig.II.2-15 The soft X-ray energy spectrum and the electron distribution function during the rf pulse. The solid circles and the solid line are the measured and calculated values, respectively. The dotted line is the estimated distribution function.

2.3 Electron cyclotron resonance heating (US-Japan Cooperation Program)

Electron cyclotron resonance heating (ECH) experiment has been successfully carried out in the JFT-2 tokamak. The newly developed gyrotron (200 kW, 28 GHz) has been operated well throughout the experiment and fruitful experimental results have been obtained.

This experiment is characterized by mainly two features. First, three types of modes have been excited, namely, ordinary mode, extraordinary mode and circular TE_{02} mode. Relatively pure modes (ordinary or extraordinary) can be launched at well-defined launching angles. Second, the net rf input power is as large as the joule heat power. The net input power of up to 110 kW has been applied to the JFT-2 plasma successfully and an effective electron heating has been obtained by both ordinary mode excitation and extraordinary mode excitation. The center electron temperature of 1.26 keV ($\Delta T_e(0) = 620$ eV) has been attained with high efficiency of 7 eV/kW at averaged density of $\overline{n_e} = 7 \times 10^{13}$ cm^{-3}.

2.3.1 Characteristics of the system[1)]

A pulse gyrotron oscillator (VGA-8050) developed by Varian has been used as the rf source. The gyrotron generates the rf output almost entirely polarized in the circular electric TE_{02} mode. The generated high power rf wave is fed to the JFT-2 tokamak by three types of launch systems:

(i) ordinary mode ($E \parallel B$) lanch system (conical horn antennas located at the low field side of the torus)

(ii) extraordinary mode ($E \perp B$) launch system (slotted array antenna located at the high field side of the torus)

(iii) TE_{02} mode launch system (open-ended circular waveguide at the top of the vacuum chamber)

For the O- and X-mode heating TE_{02} mode is converted to TE_{10} mode by a mode converter. TE_{10} mode is distributed to eight WR-42 rectangular waveguides each of which carries the rf power up to 25 kW. The loss in the mode convertor is measured to be 20 %.

Block diagram of the O-mode launch system is shown in Fig.II.2-16(a). TE_{10} rectangular mode is transformed to TE_{11} circular mode and which is supplied to eight conical horn antennas (4×2). The antennas locate in the equatorial plane of the torus at the low field side. The horns radiate with a horizontal electric field polarization in alternating pairs at +10° or -10° to the perpendicular of the magnetic field. The wave propagates nearly perpendicularly to the magnetic field ($n_{//} = \pm 0.17$). The horn gain is 21 dB and the width of emitting rf wave, $\theta_{3dB} \approx 8°$.

Block diagram of the X-mode launch system is shown in Fig.II.2-16(b). Each of the rectangular waveguides is connected to a rotary phase shifter mounted at the tokamak vacuum flange, followed by a run along the bottom inside wall of the torus. To avoid cyclotron breakdown, a BeO window is located inside of the resonance layer. The slotted array antenna locates on the inside wall at the midplane of the torus to avoid the evanescent region in the low field side of the plasma column. The fundamental X-mode is evanescent between the upper hybrid resonance layer and right-hand cut-off layer. The wave vector is steerable in the horizontal plane over a range of ±45° from normal incidence with respect to the toroidal field. The radiation is right hand elliptically polarized such as to obtain full coupling to the X-mode in a broad range of launch angles around 40° with respect to normal incidence. At normal incidence, 75 % of the power goes into the extraordinary mode while 25 % goes to the ordinary mode. At an angle of 40° in the opposite direction, 75 % of the power goes to the ordinary mode while 25 % goes to the extraordinary mode.

Two receiving horns on the outside midplane opposite the antenna were used to adjust the phases initially and to measure the beam width, which was ±8° at half power at normal incidence.

Block diagram of the TE_{02} mode launch system is shown in Fig.II.2-16(c). The TE_{02} output of the gyrotron is transferred directly to the plasma with 6.4 cm^{ϕ} flexible circular waveguides.

2.3.2 Electron heating[2,3)]

The parameters of the target plasma in the electron heating experiment is given in Table II.2-1. The filling gas is hydrogen H_2. The (45-110)kW rf pulse has been applied for (14-20)ms typically from t = 60 ms in the discharge which lasts for ~150 ms.

The calculated power absorbed in one pass at the fundamental electron cyclotron resonance layer normalized by the incident power is shown in Fig.II.2-17. P_{ab}/P_{rf} versus the angle between the incident wave vector and the magnetic field vector θ_z is plotted. Central electron temperature is taken as a parameter. P_{ab}/P_{rf} for the X-wave is expressed as the solid curve and for the O-wave expressed as the broken curve. P_{ab}/P_{rf} for both modes increases as the electron temperature increases. It is found that in the experimental condition $T_e(0)$ = (500-700)eV the extraordinary wave launched from the higher magnetic field side at $\theta_z \approx 40°$ is almost completely absorbed in the interior of the plasma in one traverse of the resonance layer. In the case of perpendicular propagation ($\theta_z \sim 90°$) damping of the X-mode is weak. The O-wave launched at $\theta_z = 80°$ from the low field side is damped by 25 % in one pass. The transmitted wave is reflected at the inner wall of the vacuum chamber back into the plasma and again passes the resonance layer. Taking account of the multi-reflection at the wall most of the power irradiated into the vacuum chamber is absorbed in the plasma

along the resonance layer. Diffusion of the wave by the multi-reflection and depolarization leads to the peripheral heating and reduces the heating efficiency. The spacial profile of the calculated damping coefficient along the resonance layer is shown in Fig.II.2-18. The X-wave with smaller parallel refractive index heats the peripheral plasma.

The examined rf-power dependences of $T_e(0)$ and $-\Delta V_l$ are shown in Fig.II.2-19 for $\overline{n_e} = 7 \times 10^{12}$ cm^{-3}. The increase of the electron temperature and loop voltage drop are almost linear with the rf power. We obtained high heating rate as 4.7 eV/kW for the O-mode and 7 eV/kW for the X-mode at $\overline{n_e} = 7 \times 10^{12}$ cm^{-3}.

Estimation of the heating efficiency can be made from the following relation: $\frac{P_{rf} + P_{\Omega,rf}}{P_\Omega} \frac{< n_e T_e > \tau_\Omega}{< n_e T_e > \tau_{rf}}$, where P_Ω is the initial joule power, $P_{\Omega,rf}$ is the ohmic power 10 ms after the rf is turned on, $< n_e T_e >$ is the volume averaged energy and τ is the confinement time. Taking $\tau \propto \overline{n_e}$ and assuming the electron temperature and density profiles with and without rf heating are the same, $P_{rf} \approx 90$ kW or the heating efficiency is 82 %.

Electron temperature profile and density profile during the rf pulse are given in Fig.II.2-19. Profiles just before applying rf power and 10 ms after were made for $\overline{n_e} = 1.0 \times 10^{13}$ cm^{-3}, at which density there is more scattered laser light but less than optimum heating. The temperature profile is changed from parabolic squared with a central temperature of 650 eV to parabolic with a center temperature of 790 eV. The rf power drops the central density by 40 % but broadens the profile from parabolic squared to parabolic to the three halves. Using the measured profiles, the efficiency of rf heating is still about 76 %, even at this density where the central heating is not large.

Power dependence of the density drop $-\Delta\overline{n_e}$ is also shown in Fig.II.2-20. $-\Delta\overline{n_e}$ is constant above $P_{rf} \gtrsim 45$ kW. Density drop is large as the density

becomes large. The line averaged and central density are both observed to drop. The edge density from a Langmuir probe was about 4 % of the central density and was unaffected by the rf power but the edge temperature increased from 10 to 16 eV. The recycling of the hydrogen may be reduced. Also the cross section for the ionization of neutral gas is a very strong function of temperature in this regime, so, stronger ionization in the limiter region may be impeding the flow of neutrals into the interior. An increase of 30 % in H_α radiation is observed during the rf pulse, indicating an affect of the rf power on the state of neutral hydrogen in the cold edge region.

Density dependence of the central electron temperature is given in Fig.II.2-21. Above the cutoff density of the wave at the fundamental electron cyclotron resonance layer, the increase of the central temperature decreases and at the density 1.5 times the cutoff density, no increase of the center electron temperature is observed. As the plasma density increases beyond the cutoff density, there grows the evanescent region at the center of the plasma column which causes the deposition of the wave power at the periphery of the plasma column and reduces the heating of the plasma core region.

Toroidal magnetic field dependence of $T_e(0)$, $-\Delta V_1$, $-\Delta\overline{n_e}$ is shown in Fig.II.2-22. The central toroidal field $B_t(0)$ in JFT-2 was varied keeping $I_p = 70$ kA and $\overline{n_e} = 7 \times 10^{12}$ cm^{-3}. For the O-mode heating, observed central temperature is maximum for 10 kG for which the cyclotron resonance is at the center of the discharge. Decreasing B_t causes the loop voltage drop and central temperature rise to decrease only slightly as B_t is reduced by 17 %. Increasing B_t moves the resonance outwards. The loop voltage drop decreases with increasing B_t but much more strongly than by decreasing B_t. The central heating also becomes negligible for $\Delta B_t/B_t = 17$ %. For 12 kG at

which the resonance is 18 cm out on the midplane, the loop voltage drop virtually disappears. The density drop has a similar dependence on B_t. For the X-mode heating $\Delta T_e(0)$ and $-\Delta V_1$ is larger when the fundamental cyclotron resonance layer is at -9 cm from the center of the plasma column. Thus there is an asymmetry of $\Delta T_e(0)$ when the resonance layer moves in the plasma column both for the O-mode heating and X-mode heating. If the cyclotron resonance is moved well off center, the damping of the O-mode should become negligible at the lower T_e and the damping of any power reflected off the inner wall in the X-mode may also be weak. This would allow power reflected in the X-mode to reach the upper hybrid resonance layer in the outside of the discharge. Linear mode conversion to electron Bernstein waves may result. This electrostatic wave propagates for $\omega > \omega_c$ and can be strongly damped. For $B_t(0) < 10$ kG, the electron Bernstein wave can propagate into the hot center and heat the center, producing the central temperature rise and voltage drop observed. For $B_t(0) > 10$ kG, the cyclotron resonance blocks the Bernstein wave from reaching the center and heating is reduced.

2.3.3 Conclusion

1) By the launch of relatively pure mode, the center electron temperature of 1.26 keV ($\Delta T_e(0) = 620$ eV) has been atained by the ECH experiment in the JFT-2 tokamak with high heating rate as large as 7 eV/kW without bad effect to the plasma. Launching the pure mode is shown to be an effective way of electron cyclotron heating.
2) The ECH system (200 kW, 28 GHz) has been constructed and operated successfully and the net rf power which is larger than the joule power as large as 110 kW has been able to launch into the plasma.
3) The heating is linear in rf power and the density limit on the

heating is no worse than theory predicts.

4) Substantial heating is observed when the fundamental electron cyclotron resonance is moved inside of the plasma column.

5) The multi-reflection of the wave at the metallic chamber wall increases the wave absorption at the resonance layer.

6) The use of ECH in the pre-ionization method is proved to be effective. The breakdown voltage drops to the half of that without rf by applying 50 kW, 5 ms rf pulse. The effect of ECH pre-ionization in JFT-2 is described in Chapter III.

REFERENCES

1) Yamamoto, T., Funahashi, A., Fujisawa, N., Iizuka, S., Kawakami, Y., Kumagai, K., Maeno, M., Moeller, C., LaHaye, R., Ro, M., Shoji, T., Suzuki, N., Takeuchi, H., Tanaka, Y., Toyama, H. and Yamauchi, T.: in Proceedings of US-Japan Workshop on Physics of High Power RF Heating, Kyoto, Japan (1980).

2) LaHaye, R.J., Moeller, C.P., Funahashi, A., Yamamoto, T., Hoshino, K., Suzuki, N., Wolfe, S.M., Efthimion, P.C., Toyama, H. and Roh, T.: Proceedings of the 4-th Topical Conference on Radio Frequency Plasma Heating, Texas (1981) D4-1.

3) Moeller, C.P.: ibid. D1-1.

Table II.2-1. Parameters of target JFT-2 plasma in the ECH experiment.

Filling gas :	H_2
Major radius :	R=90 cm
Minor radius(limiter radius) :	a=25 cm
Line averaged density :	$\bar{n}_e=(5 - 15)\times10^{12}cm^{-3}$
Toroidal field :	$B_t(0)=(6 - 12)$ kG
Plasma current :	$I_p=(70-75)$ kA
Loop voltage :	$V_l=(1.0-1.6)$ V
Electron temperature :	$T_e(0)=(450-700)$ eV
Ion temperature :	$T_i(0)=(200-250)$ eV
Effective charge :	$Z_{eff}\approx2$
Electron energy confinement time :	$\tau_{Ee}=(3-9)$ ms

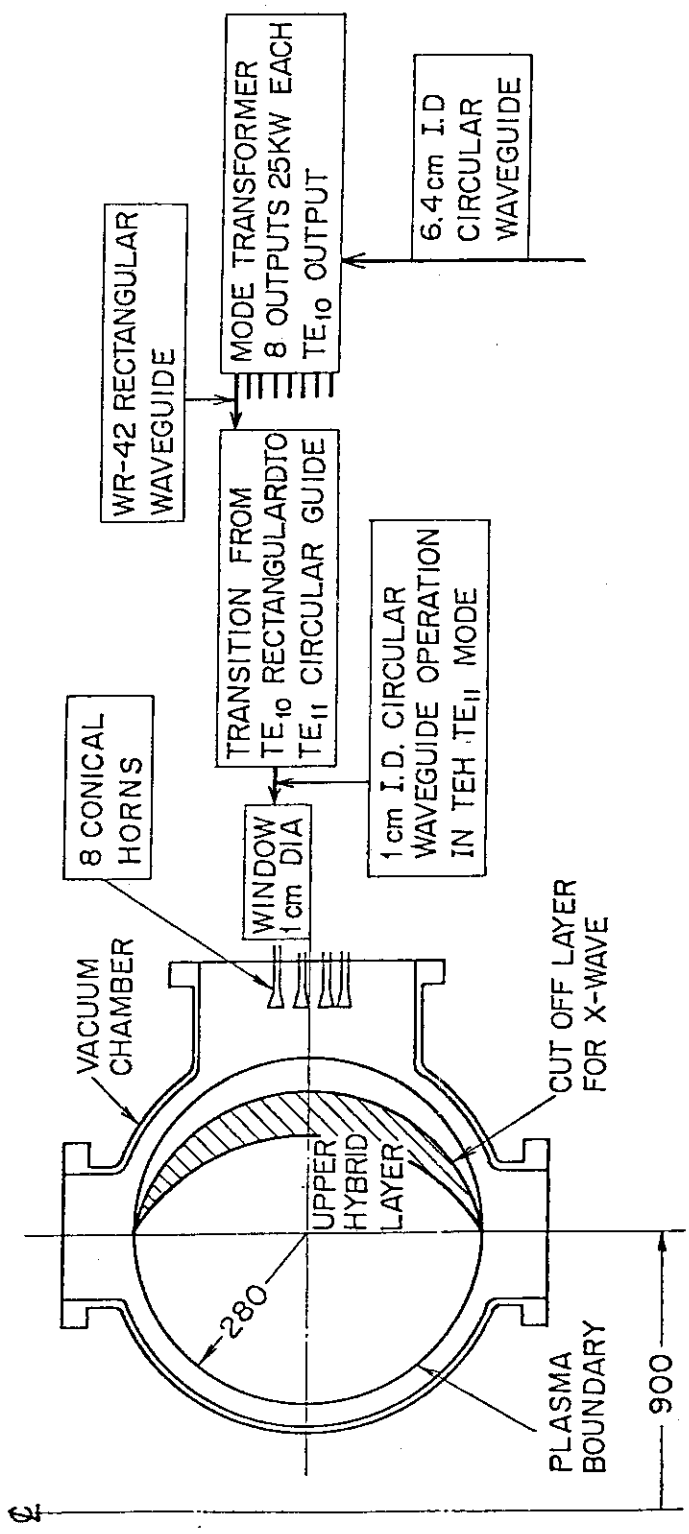

Fig.II.2-16(a) Block diagram of the O-mode launch system.

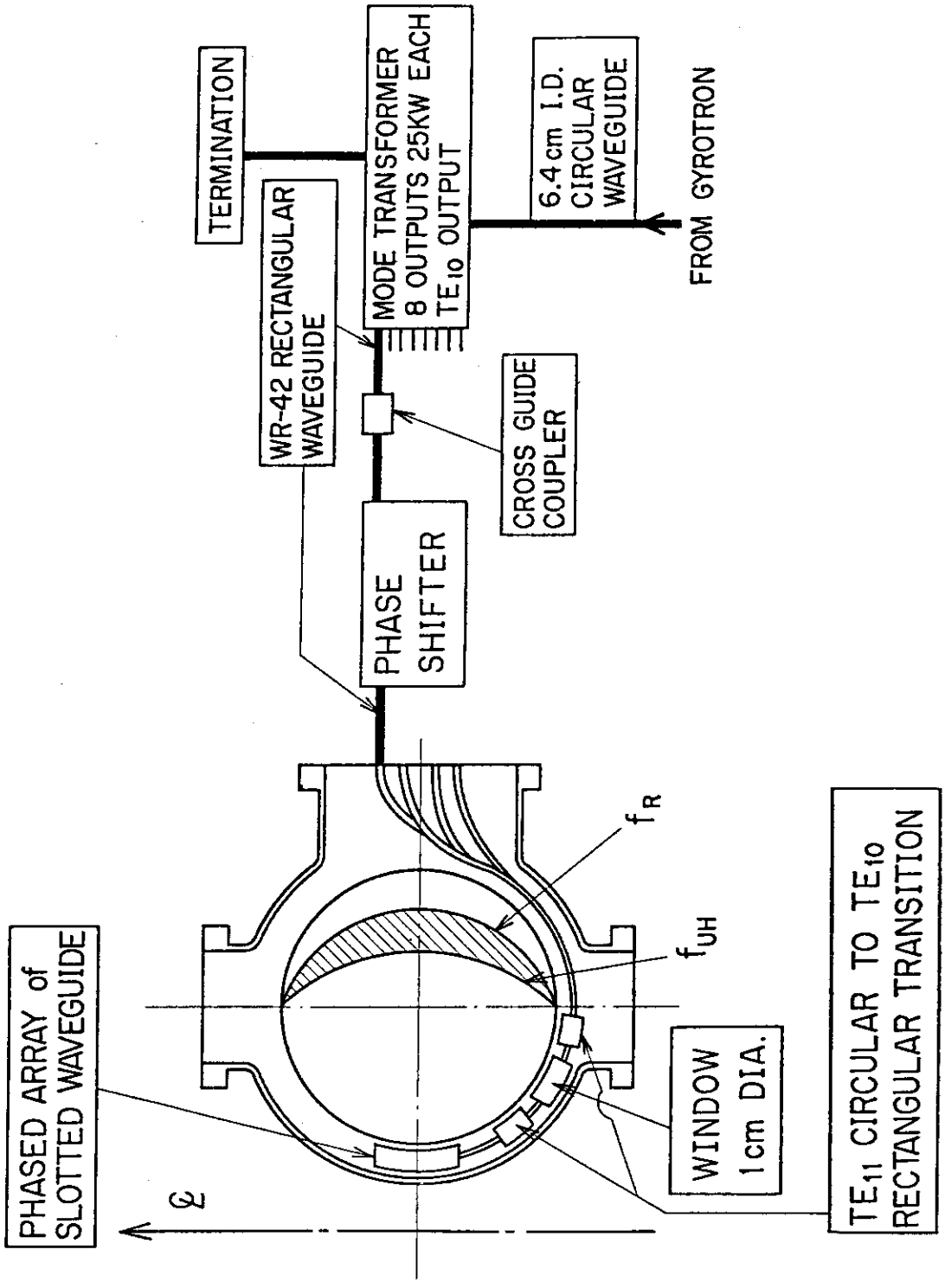

Fig.II.2-16(b) Block diagram of the X-mode launch system.

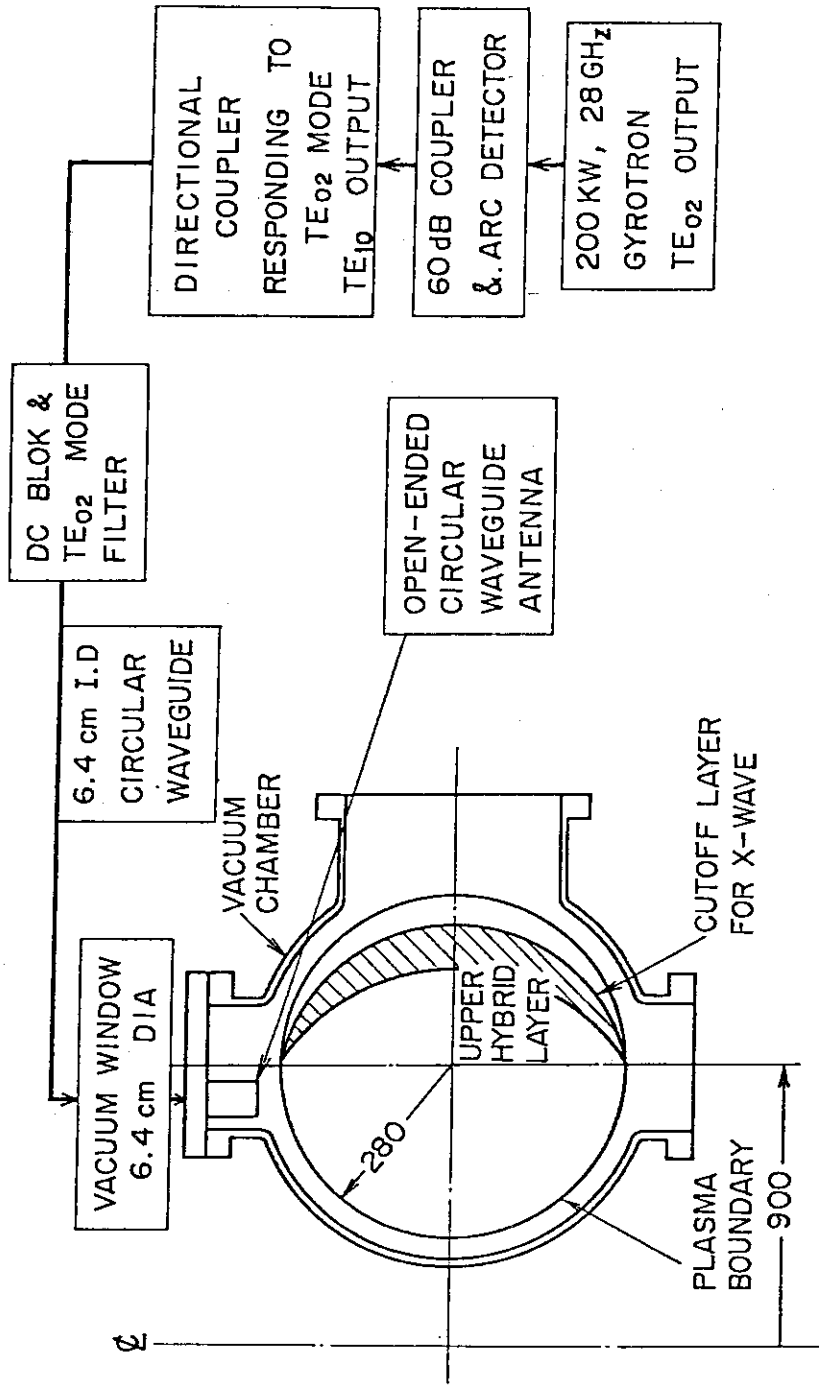

Fig.II.2-16(c) Block diagram of the TE_{02} mode launch system.

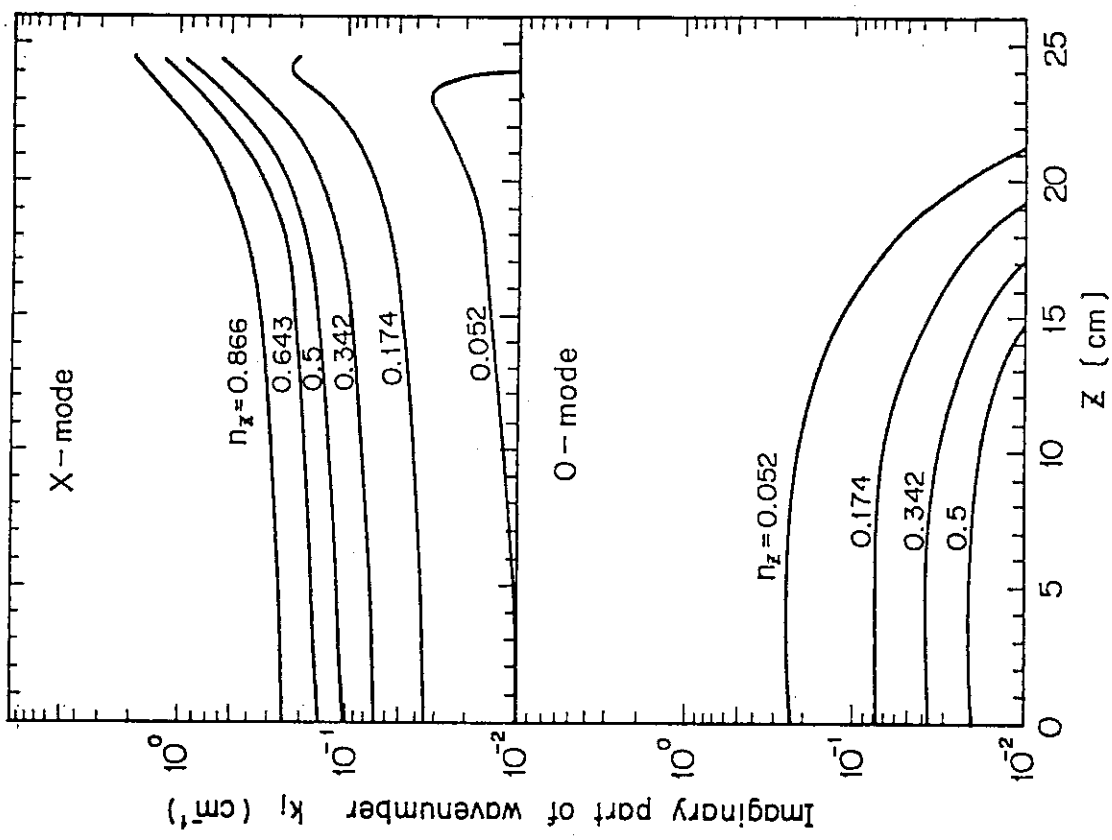

Fig.II.2-18 Spacial profile of the calculated damping coefficient along the resonance layer.

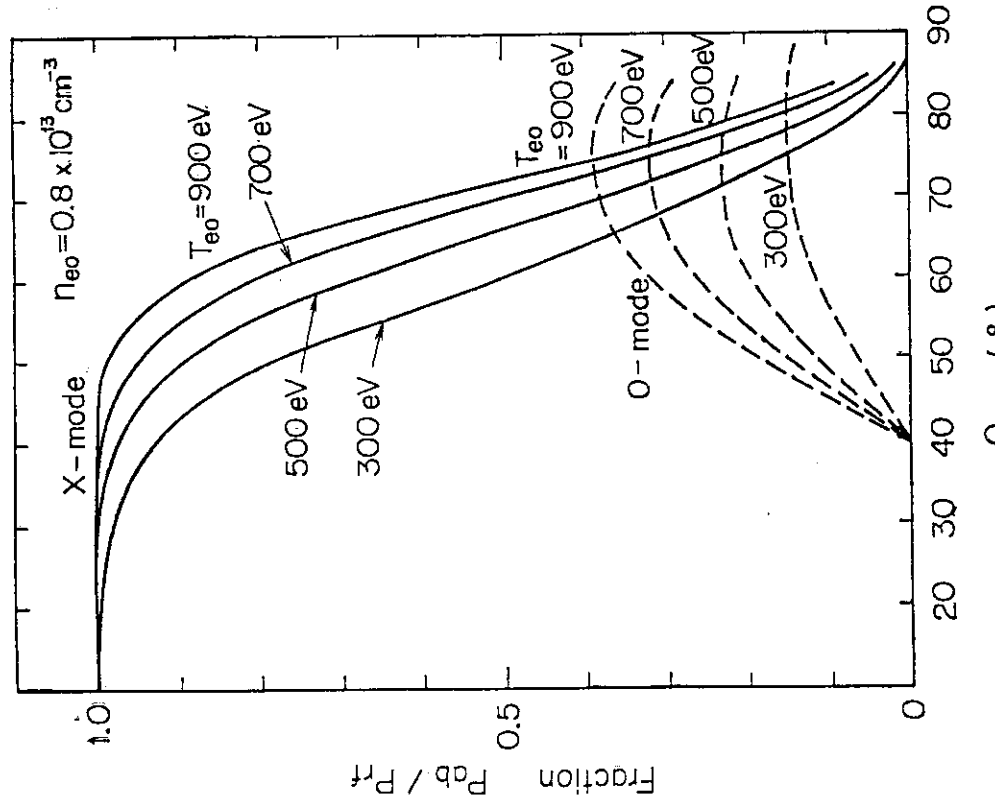

Fig.II.2-17 Calculated power absorbed in one pass at the fundamental electron cyclotron resonance layer.

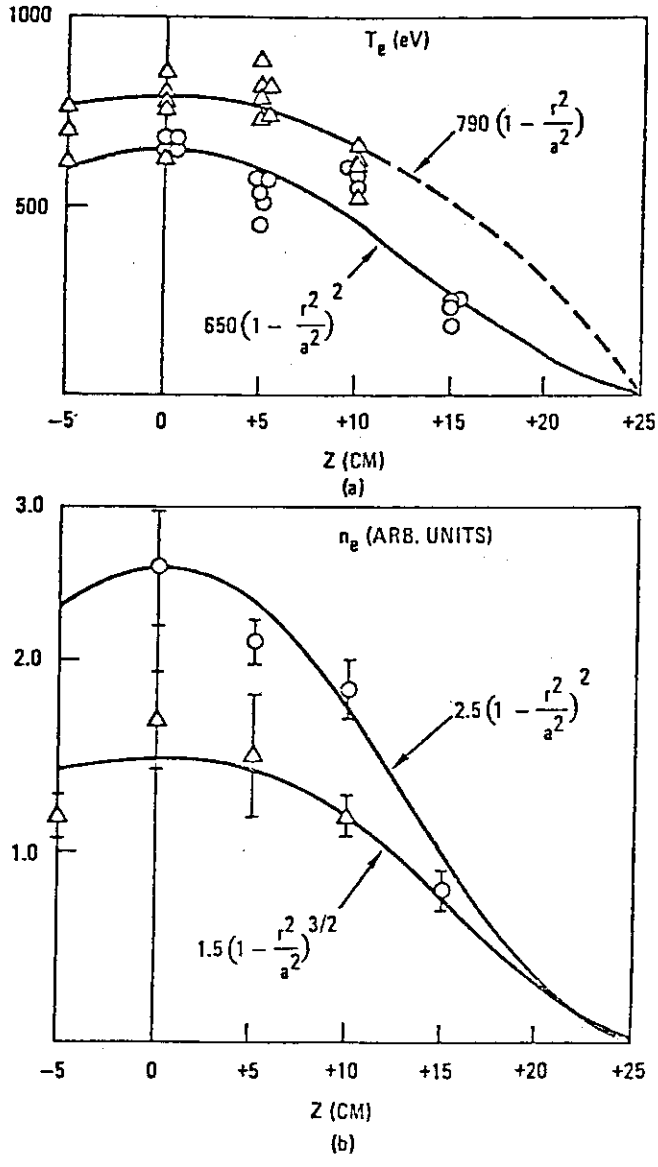

Fig.II.2-19 Electron temperature (a) and density profiles (b) just before and during the rf pulse.

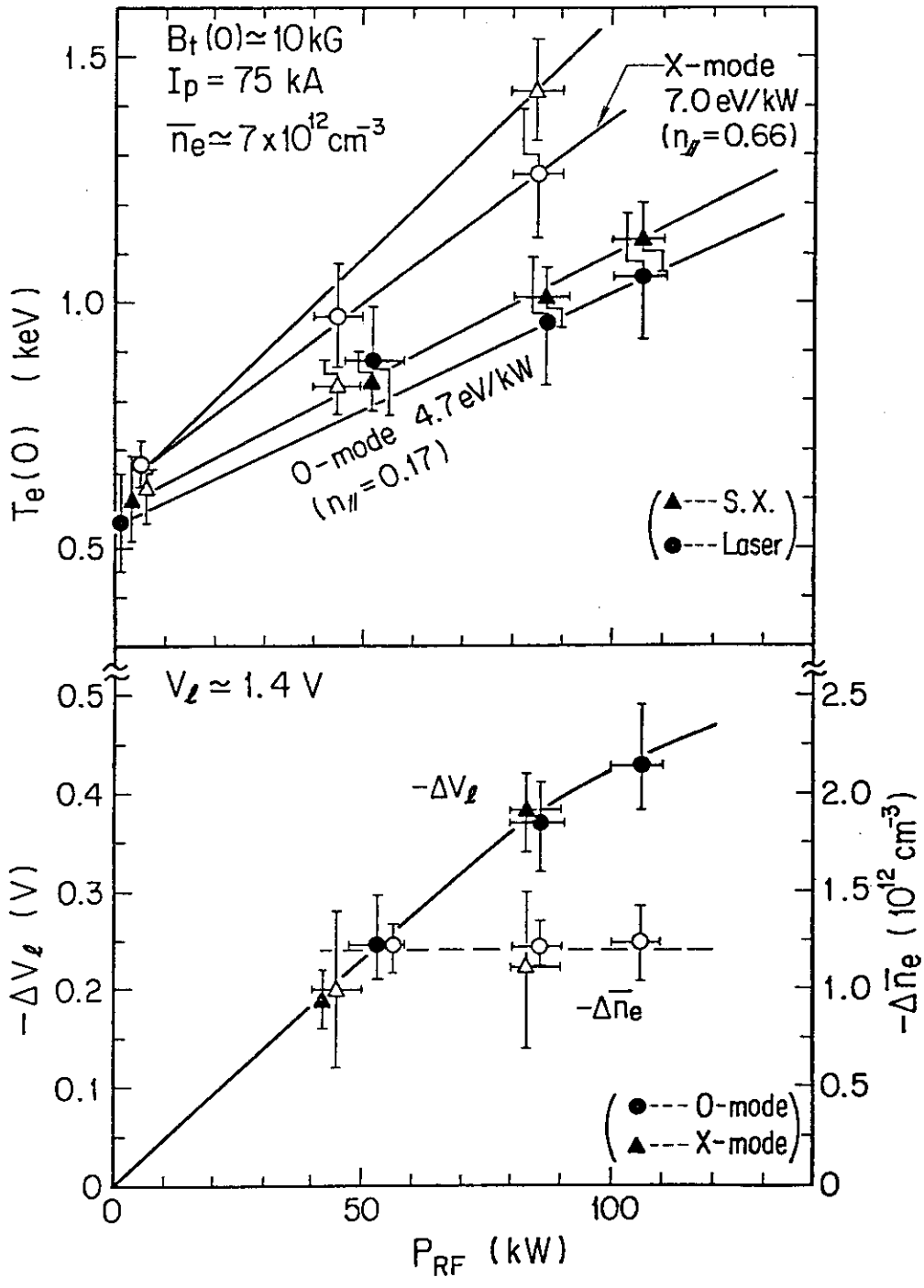

Fig.II-2-20 Power dependence of $T_e(0)$, $-\Delta V_1$, $-\Delta \overline{n_e}$.

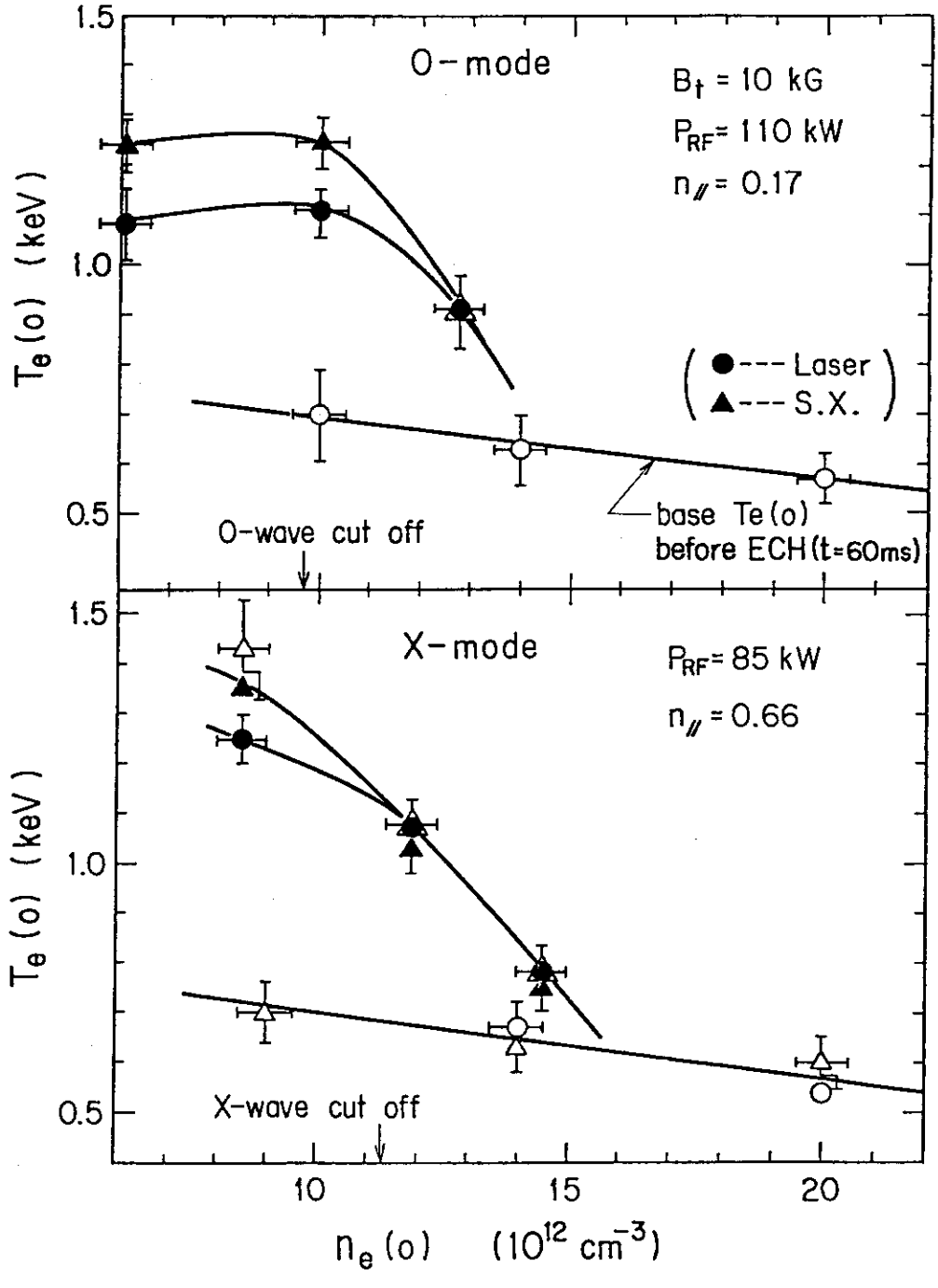

Fig.II.2-21 Density dependence of the central electron temperature.

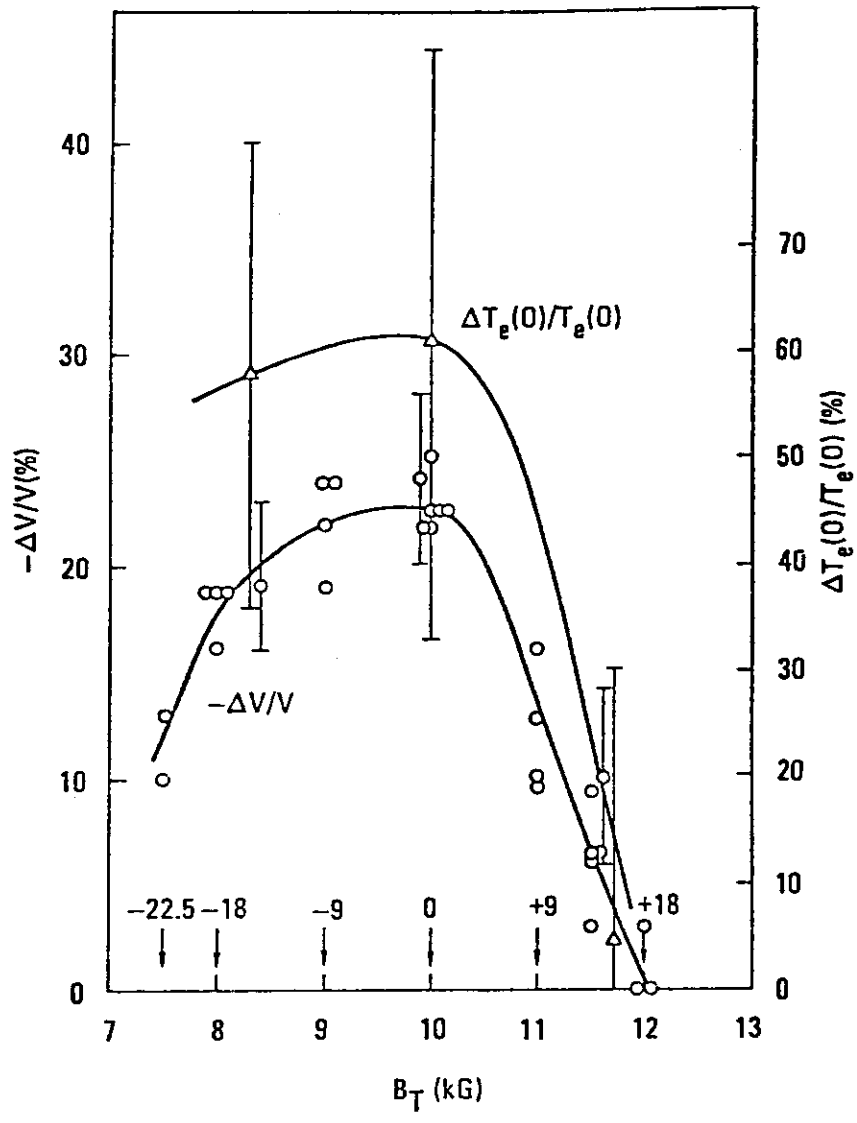

Fig.II.2-22 Toroidal magnetic field dependence of $T_e(0)$, $-\Delta V_l$, $-\Delta\overline{n_e}$ for the O-mode heating.

2.4 Ion Cyclotron Range of Frequency (ICRF) heating

ICRF heating has been recognized to be one of the most promising heating method of a tokamak plasma in competition with NBI and LH heating, for its high heating efficiency, relatively low cost and applicability to a reactor.

In JAERI, ICRF heating experiment was started since 1978 using JFT-2a (JAERI Fusion Torus-2a/DIVA) device. Following results were obtained in the DIVA experiment in 1978-1979: (i) Optimum conditions of the ion heating were surveyed in detail by varying the toridal magnetic field and the proton-to-deuteron density ratio[1]. The results were well explained by the mode conversion theory[2]. (ii) The full Faraday shield increased the heating efficiency from 3.8×10^{13} eV·cm^{-3}/kW to 8.2×10^{13} eV·cm^{-3}/kW. The gross power balance including the boundary plasma was established[3][4]. (iii) Impurity contamination during the heating was suppressed by the divertor and the T_i - gettering.

In 1980, the output of the generator which was used in the DIVA experiment has been increased from 200 kW to 1 MW. The heating experiment is restarted from March in 1981 in JFT-2. The main objectives of the experiment in JFT-2 are threefold.

(1) Investigation of the heating mechanism. In a deuteron plasma with a minority proton component, fundamental (second harmonic) cyclotron resonance layer of proton (deuteron), two-ion hybrid cut-off layer and two-ion hybrid resonance layer are formed in order from the low field side along the toroidal axis. Therefore, it is supposed that the damping mechanism of the fast wave is different whether the wave excitation is from the low field side (outside) or from the high field side (inside). In the DIVA experiment, however, the antenna was located only outside of the

torus. In the JFT-2 experiment the antenna will be located both inside and outside of the torus. The difference of the heating properties of both excitations will be examined experimentally. The result will make the heating mechanism of the ICRF heating much clearer than the recent ones of PLT[5], TFR[6] and DIVA[4].

(2) Scaling of an antenna. In order to apply the ICRF heating to a large tokamak, problems of the heat load and electromagnetic force to the antenna must be solved. For these reasons, it is important to design an antenna as compact as possible. If we know the antenna loading impedance, the most suitable design can be done about the shape, structure and insulation length of an antenna. In JFT-2 experiment, the parameter dependence of the antenna loading impedance will be examined.

In DIVA experiment, a ceramic insulator was used in the antenna. In JFT-2 experiment, we adopt an all metal antenna having no ceramic insulator except in the power feed-through. Moreover, with the assumtion that the heating is not dependent on the poloidal mode number of an antenna, we use a 1/4-turn antenna, combining two units in one poloidal cross-section as a half-turn antenna or in neighbouring two ports in the toroidal direction. Figure II.2-23 shows the antenna which will be used in JFT-2.

(3) 3 MW high power density experiment. In JFT-2, 2 MW high-β experiment has been possible with NBI only. We will explore β-limit of a circular plasma with 2 MW NBI and 1 MW ICRF.

On the basis of the results of 1 MW ICRF heating experiment in JFT-2, 4 MW heating experiment is planned in JFT-2M. The ion temperature will be increased up to multi-keV and the scaling of ICRF to a reactor will be established as well as the study of current drive and coupling with a plasma by a waveguide.

REFERENCES

[1] KIMURA, H., ODAJIMA, K., SENGOKU, S., OHASA, K., SUGIE, T., et al., Nucl. Fusion 19 (1979) 1499.

[2] IIZUKA, S., ODAJIMA, K., KIMURA, H., SENGOKU, S., MATSUMOTO, H., et al., Phys. Rev. Lett. 45 (1980) 1256.

[3] ODAJIMA, K., KIMURA, H., IIZUKA, S., SUGIE, T., TAKAHASHI, K., et al., Nucl. Fusion 20 (1980) 1330.

[4] KIMURA, H., ODAJIMA, K., IIZUKA, S., SENGOKU, S., SUGIE, T., et al., in 8th Int. Conf. on Plasma Physics and Controlled Nuclear Fusion Research (Brussels, Belgium, 1980) IAEA-CN-38/D-5-2.

[5] HOSEA, J., BOYD, D., BRETZ, N., CHRIEN, R., COHEN, S., et al., ibid., IAEA-CN-38/D-5-1.

[6] TFR-GROUP., ibid., IAEA-CN-38/D-3.

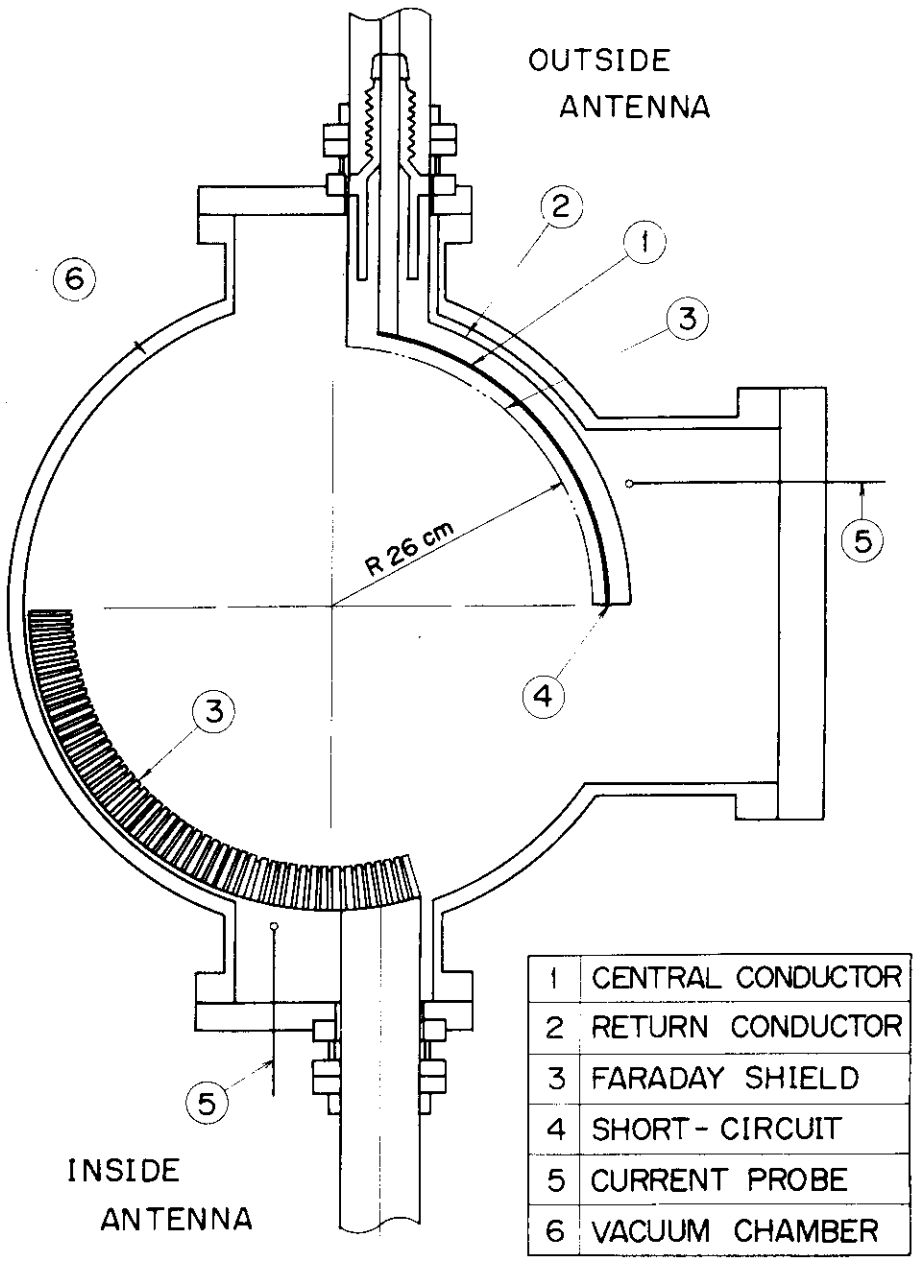

Fig.II.2-23 All-metal 1/4-turn antenna in JFT-2 ICRF experiment.

3. JFT-2M

3.1 Program

The main purpose of JFT-2M is research on the improved high-performance plasma in a tokamak reactor. The following issues are included. 1) Ion cyclotron range of frequency heating - the following research and development are studied; a) quantitative understanding of heating mechanism and optimization of heating condition in a reactor-like plasma, b) optimization of launching stracture to get a high-coupling efficiency and high-power feeding (4 MW). 2) High beta and noncircular plasma - it is very important to know the critical value of beta by optimizing the heating condition and plasma cross-section. 3) Steady state current drive - preliminary results in JFT-2 show that a plasma current is driven by the exitation of lower-hibrid wave. This result should be extended in more powerful MW level experiments on higher density plasmas. 4) Impurity control and ash exhaust - the divertor should be tested in a reactor-like plasma with the more simple configuration. 5) Control of plasma with simple and highly reliable technic - the accessibility to the low-q discharge should be established in the larger machine in order to suppress the plasma disruption and to obtain the high-beta plasma. The hibrid control of poloidal-coil system is also necessary technic in the future reactor.

JFT-2M is a flexible and easily modified facility in mid 1980s for studies relevant to the improved advance concepts of the tokamak reactors.

The design study of JFT-2M has been carried out for three years from 1978 to 1980 with assuming that both hard and soft wares established in JFT-2 and JFT-2a/DIVA are transferred to JFT-2M. The construction of the JFT-2M tokamak machine will be started in 1981, and after its completion preliminary experiments for operation of plasma current of 300 kA with

additional heatings of 2 MW/NBI, 1 MW/ICRF, and 600 kW/LHRF are planned to start in later of 1982. Then the power-up of the poloidal-coil power supply (noncircular plasma with current of 500 kA), the power-up of ICRF heating up to 4 MW, the increasing of frequency of LHRF heating (1.5 GHz), and the supplement of diagonostics will be all completed early in 1983.

3.2 Design of JFT-2M

The cross-sectional view of the main part of JFT-2M is shown in Fig.II.3-1. Its parameters are a plasma major radius 1.3 m, minor radius 0.35×0.5 m with D-shaped cross-section, maximum plasma current 500 kA, toroidal field 15 kG (capable of 40 kG with the upgraded power supply), and flux swing 2 V·sec with an iron core.

There are 16 D-shaped toroidal field coils of copper conductor surrounding the vacuum vessel. The D-shaped toroidal coil consists of a straight section and two circular sections, and the maximum tensile stress of the copper is about 11.6 kg/mm^2 in the 40 kG case.

3.2.1 Vacuum vessel

The top view of the vacuum vessel is shown in Fig.II.3-2.

The vacuum vessel, which is made of 25 mm thickness SUS-304L stainless-steel, consists of two long sections and two short connecting sections. These sections are bolted togather through flanges. The two short connecting sections are assembled after the Q_2 poloidal coils are settled between the vacuum vessel and the toroidal coils. The vessel can be heated up to 120 °C for baking. Two teflon insulating breaks are inserted between the long and the connecting sections. Each break is electrically connected with 5 mΩ resistor in order to absorb a surge voltage generated by a plasma disruption.

On the vessel there are access-ports of various sizes that are used for the maintenance. On the horizontal side of torus there are 480 mm^{ϕ} one port and 400 (in toroidal direction) × 480 (in vertical direction) mm 5 ports, and there are 160 × 415 mm race-track shaped 28 ports on the upper and lower sides of the torus. Total numbers of ports are about 130 including lots of small auxiliary ports.

Two kinds of limiter are prepared. The one is a back-up limiter which is 60 mm apart from the inner surface of the vessel, and which is made of SUS-304L stainless steel. The second is a movable limiter which consists of three parts settled on top, bottom, and outer side of the vessel. The limiter is water-cooled, and the materials of the limiter can be easily changed. On the inner surface of the vessel, there are about 1000 of screw holes that can be used to fix the liner plates, divertor plates, ICRF antenna, and magnetic probes.

3.2.2 Probe system in the vacuum vessel

Since the skin time of the vacuum vessel for poloidal magnetic field is about 7 msec, in order to detect the fast phenomena it is necessary for magnetic detectors to be included inside the vessel. They consists of following magnetic loops,

(1) A set of 24 B_{ρ}-magnetic probes which are poloidally placed along the wall.

(2) Two sets of 24 B_{θ}-magnetic probes

(3) 8 differential B_{θ}-magnetic probes

(4) Two sets of 10 flux loops

(5) A Logowski coil

(6) A diamagnetic loop.

Positions of these probes and loops are shown in Fig.II.3-2, and design

parameters of magnetic loops are presented in Table II.3-1. (1)-(5) are mainly used to determine and control the plasma equilibrium. Flux loops and differential B_θ-magnetic probes are used to measure the poloidal flux distribution directly, and shown in Fig.II.3-3.

It is desirable to determine the plasma position with the accuracy of ~ ±3 mm ($\delta/a \sim 10^{-2}$). It is advantageous to take turn area of magnetic loops (1)-(5) as large as possible in order to protect the signal from circuit noises. On the other hand, protections against electrical break down of insulations by the plasma disruption are easier with small turn area. From these consideration, turn area of ~ 0.5 m^2 is adopted. Probes cases which are made of stainless steel are effective to protect from high voltage generated by the plasma disruption. All of these magnetic loops are shielded electro-statically for noise reduction.

3.2.3 Poloidal coil system

The design of the poloidal coil system is made keeping in mind to simplify coil composition and also to reduce the electrical power supply. The poloidal coil system is composed of five kinds of coil series as shown in Fig.II.3-1, ie S-series is for joule plasma shaping and control, V-series for fast control of additional heating plasma, Q-series for changing the noncircularity with and without magnetic limiter, H for vertical position control and OH only for volt-seconds. As primary winding set (OH) on the top and bottom of the central iron yoke saturates the iron core locally, it is necessary to be wound uniformly along the central iron yoke. A variety of plasma cross section is realized by changing the coil taps and the current ratios between the coil series as shown in Fig.II.3-4. Each turn of the Q2 and OH coils is made of water-cooled rectangular hollow conductor and coiles of S-series are indirectly cooled through the insurating

material. The current density of poloidal coils is about 15-18 A/mm^2.

Table II.3-1 Design parameters of magnetic loops in the vacuum vessel

	Cable diameter (mm)	Turn	Turn area (m^2)
B_θ	0.1	7500	0.5
B_p	0.1	2250	0.5
differential B_θ	0.1	15000	1.0
flux load	~ 0.9	—	—
Logowski coil	0.2	~ 10^4	~ 0.3
dia-magnetic loop	0.9	1	~ 0.7

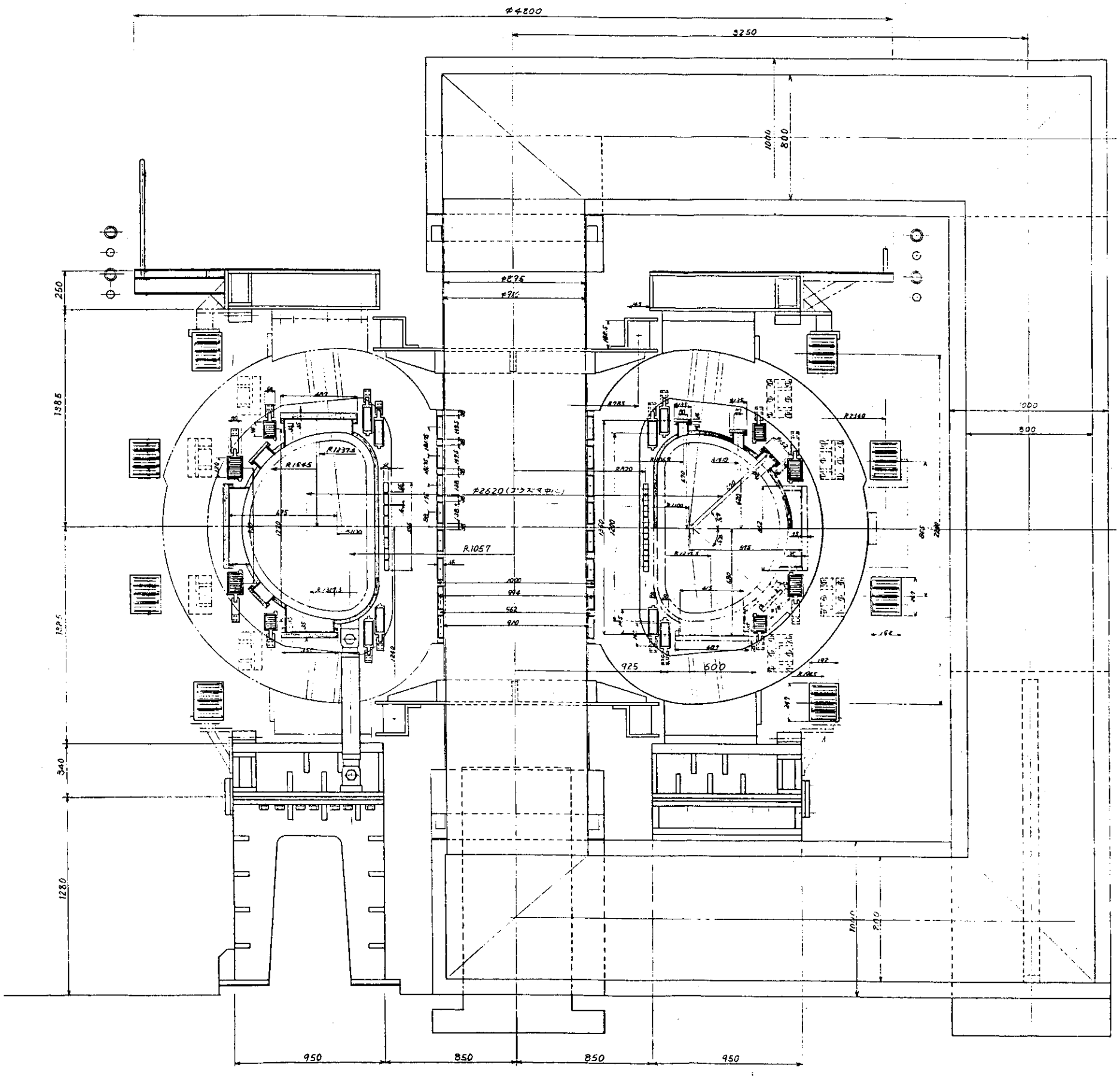

Fig.II.3-1 Cross section of JFT-2M machine

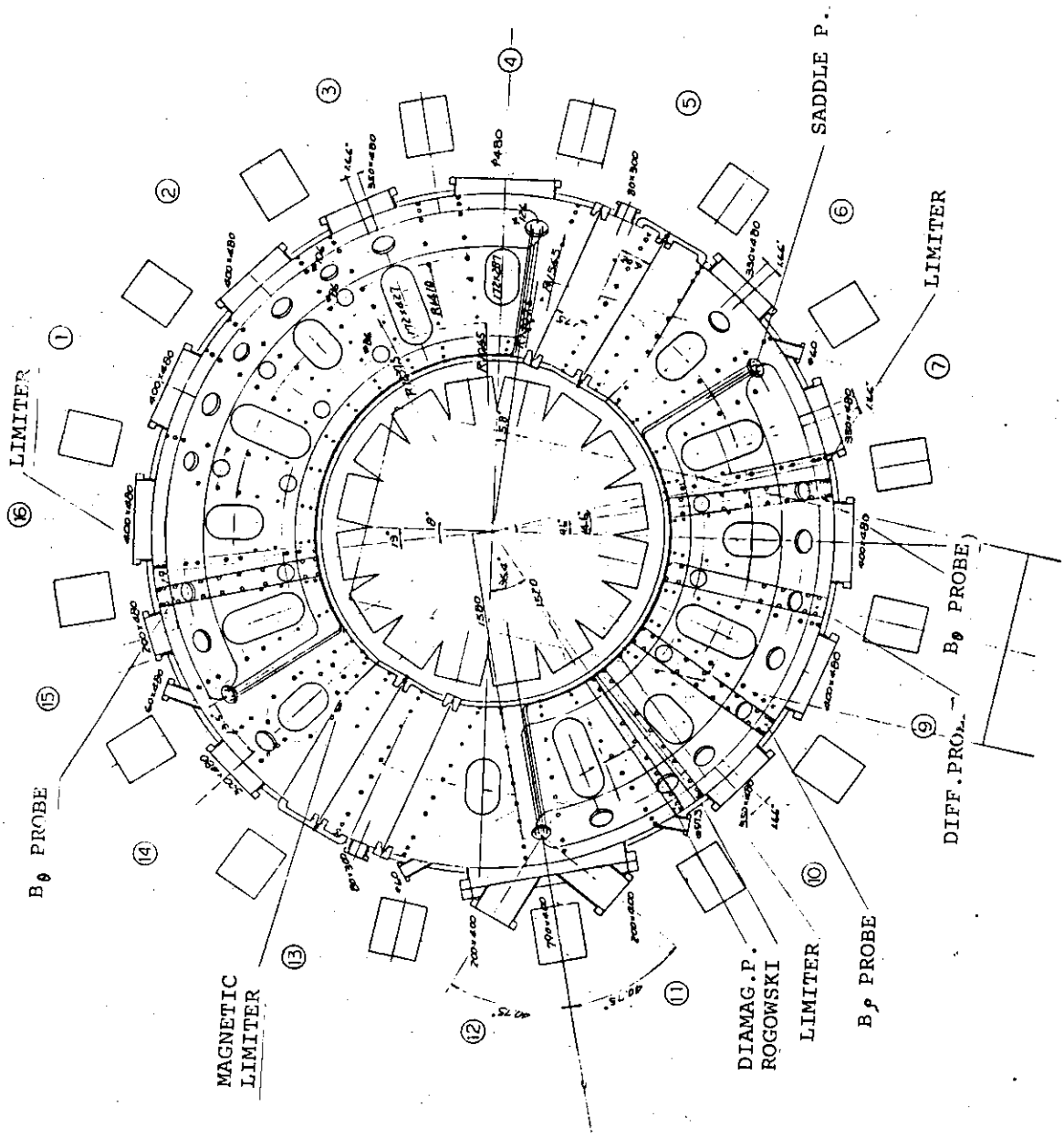

Fig.II.3-2 Vacuum vessel of JFT-2M

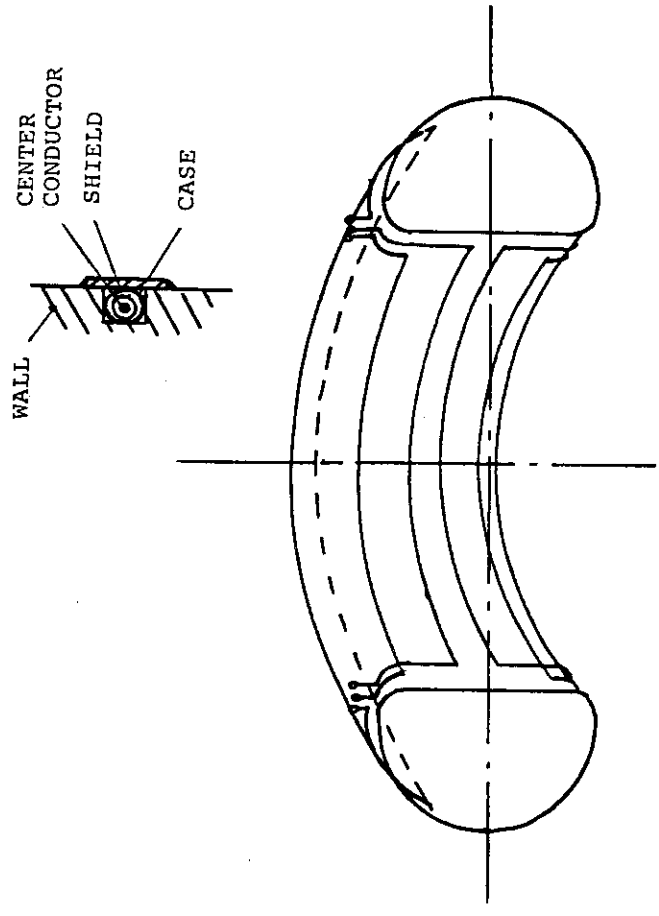

Fig.II.3-3 Configuration of flux loops; Flux loops are set in the grooves on the wall of the vacuum vessel

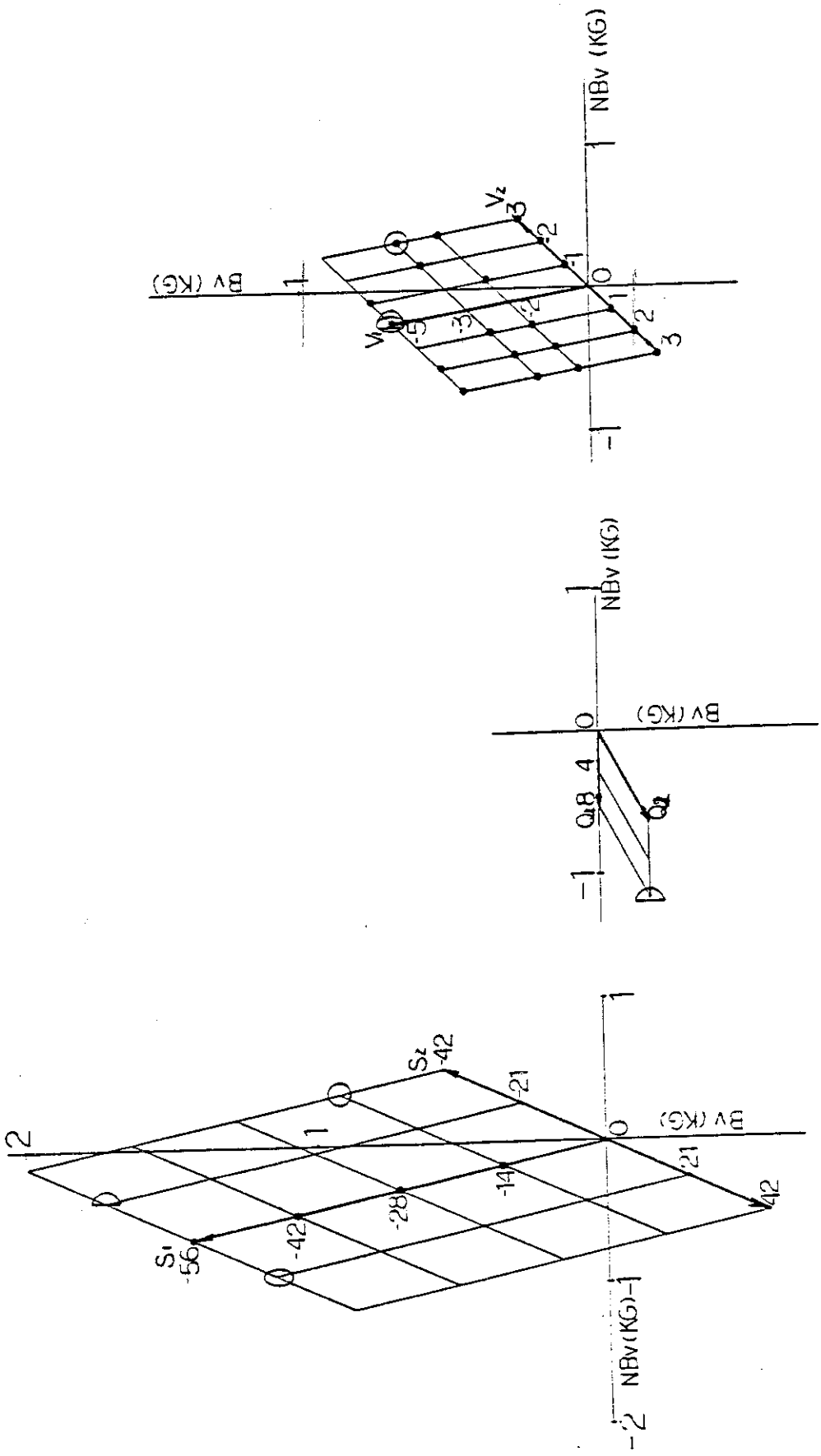

Fig.II.3-4 Control region by tap change of poloidal field coils

III. OPERATION AND MAINTENANCE

1. Introduction

Facility Operation and Engineering section has been engaged in operation and maintenance of JFT-2 Tokamak and NBI system for JFT-2 and a flyweel motor-generator, and development of auxiliary equipments and instruments.

Operation of NBI system for JFT-2 started in April 1980.

2. Operation and Maintenance

The JFT-2 and NBI system for JFT-2 and flyweel motor-generator (M-G) were operated on schdule as shown in Table III-1.

The MW-class neutral beam injection system was installed on JFT-2 in April 1980. Table III-2 shows the specification of the system.

3. Development of Equipment and Instrument

During the period under the review the following developmental works have been performed.

It is very important study to reduce a loop voltage at a tokamak start up phase for reduction of OH power supply and impurity flux. For the purposes, a pre-ionization is very useful and we made an experiment on electron cyclotron resonance heating (ECRH) pre-ionization in JFT-2 tokamak. The ECRH system consists of s 28 MHz, 200 KW Gyrotron oscillator, eight rectangular wave guides and eight horns represented at section I. The wave radiated from horns is well collimated horizontally polarized wave. (Ordinary wave)

We compare the start-up phase of tokamak discharge with and without ECRH of which power is about 100 KW, pulse width is 5 msec by measuring of one turn voltage Ve, plasma current Ip, mean electrondensity $\bar{n}e$, impurity flux O IV, radiation flux P_R and second cyclotron harmonics $2\omega ce$. The results, shown in Fig.III.3-1, shows that a break down voltage is reduced about 43 % (from 23 V to 13 V) and V·sec is 0.01 V·sec with ECRH pre-ionization. Further a plasma current and a density build up more smoothly, and a radiation flux and impurity flux are slightly reduced. From the results a plasma core grows up smoothly and the runaway electrons are largely suppressed.

We further investigate the pre-ionization effect in relation of RF incident power P_{RF} and of electron cyclotron resonance layer Xc. The effects are mainly measured by break down voltage V_{BD}. Fig.III.3-2 shows that it is the same with the break down voltage of $P_{RF} \sim 100$ KW and 50 KW. And as decreasing RF power, the break down voltage increases gradually as the same of impurity flux and radiation flux. From the results it is effective as pre-ionization over P_{RF} 50 KW. Fig.III.3-3 shows the relation of the break down voltage V_{BD} and the toroidal field Bt, namely the resonance layer Xc. As Bto increases and/or decreases, namely Xc shifts to outerside and/or inside, respectively, the break down voltage decrease。 For the correction of the effect of error field, a difference of the break down voltage with and without pre-ionization , ΔV_{BD} shows that the most effective pre-ionization occurs where Xc exists in the center of the chamber.

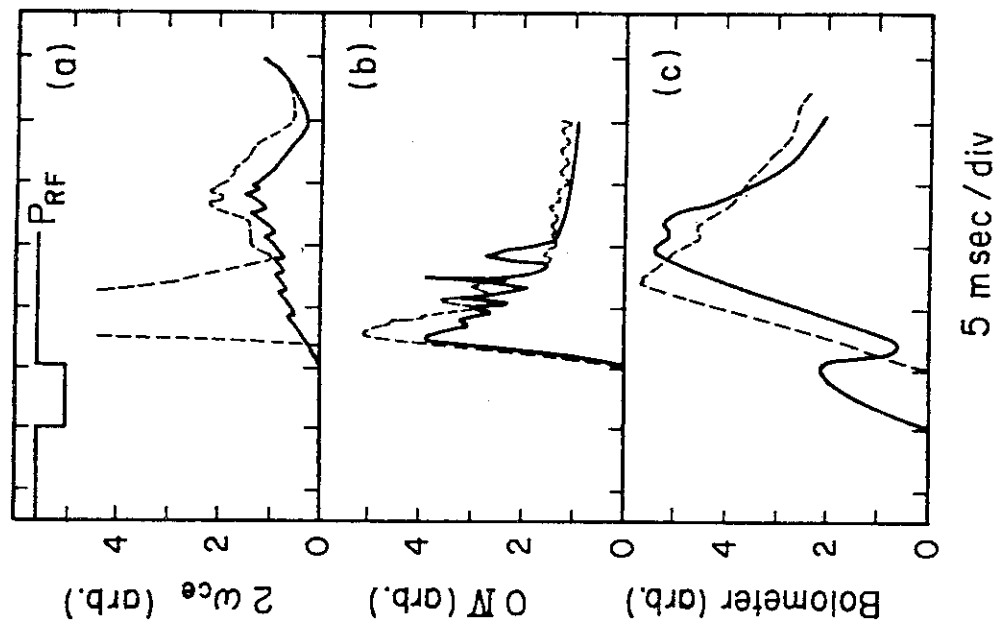

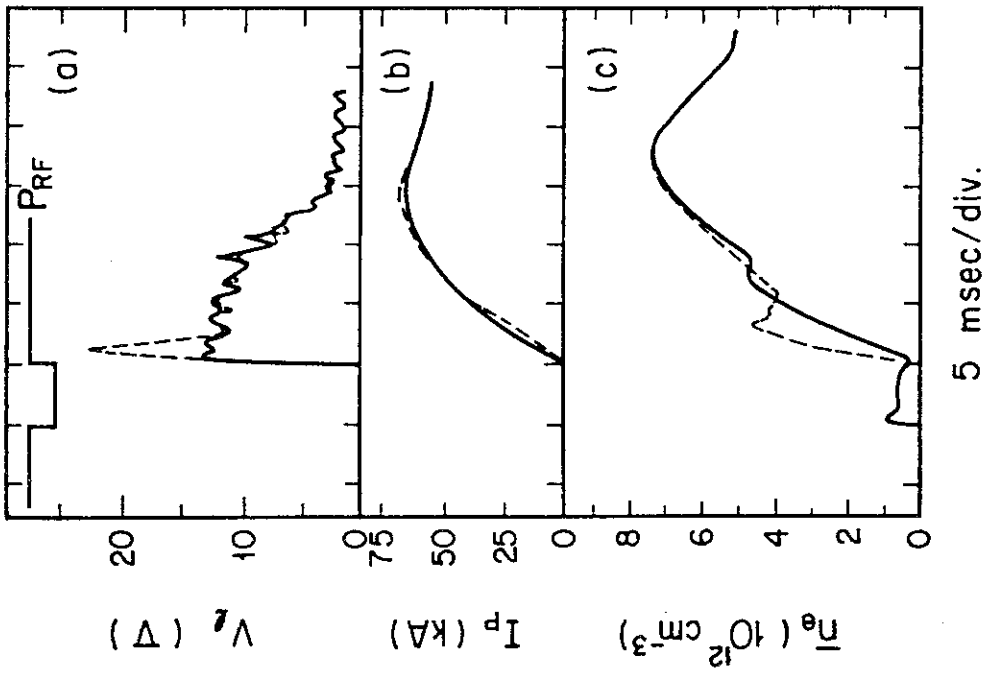

Fig. III-1 Comparisons of the start-up phase of tokamak discharge with and without ECRH

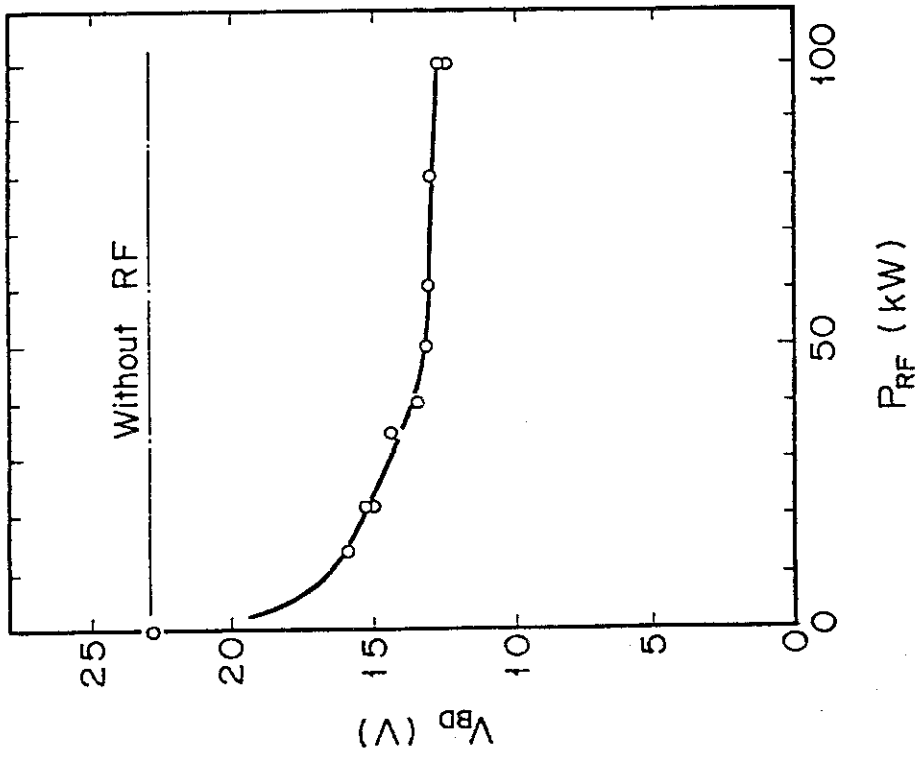

Fig. III-2 The break down voltage with of RF incident power P_{RF}

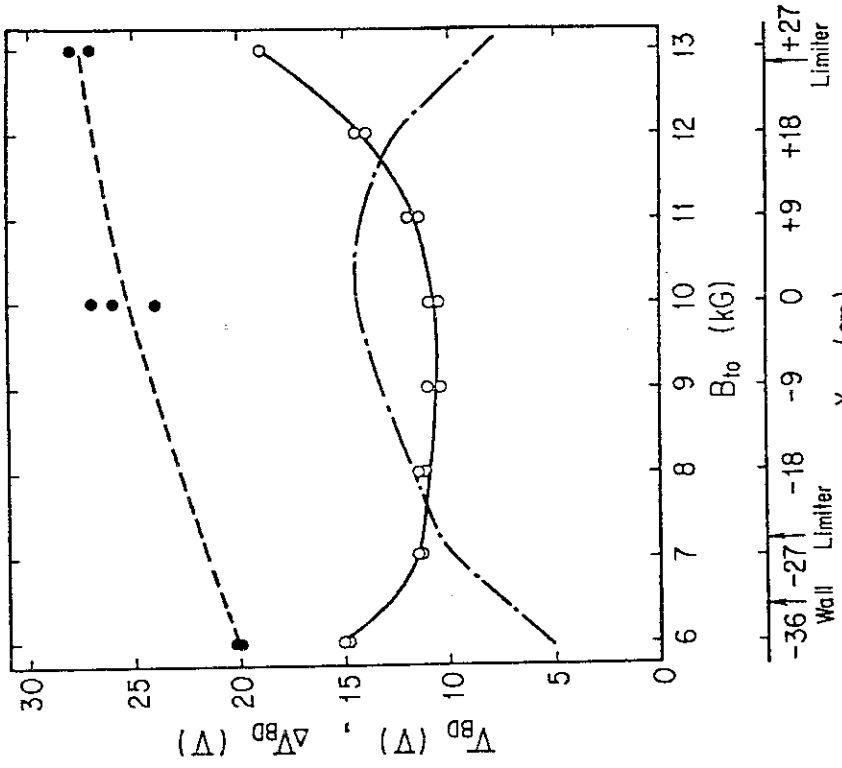

Fig. III-3 The relation of the break down voltage V_{BD} and the toroidal field B_t, namely the resonance layer X_c

Table III-1 Operation of JFT-2, NBI and motor-generator (M-G)

(Month)	1980 3 4 5 6 7 8 9 10 11 12	1981 1 2 3 4 5 6
JFT - 2	Operation and Maintenance	
NBI	Operation and Maintenance	
M - G	Operation and Maintenance	

Detail of the operation (JFT-2, NBI and M-G)

	(Fisical year)	1980	1981 APR-JUN	JUL-SEP	OCT-DEC	JAN-MAR	Total
JFT-2	Total days of operation (days)	85	40	33	38	38	149
	Number of discharges (shots)	7109	4201	3084	3787	4570	15642
	Baking (times)	6	1	2	2	2	7
	Discharge cleaning (hours)	117	37	17	36	40	130
	Vent of vacuum chamber (times)	8	2	3	4	2	11
	Ti coating (hours)	—	119	55	66	77	317
NBI	Total days of operation (days)	—	37	18	33	11	99
	Flashing and Inspection (shots)	—	A:18738 B:15054	A: 424 B: 329	A:7437 B:7471	A: 50 B: 40	A:26649 B:22894
	Conditioning (shots)	—	A:17564 B:16994	A:2320 B:2784	A:4790 B:5824	A:1180 B:1830	A:25854 B:27432
	Vent of vacuum tank (times)	—	3	2	1	1	7
	Baking (times)	—	3	2	1	1	7
	Charge of filament	—	B: 1	A: 1 B: 1	0	A: 1 B: 1	A: 2 B: 3
M-G	M - G (#1) (hours)	1271	442	246	318	330	1336
	M - G (#2) (hours)	1271	447	246	318	331	1342

Table III-2 Specification of the NBI systems for JFT-2

Specifications of the NBI systems for JFT-2		
1. Acceleration power supply		
	Output	DC 40KV, 65A, 300ms
		Duty 1/30, two sets
2. Decelaration power supply		
	Output	DC 5KV, 10A, 300ms
		Duty 1/30, two sets
3. Arc power supply		
	Output	DC 100V, 800A, 300ms
		Duty 1/30, four sets
4. Filament power supply		
	Output	DC 10V, 1200A, 5s
		Duty 1/10, four sets
5. Ion source		
	Output	40KV, 30A, four sets
6. Vacuum pumping system (TMP, two systems)		
	Pumping speed	3,700 l/s
	Expansion chamber	$20m^3$
7. Cooling system		
	Water	800 l/min
8. Beam line		
	Number of lines	2

IV. JAPAN - US RESEARCH COOPERATION IN DOUBLET III

1. JAPAN - US Joint Program

A cooperative program on thermonuclear fusion research between the United States and Japan was started in August 1979 using the Doublet III facility at the General Atomic Co., California.

A group of Japanese experimental scientists called the "JAERI team" is staying there and carrying out research as an independent group under their own leadership. They are sharing the Doublet III machine time with the American experimental team, the GA physics group.

The focus of activities on the part of the Japanese experimental team is to carry out experimental research on higher beta tokamak plasmas with dee-shaped cross sections.

The course of the research program in Doublet III is discussed and decided upon at the Japan-US Joint Doublet III Steering Committee which meets twice yearly. This committee consists of two representatives from each side with all decisions being made unanimously. As of March 1981 there had been three Steering Committee meetings.

Until March 1981, Doublet III was operated for Joule-heating experiments. It was then scheduled to shut down for several months in order to install a neutral beam injection heating system with rating values of 80 keV, 7.2 MW and 0.5 sec pulse length.

Doublet III is a tokamak device designed for research on non-circular cross sectional shapes, particularly the doublet shape. The machine is almost spherical in appearance with a diameter of ~ 6 m, as shown in Fig. IV.1-1, and it is the largest tokamak currently in operation. It has a large vacuum vessel of Inconel with a cross section 3 m high and 1 m wide. It is surrounded by 24 bundles of poloidal field shaping coils which are located immediately outside the vessel. Each shaping coil is connected to a terminal board and can be connected to any combination of coils and power supplies so that the machine has a great deal of flexibility regarding plasma cross section shape: circular, dee, doublet.

At the start of the Joint Cooperation Program the limiters were made of Inconel. In March 1980 a titanium gettering system was installed and in August 1980 a primary limiter of TiC coated carbon was installed; both followed proposals made by the JAERI team. Plasma diagnostics devices were also installed and improved upon during FY80; several of these were installed with the direct cooperation of JAERI team members.

Several noteworthy results which were obtained in the dee-shaped plasma experiments in Doublet III have been incorporated into the design of the next generation large tokamaks such as INTOR: stable control of large dee-shaped plasmas with elongations of 1.8; high plasma density of $\bar{n}_e \sim 1 \times 10^{14}$ cm^{-3} and high Murakami coefficient of $\simeq 8$; low q discharge ($q^* \simeq 1.5$); single null divertor configuration with outside coils; and helium exhaust with divertor configuration. The JAERI team owes much of these successes to the outstanding cooperation and friendship of their GA colleagues.

Higher beta plasma experiments with secondary (neutral beam injection) heating is planned for the near future. The average beta value obtained with Joule heating only attains ~ 1% for a low q discharge with a dee-shaped plasma. It is expected that an average beta of ~ 5% will be attained with a neutral beam heating of ~ 7 MW if any adverse effect does not deteriorate the plasma property.

2. Experimental Results

2.1 High Plasma Density

Because the minimum density required for a neutral beam of 80 KeV perpendicular injection is 5 - 6 x 10^{13} cm^{-3} line-averaged density the achievement of high plasma density was given the first priority. This target density was attained in Dec. 1979. A higher plasma density of ~ 1 x 10^{14} cm^{-3} was obtained in April 1980 after the titanium gettering system was applied; both had a toroidal field of 24 kG.

2.2 High Elongation and High Plasma Current

After a trial and error method of plasma control, an elongation K (ratio of height-to-width) of the dee-shaped plasma was gradually increased and in Dec. 1980 plasmas with elongations as high as 1.8 were stably controlled. The stability of the elongated plasma was experimentally investigated with regard to both elongation K and triangularity δ and it was shown that K ~ 1.8 is almost the limit of the elongation under present conditions; i.e., the present plasma control system and no particular control of the plasma current density profile. Typical plasma cross section shapes are shown in Fig. IV.2-1.

2.3 Low q Discharge

The plasma properties were improved in two steps: with titanium gettering and with a TiC coated carbon primary limiter which were installed in March and September, respectively. The plasma parameters obtained are shown in Fig. IV.2-2. DIII[a] shows the first parameter; DIII[b] shows the improvement after the start of titanium gettering; and DIII[c] shows the present status of the parameter region after the addition of the carbon primary limiter. The lowest q in Doublet III is ~ 1.5 of the geometrical definition. The real q (or MHD q) is nearly 1.0 from the plasma center up to more than half the minor radius and increases steeply to $\gtrsim$ 2 at the plasma edge. Our dee-shaped plasma in Doublet III is the first one to obtain q* well below 2.0 in a large (R ~ 1.5 m), shell-less tokamak. The Murakami coefficient $\bar{n}_e$ / (B_T/R) also increased with low q discharge with a highest value of ~ 8. A line-averaged plasma density of ~ 7 x 10^{13} cm^{-3} can be obtained with 12 kG, with an average beta value reaching ~ 1% with Joule heating only.

2.4 Confinement

Energy confinement was studied while periodically verifying that the machine condition remained constant. By using titanium gettering between discharges, data was taken for various densities, plasma current (q values), and elongations. Using the temperature profile taken mainly with a soft X-ray energy analyser, the confinement of the central core of the plasma up to 1/2 of the minor radius was studied. The ratio of the radiation power to the Joule heating input power within the central part remains $\lesssim$ 30%.

An experimental scaling which has the best fit for a wide range of plasma parameters, including low q cases, was obtained. The electron energy confinement is consistent with

$$\tau_{E_e} \propto \frac{\bar{n}_e \cdot B_T}{I_p} \cdot \frac{1 + K^2}{2} \qquad (\propto \bar{n}_e\, q^*)$$

and the ion energy confinement is expressed as

$$\tau_{E_i} \propto \frac{I_p^2}{B_T^2\left(\frac{1+K^2}{2}\right)^2} \cdot \frac{K^2}{\bar{n}_e} \qquad \left(\propto \frac{K^2}{\bar{n}_e\, q^{*2}}\right)$$

The absolute value of the ion energy transport coefficient is 1 - 2 times the neoclassical theory. The experimental data and the analytical model calculation corresponding to each of the experimental data are shown in Fig. IV 2-3 (a) and (b), respectively. It is shown that the energy confinement is improved by elongation in the higher density region where the ion transport is dominant.

2.5 Remote Radiative Cooling and Helium Ash Exhaust in Single-Null Divertor Configurations

A unique plasma configuration with a single null poloidal divertor as shown in Fig. IV.2-4(A) was realized with the poloidal coils located outside the vacuum vessel. Even without any particular divertor chamber or throat, distinct reduction of impurities contained inside the main plasma and also reduction of the radiated power loss from the main plasma were achieved as shown in Fig.IV.2-4(B). Several new phenomena were also found at the divertor

region because of its large volume and the ease of observing separately from the main plasma. The plasma density as well as plasma particle recycling at the divertor region increases sharply with an increase in the main plasma density. The radiation power from the divertor region also increases sharply with an increase in the main plasma density, which strongly reduces the heat flux to the divertor plate as observed with an infrared TV. The result is shown in Fig. IV.2-5.

Another unique discovery was finding the helium exhaust function of the divertor configuration. Artificially injected helium is removed from the main plasma region and compressed at the lower chamber. This helium exhaust is also a result of high plasma density, and the helium pressure rises as high as $\sim 10^{-4}$ Torr at the high density region as shown in Fig. IV.2-6. The helium concentration in the main plasma at those conditions is kept low ($\sim$ 1.6%). By simply extrapolating this result to an INTOR class device, the required pumping speed is $\sim 7 \times 10^3$ ℓ/s which relaxes the presently proposed pumping speed for the INTOR by a factor of 70.

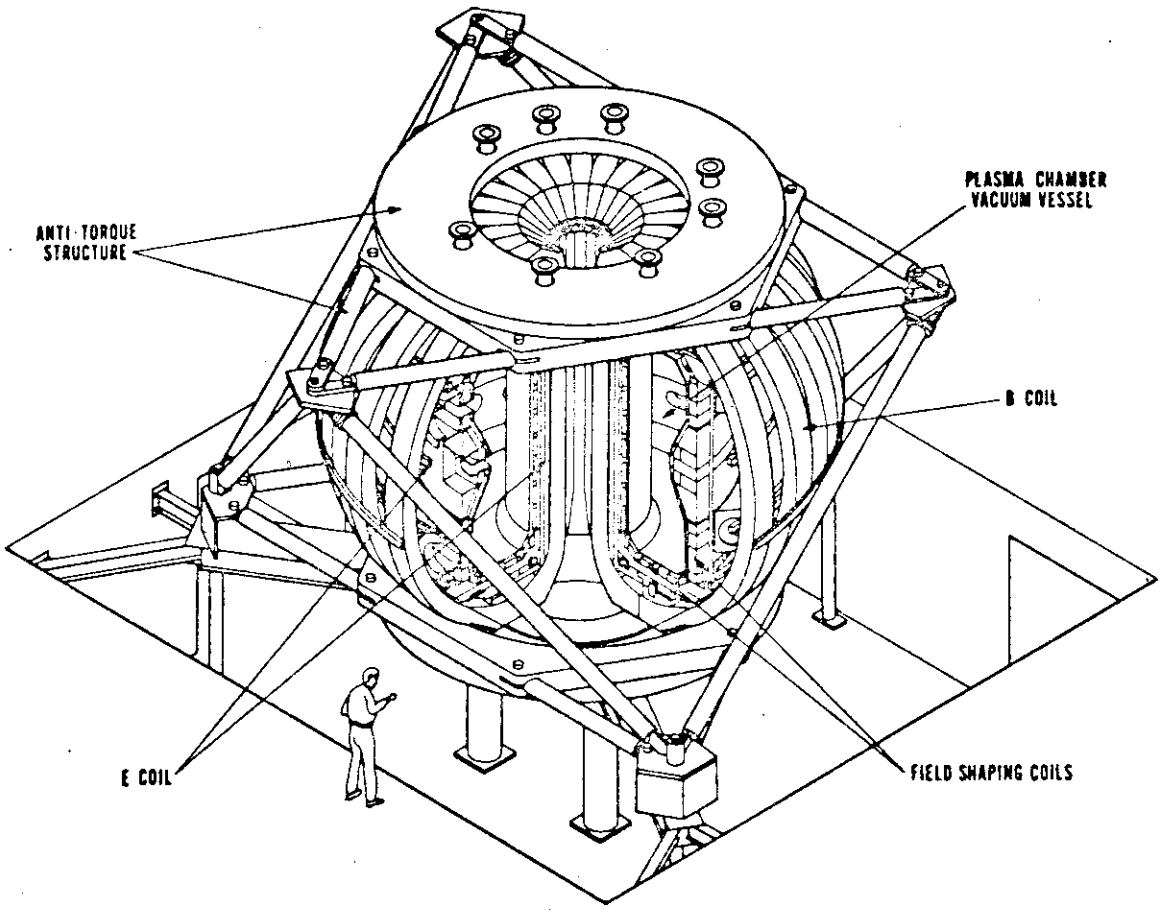

Fig. Ⅳ.1-1 Schematic of Doublet III

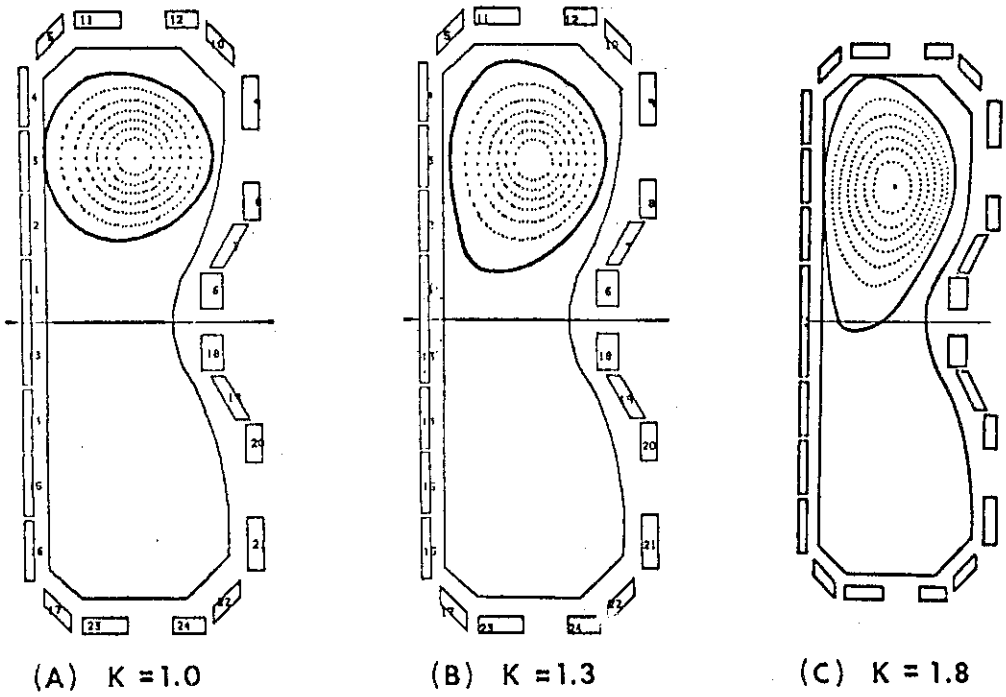

Fig. IV.2-1 Typical shapes of dee-plasmas in Doublet III

K is the elongation (height-to-width ratio)

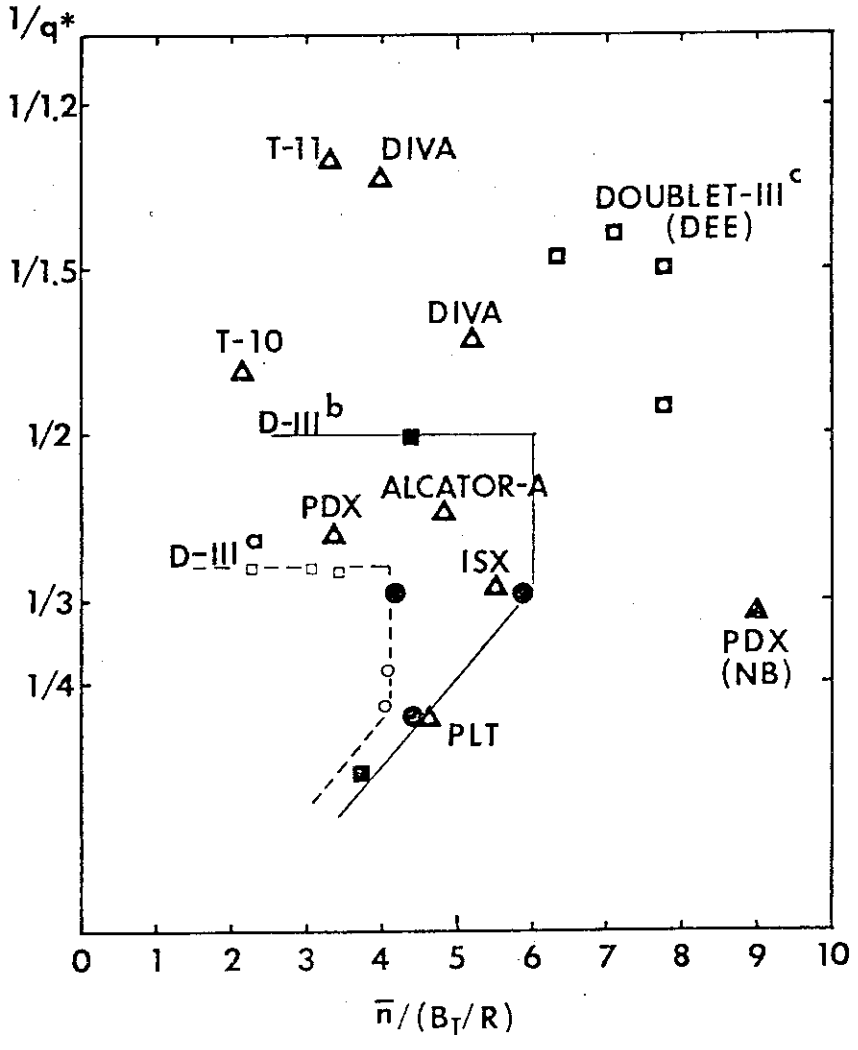

Fig. IV.2-2 $1/q^*$ and $\bar{n}/(B_T/R)$

D-III^a (dotted line) : at the start of cooperation

D-III^b (sold line) : after titanium gettering

D-III^c (□) : after carbon primary limiter

Δ : other tokamaks

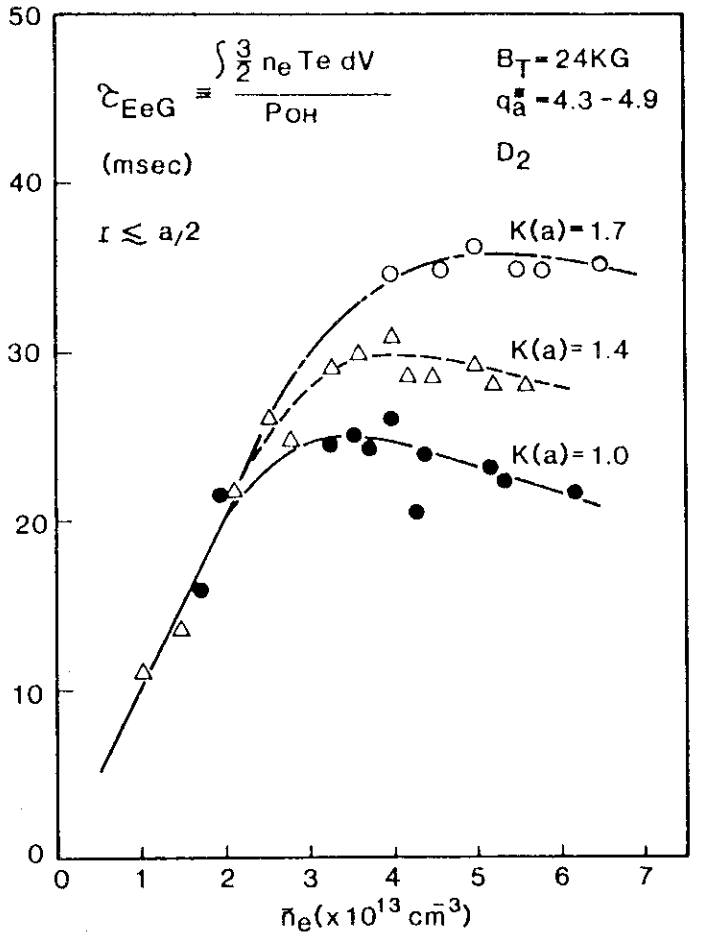

Fig. IV.2-3 (a) Comparison of $\tau_{E_{eG}}$ for discharges of K(a) = 1.0, 1.4 and 1.7 with constant q_a^*. At high density region, $\tau_{E_{eG}}$ is improved by 65% with the vertical elongation from K(a) = 1.0 to 1.7.

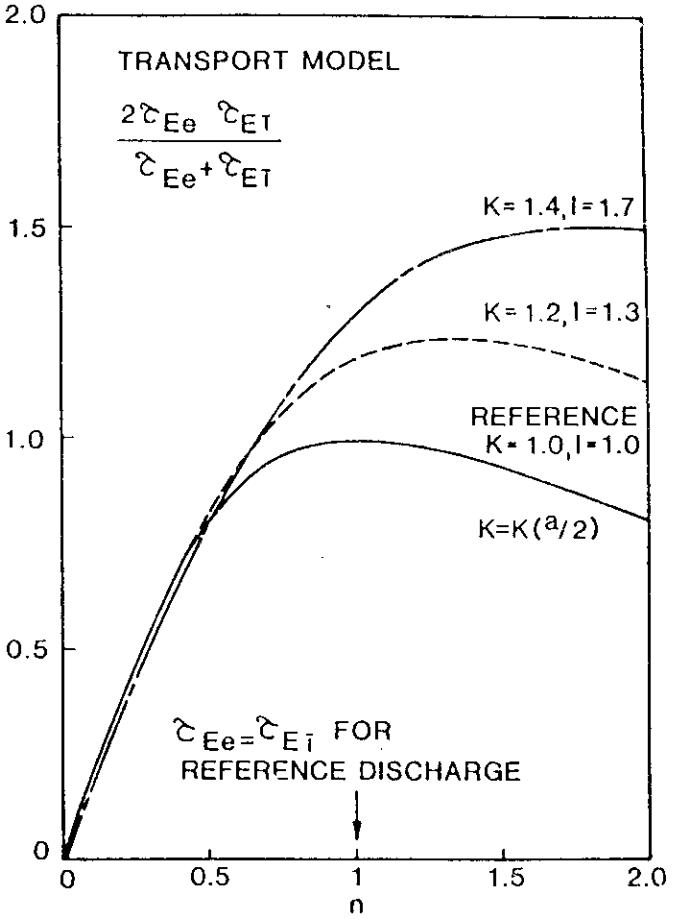

Fig. IV.2-3 (b) Transport model calculation based on equation (1) and (2). n and I are non-dimensional electron density and plasma current.

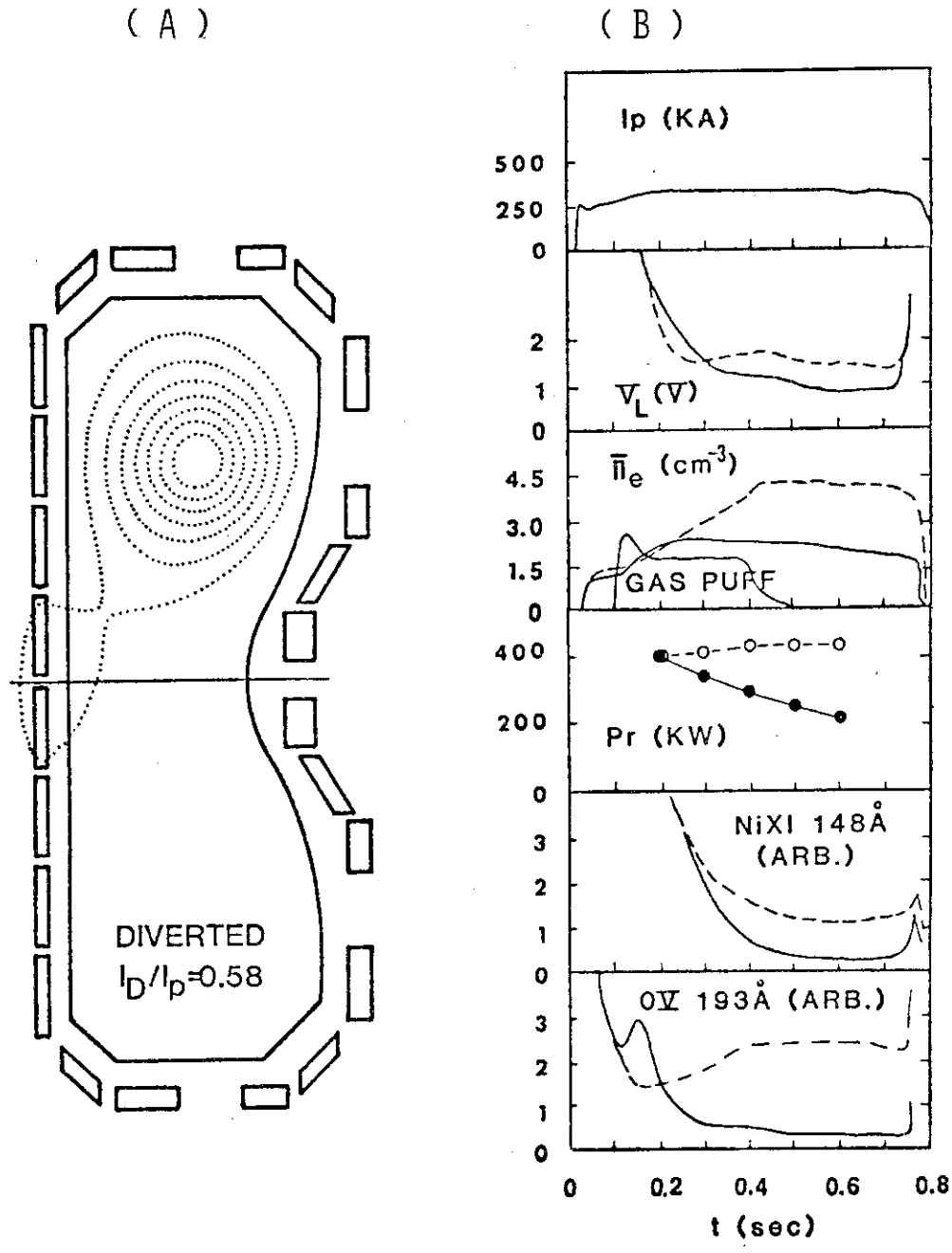

Fig. IV.2-4 Cross section of single null divertor configuration in Doublet III and comparison of waveforms of the diverted (solid line) and non-diverted (broken line) discharges. The divertor coil current is increased during discharge and the divertor configuration is produced at ~ 300 ms. I_p : plasma current, V_L : plasma loop voltage, $\bar{n}_e$; line-averaged plasma density of the main plasma region, P_r : total radiation loss power, and intensities of NiXI 148Å and OV 193Å line emission from the main plasma.

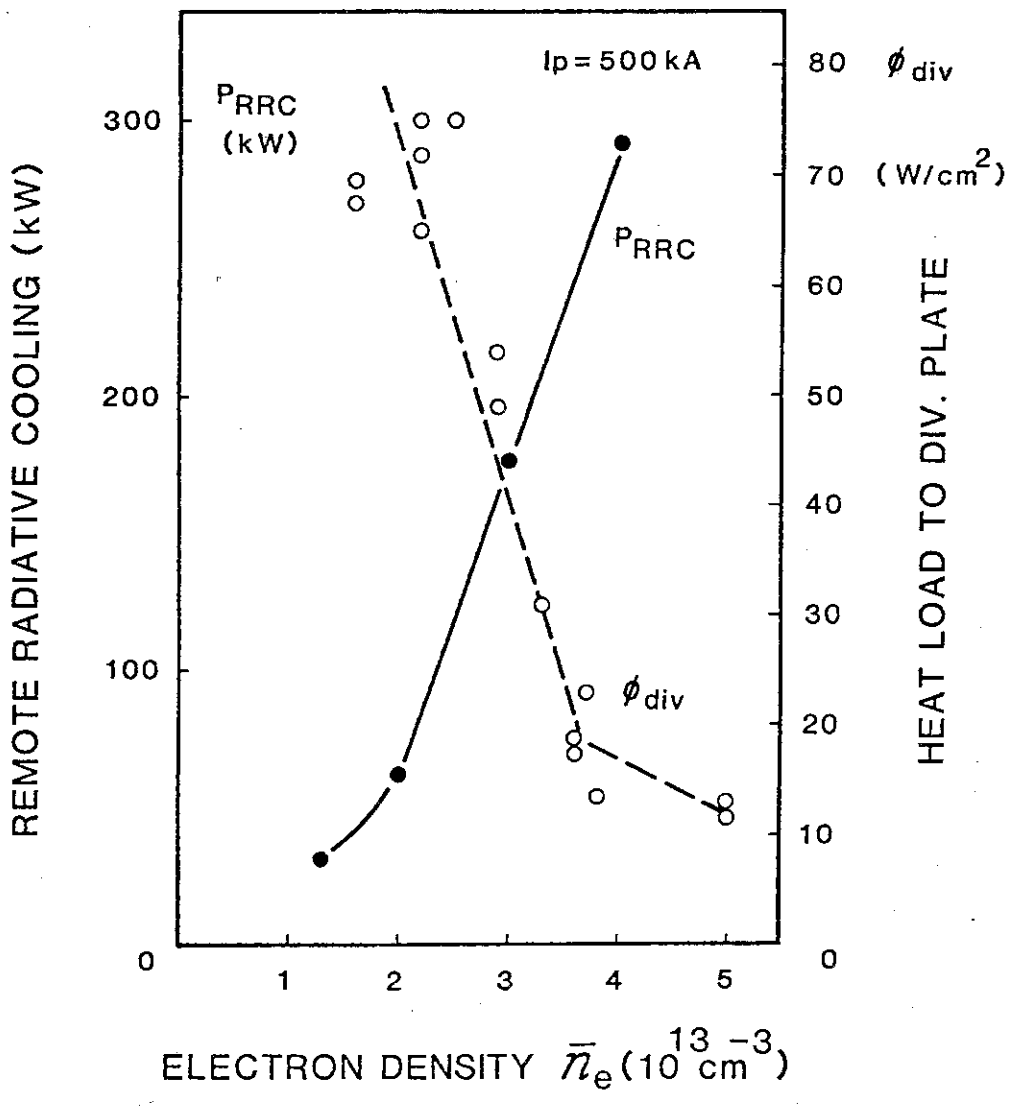

Fig. IV.2-5 Reduciton of heat load on the divertor plate by remote radiation cooling of the divertor configuration. The radiation power from the divertor region P_{RRC} increases, and the heat flux to the divertor plate ϕ_{div} decreases, both with the increase of the main plasma density $\bar{n}_e$. P_{RRC} is mesured by a bolometer and ϕ_{div} by infrared TV and thermocouples. ($I_p \simeq 500$ kA)

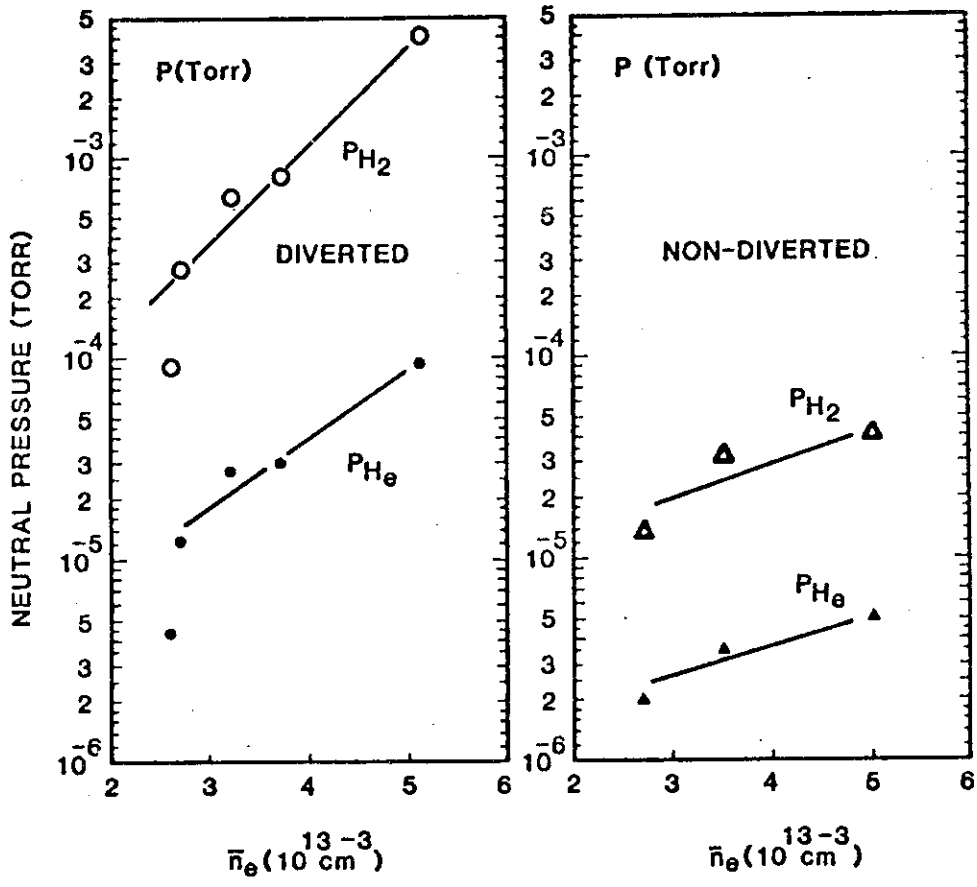

Fig. IV.2-6 Helium pressure at the lower chamber (divertor chamber) with and without divertor. With divertor, the helium pressure reaches $\sim 10^{-4}$ Torr, which is enough for helium ash exhaust in future machines.

V. DEVELOPMENT OF PLASMA HEATING SYSTEM

1. Introduction

Neutral beam injection and radiofrequency (RF) heating systems are under development.

In the neutral beam injection system, ion source development and beam line studies for JT-60 injectors have been made using test stands ITS-2 and ITS-3. The prototype-I ion source of which extraction grids are the same size as that of JT-60 injectors has been fabricated and tested. An ion beam of 75 keV/35A has been extracted for a duration of 0.1 sec. From one sixth section of the extraction area, longer pulse beams of 70 keV/6A have also been extracted for up to 10 sec.

The prototype unit of neutral beam injectors for JT-60 are under construction and will be completed in autumn of 1981.

In the RF heating system, R&D work of 1.4 MW klystron and construction of the power test facility of the klystron have begun. Test stand of coupling system with short pulse length was constructed and it is started to study conditioning and power limit of the launcher. Preliminary design work of the Lower Hybrid Range of Frequencies (LHRF) heating system has continued and a conceptual design of the Ion Cyclotron Range of Frequencies (ICRF) heating system has also been performed.

2. Neutral Beam Injection System

2.1 Ion source development

The ion sources of JT-60 neutral beam injectors must satisfy the following performance characteristics;

(1) Beam energy : 75 keV (50 - 100 keV)

(2) Beam current : 35 A

(3) Pulse duration : $\leq$ 10 sec

(4) Divergence (ω 1/e) : $\leq$ 1 deg.

(5) H^+ species : $\geq$ 75 %

(6) Impurity : $\leq$ 1 % (low Z)

$\leq$ 0.1 % (High Z)

(7) Gas flow rate : $\leq$ 20 torr · ℓ/sec

(8) Cathode life : $\geq$ 1/year

(9) Grid heat loading : $\leq$ 2 % of total beam power

These items except (8) have already been achieved individually. In order to improve the life time, we have developed a technique for surge protection of tungsten filaments and hollow cathodes. The demonstration of the total source performance will be performed at the prototype unit of JT-60 injector units in late 1981.

2.1.1 A 75 keV/35A ion source

To obtain an ion beam of 35 A at 75 keV, the prototype-I ion source has been developed. The plasma generator is a bucket type plasma source, which is shown in Fig.V.2.1-1. The rectangular arc chamber (21 cm × 36 cm wide, 18 cm deep) is surrounded by samarium-cobalt magnets arranged in a line cusp configuration. A schematic of the prototype-1 ion accelerator is shown in Fig.V.2.1-2. The accelerator comprises a rectangular alumina insulator and a two-stage acceleration grid assembly. The grid assembly is composed of four grids. Each grid is made of oxygen free copper plate which has 1032 apertures within the area of 12 cm × 27 cm. Each aperture is carefully drilled and shaped to obtain

a small beam divergence. Since 0.3 - 1.5% of the total beam power is dissipated in each grid, forty four cooling pipes are frazed within the extraction area to remove the heat loadings.

Using the prototype-I ion source, a 75 keV/35A hydrogen ion beam was extracted for a duration of 0.1 sec. The e-folding half width divergence measured is 1.2° - 1.7°, which is fairly large compared with the divergence obtained by the small size grid. The deterioration of beam optics turned out to be due to the plastic deformation of the plasma grid, which is resulting from thermal stresses induced in a grid repeatedly. A deformation of about ±0.5 mm was found within the area of 12 cm × 27 cm.

2.1.2 Development of molybdenum plasma grid

To eliminate the deterioration of beam optics caused by plastic deformation of the plasma grid, new grid materials and structures must be developed. A molybdenum is one of the most attractive materials because it has low thermal expansion coefficient, high Young's modulus and high tensile strength. As a result of structural analyses of the molybdenum grids, we have developed two types of molybdenum grids. One type is shown in Fig.V.2.1-3. This grid comprises four molybdenum plates. Each plate has 258 apertures and eleven copper cooling pipes. Both ends of each plate are rivetted to the oxygen free copper flange which has bellows. Each plate can expand freely by the effect of the bellows. The other type of the grid is shown in Fig.V.2.1-4. Both of the plate of the plasma grid and cooling pipes are all made of molybdenum. Since the circumference of the grid is fixed tightly, the grid cannot expand. This molybdenum grid is now manufactured. The former plasma grid has been fabricated and tested with the prototype-I ion source.

The e-folding half width divergence of 0.93° was obtained when an ion beam of 22A at 60 keV was extracted for 0.1 sec. The perveance per grid aperture is same as that of a 35A/75 keV ion beam. To test the durability of the molybdenum grid, the long pulse operation was performed using a one sixth section of the grid. Ion beams of 6A at 70 keV were extracted for 10 sec. The beam current density equals that of ion beams of 35A, and the heat loading of the plasma grid reaches up to 200 W/cm^2. In spite of this large heat loading, we could extracted a long pulse beam without any difficulties. Using the multichannel photo beam monitor, no change in the beam divergence was observed during 10 sec.

2.1.3 Measurement of hydrogen species and impurities

The hydrogen species in the beam produced by the prototype-I ion source have been measured by three different methods, i.e. momentum analysis with thick target, that with thin target and optical analysis. Figure V.2.1-5 shows the hydrogen species as a function of extraction currents. The values measured by momentum analysis with thin target is considered to be accurate, because they were measured directly. Optical analysis was performed by observation of the Doppler shifted H_α lines emitted by fast atoms in the beam. From these measurements, it was varified that the proton ratio of the prototype-I ion source reached over 75%.

Impurity concentration in the beam is also an important factor. Table V.2.1-1 shows the result measured by momentum analyzer. These values are corrected for zero line density. Low Z impurities such as C, O can be reduced to a level of 1% after the sufficient source conditioning. And metal impurities such as Cu, W can be reduced to

a level of 0.1% with the good choice of source materials and operating parameters.

2.1.4 Grid inspection by a infrared camera

The grids of the accelerator are water-cooled by a lot of small diameter pipes which are brazed on the grids. In the process of brazing, some cooling pipes may be choked by the solder. The choking of the pipes may easily break the grid. Therefore, it is important to develop a technique to inspect the choking and to measure the flow rate of the cooling water in each pipe without destruction of grids.

Fundamental experiments of measuring the flow rate in pipes have been performed using a model copper grid with three cooling pipes. The flow rate in the center pipe can be changed. When a burst of hot water is supplied to the three pipes, the time dependence of grid temperature is observed by a infrared television camera. The temperature pattern of the grid is displayed on the color monitor system and all frames of one run are memorized in the system and can be copied on video tapes or floppy disks later. Figure V.2.1-6 shows the time dependence of temperature of the center pipe as a parameter of flow rates. As a result of these experiments, it is proved that the reduction of the flow rate by 50% can be measured by this technique.

2.1.5 Surge protection of tungsten filaments

The life time of the bucket type plasma source is limited by that of tungsten filaments. To protect tungsten filaments from damages is an important problem. The most serious damage is the arc spotting caused by the surge when a breakdown occurs between acceleration grids. If large capacitors are installed between filaments and the plasma

grid, the surge voltage may be reduced and the damages will become small.

In order to confirm the effectiveness of surge protection, the prototype-I ion source was operated with and without the capacitors of 10 μF. After several thousands of shots, filaments without surge protection were subject to several large (∿1mm) damages and small (0.1 ∿ 0.2mm) damages over the full surface of filaments. However, filaments with the capacitors were subject to only small (∿0.1mm) damages. From these experiments, it turned out that the capacitors installed between filaments and the plasma grid effectively protected the filaments from the arc spotting.

2.1.6 Development of hollow cathode

A hollow cathode may have the advantage of a hair-pin shaped tungsten filaments, since it has a long life time and is indirectly heated. For practical point of view, it is a probelem that the gas flow rate through a hollow cathode is too high. Experimental studies to reduce the gas flow rate have been made, using a circular ion source with magnetic multi-line cusp field. Figure V.2.1-7 shows a schematic view of the experimental setup. At the arc current of 400A, the gas flow rate was reduced to 2.4 torr · ℓ/sec by using both a molybdenum button placed in front of the orifice and the aixal magnetic field directed anti-parallel to the field generated by the cathode heater current. This flow rate satisfy the specified flow rate of the ion source of JT-60 injectors.

Since ion sources of JT-60 injectors will need four hollow cathodes, the parallel operation of the hollow cathodes must be performed stably. As a result of the parallel operation of four hollow cathodes, it was

proved that:

(1) hollow cathodes could be operated stably with parallel gas feed,

(2) a resistance of 0.1 Ω installed between each hollow cathode and the negative terminal of the arc power supply could reduce the inhomogenity of the arc current under 10%, whre the maximum are current was 800A.

2.2 Development of the JT-60 neutral beam injection system

Neutral beam injection is expected to play an important role in the stage of additional heating of JT-60 plasma beyond 5 keV. Performances of the injector are specified as follows.

(1) Beam energy: 50 - 100 keV

(2) Total neutral beam power: 20 MW

(3) Pulse width of injection: 10 seconds

(4) Number of injector unit: 14 units

(5) Permissible cold gas influx into the torus: a value corresponding to 15% of the fast neutral atoms.

Prior to fabrication of the fourteen units, a prototype unit is now constructed to test and demonstrate a single unit performance. The prototype injector unit consists of a beam fine unit, a power supply unit, a target chamber and auxiliary systems. A scheme of the beam line and the target chamber is shown in Fig.V.2.2-1. The most significant feature of this unit is its long beam pulse of 10 sec, producing as much as 15 MJ neutral beam. From a thermal view point, this is technologically in the same degree of difficulty as in the case of continuous beam production. A forced water cooled beam dump (Fig.V.2.2-2) can handle an ion beam of up to 5.6 MW by the aid of a carefully designed reflecting magnet

(Fig.V.2.2-3) and a dump structure.

A liquid helium refrigeration system and a liquid nitrogen system are provided to cool down the cryopumps that are installed in the main vaccum and the target chambers. A cooling water system consists of a secondary open loop and a primary demineralized closed loop, which transfers heat caused by beam extraction from all the heat absorbing surfaces.

An auxiliary pumping system consists of a pair of turbomolecular pumps and is used as a roughing pump before the cryopumps start to operate.

After completion of this unit in autumn of 1981, the performances will be tested and the results will be reflected for the construction of the JT-60 neutral beam injection system from 1982.

Table V.2.1-1 Impurity concentration of the prototype-I ion source

IMPURITY CONCENTRATION (60 KEV, 5.3 A , NL= 0 TORR·CM)

H	H_1^+ , H_2^+ , H_3^+	100 %	100 %
LOW Z	C^+, CH_N^+	0.1 %	1.4 %
	O^+, OH^+, H_2O^+, H_3O^+	1.3 %	
	N_2^+ , O_2^+ , ETC.	0.02 %	
HIGH Z	Cu^+, Zn^+	0.03 %	0.11 %
	Mo^+	0.03 %	
	W^+	0.05 %	

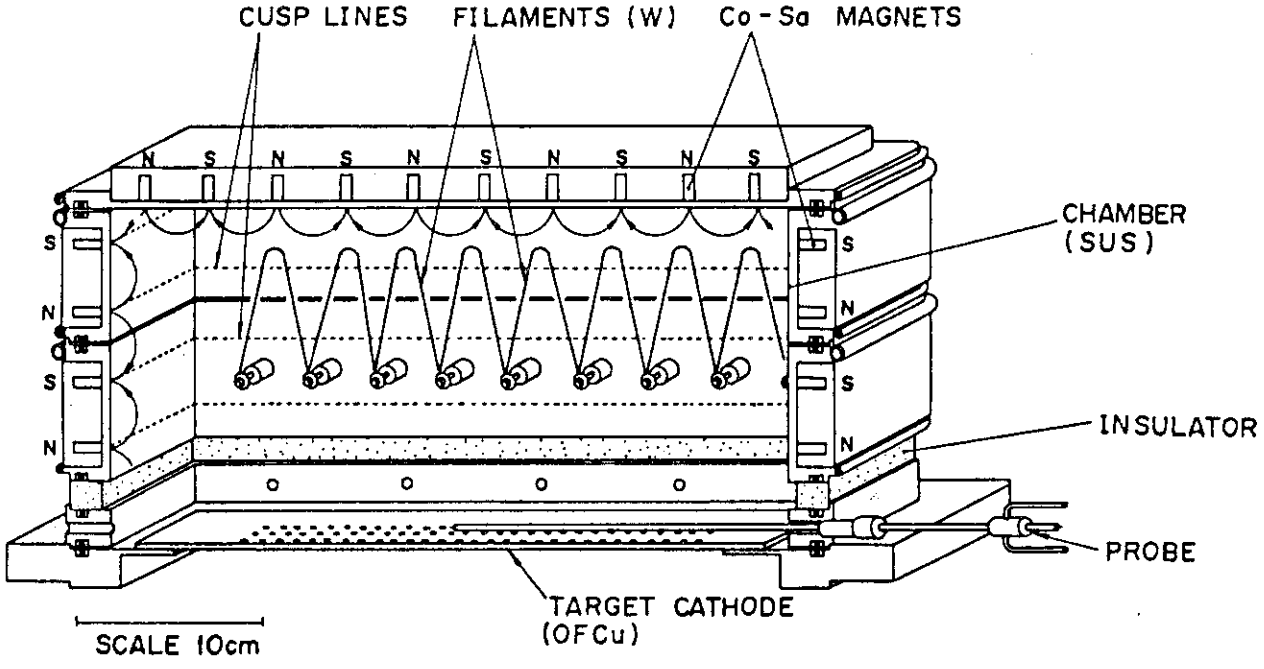

Fig. V.2.1-1 Schematic of the rectangular bucket plasma source of the prototype-I ion source

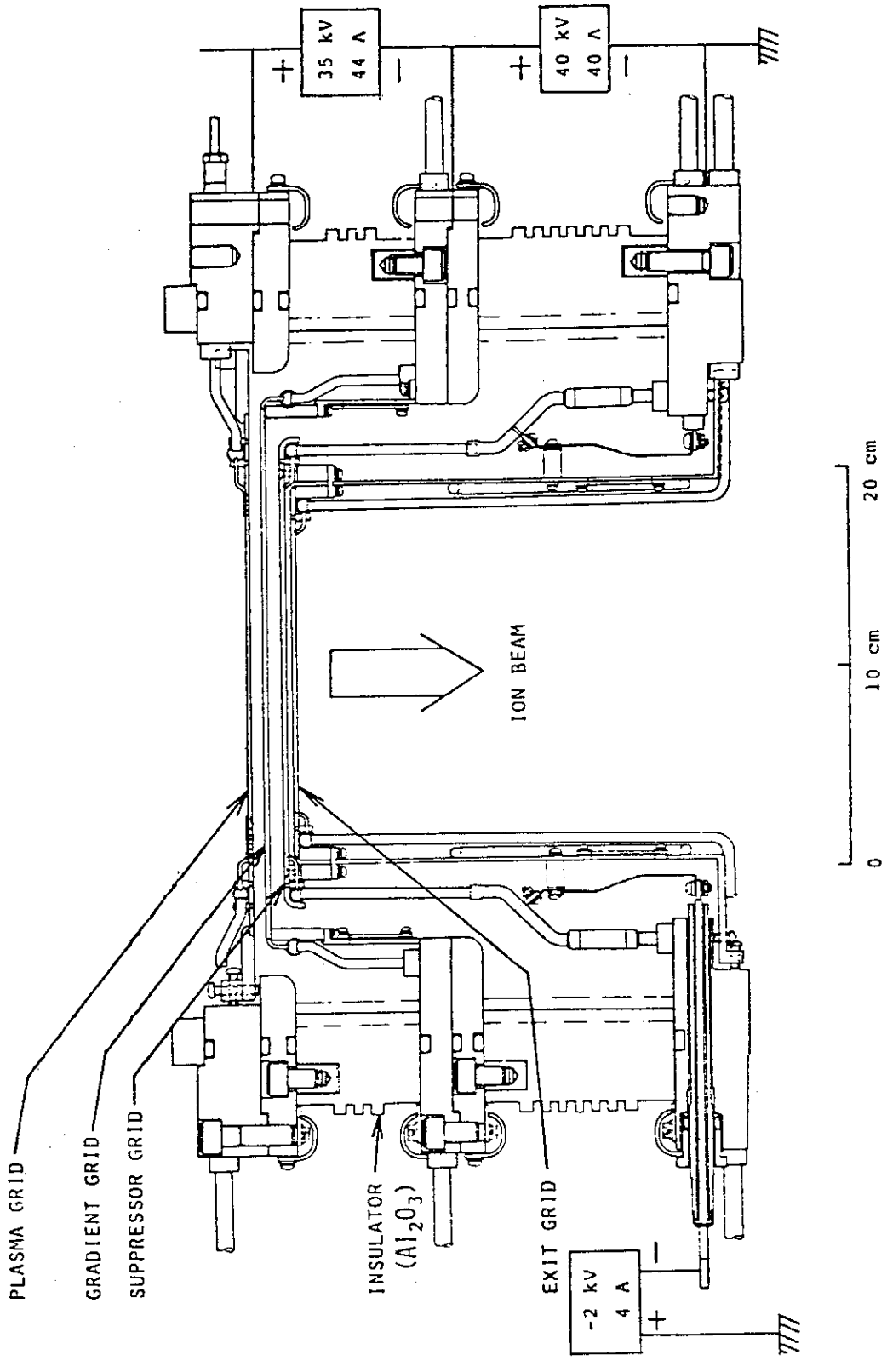

Fig. V.2.1-2 Schematic of the two-stage accelarator of the prototype-I ion source

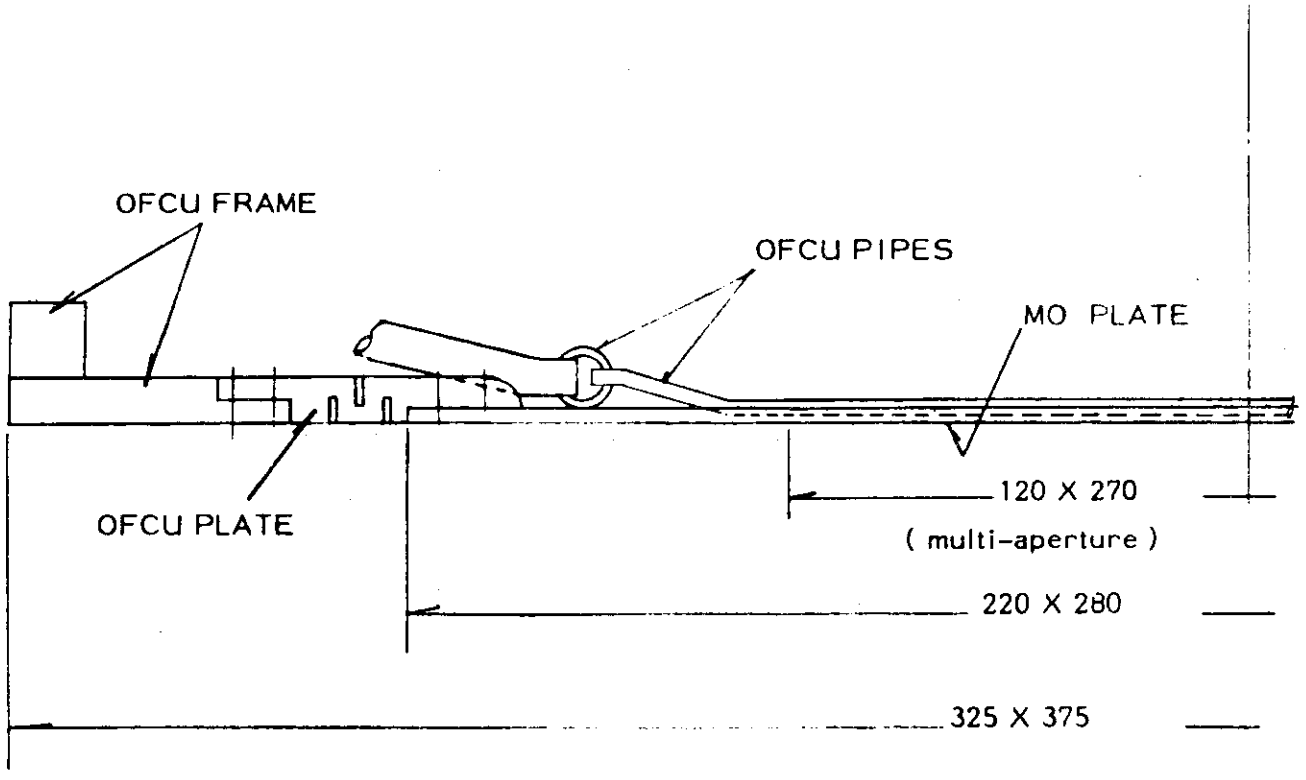

Fig.V.2.1-3 A cross sectional view of the molybdenum grid TYPE-I

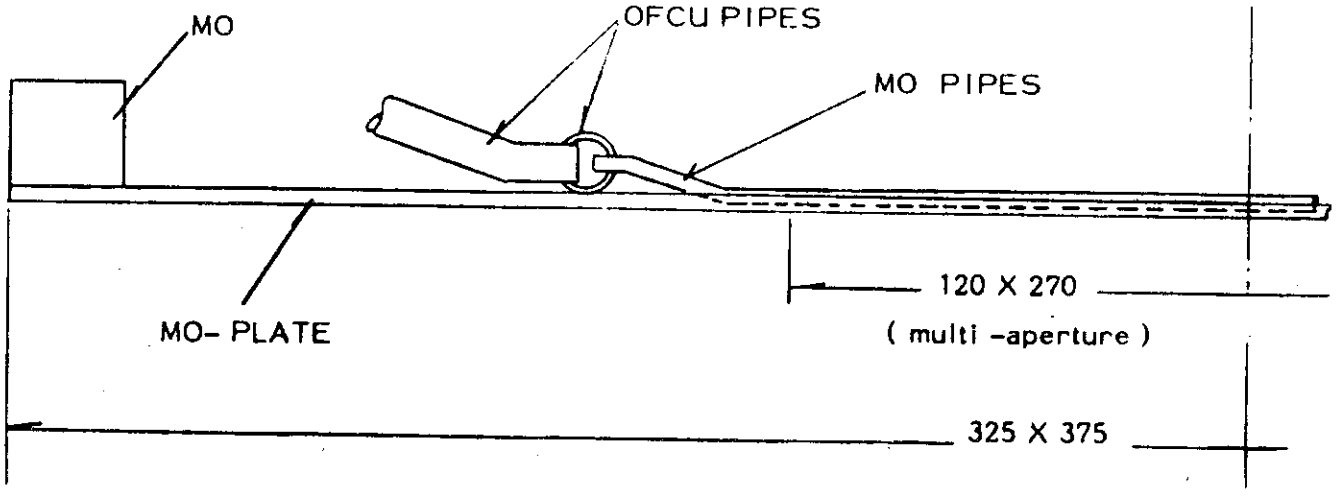

Fig.V.2.1-4 A cross sectional view of the molybdenum grid TYPE-II

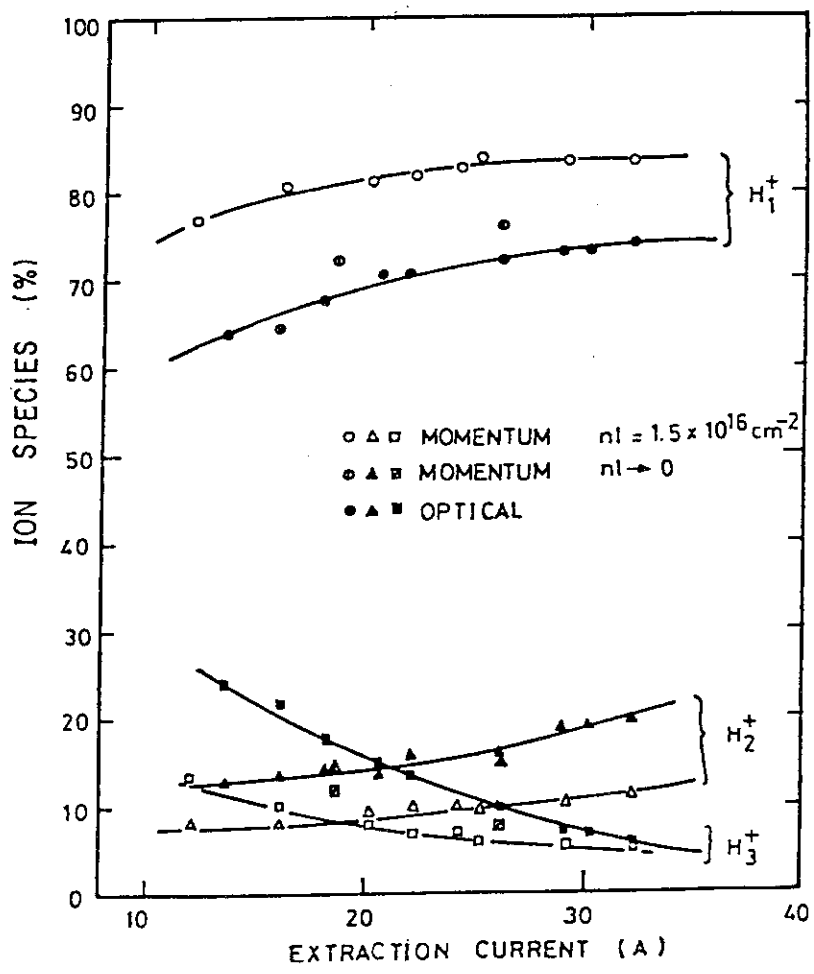

Fig.V.2.1-5 Proton fraction of the prototype-I ion source measured by three different methods

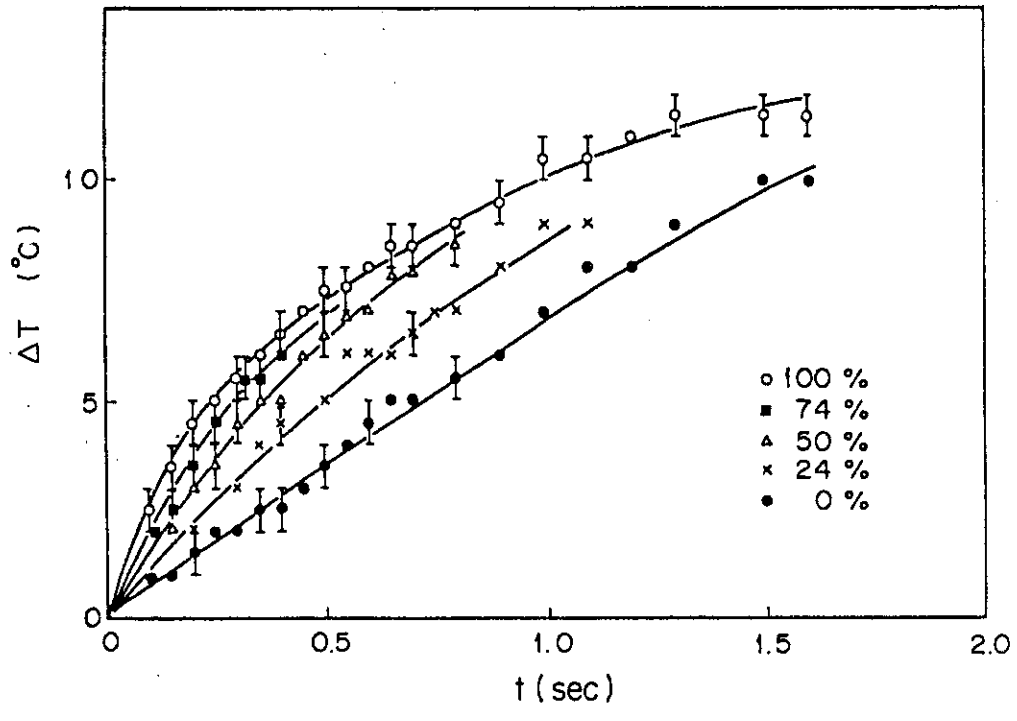

Fig.V.2.1-6 Time dependence of the center pipe temperature

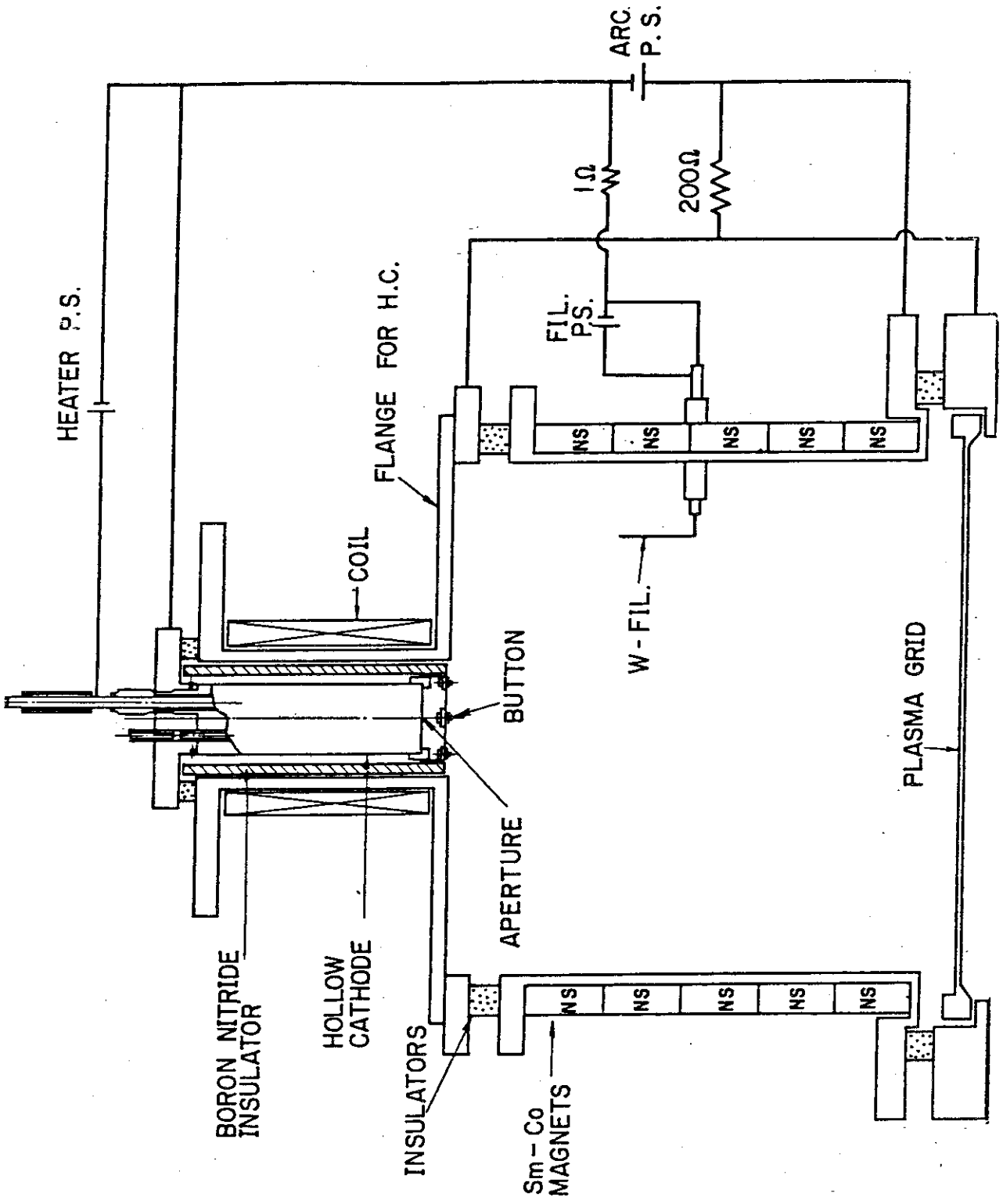

Fig.V.2.1-7 Sketch of the experimental setup of the hollow cathodes

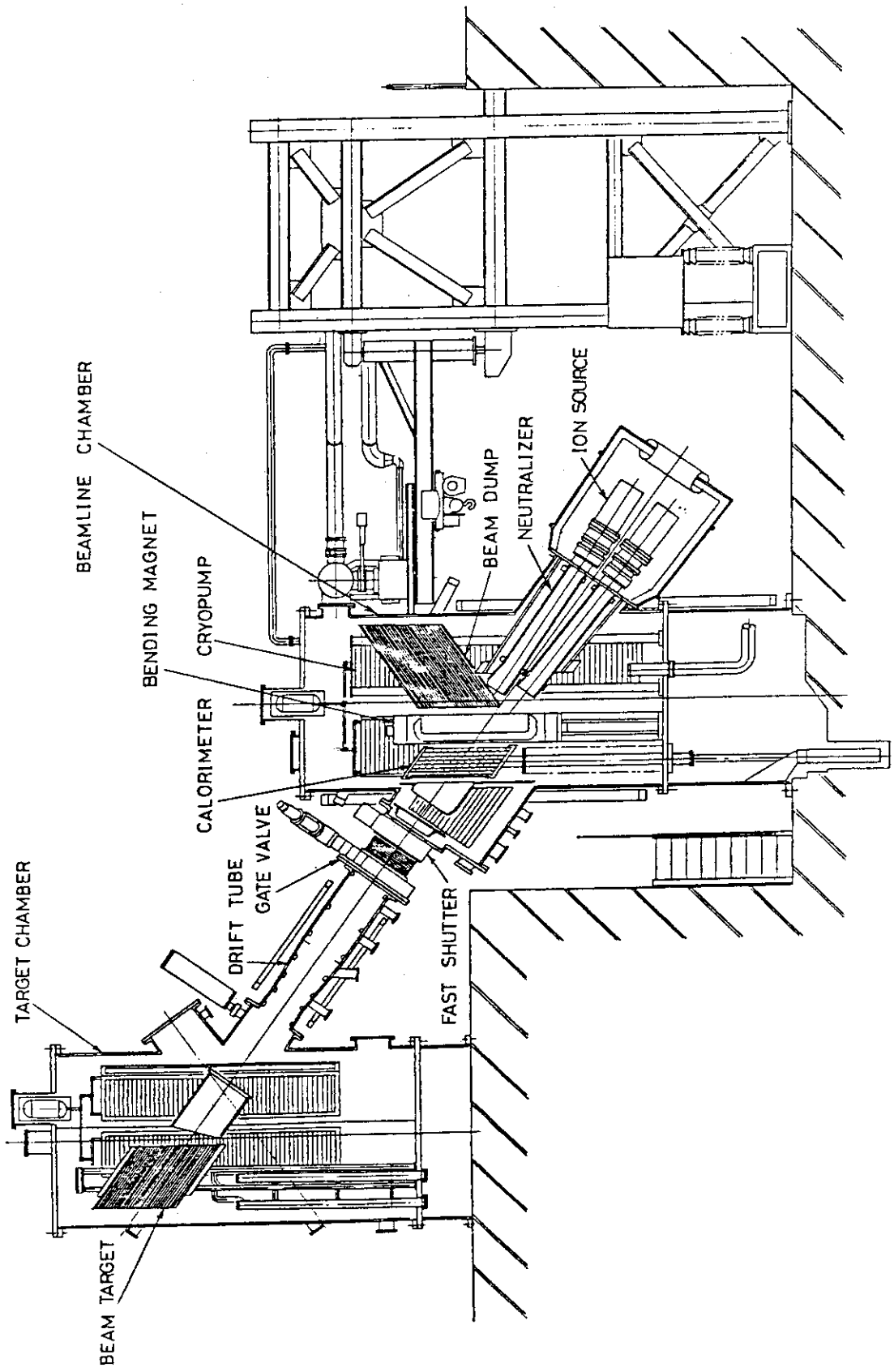

Fig.V.2.2-1 A cross sectional view of the prototype unit of the JT-60 NBI

Fig.V.2.2-2 The beam dump

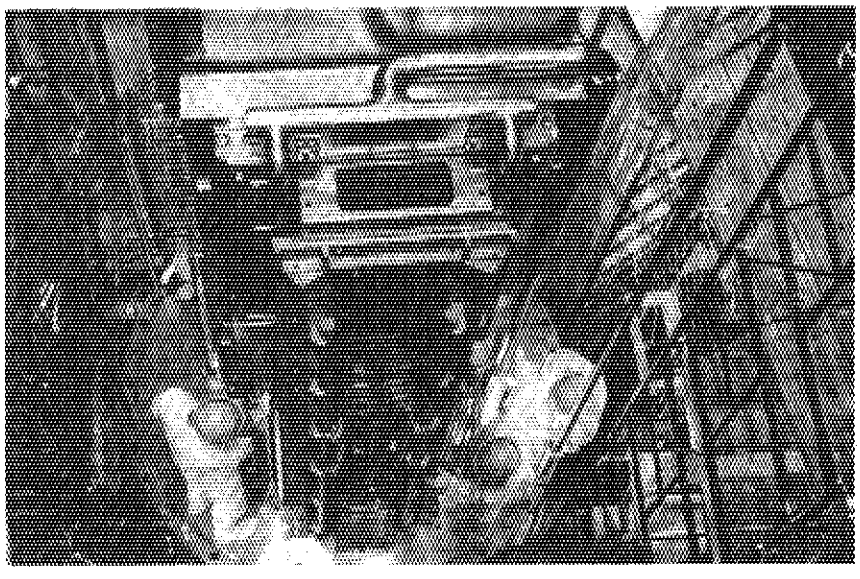

Fig.V.2.2-3 The reflecting magnet

3. Radio-Frequency Heating System

3.1 R&D study for RF heating system

Key components of the RF heating system are a high power tube and a coupler. Extensive study including R&D of these two parts are being conducted in JAERI. In JT-60, both Lower Hybrid Range of Frequencies (LHRF) and Ion Cyclotron Range of Frequencies (ICRF) heatings are in scope. In the LHRF, waveguide coupler is easily applicable to the JT-60 and is being developed smoothly based on the successful results in the JFT-2 experiments.[1-3] An application of a ridged waveguide to the ICRF heating has also begun to study in the cooperation with the Tokyo Institute of Technology. R&D of 1.1 MW klystron specially designed for fusion application is also proceeding in the cooperation with Toshiba electric company and Nippon electric company.

3.1.1 Development of waveguide coupler

A phased array of 8 waveguides of 4 stories (32 waveguides in total) will be used as a launcher for the LHRF heating in the JT-60. An example of the front shape of the launcher is shown in Fig.V.3.1-1. Four launchers will be placed in four ports of the vaccum chamber to inject 10 MW of a net RF power into the plasma core, which requires RF power density of 3.5-4.0 kW/cm^2 with 10 sec. at the mouth of the launcher. Available power density in the present time is $\sim$2 kW/cm^2, because of the limitation of power source. Several improvements of the launching system have been done to get the present level of the power density. From our cumulative data in the JFT-2 experiment, the follwoing points are important in the tokamak environment.

(1) To reduce the electric field strength near the ceramic window.

(2) To keep the low pressure both in the vacuum waveguide and the vacuum side of the ceramic window.

(3) To reduce the secondary electron emission of the narrow mouth of the launcher.

(4) To eliminate the seeds of the arc.

Large area ceramic window is effective for the (1), but it also make the volume of the vacuum waveguide large because the ceramic window must be placed far from the plasma to get the large area. If the conductance of the waveguide is small, the outgas due to the RF should accumulate and it must be the cause of the breakdown in the waveguide or the ceramic window. This accumulation must be reduced, as pointed out in the (2). The differential pumping of the waveguide was employed together with the expansion manifold to pump out the outgas in the experiment of the JFT-2. Titanium coating or pure titanium launcher was used for the (3). Contact reformation with copper wires and rounding of the sharp edge were done for the (4). Details of the result of these improvements will be reported elsewhere.[4)]

Outgas from the surface of the vacuum waveguide during the RF shot will be extremely important problem in the JT-60, since the launcher will be operated in the long pulse of 10 sec. and the high power density. Therefore the launcher of the JT-60 will be baked out with the temperature of 400 - 500°C.

As for the ridged waveguide for the ICRF, we are planning to use the modified ridged waveguide without a ceramic loading, which is proposed by Perkins and Goto.[5),6)] Due to the limitation of the port size in JT-60, frequency of more than 90 MHz is required to achieve the significant power injection to the plasma. A simplified example of the front shape of the LCRF waveguide for the JT-60 is shown in

Fig.V.3.1-2.

3.1.2 R&D work of 1.4 MW klystron

R&D works of the high power klystron has started in the middle of the 1980. The desired specifications of the tube aimed at the fusion application is shown in Table V.3.1-1. Key features of the klystron for JT-60 are (1) high power output 1.1 MW, (2) wide mechanical tuning range (f_0 ± 15 %) and (3) large load VSWR of 2-3. Some of these specifications have become to be in scope by using CAD study and cold test of the compornents. But more extensive study and manufacturing of the test tube are needed to approarch the specification in Table V.3.1-1. An example of the outside view of the klystron is shown in Fig.V.3.1-3.

References

1) Nagashima, T. and Fujisawa, N.: In Proceedings of the Joint Varenna-Grenoble Int. Symp. on Heating in Toroidal Plasma, Grenoble (1978).

2) Fujii, T., et al: In Proceedings of the 7th Int. Conf. Plasma Physics and Controlled Nuclear Fusion Research, Innsbruck (1978) IAEA-CN-37/A4-2.

3) Imai, T., et al.: In Proceedings of the 4th Topical Conf. on RF Plasma Heating, Austin (1981) C2.

4) Fujii, T., et al.: to be published.

5) Perkins, F.W.: ibid of Ref. 3), B13.

6) Goto, N., et al.: Private Comunication.

Table V.3.1-1 Specifications of 1.4 MW klystron.

Frequency	2.0	GHz
Output Power (Saturation)	1.4	MW
Instantaneous Band Width (1dB)	6	MHz
Mechanically Tunnable Band Width	± 150	MHz
(Desired Value)	± 300	MHz
Efficiency	$\geq$ 50	%
Power Gain	$\geq$ 40	dB
VSWR Capability	$\geq$ 2	
(Desired value)	$\geq$ 3	
RF pulse length	10	sec.
Repetation Period	10	min.
Typical Output Power	1.1	MW
Driving Power	$\leq$ 200	W
Beam Voltage	87	kV
Beam currents	30	A

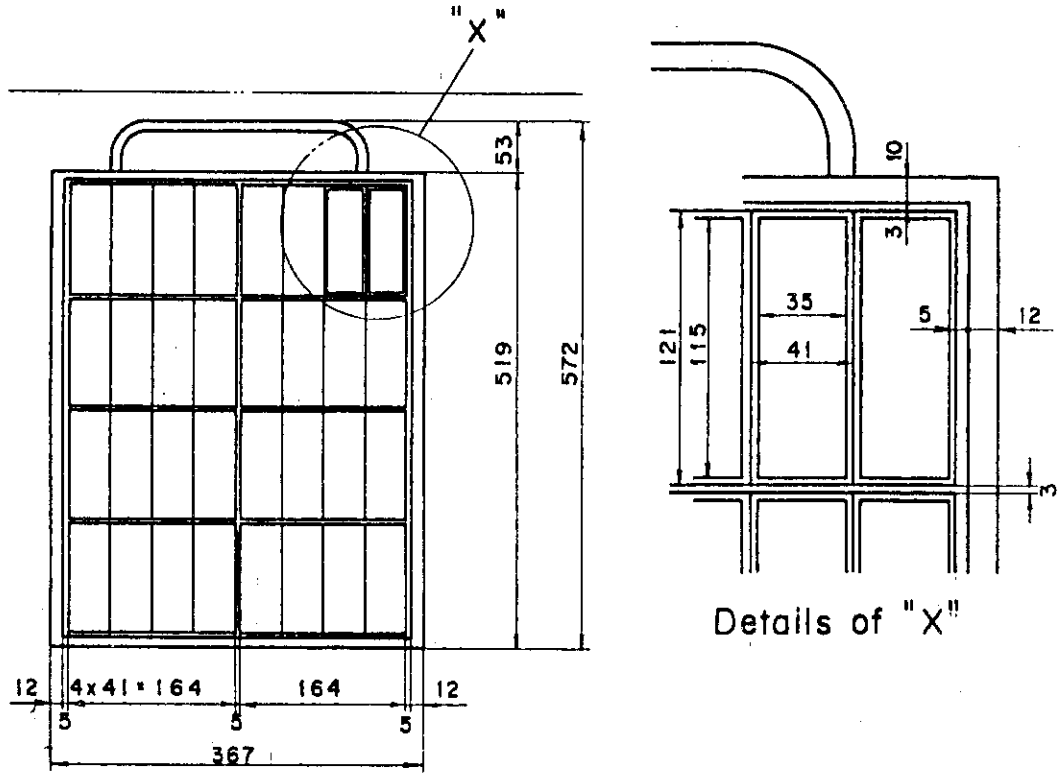

Fig.V.3.1-1 Front shape of the phased array for JT-60.

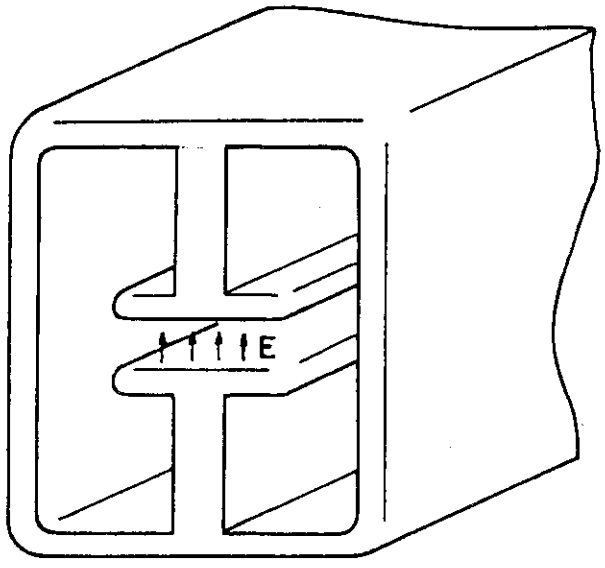

Fig.V.3.1-2 Simplified schematics of the ICRF waveguide.

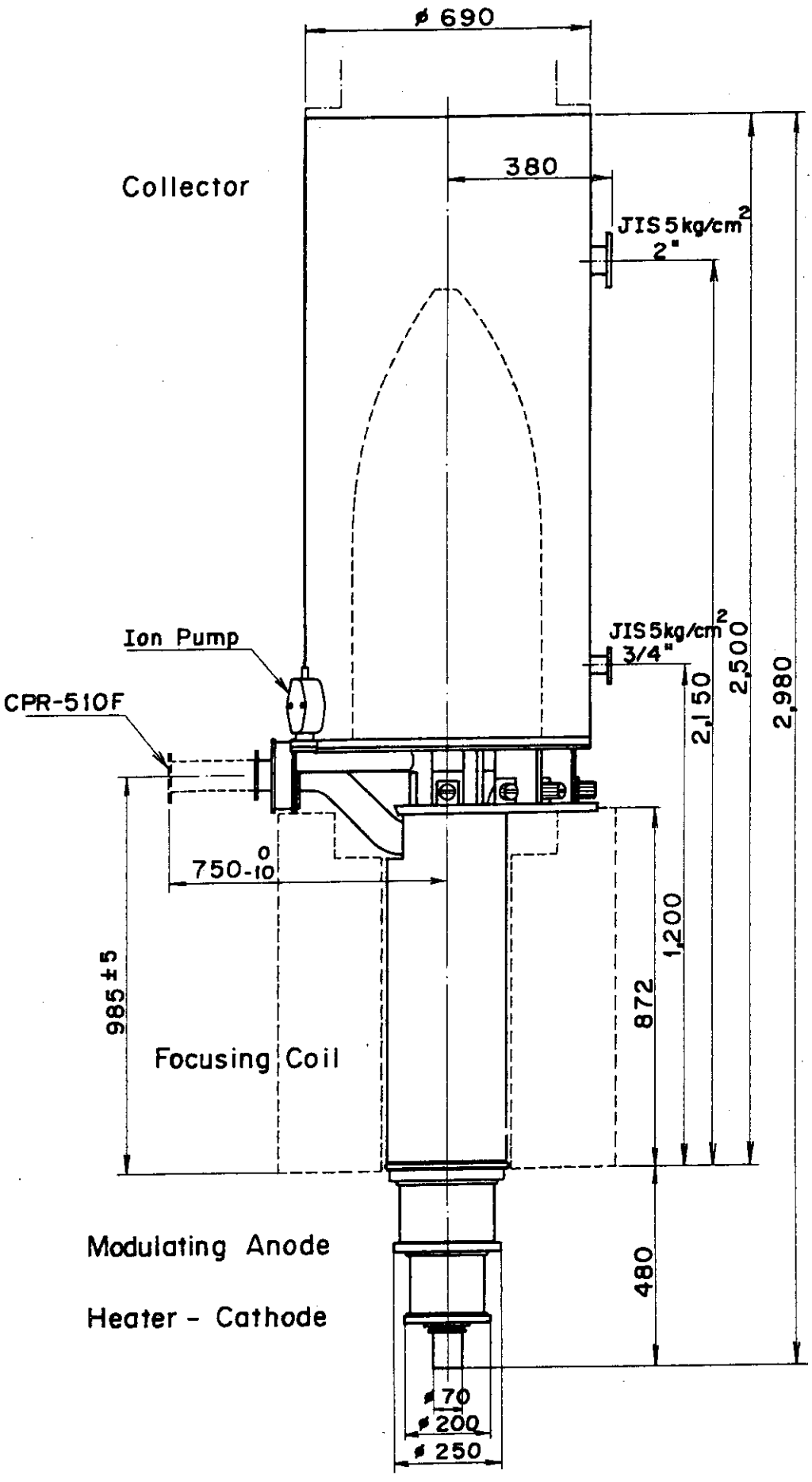

Fig.V.3.1-3 Example of the outside view of the JT-60 klystron.

3.2 Radio-Frequency heating system in JT-60

RF heating power required in JT-60 is 10 MW into the plasma core. Overview of the whole LHRF heating system had been already made public in the last report.[1),2)] Basic specification of the system is described in the Table V.3.2-1. The LHRF system consists of four units of high power RF generator apparatus and launcher with D.C. power supplys and control system. Each unit has 8 klystrons of 1.1 MW/tube. Overview of the system is shown in Fig.V.3.2-1. Details of some subsystem have been further advanced in accordance with the requirement of the JT-60 program. They are (1) the design of the support structure of the launcher against the earthquik, (2) control system and (3) D.C. power supply. Design of the other parts are also reformed in accordance with the experimental need.

Conceptual design of the ICRF heating system of 2-3 MW injection has also been performed.

3.2.1 LHRF heating system

(1) Low power drive train

One of the attractive points of the RF heating is the flexibility of the control of RF parameters of RF power p_{RF}, phase difference $\Delta\phi$ and, in some case, frequency f. In the JT-60 experiment, Real Time Feed-back Control (RTFC) of whole tokamak system will be required to attain the aimed plasma parameters. The flexibility of the RF system is one of the key measures of the RTFC. This flexibility of the RF is condensed in the low power drive train. Block diagram of the low power drive train is shown in Fig.V.3.2-1. The μ-processor of the excitation controller enables to switch the pin attenuators and phase

shiteres of excitation modulators within 1 ms.

(2) High power Amplifier

Heart of this section is the klystron of the saturation power of 1.4 MW, which is now underdevelopment, as described in the section 3.1.2. The specifications of the klystron are high power (1.1 MW), wide mechanically tunable band (1.7-2.3 GHz) and strong against the VSWR ($\leq$ 3), though they are expected values. These features give an exclusion of high power circulators and make it possible to control frequency in real time in accordance with the plasma parameters.

(3) Control system

RF heating system is one of the key blocks which enable the RTFC in JT-60. Therefore the control system should have organic connection with the total control system in JT-60 (ZENKEI). Block diagram of the control system is shown in Fig.V.3.2-3. Mini-computer system and CAMAC system are adopted to make an automatic control of the RF plant. The real time feed back control of the RF parameters is also performed with this CAMAC system.

P_{RF} and $\Delta\phi$ are controlled with the time constants of 1 ms and 10 ms, respectively, in accordance with the plasma parameters. The command of the control is transmitted from ZENKEI computer through the bite serial high way. RF mini-computer system also provides the flexible function to control the RF parameters at the center console in order to carry out the aging and conditioning of the launcher.

(4) Wave launching system

Detailed design of the support structure was accomplished. Simplified schematics of the support structure is shown in Fig.V.3.2-4. Some reformation of the design of the phased array of 32 waveguides was made. Baking temperature of the launcher is increased from 250°C

to 400-500°C, corresponding to the result of the experiment of 3.1.1.

(5) D.C. power supply

One klystron needs 90 kV × 30 A D.C. power supply to yield the saturation RF power of 1.4 MW. We designed 90 kV × 70 A D.C. power supply to drive two klystrons. 16 D.C. power supplys will be used in total. Half of them are planned to be able to use as the D.C. power supply for the ICRF system by changing the connection of the D.C. generator module. One module has the capacity of 22.5 kV × 35 A. Series and parallel connections of 4 modules enable to use them for the LHRF and ICRF, respectively.

3.2.2 ICRF heating system

2-3 MW experiment of the ICRF heating to testify the waveguide coupling and to compare the difference between the waveguide coupling and loop antenna is planned in JT-60. Frequency range for the ICRF is from 45 to 90 MHz, corresponding to the toroidal field and heating scheme. Lower limit of the frequency to be able to use the ridged waveguide is about 80 MHz. Therefore, final power tube will be TH 518 of Thomson CSF or Eimac 2170 tetrode. Line up of the ICRF system is shown in Fig.V.3.2-5.

References

1) Annual Report of the Fusion Research and Development Center for the Period of April 1, 1979 to March 31, 1980, JAERI-M 9421 (1981).

2) Nagashima, T., Imai, T., Uehara, K., Shirakata, H. and Fujii, T.: First Report on the RF Heating Systems for JT-60, unpublished.

Table V.3.2-1 Specifications of the LHRF system for JT-60.

RF Parameters

Frequency f	1.85-2.15 (1.7-2.3)	GHz
Injection Power P_{RF}	0 - 10	MW
Phase Difference $\Delta\phi$	0 - 360	Deg.
RF Pulse Length t_p	0 - 10	sec.

Launching System

Type	A Phased Array of 8×4 Waveguides
Number of Launcher	4
Size of Each Waveguide	115 mm × 35 mm
Baking Temperature	400 - 500 °C
Base Material	SUS 304 or 316

High Power RF Generator

Power Tube	1.4 MW klystron
Number of Tubes	32
Circulator to protect Tubes	NONE
Total Transmission Loss	< 2.0 dB

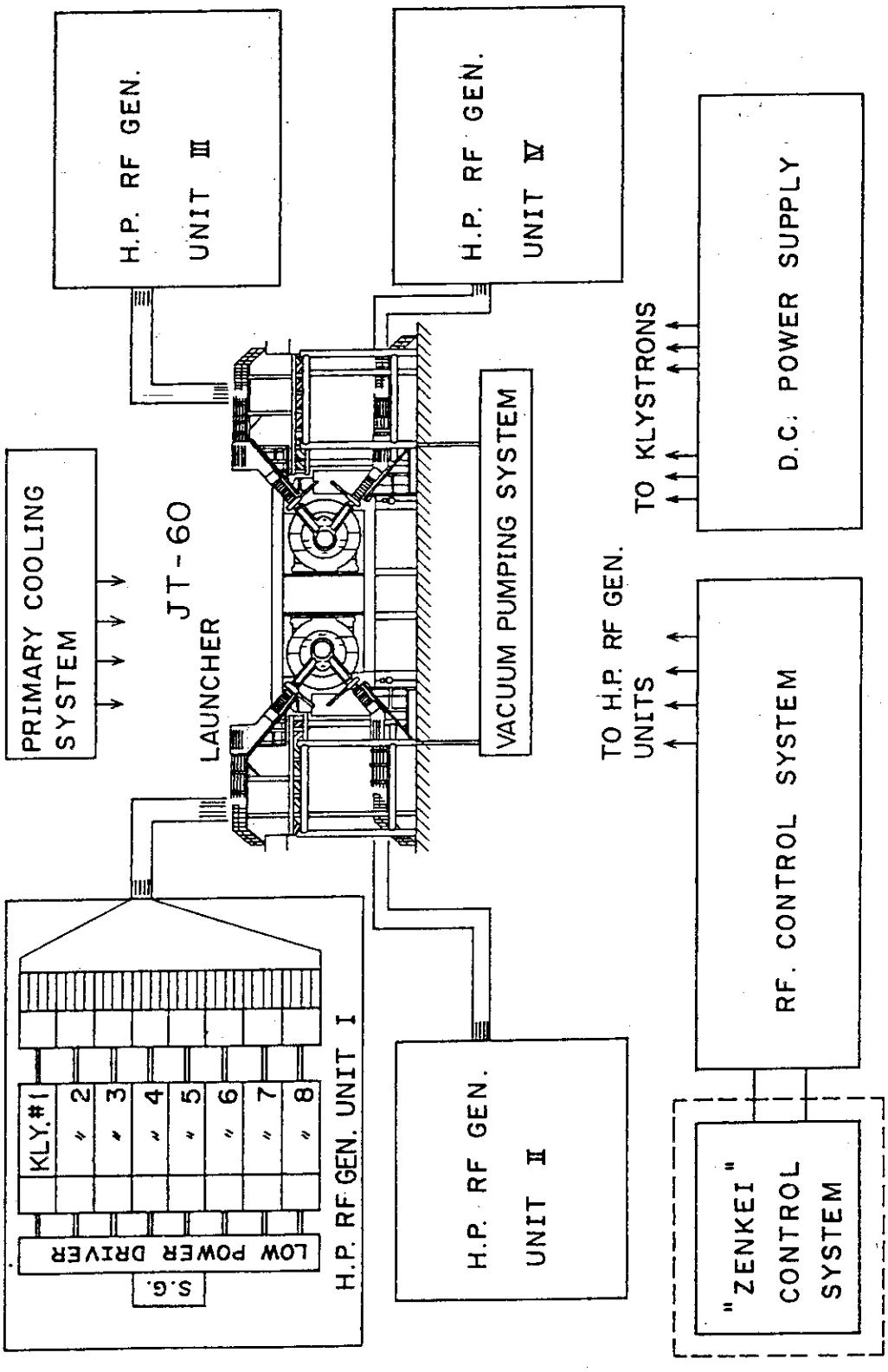

Fig.V.3.2-1 Over view of the LHRF system for JT-60.

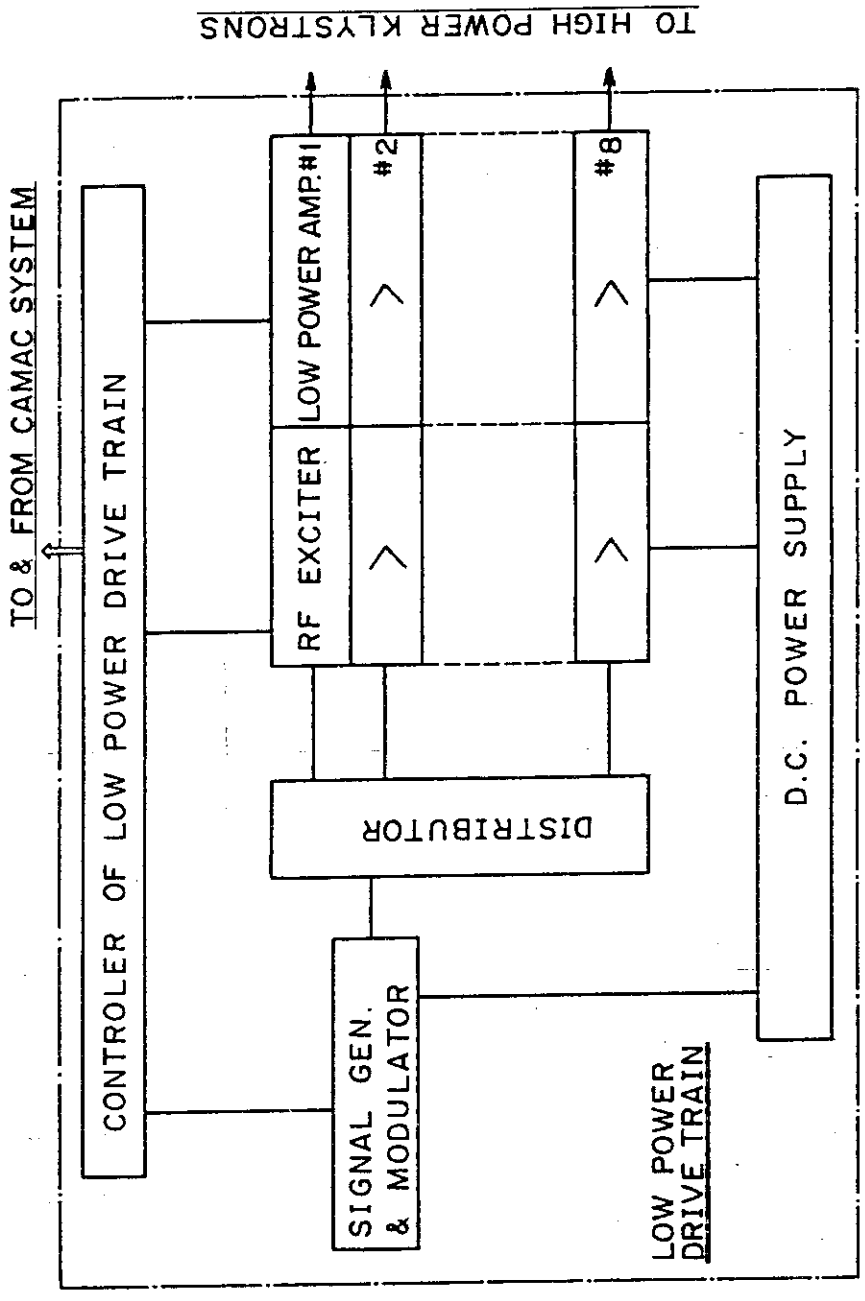

Fig.V.3.2-2 Block diagram of the low power drive train.

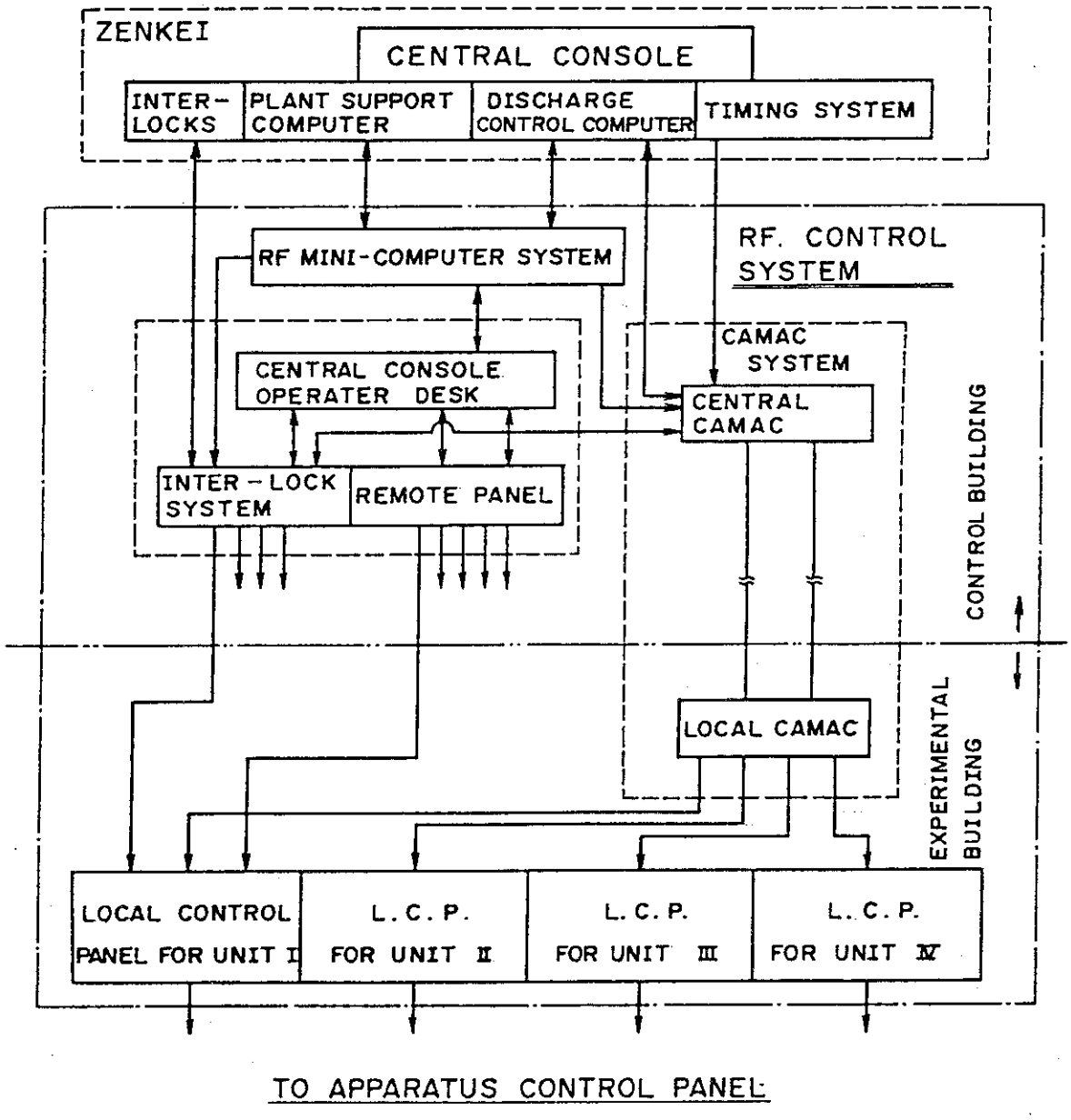

Fig.V.3.2-3 Block diagram of the RF control system.

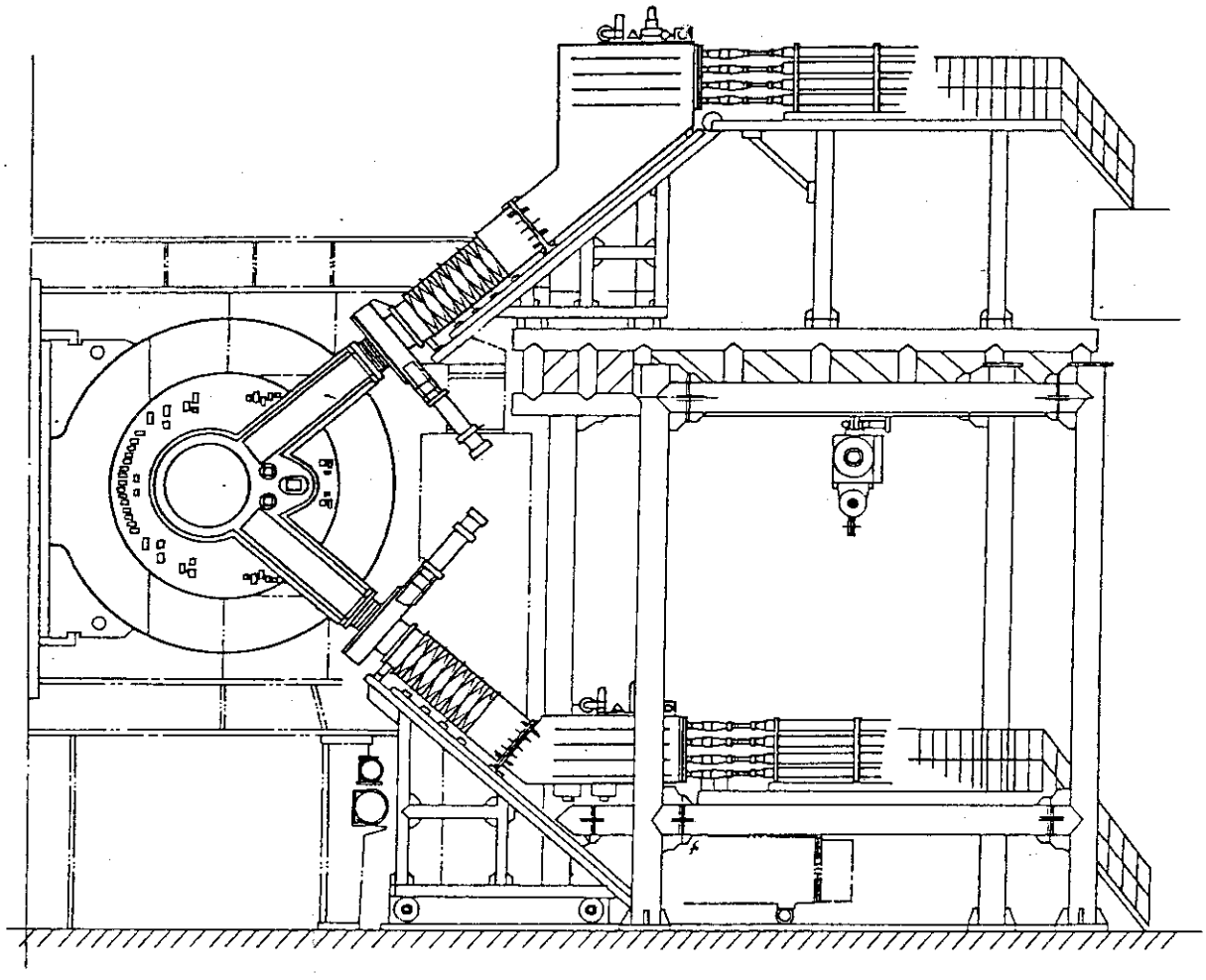

Fig.V.3.2-4 Support structure of the launching system.

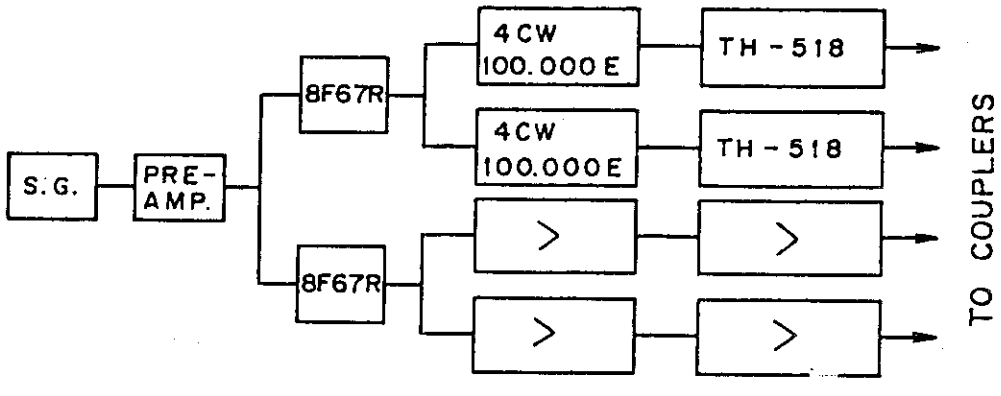

Fig.V.3.2-5 An example of the line up the amplifiers of the ICRF system for JT-60.

VI. SURFACE SCIENCE AND VACUUM TECHNOLOGY

1. Introduction

In JAERI, the plasma surface interaction study for fusion materials was started in 1975, and has been continued in close connections with the JT-60 project, JFT-2, and JFT-2a experiments. The primary objective of this study is to investigate the surface processes such as sputtering, blistering, chemical reaction, arcing, evaporation and trapping/detrapping by using ion accelerators and in some cases by using tokamaks. Three ion accelerators, LSP (0.1 - 6 keV), MSP (up to 30 keV) and HSP (up to 400 keV), have been provided for the experiments. A heavy ion source is under construction for self-sputtering experiment. The second objective of this study is to develop wall fabrication techniques which include surface coating, surface cleaning and related vacuum technology. Vacuum Technology Group in JT-60 Project Office I has the responsibility for the second objective (see Chapter X). A study on the vacuum technology for tokamak reactors is also advanced.

In this fiscal year of 1980, an emphasis was laid on the evaluation of low-Z materials and low-Z surface coatings since results from recent plasma experiments with additional heatings raised serious questions about the use of conventional first walls with high atomic number. Chemical sputtering yields of sintered TiC and vapor-deposited TiC were measured with hydrogen ions in the energy range of 0.1 - 6 keV. Surface deformation and re-emission characteristic of various types of carbon were measured with 200 keV helium ions at ambient temperature. For the evaluation of low-Z surface coatings, thermal fatigue and thermal shock tests were made on small samples of C/Mo, TiC/Mo, TiN/Mo, C/Inconel,

TiC/Inconel and TiN/Inconel. Besides these experiments, mechanisms responsible for the initiation of unipolar arcs was studied in JFT-2. As to vacuum technological studies, considerations were made on helium pumping with cryosorption pumps and mercury diffusion pumps.

2. Construction of Self-sputtering Testing Accelerator

The construction of a Self-Sputtering testing accelerator (SSP) was started in the fiscal year of 1980 and completed in July 1981. It was intended to cover the ion species lacked in LSP and MSP. Thus, a sputtered ion source was employed. The available ion energy ranges from 0.1 to 30 keV.

A schematic diagram of SSP is shown in Fig.VI.2-1. Some characteristic features of SSP are as follows: Beams of positive ions from both solids and gases are available. Ions in the sputtered ion source which is kept at potential V_a are extracted at an energy of $e \cdot V_{ext}$ and the emergent beam is analysed with a sector magnet (radius: 20 cm, deflection angle: 90°). The mass-analysed beam with the kinetic energy $e \cdot V_{ext}$ in a beam drift tube is decelerated down to the final energy $e \cdot V_a$ before the impingement on a sample target. A 400 liter/sec turbo-molecular pump and a 400 liter/sec sputter-ion pump serve to evacuate the beam line and the target chamber, respectively. A pressure of 3×10^{-6} Torr was recorded in the target chamber under the operating condition. Typical beam currents obtained at the energy of 10 keV are 8 μA, 10 μA and 6 μA for Mo^+, Ti^+ and C^+ beams, respectively.

3. Experiments on Chemical Sputtering of TiC

Measurement of chemical sputtering yields of sintered TiC and

physical-vapor-deposited TiC* was made at the proton energies of 0.1, 1 and 6 keV. The target temperature ranged from 30 to 700°C. (* Reactive ion plating of TiC on molybdenum was done in ULVAC).

In Figs.VI.3-1 and 3-2 are shown the measured equilibrium production rates of methane from the sintered TiC and the vapor-deposited TiC, respectively. In both cases, the methane production rate increases with increasing the target temperature in the temperature range between 400 and 700°C. The main difference in temperature dependence between the two samples appears below 400°C. The rate from the sintered TiC is nearly constant, whereas the rate from the vapor-deposited TiC increases with decreasing temperature in this low temperature range. In both cases, however, the methane production rate from TiC is about one order of magnitude lower than that from carbon at 1 keV.[1] The chemical sputtering yield of chemical-vapor-deposited TiC is under investigation.

4. Experiments on Surface Erosion of Various Types of Carbon[2]

Surface observations and re-emission measurements were made on pyrolytic graphite, reacotr grade graphite and glassy carbon with polished and non-polished surfaces under 200 keV helium-ion bombardment at ambient temperature.

Table VI.4-1 shows the summary of the results on surface deformation and re-emission characteristic of the carbon materials examined. The main results are as follows:

(1) Surface deformation mode and re-emission behavior depend strongly on the types of carbon materials as well as their surface states.

(2) Remarkable surface deformation such as cracking and exfoliation of

the surface layer takes place in both basal- and edge-oriented pyrolytic graphite accompanying with a helium-gas burst.

(3) Eroded surface morphologies in reactor grade graphite are characterized by an agglomerated structure with micro-grains as well as their anisotropic nature.

(4) Little topography change takes place in glassy carbon.

(5) Severe erosion occurs more in polished surface than in non-polished surface.

5. Thermal Fatigue Test of Low-Z Surface Coatings

In order to screen candidate low-Z surface coatings for the JT-60 first walls, thermal fatigue test was made on small samples of C/Mo, TiC/Mo, TiN/Mo, C/Inconel, TiC/Inconel and TiN/Inconel. The coating specifications are summarized in Table VI.5-1.

In this experiment, the small samples of 10 mm × 10 mm × 0.5 mm were subjected to infra-red heat irradiation. The infra-red heat irradiation was done under a high vacuum ($<10^{-4}$ Pa) by using a conventional infrared lamp furnace. A thermal cycle with a steep temperature rise (ca.160 deg/sec from 250 to 1400°C for the molybdenum substrate samples and from 250 to 1000°C for the Inconel substrate samples) was applied to the samples. The carbon on both substrates showed partial peeling off after one cycle of the heat irradiation. In the TiC and TiN films on molybdenum cracks grew with the thermal cycles, but the films never peeled off even after the maximum number of heat cycles of 3000. In the TiC and TiN films on Inconel there was no evidence of cracking or peeling off after the maximum cycles of 50. Figures VI.5-1 and 5-2 show the crack growth in the coated layers with the

thermal cycles.

6. Thermal Shock Test of Low-Z Surface Coatings

Thermal shock test was made on small samples of TiC/Mo, TiN/Mo, TiC/Inconel and TiN/Inconel by using a neutral beam apparatus, ITS-2. In this experiment, the small samples of 10mm × 10 mm × 0.5 mm were subjected to pulsed hydrogen beam irradiation. The hydrogen beam apparatus was operated at an accelerating voltage of 44 kV and a power density of 2 kW/cm^2. The pulse length was varied from 0.1 to 0.4 sec. During the irradiation surface temperature of the samples was monitored with an infra-red camera.

Thermal shock test showed that, in the case of chemical-vapor-deposited TiC on molybdenum, there was no evidence of failures until the melting of the substrate under the coated layer. The melting of the substrate resulted in a very sudden failure of the coated layer since the heat transfer from the film to the substrate was severely reduced when the melting occurred. Figure VI.6-1 shows the samples after an irradiation with different pulse lengths. On the other hand, for ion-plated TiC on molybdenum the allowed maximum pulse length (or beam flux) was limited by exfoliation and spalling of the coated layers. This may be due to a poor thermal contact between the film and the substrate. In the case of chemical-vapor-deposited TiN on molybdenum, there was no evidence of exfoliation or spalling until the melting of the substrate, but the golden-colored film was faded away into grey by the hydrogen beam irradiation. This may be due to the thermal decomposition of TiC.

7. Plasma Wall Interaction Studies in JFT-2

Mechanisms responsible for the initiation of unipolar arcs on the tokamak first wall were studied by mesuring plasma parameters in the scrape-off layer at the onset of arcing. It was shown that a large electric field in the sheath region produced by runaway electrons is the dominant cause of the arc initiation. The boundary plasma temperature and density at the moment of arcing also contribute the arc initiation. Moreover, a difference of the arc frequency in the toroidal direction on limiter surfaces, which has been observed in several tokamaks, was explained by an asymmetry of ion flux as a result of the ion drift motion. Figure VI.7-1 shows the asymmetry of the ion flux in the plasma boundary obtained by a directional probe.

References

1) Yamada, R., Nakamura, K., Sone, K. and Saidoh, M., J. Nucl. Materials 95 (1980) 278.

2) Saidoh, M., Yamada, R. and Nakamura, K., J. Nucl. Materials 102 (1981) 97.

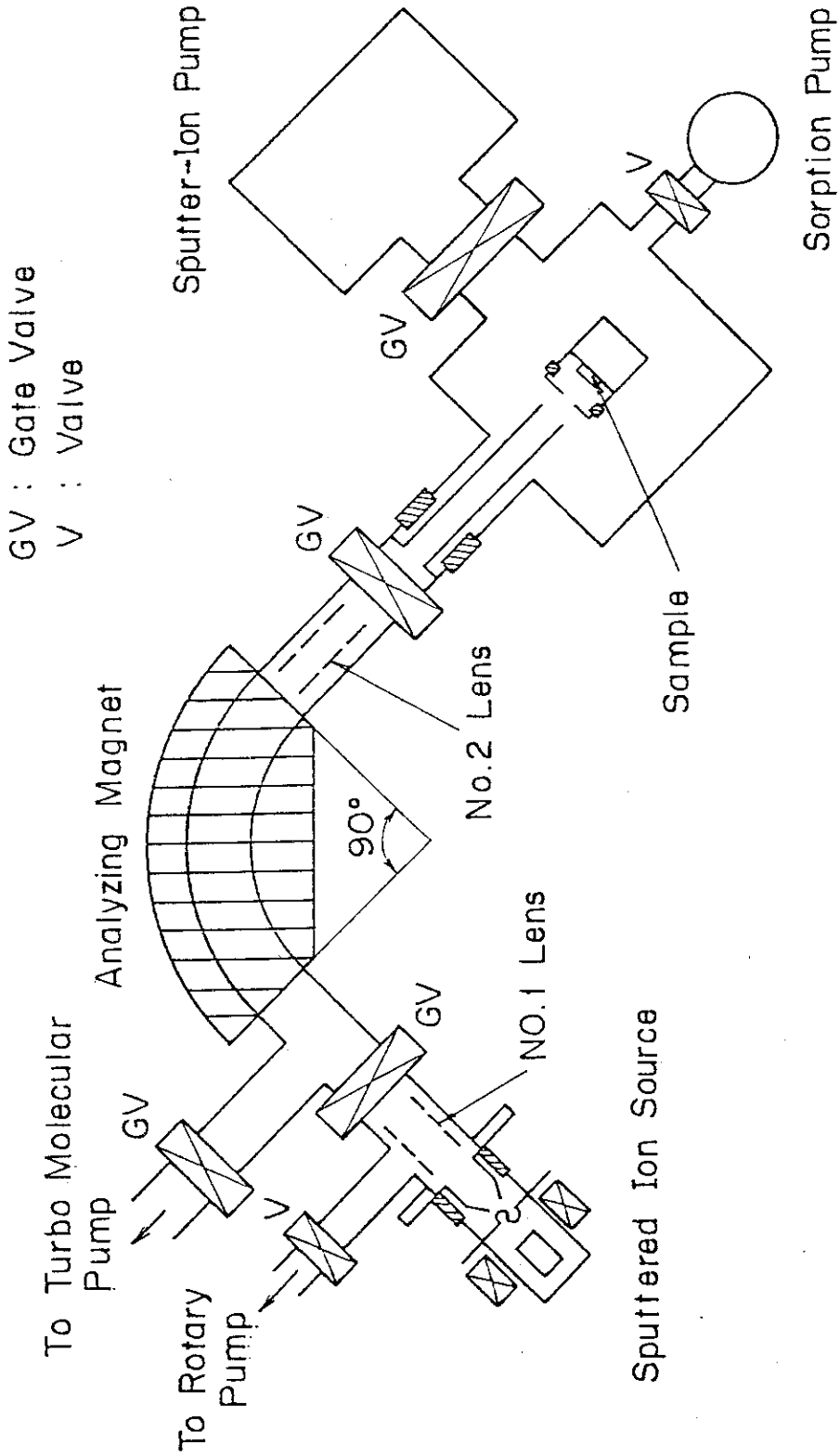

Fig. VI. 2-1 Schematic diagram of self-sputtering testing accelerator.

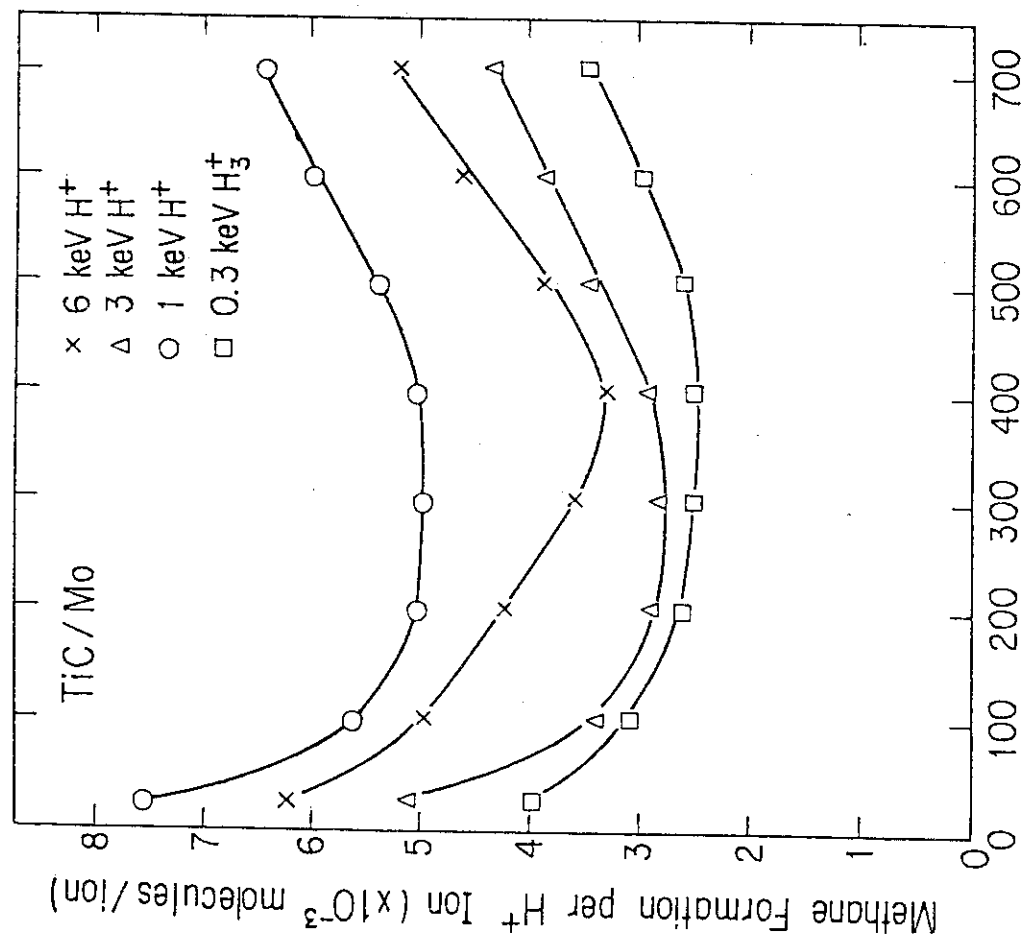

Fig. VI. 3-2 Measured methane production rates from ion-plated TiC.

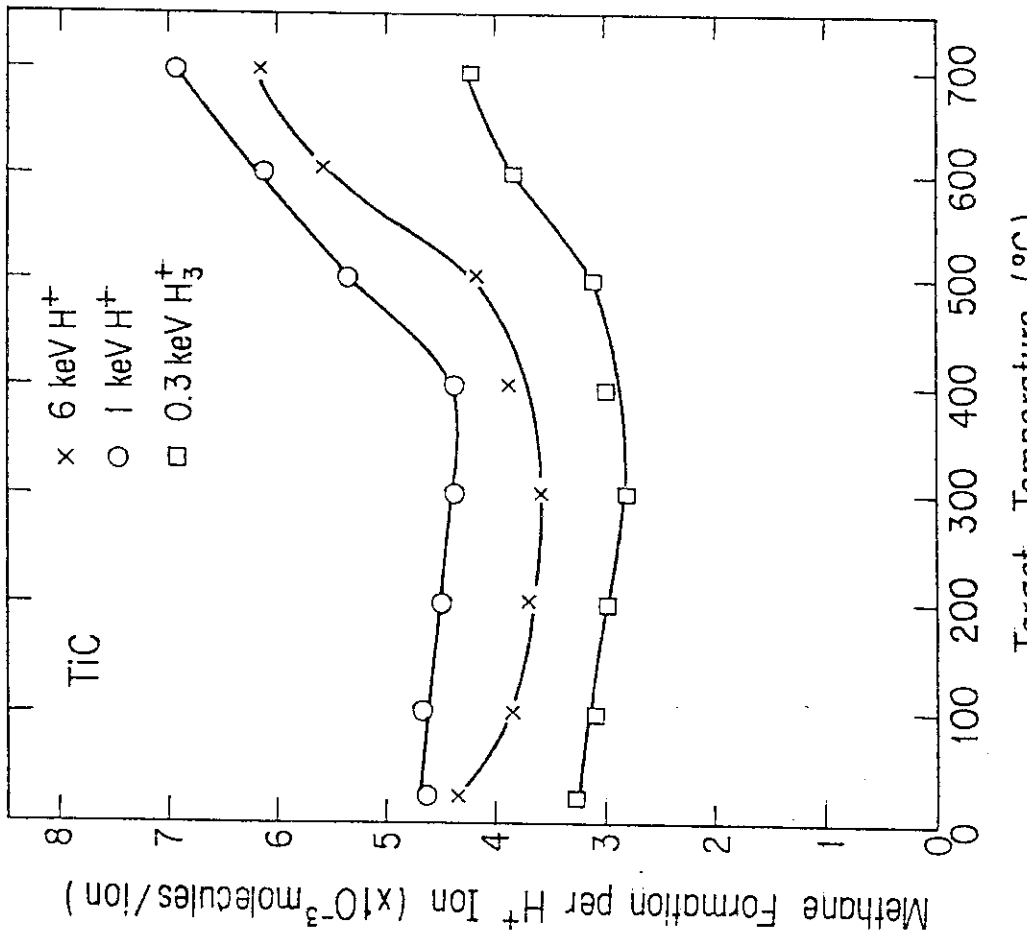

Fig. VI. 3-1 Measured methane production rates from sintered TiC.

Table VI. 4-1 Fluences for onset of helium re-emission, for attainment to a steady state and for initial occurence of gas burst and surface deformation mode in various types of carbon bombarded with 200 keV helium ion up to a fluence of 2.5×10^{18} He^+/cm^2.

			Fluence (He^+/cm^2)			Deformation mode
			Onset of re-emission	Steady state	First gas burst	
PG-A	Basal plane	Polished	2.0×10^{17}	1.6×10^{18}	7.8×10^{17}	Crack + cone/roundish protrusion
		Non-polished	0.6×10^{17}	1.0×18^{18}	3.4×10^{17}	Crack + roundish protrusion/layer
	Edge plane	Polished	2.5×10^{17}	4.5×10^{17}	3.6×10^{17}	Exfoliation + ridge and groove (fibrous structure)
		Non-polished	Onset of irradiation	3.0×10^{17}	None	Ridge and groove (fibrous structure)
7477PT		Polished	1.5×10^{17}	8.2×10^{17}	None	Ridge and groove (fibrous structure + spheroidal structure)
		Non-polished	Onset of irradiation	8.2×10^{17}	None	Ridge and groove (spheroidal structure)
GC-30		Polished	0.5×10^{17}	3.0×10^{17}	None	No change
		Non-polished	Onset of irradiation	0.3×10^{17}	None	No change

Table VI. 5-1 Materials and coating methods examined.

Coating Materials	Coated Film Thickness (μm)	Substrate Materials	Coating Methods
C	20	Mo	DVD
C	20	Inconel	DVD
TiC	20	Mo	RIP
TiC	20	Inconel	RIP
TiC	20	Mo	CVD
TiN	20	Mo	CVD
TiN	20	Inconel	CVD

DVD: Discharge vapor deposition
RIP: Reactive ion plating
CVD: Chemical vapor deposition

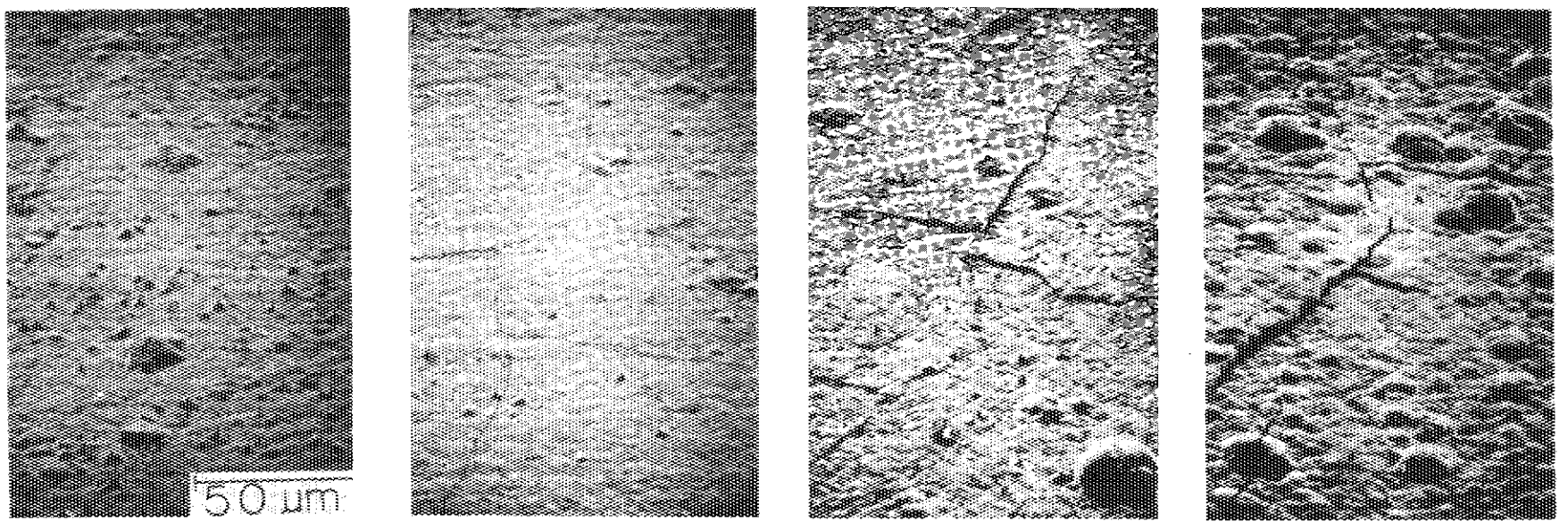

Fig. VI. 5-1 Scanning electron micrographs of chemical-vapor-deposited TiC on molybdenum before and after heat cycles. The numbers below photographs indicate the number of heat cycles.

TiC on Mo (RIP)

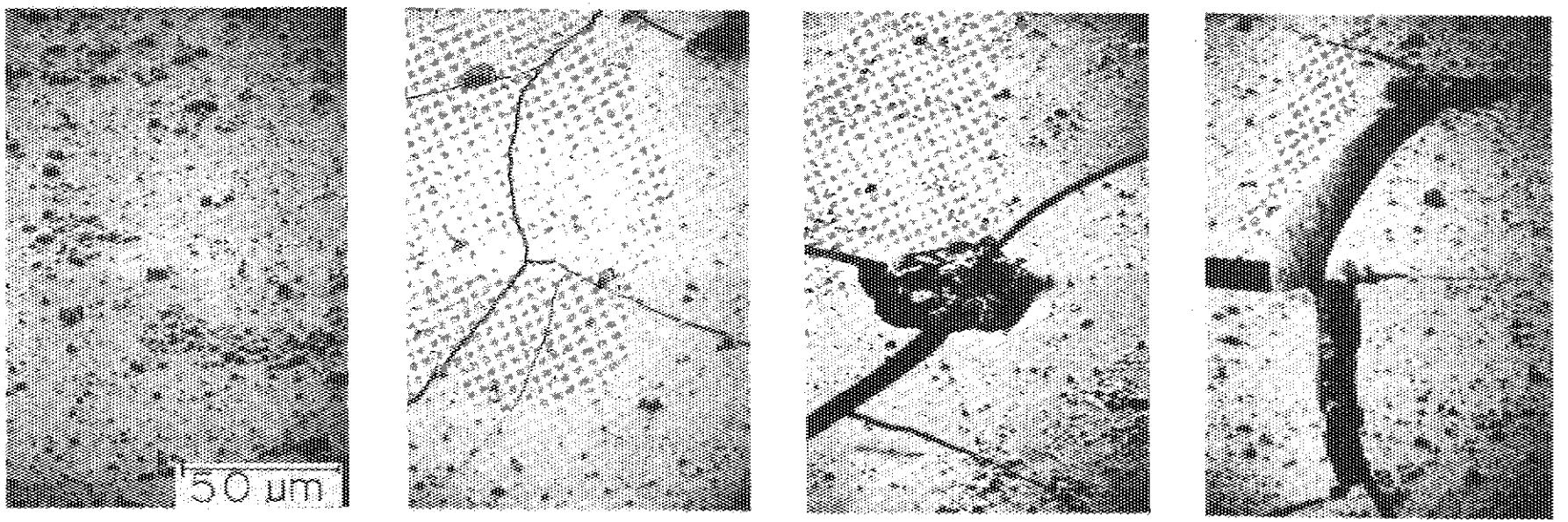

as deposited | after 100 cycles | after 1000 cycles | after 3000 cycles

Fig. VI. 5-2 Scanning electron micrographs of ion-plated TiC on molybdenum before and after heat cycles. The numbers below photographs indicate the number of heat cycles.

TiC on Mo (CVD)

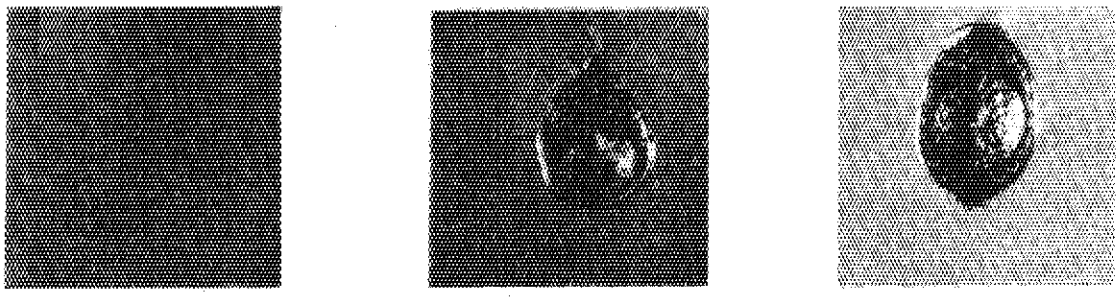

0.3 sec　　0.35 sec　　0.4 sec

Fig. VI. 6-1 Photographs of chemical-vapor-deposited TiC on molybdenum after a single pulse of hydrogen beam irradiation with different pulse lengths.

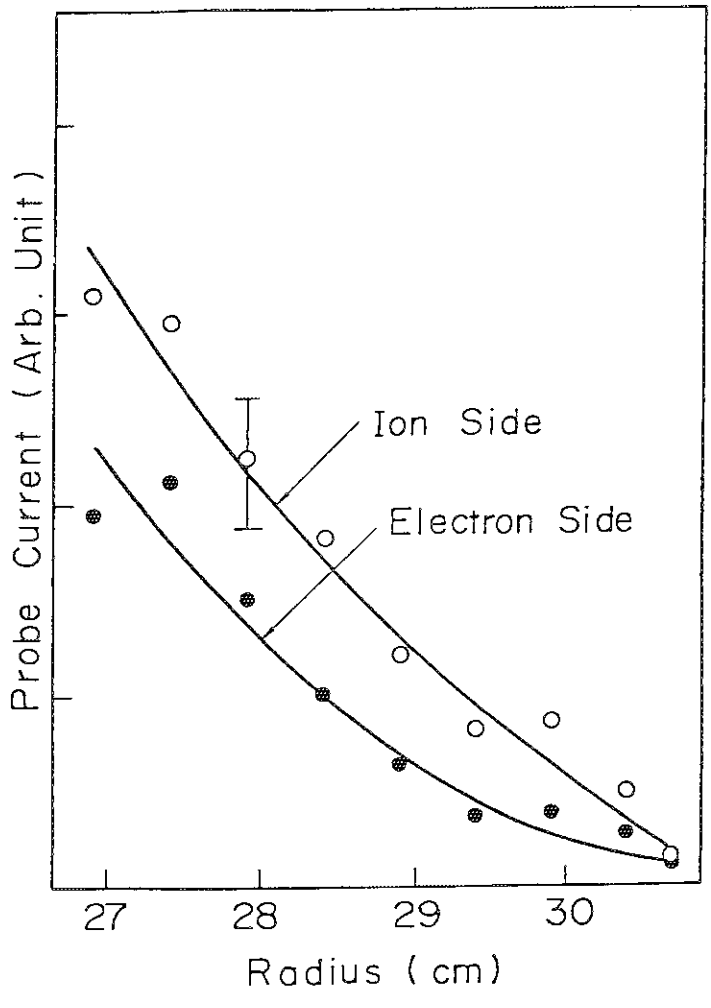

Fig. VI. 7-1 Radial profiles of the ion saturation current at the moment of arcing obtained by a directional probe.

VII. SUPERCONDUCTING MAGNET DEVELOPMENT

1. Introduction

The main objective of superconducting magnet system development work is to establish a capability of construction of the Next Engineering Tokamak after realization of JT-60.

For this purpose, two main projects, Cluster Test Program and Large Coil Task, have been evolved in JAERI since 1977 for toroidal coil development. In FY 80, besides these two projects which will continue for a few years, the conductor development for poloidal coil has been started. The following works have mainly done in FY 80.

i) The successful first operation of Cluster Test Facility

ii) Fabrication of 10T Nb_3Sn Test Module Coil

iii) Fabrication of the Japanese LCT coil

iv) Construction of the domestic test facility for the LCT

v) Measurement of mechanical properties of structural material at 4.2 K

iv) Development of 10 kA poloidal conductor

vii) Conceptual design and analysis of superconducting magnet system for the Next Engineering Tokamak

2. Cluster Test Program

2.1 Operation of the cluster test facility

The Cluster Test Facility (CTF), in which a test module coil (TMC) is tested, is composed of two Cluster Test Coil (CTC), a 100 1/h helium liqefier/240 W at 4.2 K refrigerator system, a 3000 A-10V D.C. power

supply and magnet protection system, and a data aquisition and control system. This facility is significant to design the superconducting tokamak coil system after JT-60.

The construction of CTF was finished in May 1980, and the first operation was successfully carried out from the end of July to the middle of August. The detail of the test results were described in reference[1]. And the advanced operation was carried out in April 1981.

2.1.1 Test operation

As the first operation, the cool down was carried out modestly in order to avoid excessive thermal atress. Since the cooling time of the supporting legs was long unexpectedly, about 270 hours was spent for cool down. In Fig.VII 2-1, it is shown a comparison of the actual cool down characteristics with a theoretical calculation.

Next, temperature in supporting legs was discussed. Below 100 K, the measured temperature was higher than that calculated. Two reasons were considered as follows:

(1) In the higher temperature zone, down to 40 K, supply of coolant on legs was small unexpectedly, especially at the joint between the stainless steel and epoxy leg.

(2) In the lower zone, around 30 K, there existed excessive heat input to the epoxy leg probably causing a radiation.

Now, the more accurate analysis is carring on, and the modification of structure of leg is planning.

Azimuthed stress distribution was measured. In general, it was found that; the stress values were unexpectedly high for winding, and were very low for the helium vessel. In order to match the measured stress, in calculation, Young's modulus in the outer part of winding

must be lowered. From this analysis, it can be understood that the electromagnetic force is not sufficiently transmitted to the outer ring of the helium vessel. This is due to insufficient filling or rigid spacer between the winding and the helium vessel, or due to thermal contraction. Therefore, to establish a stress design for a large coil, it is important to clarify the interface condition between a winding and helium vessel and to make the accurate data of Young's modulus of a winding at low temperature.

2.1.2 Advanced operation

The purpose of the second test was to inspect some improvement and to varify the additional capacity, automatic control, and setting method for TMC operation.

The reformed points are as follows.

1) Radiation through a 30 cm glass window was elminated by blocking the window.
2) A thermal bypass circuit and super-insulation on the surface were added to CTC legs.
3) The valve which caused a cold leak was repaired.
4) The communication lines between computer system and refrigerator system were added. The flow diagram is shown in Fig.VII 2-2.

The results obtained during the second test showed the excellent improvement of the CTF. Fig.VII 2-3 shows the test results of the automatic cool down. The inlet gas temperature was controlled depending on a thermal difference criterion between temperatures at the coil case, the winding, and the support between the two CTC coils. The inlet gas flow was controlled depending on the thermal difference between the two CTC coils. This automatic control method will be applied to

the five coils cool down (CTC × 2, CBC × 2, and TMC) and a final tokamak system. The effect of the thermal bypass and the super-insulation is effective to shorten the cool down time. The heat leak to the two CTC coils at 4.2 K was 45 W, which was less than the design value. The warm up of the CTF was also controlled by the computer, using the same criterion as the cool down.

Other test items included refrigeration operation, a continuous charge hold (6 hours), and a full current dump test, these were carried out to check the facility before installing the TMC.

reference

1) S. Shimamoto et al. "Test Results and Perspective of the Cluster Test Program", MT-7, Karlstruhe, March 1981.

2.2 Fabrication of test module coil

A fabrication of the first Test Module Coil (TMC) was started. The purpose of this coil is to demonstrate the reliability of Nb_3Sn for large current carring conductor in the region of 10T magnetic field.

The main parameters of TMC are shown in Table VII.2-1. The circular TMC has a winding inner diameter of 60 cm, a winding outer diameter of 160 cm, and thickness of 30 cm. The 10-T magnetic field is produced at a operating current of 6,050 A with a background field of 3T from the CTC. The total stored energy, including CTC, is around 30 MJ. The coil's 20 double pancakes are pool-cooled at 4.2 K.

Two conductor grading are employed using Nb_3Sn conductor for field higher than 6.2 T and Nb-Ti for lower field region. Both conductor have the same size of 12.6 mm × 13.0 mm and they are composed of six

stranded cables soldered in the center of a copper stabilizer. The Nb_3Sn strand in fabricated with a bronze method and is composed of 77,454 filaments (331 filaments × 129 units) embeded in the copper matrix. Fig.VII.2-4 shows a whole of Nb_3Sn conductor. The Nb-Ti strand has 1,350 filaments and a copper/superconductor ratio is 2.1. Two conductor surfaces exposed to liquid helium are roughened and oxidized to obtain a high heat flux. This method was developed at JAERI and was used for the Japanese LCT conductor.

Between pancakes is a glass epoxy flat bar spacer whose thickness is 2.6 mm. This spacer is stuck on pancakes and covers 25-% surface of the conductor flat side. The insulation between turns is epoxy impregnated glass tape of 0.3-mm thickness which covers fully the narrow side surface conductor. The allowable gap between turns is less than 0.1 mm so as to avoid conductor movement and to obtain high rigidity. A winding tention of 350 kg is to be used. 316L stainless steel is selected as the structural material for the outerring of helium vessel, whose the stainless steel is used. Final assembly is performed by the electron beam welding.

The fabrication of TMC will be finished in the end of 1981 and testing will be done in the begining of 1982.

3. Large Coil Task of IEA

3.1 LCT coil

JAERI, representing Japan, is now fabricating one of six coil for the International Energy Agency's (IEA) Large Coil Task. All six test coils will be brought together and tested in a toroidal array

at Oak Ridge National Laboratory (ORNL) in the United States.

On the basis of LCT specification issued by ORNL, JAERI carried out the detailed design work in collabolation with three electro-technical companies and three cable campanies in Japan for a year from the middle of 1978. The final design and fabrication of the Japanese LCT coil was started in 1979 with an electro-technical company in parallel with a number of verification tests for the coil. Major parameters of the Japanese LCT coil are shown in Table VII.3-1.

The fabrication of the Japanese test coil will be finished in October, 1981, and it will be tested in the newly constructed domestic test facility up to rated current before transportation to ORNL.

3.1.1 Fabrication of LCT coil

The fabrication of the helium vessel which contains the winding has been continuing since November, 1980. The helium vessel of the Japanese test coil consists of three major assemblies shown in Fig. VII.3-1. These are inner ring, two side plates, and an outer ring. All these parts were manufactured by nitrogen strengthened stainless steel to accommodate the high stress in the "ALT B" test condition defined by ORNL specification. Welding of each assembly was finished by the end of February, 1981, and the results of nondestructive tests showed no problem. Fig.VII.3-2 and Fig.VII.3-3 show the inner ring and outer ring which were welded by the covered electro welding method. The machining of welded structure is now continuing and it will be completed at the end of April 1981.

The conductor winding of twenty double pancakes was carried out in parallel with the fabrication of helium vessel after several practice windings. A schematic view of the winding facility is shown in Fig.VII.3-4.

As a stabilizer of conductor is hard copper, a over bending winding technique is employed. In this method, at first, a certain length of conductor is formed into a small radius with a special jig on the winding frame. Then, this conductor portion is wound back slightly to remove the jig and finally it is wound in the final position. For the insulation between turns, two tapes of 0.22 mm thick impregnated glass cloth are used. The dimensions, flattness, thickness of each pancake, and the damage of the conductor surface were carefully checked and controlled in the winding work. These values were also checked after curing. Fig.VII.3-5 and Fig.VII.3-6 show the view of winding facility and one double pancake of the Japanese test coil, respectively.

The coil is being wound at present and more than half of all pancakes have been completed. In order to shorten the winding time, a second winding line was constructed in the same plant. The new line will come into service in late April 1981, and the winding work will be finished by July 1981. After the completion of the winding work, the wond twenty double pancakes will be installed in the helium vessel by shrink fit technique.

3.1.2 Verification works

In order to verify the reliable operation of the Japanese LCT coil, many verification tests were carried out. The principal tests, described below, were mechanical tests of the conductors and the coil case, and ac loss measurement of the conductors.

1) Tensile test of the conductor

In the detailed design of the Japanese LCT coil, the superconducting stranded cable was not accounted for as a structural member supporting electromagnetic stress. As the design advanced, we realized that the

calculated stress in the conductor was greater than the design value. Therefore, the stress safety margin in the conductor was smaller than desired. To obtain the measured value of ultimate stress, 0.2 % yield stress, and Young's modulus, tensile tests of the full-sized conductor, the soldered strand pack only, and the copper housing only, were carried out at 4.2 K.

Fig.VII.3-7 shows the tensile test results for the full-sized conductor, the soldered strand pack, and the copper housing. From these results, the 0.2 % yield stress of the full-sized conductor is 295 MPa. This value is about 1.5 times larger than the calculated stress. Therefore the Japanese LCT conductor has enough strength.

2) Mechanical tests of the coil case

In order to verigy the mechanical integrity of the coil case against large electromagnetic stress, the tensile test, Charpy test, and fracture toughness test were carried out for the structural material (SUS 304LN) and the weldment at 4.2 K. These results are shown in Fig.VII 3-8. The structural material and the weldment have enough strength and toughness for planned tests of this coil at ORNL.

To clarify the influence of nitrogen and carbon on the meachnical properties, mechanical tests were carried out for candidate structural stainless steel (SUS 304 and SUS 316) with various nitrogen contents. These results of the tests and analysis can be summarized as follows;

i) The ESR method, used in the Japanese LCT coil case, enhances the impact toughness of SUS 304 by a factor of three over the impact toughness of SUS 304 produced by the inductionmelt method.

ii) As the combined nitrogen and carbon content increases from 0.1 wt% to 0.25 wt%, the yield stresses of SUS 304 and 316

increase linearly to about 1.8 time their respective 0.1 wt% values.

iii) Nitrogen is more effective in raising yield stress than carbon.

iv) Addition of nitrogen and carbon has no negative effect on ductility.

v) As the nitrogen and carbon contents increase, the impact energy decrease gradually.

3) Ac loss measurement of the conductor

It is necessary to evaluate the heat generation due to the ac losses in the conductor because the refrigeration power is restricted. We estimated the pulsed field losses both of a signal started and the strand pack by measuring the magnetization. In this measurement, data acquisition and numerical calculation were performed by a minicomputer, PDP-11/34. We compare the measured and calculated losses by means of the time constant of the coupling current, which is a useful figure of merit for ac losses. The measured and calculated values are listed in Table VII.3-1. These calculated values agree reasonably well with the measured ones. Thus, the ac loss of the LCT coil, averaged over one cycle, can be calculated reliably, and is about 8.8 W.

3.2 Domestic test facility

The new building for the domestic test of the Japanese LCT coil was completed on January 7th, 1981. The building is ready to accept the domestic test facility which consists of a cryogenic system, a vacuum system, a data acquisition system, and a power supply with a protection system. By March, 1981, each of these systems was almost completed by the company responsible for it. After technical inspection

by JAERI at the works, some compoennts of the system were delivered to the new building on schedule. Therefore, installation work at JAERI was started.

3.2.1 General lay-out

In the new building, there are about 1760 m^2 of floor space in the experimental area, which is devided into an LCT experimental area, a conductor development and investigation area, and a work shop and machine room. There are about 800 m^2 in the LCT coil experimental area.

3.2.2 Cryogenic system

The cryogenic system for the domestic test consists of a helium liquefier/refrigerator, a pair of helium purifiers, a helium recovery unit, and instruments. Fig.VII.3-9 shows the flow diagram of the system incorporating the main components. The capacity of the helium liquefier/refrigerator is specified as 300 liters of liquefaction perhour or 1 KW of refrigeration at 4.5 K; this permits cooling the coild down in 120 hours and warming up in 60 hours. The flow rate and temperature of the helium gas supplied by the refrigerator can be controlled manually or by the computer so as to avoid excessive thermal stress during cool-down and warm-up. In addition, the turbo-expander circuit is completely separated from the coil circuit (J-T circuit) so that long-term operation can be achieved in safety against thermal and pressure disturbance from the coil. The double J-T method was employed to increases the thermodynamic efficiency of the system. Using this method, the thermodynamic efficiency can be increased to 1/500. Because the ordinary efficiency is around 1/1000-1/1500, this method is very useful for

the cryogenic system in fusion reactors. There are a pair of helium purifiers to clean up the system and the LCT coil before cool-down, and to supply pure helium gas to the system during the liquefaction and refrigeration operation. A single purifier can purify 21 g/s of helium gas, and one can automatically switch from one purifier to others after 24 hours. Returning gas from the LCT coil and other experiments can be stored in the gas bag, which has a maximum capacity of 400 m^3. When the gas bag is filled with gas, a high-level swithch automatically starts a recovery compressor; the compressed helium gas can be stored in an impure gas tank (100 m^3) directly, or in a pure gas tank (100 m^3) directly, or in a pure gas tank (100 m^3) after passage through the helium purifier. The maximum capacity of the recovery compressor is 21 g/s and its outlet pressure is 18 atm. The cold box (helium liquefier/refrigerator) and main helium compressor were delivered to the new building in March, 1981, when the installation and piping work were started. The first test run of the cryogenic system will take place beginning in June, 1981, after several preliminary tests, such as a helium leak test and a proof pressure test.

3.2.3 Vacuum system

The vacuum chamber, the diameter and height of which are 5 m and about 8 m, respectively, was completed at the works (Toshiba Co.) in December, 1980. The results of the vacuum test, proof test, and leak test satisfied JAERI specifications. The vacuum test, proof test, and leak test satisfied JAERI specifications. The vacuum chamber, the vacuum pumps, and the control unit were delivered to the new building on March 15th. On March 26th, the vacuum system was installed and the vacuum test and the leak test for the chamber will be carried

out in April. Fig.VII.3-10 shows the vacuum chamber at the new building.

3.2.4 Data acquisition system

The PDP-11/70 computer for data acquisition and automatic control was installed at the new building on January 16, 1981. Other units for the system (CAMAC modules, CAMAC crates which drive the CAMAC system, and so on) have also been installed. Remaining work includes the interconnection of the many components for this sytem. Since completion of the software design at the end of 1980, computer programs were installed and by the end of March, 1981, each function had been confirmed.

All program outputs (list graphs, plant status, file making on magnetic tape) operate properly.

The performance of the computer system, including value control, will be tested after the cryogenic, vacuum, and power supply system are completed.

3.2.5 Power supply system

The power supply was designed to provide stable, high current to the LCT coil for a long time. It consists of a DC power supply and a high-energy protection system, as shown in Fig.VII.3-11.

The current ripple of the DC power supply, which has a maximum capacity of 30 KA and 12 V, is 6.0×10^{-4} rms. Thus the signals from sensors in the coil can be measured without any electrical noise from the power supply. The DC power supply consists of transistors to control the output current and thyristers to control the voltage of the transistors, as shown in Fig.VII.3-12. The bridge-circuit method was employed to detect the voltage when the LCT coil quenches. The high-speed, DC, air circuit breaker consists of two commercial 8000-A breakers.

A dump resistance and breaker are installed in the dump circuit, the maximum voltage of which is 1500 V. An aluminum bar (400 mm × 700 mm) was employed for the current lead from the DC power supply to the LCT coil. The power supply system were delivered to the new building in March, 1981. Thereafter, installation was satrted.

4. High Field Magnet Development

Concerning the development work for high field superconducting magnet, the achievement of a 10T-15 cm bore coil would with reacted multifilamentary Nb_3Sn superconductor was described in the last annual report. However, that test was carried out with the external Nb-Ti coil in series connection with a power supply and a circuit breaker from the limit of the instrument. After that, by preparating two power supply and two circuit breaker, as a result, with a backgrand field of 8.5T, the first onset of resistivity in the Nb_3Sn coil occurred at a current of 1,040 A, and a field of 11.0 T corresponding to the short sample limit. At a current of 1,090 A and a field of 11.2 T on the conductor, the quench detector initiated a quench after sensing a voltage of 0.5 V for 0.1 sec.. At a current of 1,040 A, the current density in the winding and on the conductor were 64.4 A/mm^2 and 94 A/mm^2, respectively. The estimated total strain at 11T operation was 0.7 %.

This successful result demonstrates the potential feasibility of using reacted multifilamentary Nb_3Sn for the application of larger high field superconducting magnets in a future fusion magnet.

5. Pulsed Poloidal Conductor Development

In the course of the basic study for the Next Engineering Tokamak after JT-60, the necessity of the superconducting poloidal coil system was strongly recommended. Therefore, a development work was initiated in JAERI in 1980.

For the plasma current induction and control in the Next Engineering Tokamak, superconducting poloidal coils should be operated in a strong pulsed mode such as 10 T/sec. Even based on the present achievement of the DC toroidal coils, the development of superconducting poloidal coils has new problems such as, large current (30-100 kA0 and low loss (less than 0.2 % of the stored energy) conductor at the same time, fatigue toughness against 10^6 cycles of pulsed operations, large diameter (3-20 m) and small thickness (less than 1 m) coil, insulation against high voltage (1-5 kV), cooling of pulsed heat generation, in which the peak heat generation is about 20 times greater than the averaged value, and so on.

Japan has relatively few experiences in pulsed coil development. However, an analytical and experimental research has been developed rapidly in JAERI regarding the pulsed field test of the LCT program. Based on this experience, large current poloidal conductor development was initiated in JAERI in 1980. The first step of development work is the fabrication of a 10 -kA poloidal conductor and two designs of configuration were selected as follows,

1) twisted strands around a flat stainless steel core (Type JA-10)
2) twisted strands which have stainless steel structure both in inside and outside (Type JB-10)

We started R&D and fabrication of both type of poloidal conductors in April 1980 and the full-sized conductors were fabricated by March

1981. Figures VII-5.1 and VII-5.2 show the configuration of the JA-10 and the JB-10 respectively.

6. A Conceptual Design of the Superconducting Tokamak Test Assembly (STTA)

A superconducting tokamak system is a complicated system in which four bodies, toroidal coils, poloidal coils, structure, and plasma, are electromagnetically and mechanically coupled to each other.

The large, superconducting TF coils for the Next Engineering Tokamak, which may store as much as 20-30 GJ, may possibly quench in the event of a plasma disruption. Even though the coils will be designed to be cryostable against small disruption, such as wire motion, a plasma disruption may quench them. Therefore it is indispensable that they be protected.

It may not be so difficult to design the protection system analytically. But to verify the operation of the protection system without any previous testing may involve serious expenditures of man power and resources. It is therefore important to construct a medium-sized tokamak whose stored energy is about 1/10 of that of the Next Engineering Tokamak so as that operation of the protection system can be verified under realistic conditions.

In Japan, the working group for superconducting magnets of the Fusion Council proposed such a medium-sized tokamak, called STTA (Superconducting Tokamak Test Assembly), as part of the long term development program for the Fusion Experimental Reactor.

Major objectives of the STTA are,

1) construction of the first superconducting coil system as a tokamak,
2) verification of coil protection under the existenc of noisy and

disruptive plasma,

3) verification of the systematic control of many superconducting toroidal and poloidal coils,

4) fatigue and reliability testing by repetitive operations, and

5) verification of complicated cryogenic system for the tokamak.

Although projects of T-15 and Torus-II are progressing in the USSR and France, no actual project, in which these complicated problems of superconducting tokamak are investigated, has been started in Japan no the U.S. Therefore, JAERI is now examining the possibility of constructing the STTA which will use the actual LCT coils for toroidal coils based on the tentative parameters as shown in table VII-6.1

Table VII. 2-1 Characteristics of the Test Module Coil I

COIL SHAPE	CIRCURAR
COIL SIZE	
WINDING INNER DIA.	600 mm
WINDING OUTER DIA	1600 mm
WIDTH	300 mm
WINDING CONCEPT	DOUBLE PANCAKE
COOLING CONCEPT	POOL COOLING at 4.2 K
GRADING CONCEPT	TWO GRADES (10T, 6.2T)
NORMINAL MAGNETIC FIELD	10 T
NORMINAL OPERATING CURRENT	6,050 A
NUMBER OF TURNS	730
MAGNETMOTIVE FORCE	4.4 MAT
AVERAGE CURRENT DENSITY	30 A/mm^2
SELF INDUCTANCE	0.46 H
SUPERCONDUCTING MATERIALS	Nb_3Sn and Nb-Ti
STRUCTURE MATERIAL	304L and 316L
FINAL ASSEMBLE	ELECTRON BEAM WELDING

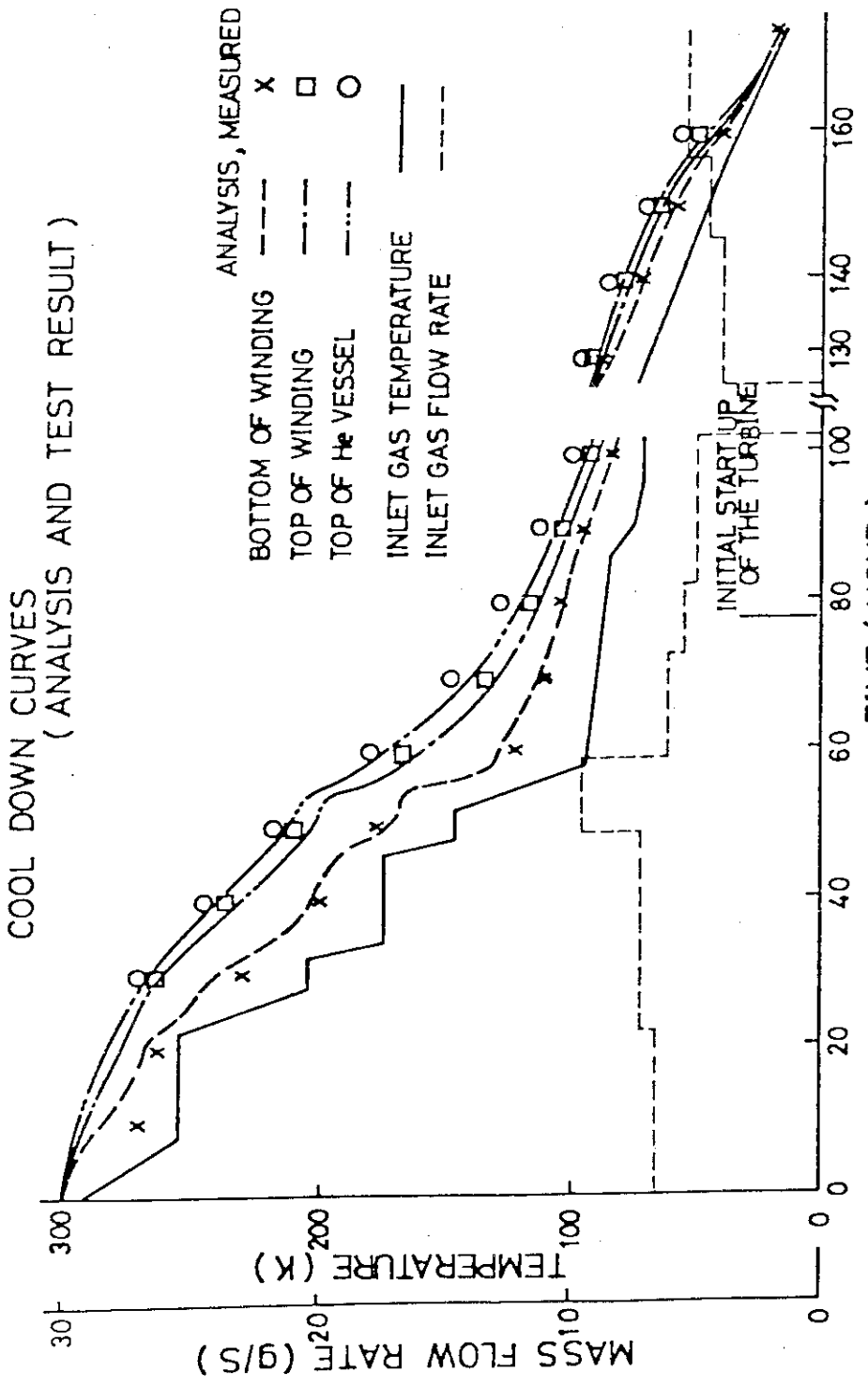

Fig. VII.2-1 Cool down characteristic of the Cluster Test Coil

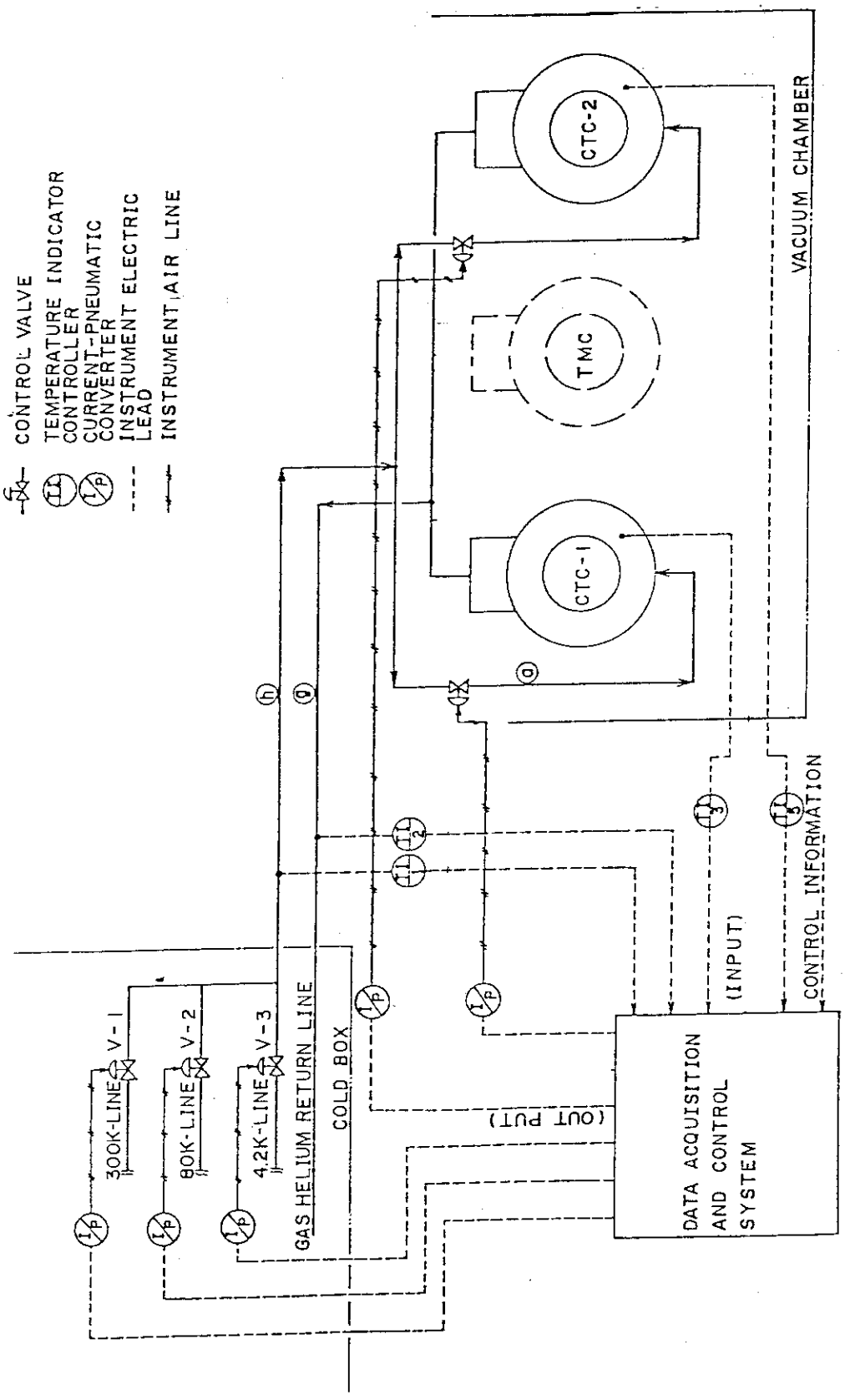

Fig. VII. 2-2 Flow diagram of the automatic cool-down

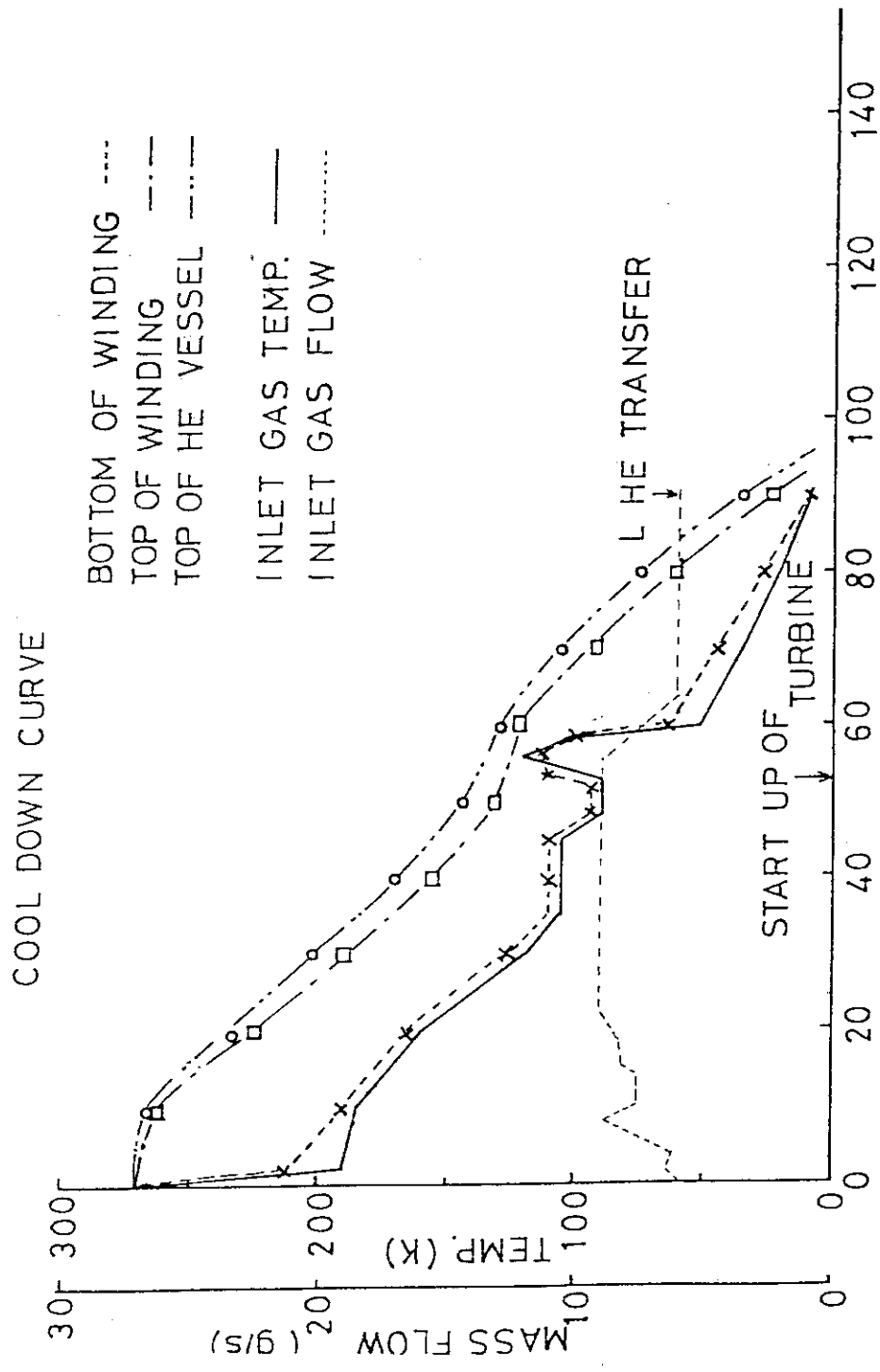

Fig. VII. 2-3 A cool down curves of the Cluster Test Coil in the second test

TMC Nb_3Sn CONDUCTOR

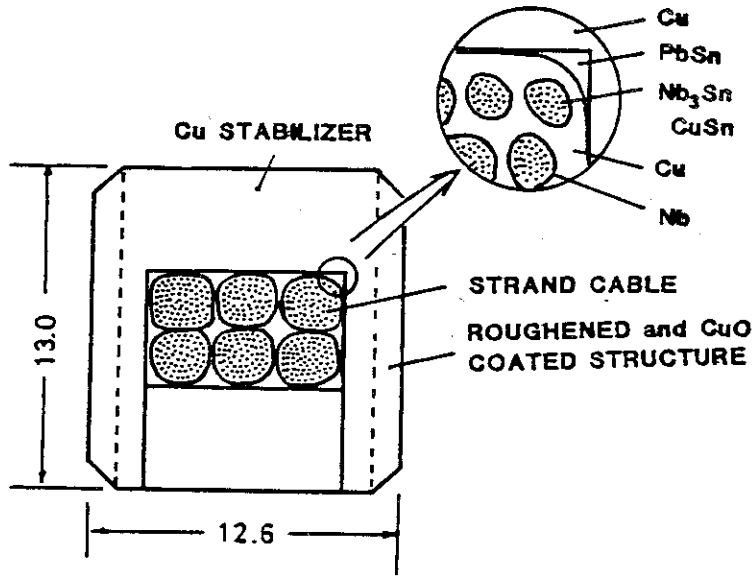

CRITICAL CURRENT	10 KA
CURRENT DENSITY(in conductor)	37 A/mm^2
FILAMENT DIA.	4 μm
FILAMENT No.	(331)x234
STRAND DIA.	2.48 mm
STRAND No.	6
STRAND TWIST PITCH	35 mm
CABLE TWIST PITCH	75 mm
Cu/non Cu (in strand)	0.65
Cu STABILIZER	
RESISTIVITY	5.7x10^{-9}Ω-cm
0.2 % YIELD STRESS	34 kg/mm^2

Fig. VII. 2-4 TMC Nb_3Sn Conductor

Table VII. 3-1 Major characteristics of the Japanese LCT coil

COIL SHAPE	OVAL
COIL SIZE	
WINDING INNER DIMENSION	2.48 × 3.48 (m)
He-VESSEL INNER DIMENSION	2.35 × 3.60 (m)
OUTER DIMENSION	3.35 × 4.54 (m)
WIDTH	0.748 m
WINDING CONCEPT	DOUBLE PANCAKE and EDGE WISE
COOLING CONCEPT	POOL COOLING
GRADING CONCEPT	TWO GRADINGS (8, 5 T)
NORMINAL CURRENT	10,220 A
NUMBER OF TURNS	658
MAGNETMOTIVE FORCE	6.725 MAT
AVERAGE CURRENT DENSITY	26.56 A/mm^2 (in winding)
MAXIMUM MAGNETIC FLUX DENCITY	8.1 T
SELF INDUCTANCE	2.03 H
SELF STORED ENERGY	106.0 MJ
NUMBER OF PAN-CAKES	20 DOUBLE PANCAKE
COOLING CHANNEL DEPTH	2.9 mm
SUPERCONDUCTING MATERIAL	Nb-Ti
STRUCTURE MATERIAL	304L (including N)
FINAL ASSEMBLY	BOLTED and SEAL WELDED
TOTAL WEIGHT	40 TON
PERMISSIBLE MAXIMUM VOLTAGE	1 KV (between terminals)
	1 KV (for ground)

Table VII. 3-2 Coupling time constant of the conductor

	measured (m sec.)	calculated (m sec.)
single strand	22	30
strand pack	100	140

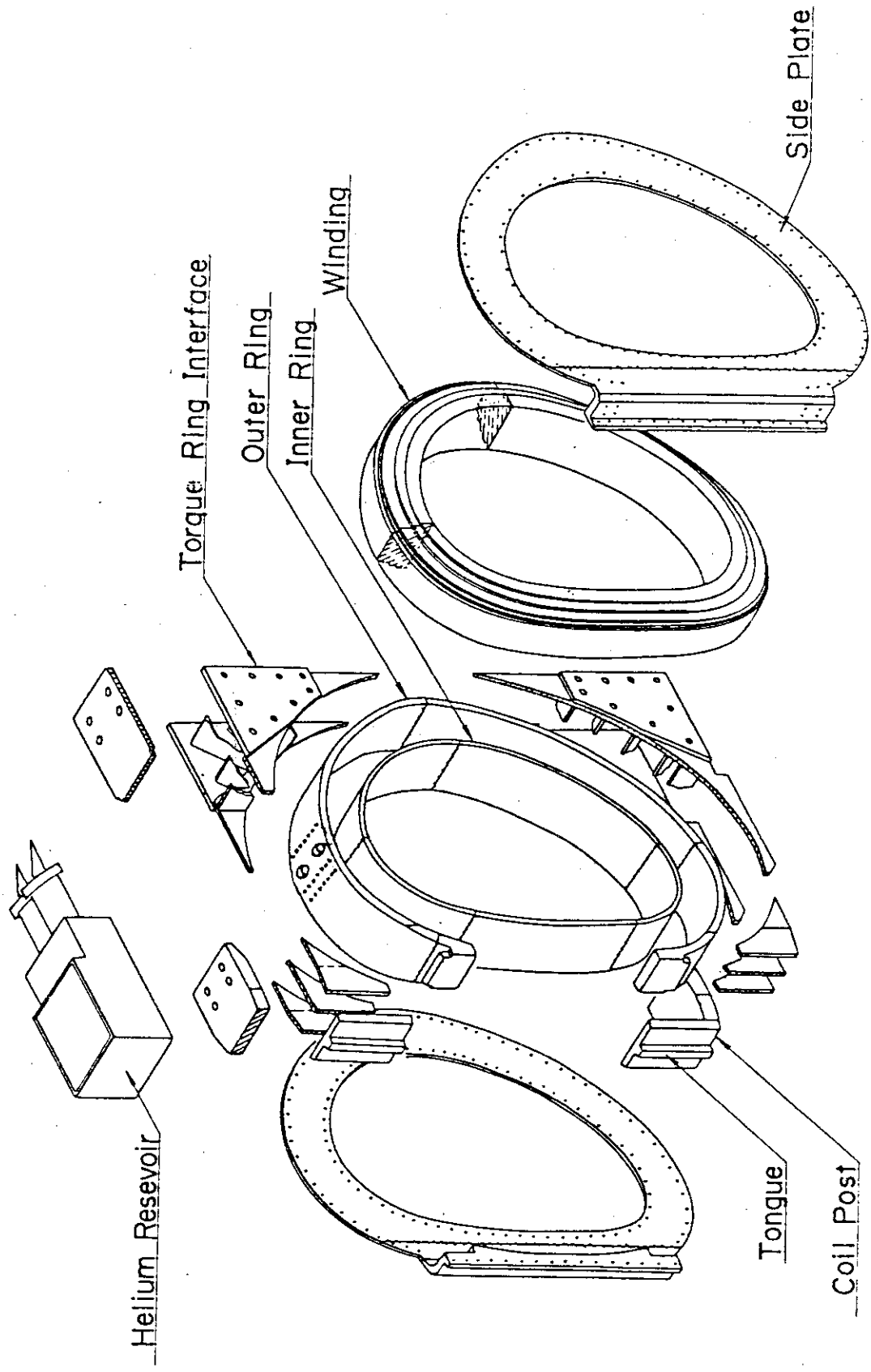

Fig. VII. 3-1 Major assemblies of the Japanese LCT coil

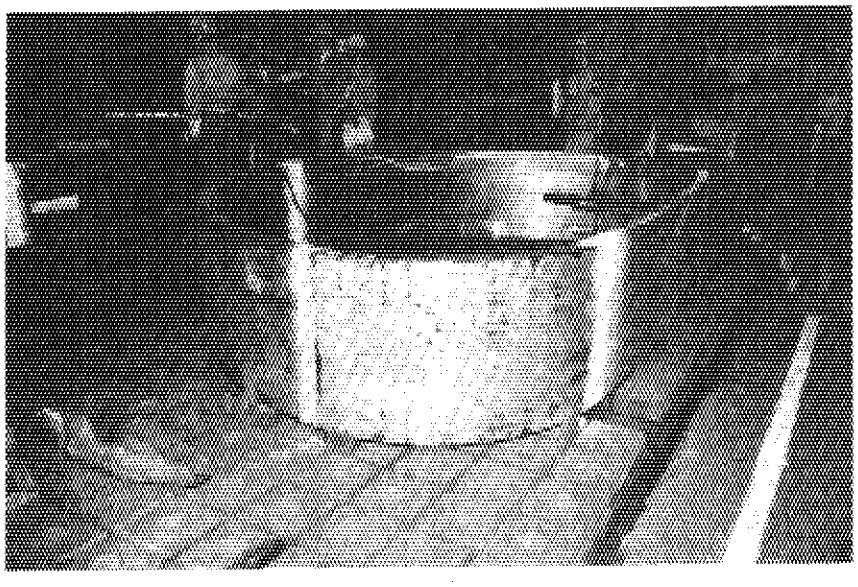

Fig. VII. 3-2 The inner ring of Helium Vessel

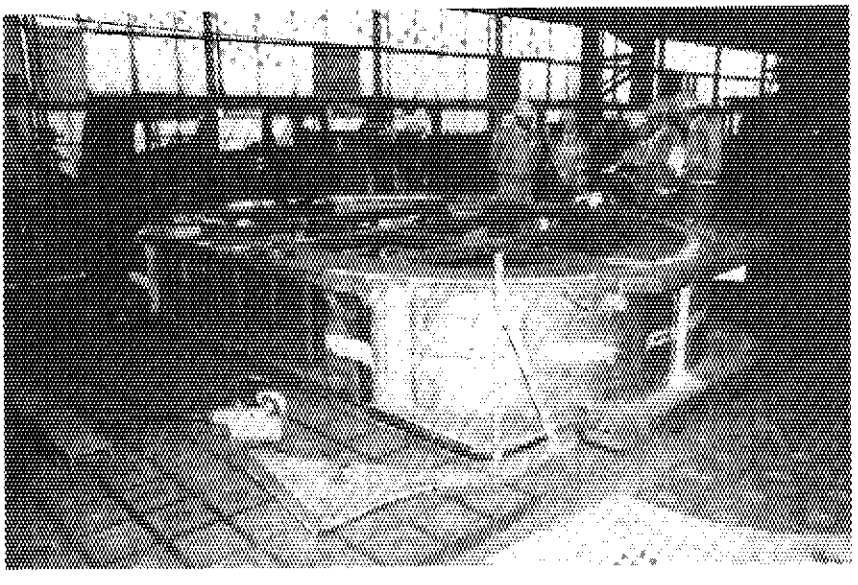

Fig. VII. 3-3 The outer ring of Helium Vessel

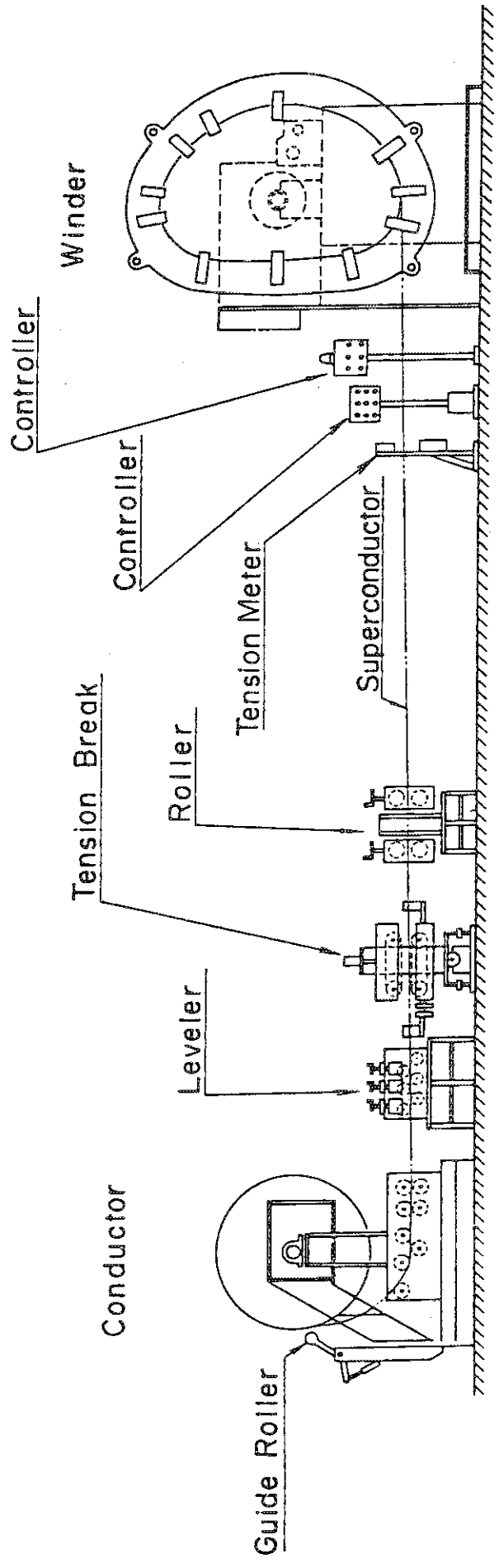

Fig. VII. 3-4 The arrangement of winding facility

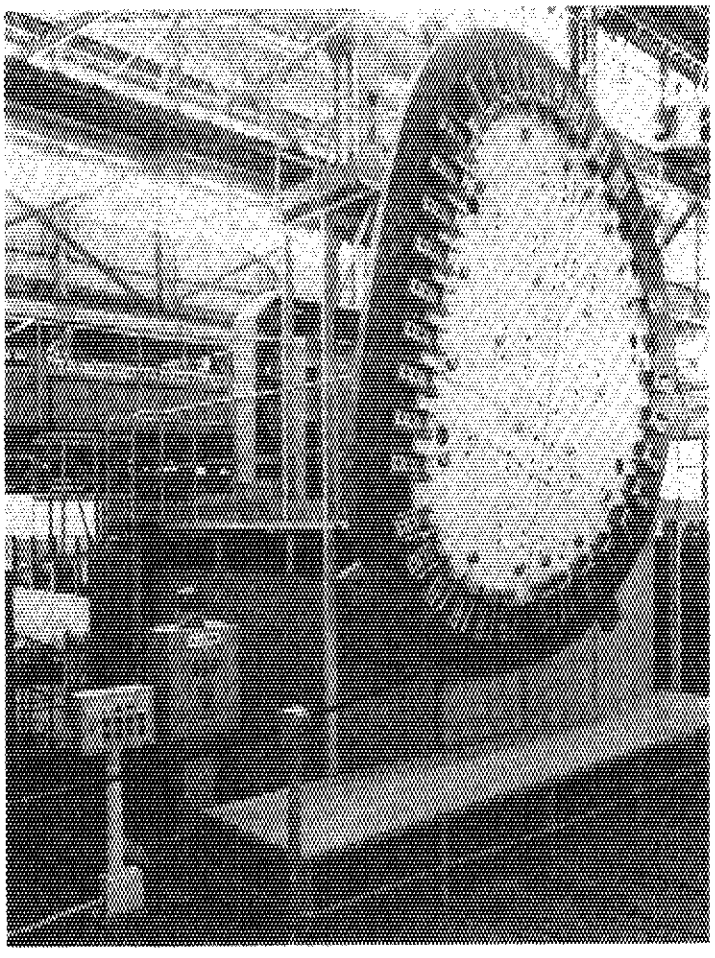

Fig. VII. 3-5 The view of winding facility

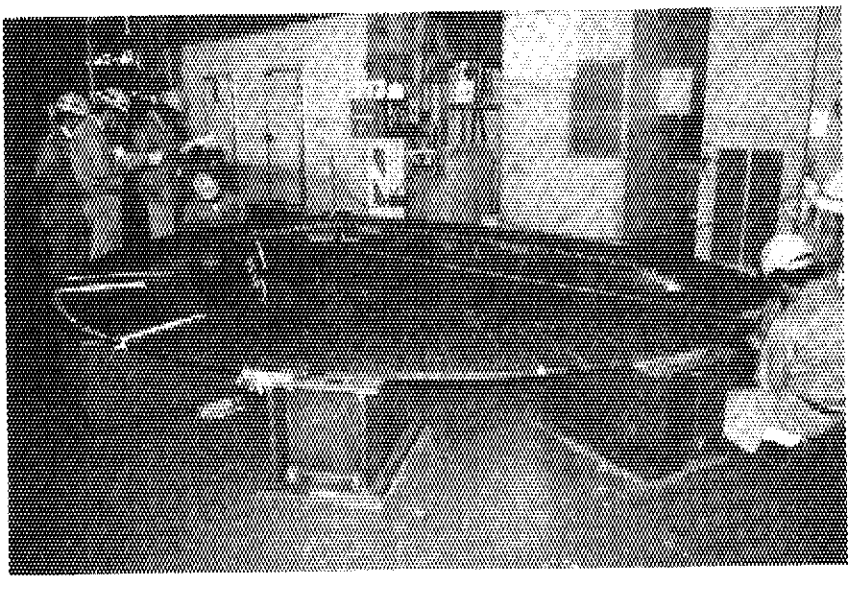

Fig. VII. 3-6 One double pancake of the Japanese LCT coil

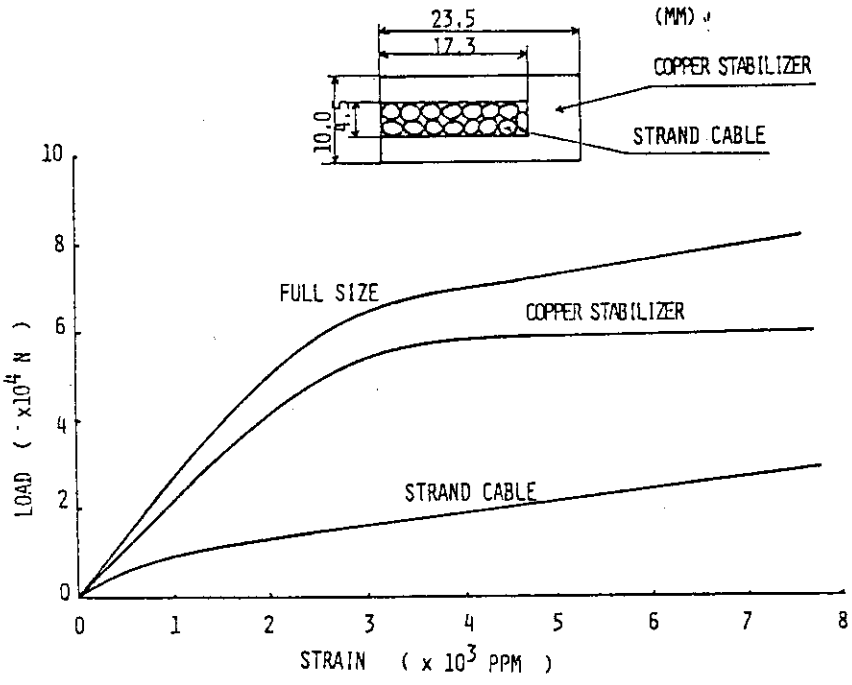

Fig.VII.3-7 Stress-strain curves of copper stabilizer, strand cable, and full sized conductor

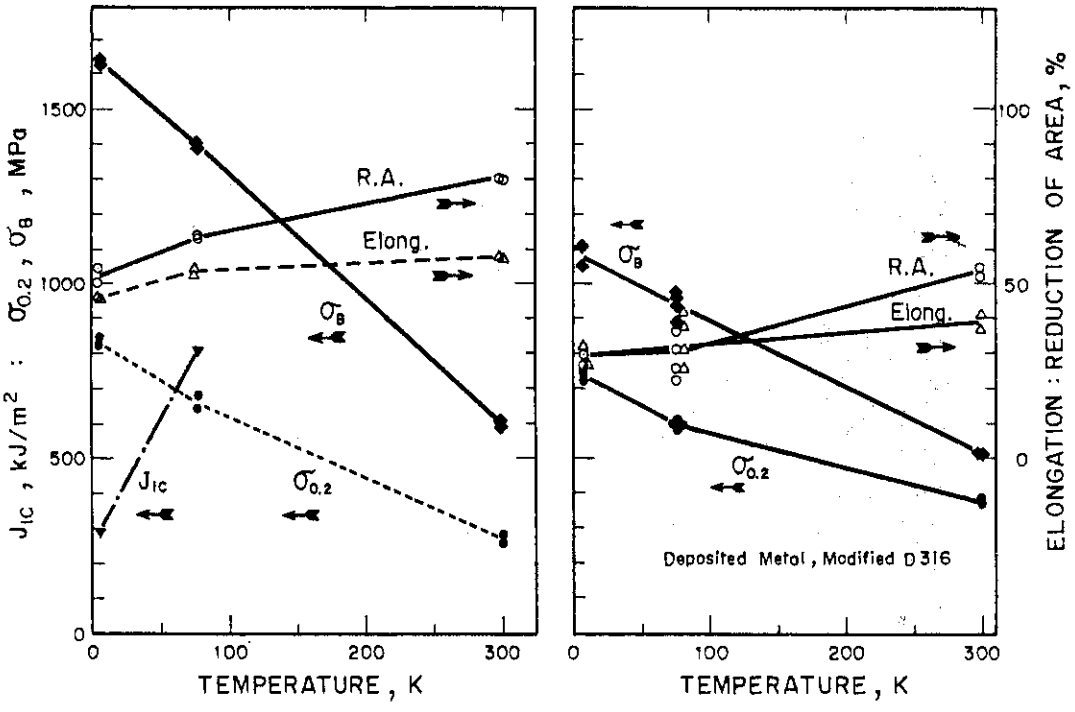

Fig.VII.3-8 The mechanical properties of the Japanese LCT coil case

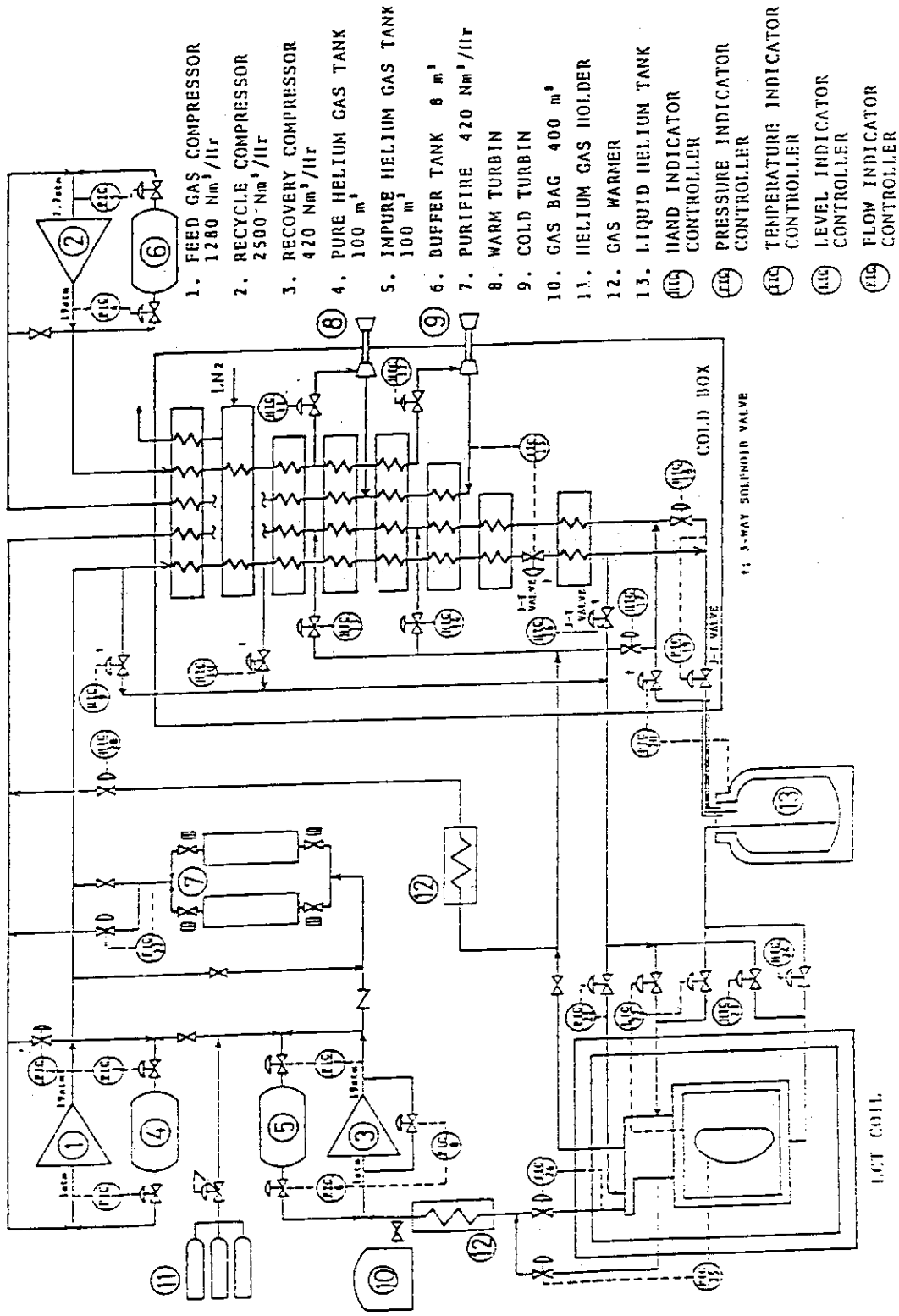

Fig. VII. 3-9 300 l/hr Liquefier/Refrigerator System

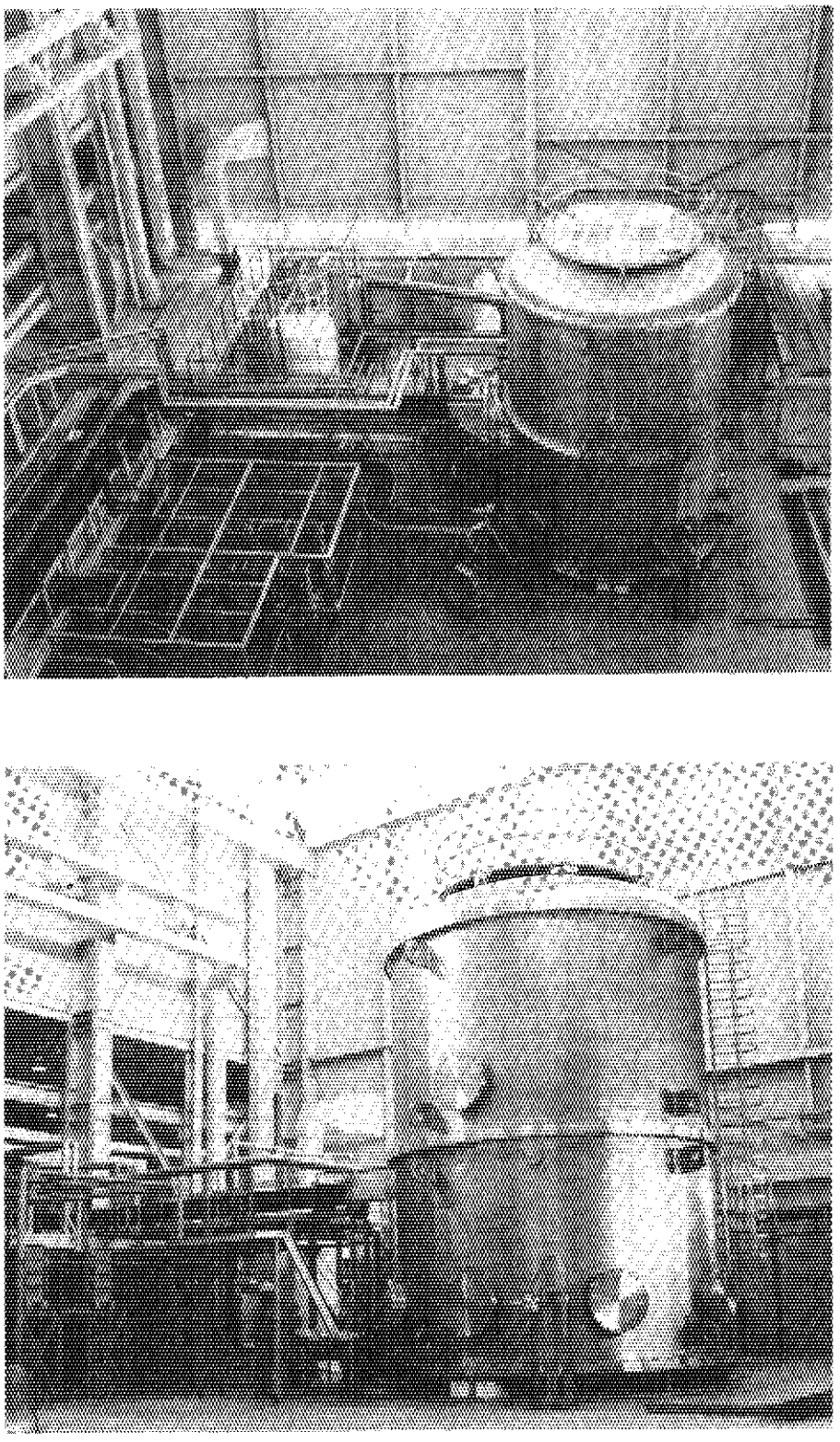

Fig. VII.3-10 Vacuum chamber (5-m dia. and 8-m high)

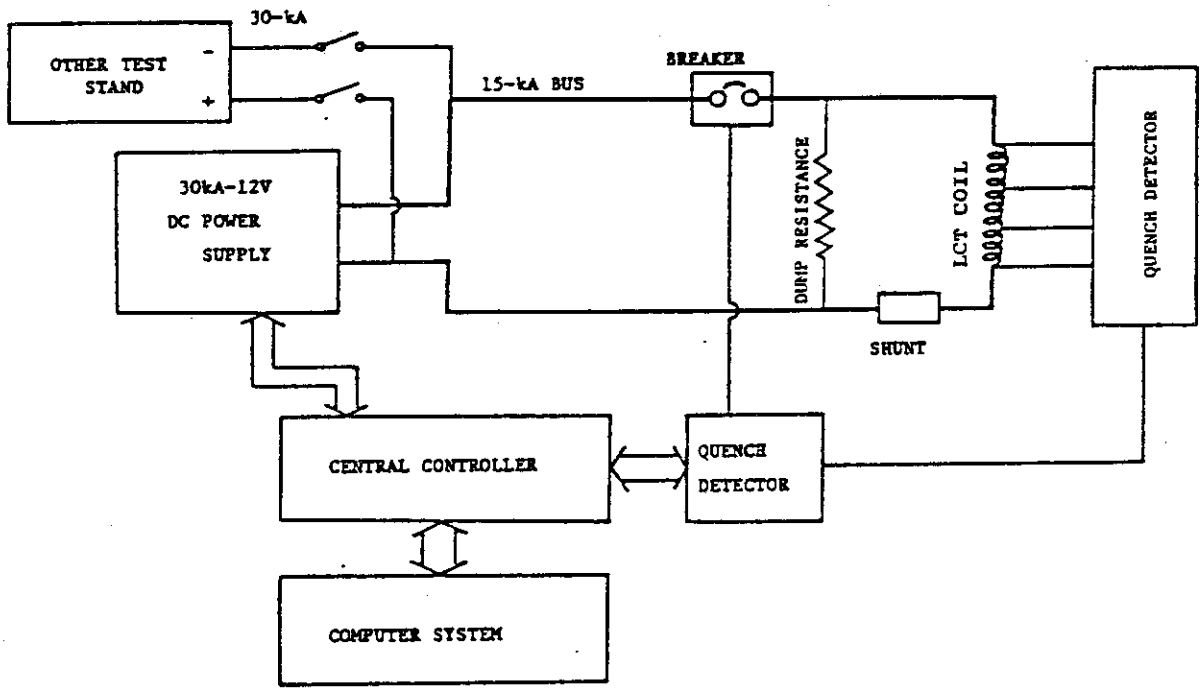

Fig. VII. 3-11 A DC power supply and a high-energy protection system

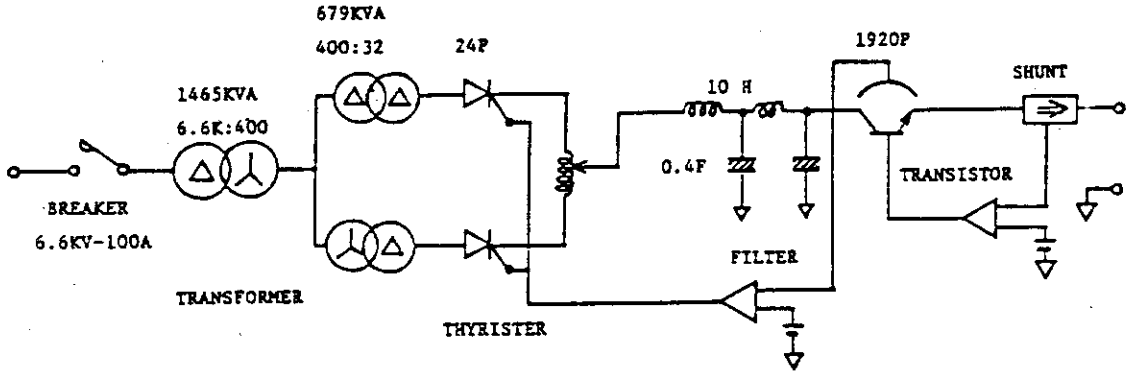

Fig. VII. 3-12 A circuit of the DC power supply

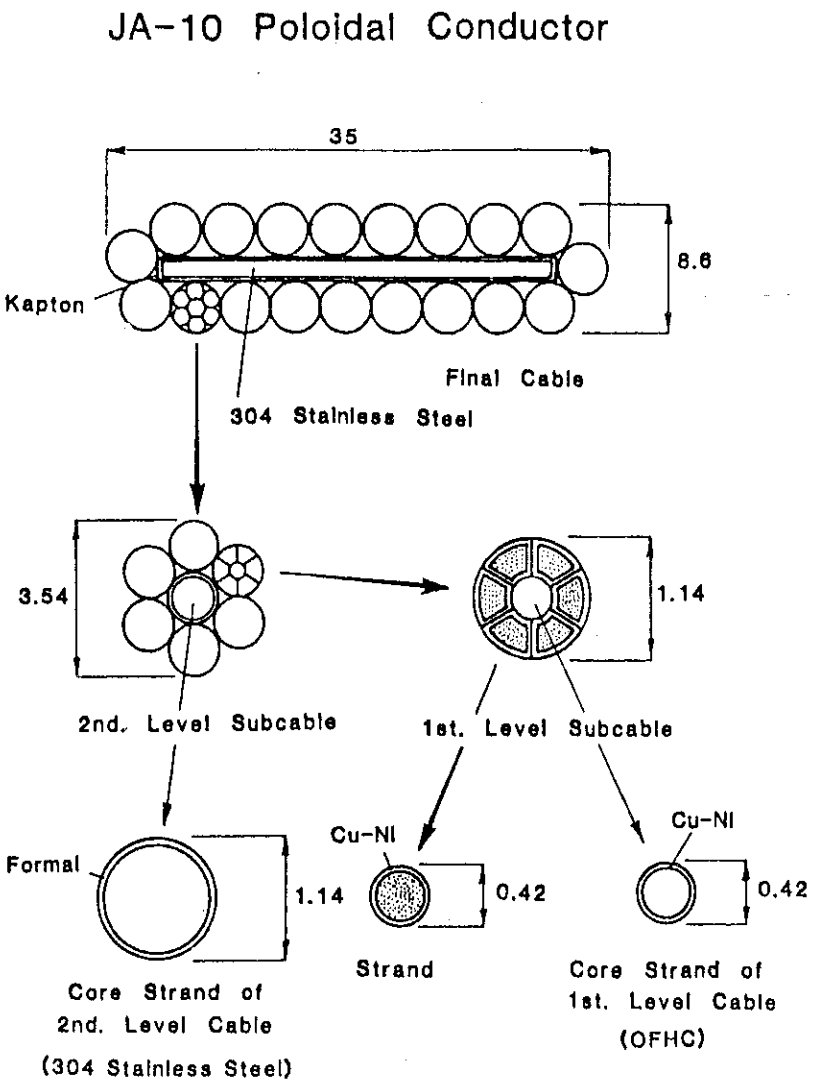

Fig. VII. 5-1 Cross sectional configuration of the JA-10 conductor

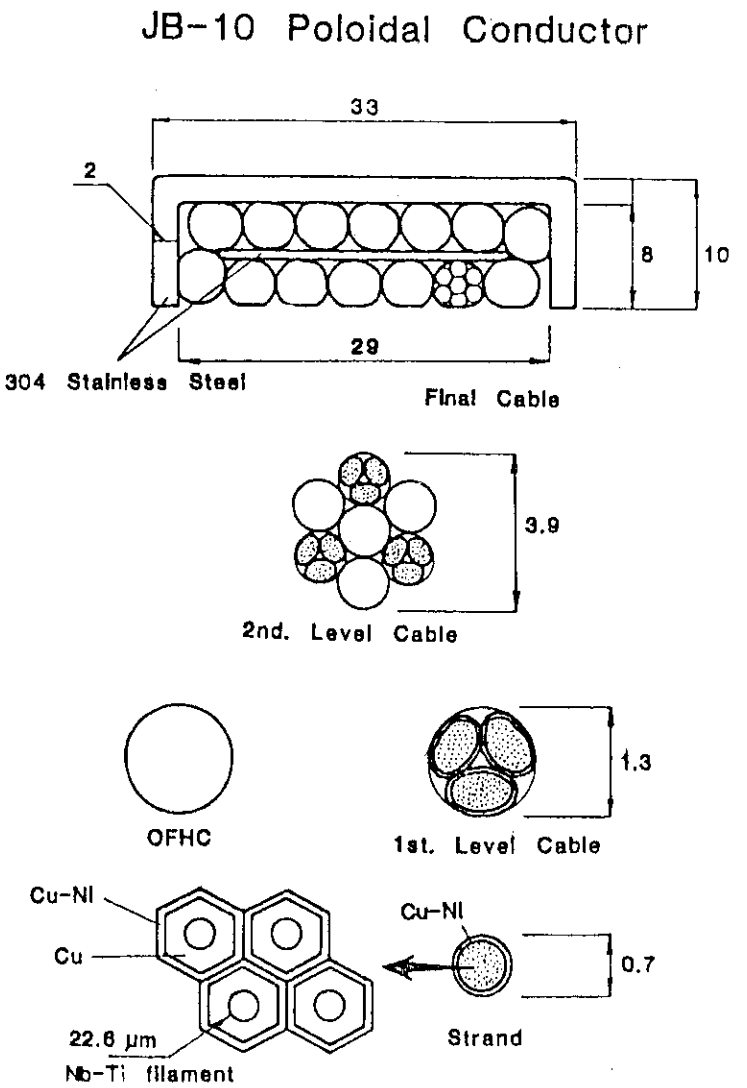

Fig. VII. 5-2 Cross sectional configuration of the JB-10 conductor

Table VII. 6-1 Tentative parameters for the STTA-LCT

TENTATIVE PARAMETERS FOR THE STTA-LCT

MAJOR RADIUS	Ro	2.40 ± 0.10 M
MINOR RADIUS	A	0.55 ± 0.05 M
	B	1.00 ± 0.10 M
	K	1.8
TOROIDAL COILS		LCT COILS
TOROIDAL FIELD	Bo	5T OR MORE
PLASMA CURRENT	Ip	2.7 MA
SAFETY FACTOR	Ga	2.5
TOROIDAL BETA	β_t	5 %
CYCLE DURATION	CT	100 SEC (TOTAL)
NUM. OF OPERATIONS	NOP	2×10^5
INTEGRATED DURATION	IT	8 MONTHS
MAXIMUM FIELD	Bmax	8 T
NUM. OF TF COILS	Ntf	12
TOROIDAL COIL CURRENT	Itf	93% OF SPECIFIED VALUE
TOROIDAL RIPPLE	Rt	LESS THAN 2%
NUMBER OF PF COILS	Npf	12

VIII. TRITIUM

In order to develop tritium engineering technologies in relation to R/D program of fusion reactor, it is necessary to provide the safe facility which has the functions of protecting radiation exposure of working personnels from tritium activity and preventing tritium release to the environment. Detailed design study and safety analysis of Tritium Processing Laboratory (TPL), in which gram levels of tritium were to be handled, were carried out.

In parallel with the design study of TPL, several fundamental experiments using H_2, D_2, etc. and computor simulation studies of the main components in Fuel Gas Circulation System were performed as the first stage of R/D.

1. Development of Tritium Processing Technology

1.1 Separation characteristics of thermal diffusion column

Thermal diffusion method is considered to be one of the most useful technologies for the hydrogen isotope separation in the tritium production process by neutron irradiation of ^{6}Li-Al alloy and ^{6}Li-compounds, because of small tritium inventory, leak tightness and handling ease in batch operation. Separation experiments were carried out with H_2-HD-D_2 mixture in advance of the separation of tritium gas mixture.

Fig. VIII. 1-1 shows the relation between overall separation factor of the column and operation pressure. Separation factor greatly increases with increasing of temperature of hot wire. Optimum operating pressure was observed in each temperature. In this case equilibrium time was less than 30 minutes. As shown in the figure, the overall separation factor markedly varied with the feed gas content, and in the design of thermal diffusion column, this effect should be considered.

1.2 Simulation test of tritium removal system

A series of simulation tests were performed with H_2, D_2, CH_4 and H_2O vapor to study the characteristics of detritiation system composed of

catalytic oxidizer packed with precious metal-alumina catalyst, dryer with molecular sieve-5A and so on.

Fig. VIII. 1-2 shows the conceptual flow sheet of experimental apparatus. Specifications of the main components are : volume of enclosure ; 300 l, maximum flow rate of circulation pump ; 4 m^3/hr, effective dimension of oxidizer ; 53.3 mm I.D. x 388 mm L, maximum packed weight of catalyst ; 0.8 kg, effective dimension of dryer ; 83.1 mm I.D x 920 mm L, maximum packed weight of molecular seive-5A ; 3.5 kg.

Table VIII. 1-1 summarizes the conversion ratio of D_2 and CH_4 obtained under various operating conditions of oxidizer. These experimental results indicate that conversion ratio of tritium in the form of hydrogen gas can be obtained as high as 99.99 % at 100 °C, and 99.9 % at room temperature, whereas for tritiated methane, the operating temperature should be more than 350 °C to attain much higher conversion ratio than 99.6 %.

Fig. VIII. 1-3 shows that the amount of water vapor adsorbed on the catalyst comes up to about 10 % of that on the molecular sieve-5A. Although the effect of adsorbed water on the conversion ratio was not detected in our study, consideration for the adsorption on the catalyst should be taken into the evaluation of tritium material balance and inventory in the detritiation system.

Fig. VIII. 1-4 illustrates the operation characteristics of the detritiation system during long period of its operation. Water vapor in the outlet of the dryer was proved to maintain lower than 10^{-2} ppm until the break-through in the dryer was initiated. The maximum reduction rate of water vapor was 99.9998 %.

1.3 Hydrogen purification experiment

Extracted gas from tritium production target (^{6}Li-Al alloy) and plasma effluent gas from fusion reactor include many species of impurities (He, N_2, O_2, CO, CO_2, CH_4, NH_3 etc.). Therefore, purification process is necessary to remove these impurities prior to the hydrogen isotope separation process. Palladium-silver alloy membrane method, which has been established as a production technology of pure hydrogen, is expected to be a feasible one, because of its simplicity of the system and its handling ease in continuous operation. However, impurity effects on the hydrogen permeability has not been proved under comparatively high temperaure and pressure.

In the experimental study, permeation characteristics of Pd-25wt%Ag alloy tube were measured with hydrogen, which contains such impurities as above mentioned. Effective dimension of the tube is 1.6 mm O.D. x 1.44 mm I.D. x 96.7 mm L.

Fig. VIII. 1-5 shows hydrogen permeation flow rate against operation time. In our experimental conditions, effects of impurities on permeability were not observed. When poisoned by oil vapor from vacuum pump, the membrane could be decontaminated by regeneration treatment(oxidation and reduction), and initial permeability was easily recovered.

1.4 Basic experiment on tritium recovery from blanket materials

Tritium release behavior in neutron-irradiated lithium compounds has been studied with the purpose of accumulating the basic data necessary for the selection of a suitable blanket materials. When the neutron-irradiated materials such as Li_2O, $LiAlO_2$, Li_2SiO_3, Li_2C_2, LiAl and LiH were heated under vacuum, the tritium was released in the chemical forms of HT, HTO, CH_3T and $C_2H_{2n+1}T$ (n=1,2,3). Table VIII. 1-2 summarizes the distribution of tritiated species analyzed by using a radiogas chromatograph.

On the basis of kinetic studies, the reaction $2LiOT(S) \rightarrow Li_2O(S) + T_2O(G)$ was revealed to play an important role in the tritium release process of neutron-irradiated Li_2O, although the rate-controlling step was diffusion of tritium. The diffusion coefficent of tritium obtained for the sample irradiated to nvt = 8.9×10^{17} cm^{-2} was shown by the following equation.

$$D = 5.1\times10^{-3} \exp[-(100.0\pm7.1)\times10^{3}/RT] \quad cm^2 s^{-1}$$

$$R = 8.314 \text{ Joule } K^{-1} \text{ mol}^{-1}$$

1.5 System analysis

(1) Cryogenic distillation column for hydrogen isotope separation

There are three major factors which are expected to have large effects on separation characteristics : differences of latent heat of vaporization among the six isotopic species (Factor 1)(See Fig. VIII. 1-6) ; decay heat of tritium (Factor 2) ; and nonideality of the solutions (Factor 3). These effects were investigated by using a rigorous simulation model developed for the present study. It was revealed that Factor 1 has negligible effects, but

Factor 2 in the case of high tritium concentration and Factor 3 have significant effects on column performance. However, the expected performance can be obtained by increase in number of total theoretical stages by about 30 %, even if the design calculation is made neglecting all of these factors.

A dynamic simulation study was carried out for a single column. A parameter setting method was proposed for the PI controller. This method has two important features : it accounts for strong nonlinearity of the column ; and it allows us to predict unstable region which must be avoided in the actual operation.

(2) Hydrogen isotope separation cascade by porous membrane method

A new mathematical simulation procedure was developed for multicomponent separating cascades. This procedure is applicable and effective under such conditions that the cut of mixture of each stage is prescribed and required to be independent of concentration, and stage separation factors are given as input variables, and these values are very large. By use of the procedure, system analysis was made for hydrogen isotope separation system by porous membrane method. It was revealed that the system configuration illustrated in Fig. VIII. 1-7 could meet the separation requirement for hydrogen isotope separation in the fuel gas circulation system for fusion reactor. Porous membrane method is worth-while to investigate in further studies as one of the promising method.

(3) Falling liquid film condenser for removal helium from hydrogen isotope

A preliminary design model was developed for falling liquid film condenser processing helium and the six molecular species of hydrogen isotopes. A design study of this unit was performed under flow conditions of the Tritium Systems Test Assembly (TSTA) which was ongoing at Los Alamos National Laboratory. Several attractive features were revealed : helium can be removed almost perfectly from hydrogen isotopes ; separation of hydrogen isotopes is promoted at the same time and helium can be directly transfered to the Tritium Waste Treatment because of low tritium concentration in it (less than 1 %) ; both required refrigeration capacity and tritium inventory appear to be sufficiently small in comparison to those of the Isotope Separation System (TSTA). This unit may be constructed and incorporated in TSTA in the last stage of the program.

2. Detailed Design Study of Tritium Processing Laboratory

On the basis of the preliminary and conceptual design studies carried out for the last three years, the more detailed design work for constructing Tritium Processing Laboratory (TPL) was made to determine the specifications of the building and its auxiliary equipments, the safety equipments including tritium containment systems, and various kinds of experimental apparatus. And also, the safety analysis was performed to meet the controlled criteria of tritium. In this section, the safety analysis on accidental release of tritium gas is briefly described.

2.1 Scenario of accidental release of tritium

It is postulated that a tritium storage equipment containnig 35,000 Ci of tritium is damaged and all of the tritium is abruptly released into the atomsphere of the glovebox as the chemical form of T_2. Fig. VIII. 2-1 shows the path way of tritium released at the accident. The analysis is made assuming the following simple model.

1) The glovebox, in which the accidental emission of tritium occurs, is immediately isolated from the other gloveboxes. Volume and changing rate of the concerned glovebox are 8.6 m^3 and 17.5 hr^{-1}, respectively. Tritium concentration in the glovebox is calculated using perfect mixing model.

2) The glovebox atmosphere containing tritium is detritiated through Glovebox Purification System (GPS). The specification of the main components related to tritium removal is as follows.

Conversion factor of catalytic oxidizer : 200

Water vapor adsorption factor of dryer : 200

3) The glovebox is maintained at negative pressure to the surrounding area. The effluent gas equivalent to 0.1$^{vol\%}$/hr of the glovebox leak rate is led to Effuent Removal System (ERS), and stored in the holding- tank.

4) Tritium transfer from glovebox to operating room I is due to the permeation through glove materials.

Material of glove : Hypalon(Chlorosulfonated polyethylene)

Number of glove used : 4 pairs of glove

Surface area of glove : 1 m^2/ 1 pair

Thickness of glove : 0.8 mm

Permeation factor of glove material :

$HT(T_2) = 1 \times 10^{-7}$ cm^3(STP) cm/cm^2 s, atm

$HTO(T_2O) = 5 \times 10^{-6}$

Tritium concentration in the operating room I is diluted by the ventilation air. Volume and changing rate of the concerned room are 900 m^3 and 5 hr^{-1}, respectively.

2.2 Tritium release to the environment

Fig. VIII. 2-2 shows the relation between tritium concentration and lapse of time. Tritium concentration in the glovebox decreases exponentially with lapse of time. On the other hand, tritium concentration in the operating room I shows the maximum value, and then decreases exponentially to be the controlled level in the same way within about 1 hr after the accidental release of tritium happened. Effluent gas discharged from the operating room I is diluted with other ventilation gas, and average tritium concentration at stack is kept less than the permissible level. In this case, total tritium release to the environment is estimated to be about 0.04 Ci, and therefore the tritium containment system in TPL is evaluated to meet the safety criteria of tritium.

Table VIII. 1-1 Conversion Factor for D_2 and H_2

BED TEMPERATURE T_1(°C)	FLOW RATE F (m^3/hr)	SPACE VELOCITY SV(hr^{-1})	CONCENTRATION D_2(%)	CH_4(%)	O_2(%)	CONVERSION RATIO σ(%)
100	1.5	1800	0.857	-	4.89	>99.99
100	2.6	3100	1.389	-	5.12	"
100	4.1	4900	0.767	-	5.55	"
50	3.9	4700	0.689	-	4.99	"
28	4.1	4900	0.7	-	5.0	"
26	4.1	4900	0.031	-	0.136	>99.9
23	4.2	5100	0.033	-	0.138	"
500	1.7	2000	-	0.114	1.089	99.7
450	"	"	-	0.090	1.047	99.8
400	"	"	-	0.095	1.040	99.7
350	"	"	-	0.092	1.077	99.6
300	"	"	-	0.105	0.949	68.0
250	"	"	-	0.080	1.016	23.6
200	"	"	-	0.184	1.796	6.2

Table VIII. 1-2 Cumulative Distribution of Tritium Released from Neutron-irradiated Lithium Compounds during Heat Treatment under Vacuum

Lithium compound	Neutron fluence cm^{-2}	Upper temp.§ K	Tritiated species % HT	HTO	CH_3T	$C_2H_{2n-1}T$ (n=1,2,3)	Retained in the target
LiH	3.0×10^{15}	1023	99.4	0.3	0.3	0.03	0.07
Li_2C_2	3.0×10^{15}	973	95.9	1.2	0.4	2.6	0.01
LiAl	3.0×10^{16}	1073	93.2	5.3	1.2	0.03	0.3
Li(1wt%)-Al	3.6×10^{17}	1023	44.5	53.7	1.8	0.03	0.01
LiOH	3.6×10^{16}	873	0.3	99.4	0.1	0.2	0.01
Li_2O	3.6×10^{16}	873	0.9	98.0	0.9	0.1	0.1
Li_2CO_3	3.6×10^{16}	873	1.7	96.9	0.3	1.0	0.1
$LiAlO_2$	3.0×10^{15}	1023	8.1	87.1	1.2	3.6	0.03
Li_2SiO_3	3.0×10^{15}	1023	2.5	97.1	0.4	—	0.01

§ The sample was heated for 20 min at each temperature which was raised stepwise from 473 K to the upper one with a 50-100 K interval.

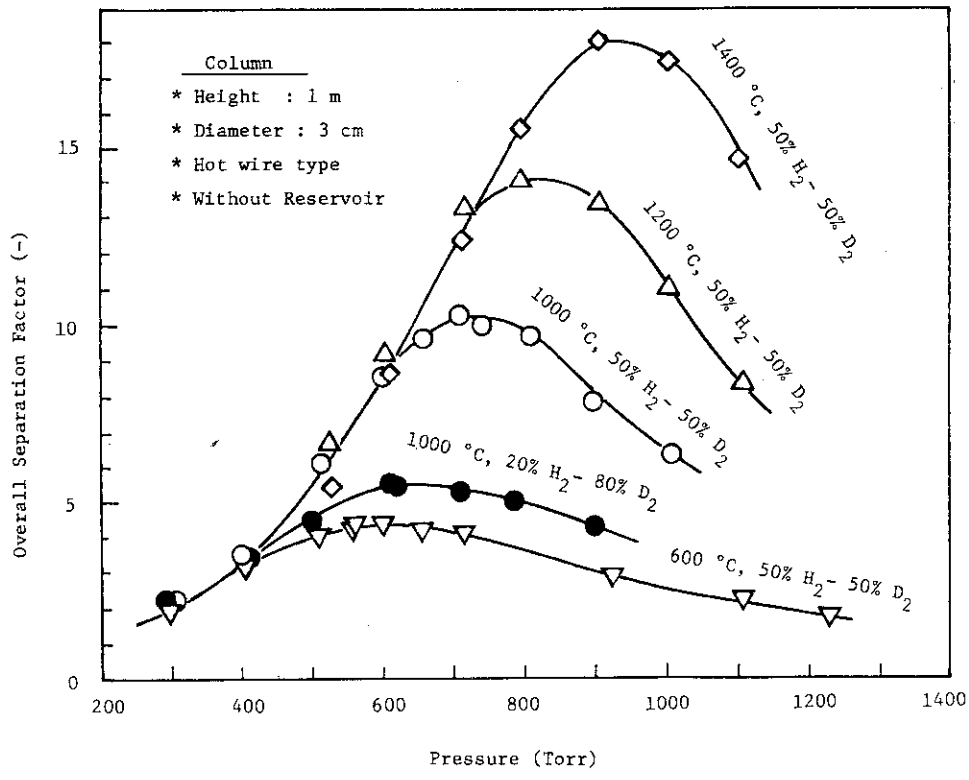

Fig. VIII. 1-1 Overall Separation Factor of Thermal Diffusion Column

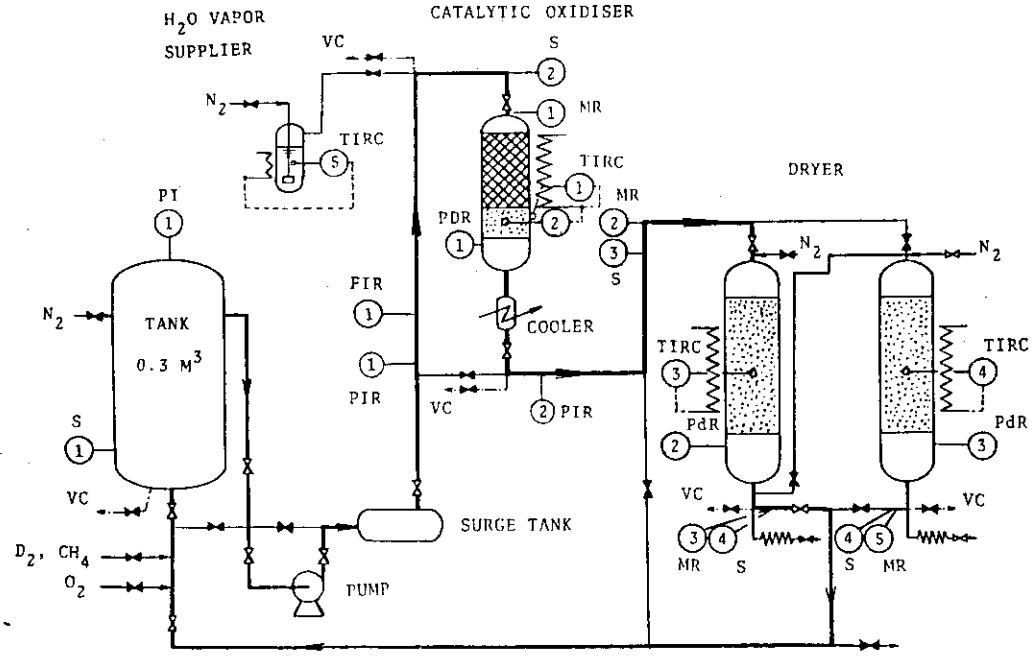

Fig. VIII. 1-2 Conceptual Flow Sheet of Experimental Apparatus

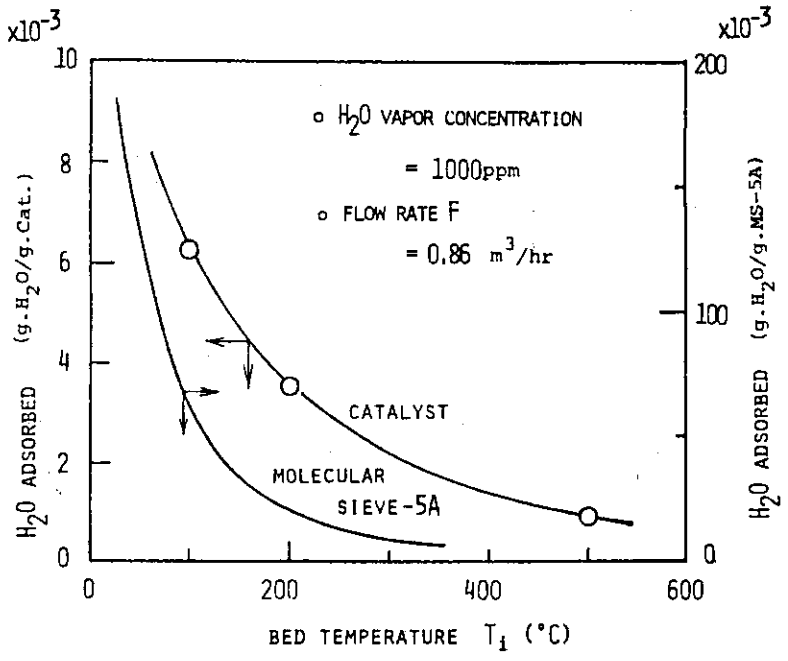

Fig. VIII. 1-3 Amount of Water Vapor Adsorbed on Catalyst

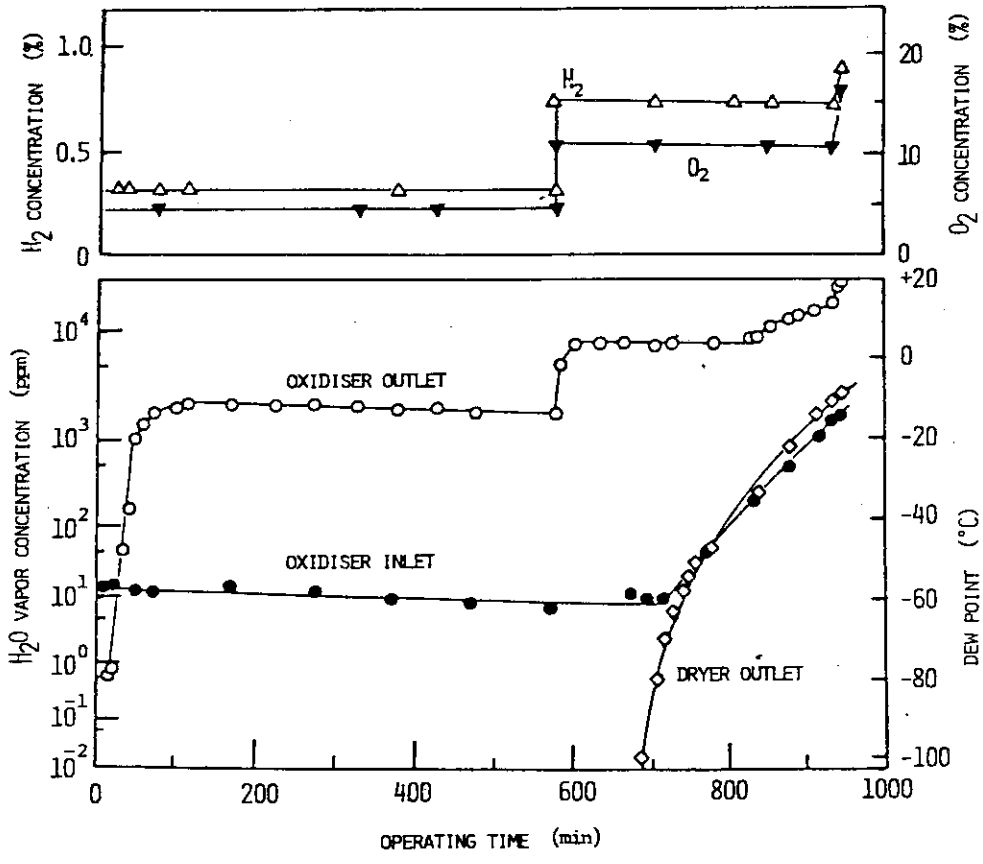

Fig. VIII. 1-4 Operation Characteristics of Detritiation System

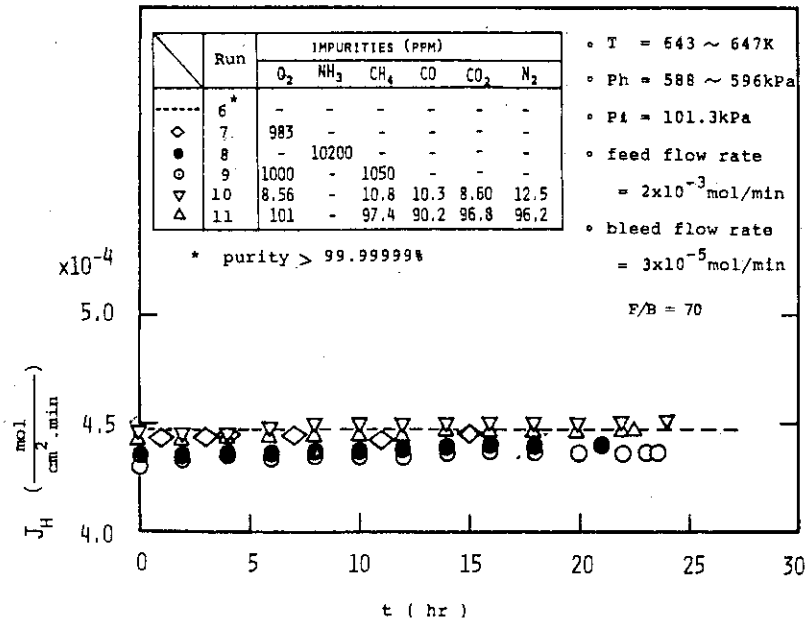

Fig. VIII. 1-5 Effect of Impurities on Hydrogen Permeability

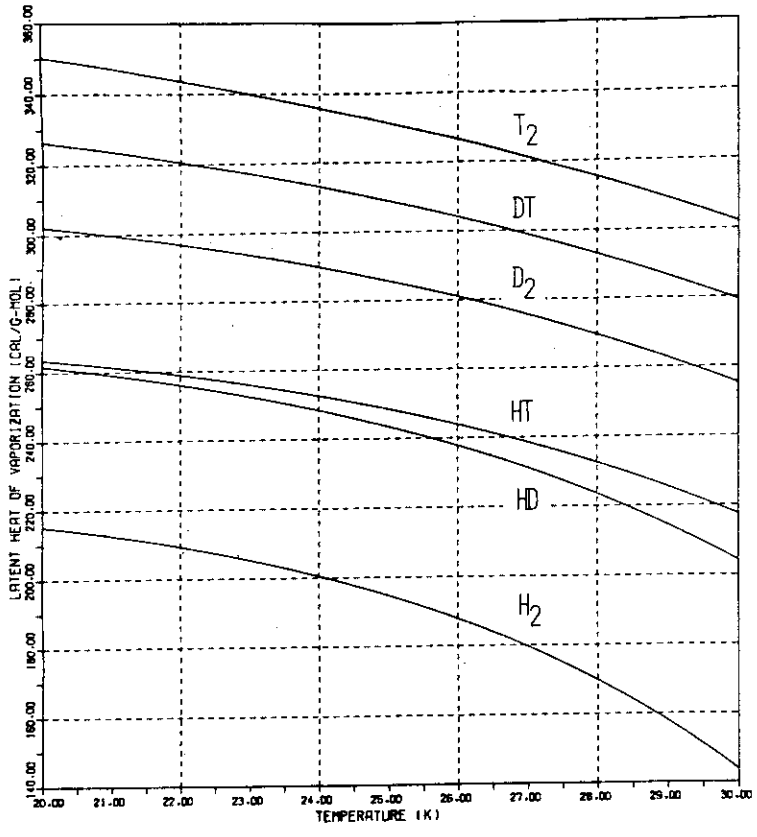

Fig. VIII. 1-6 Latent Heat of Vaporization of Hydrogen Isotopes

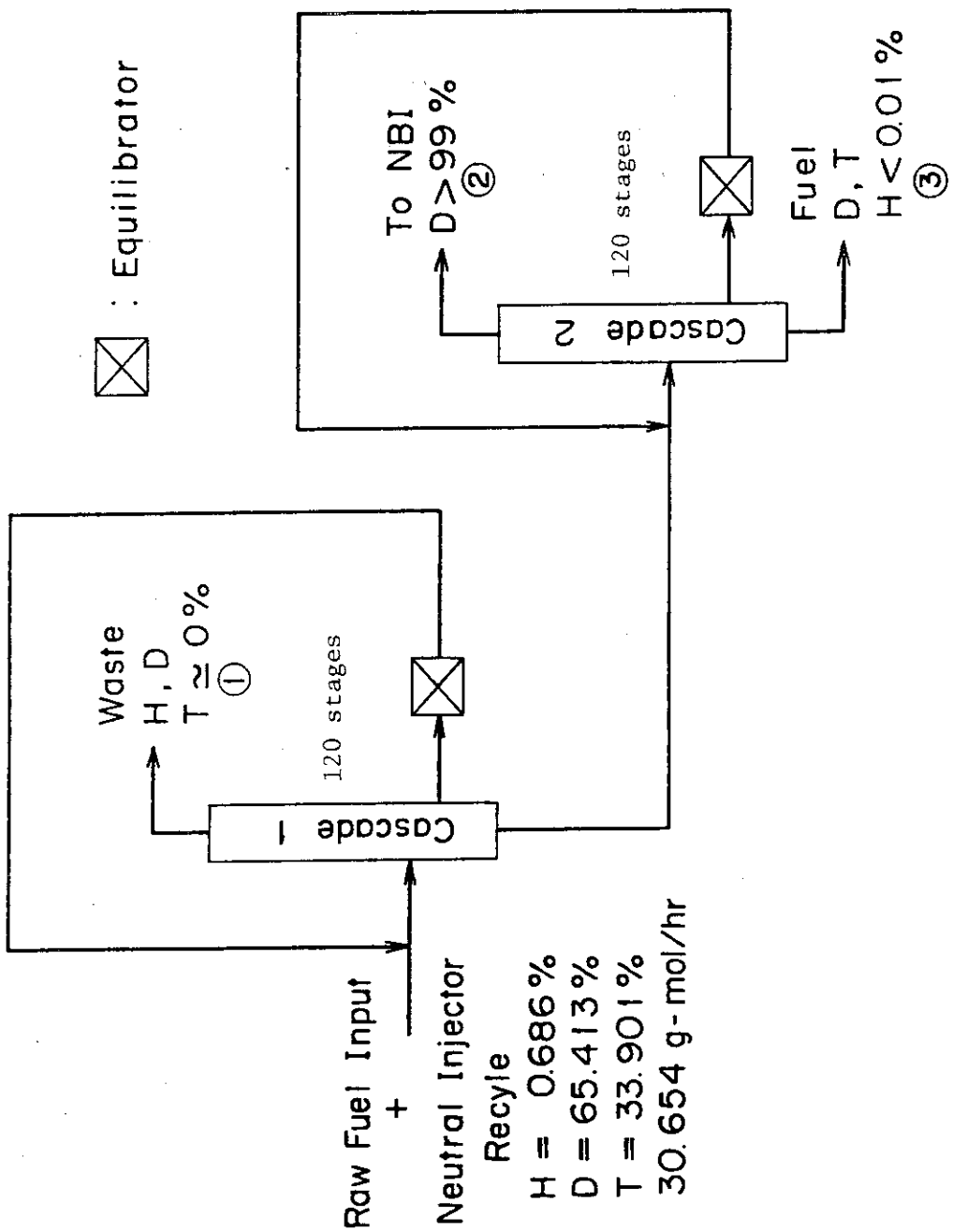

Fig. VIII. 1-7 Hydrogen Isotope Separation Cascade by Porous Membrane Method

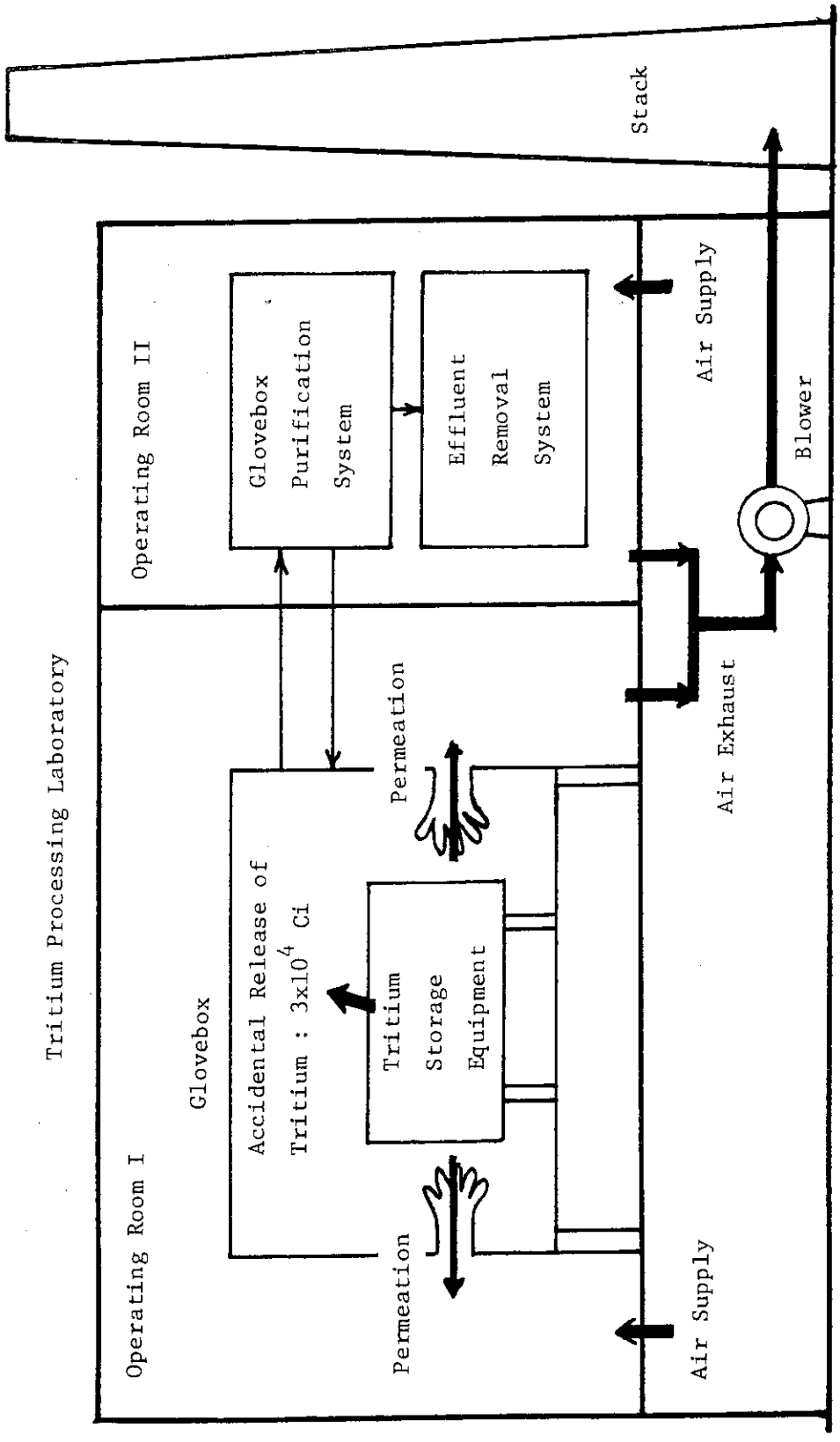

Fig. VIII. 2-1 Pathway of Tritium Released at Accident

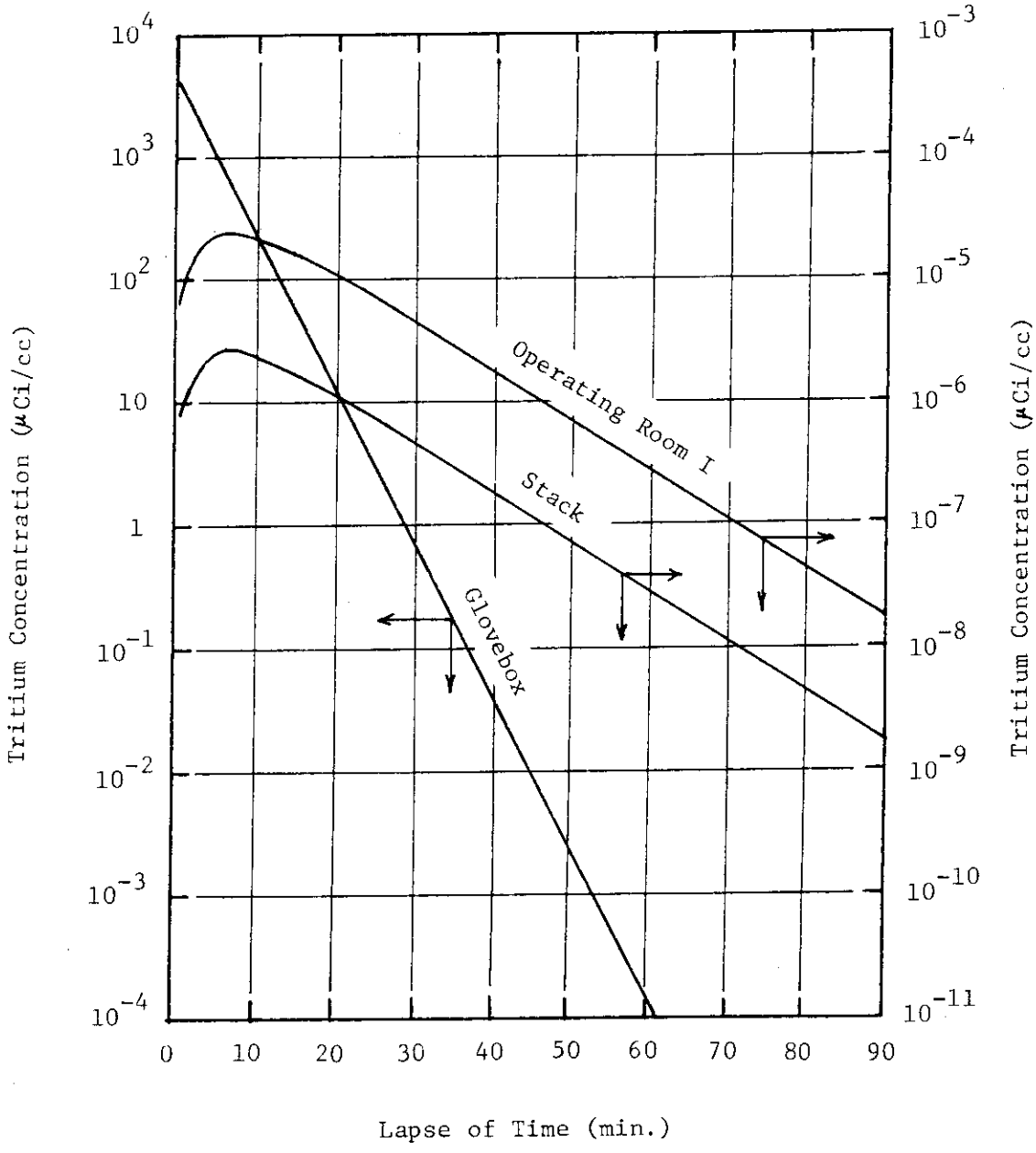

Fig. VIII. 2-2 Tritium Concentration vs. Lapse of Time

IX. DESIGN STUDY OF FUSION REACTOR SYSTEM

1. Analysis of Reactor System

The following issues related to the design study of INTOR and the Next Tokamak Reactor were investigated.

(1) Reactor Structure
   (a) Effects of toroidal field ripple on the loss of energetic injected ions and the toroidal coil configuration[1]
   (b) Structure of high heat flux divertor[2]
   (c) Structure of Li_2O-Pb breeding blanket[3]
   (d) Tritium inventory in blanket

(2) Neutronics
   (a) Tritium breeding and shield
   (b) Improvement of neutron-gamma coupled cross section file

(3) Swimming Pool Type Tokamak Reactor (SPTR)[4]
   (a) Structure of blanket and vacuum vessel
   (b) Repair and maintenance
   (c) Shield effect of water

(4) Safety and Environment
   (a) Tritium system
   (b) Tritium release from stack
   (c) Magnetic exposure
   (d) Skyshine
   (e) Accident analysis

2. Development of a Calculational System for Fuel Producing Blanket

A calculational system of a nuclear fuel producing blanket utilizing a fusion reactor has been developed and tested.

A one dimensional discrete ordinates radiation transport code called ANISN-SP is developed to reduce the computation time required in obtaining the neutron flux distribution in a nuclear fuel producing blanket of a fusion reactor. This code employs the separation method proposed by Youssef and Conn[5] which solves separately, the distribution of the neutrons coming directly from the plasma and that of the neutrons resulting from the fission reactions. This code is made by modifying

the original ANISN code[6] and uses the coupled neutron-gamma ray cross section GICX40.[7] A preliminary test of the code resulted in the reduction of 30 - 50% computation time without loosing the accuracy of calculated neutron flux when compared with the direct calculations.

A library of cross sections for the burn-up calculations including the (n,γ), (n,f), (n,2n) and (n,3n) reactions for heavy nuclides is produced mainly from the ENDF/B-4 file.[8] This library also includes cross sections of lumped (n,γ) reactions of the fission products (FP) of ^{232}Th, ^{233}U, ^{235}U, ^{238}U and ^{239}Pu made from the FP nuclides file of Japan Nuclear Data Committee. In addition, the decay chain data for the burn-up calculations are compiled in the form compatible with the induced activation calculation code system THIDA.[9]

References

(1) Tone, Y., et al.: JAERI-M 8938 (1980)
(2) Iida, T., et al.: JAERI-M 8944 (1980)
(3) Iida, T., et al.: JAERI-M 8925 (1980)
(4) Sako, K., et al.: JAERI-M 9050 (1980) (in Japanese)
(5) Youssef, M.Z. and Conn, R.W.,: Nucl. Sci. Eng. 74 (1980) 130
(6) Engle, W.W.: Jr. K-1693, Computing Technology Center, Union Carbide Corporation (1963)
(7) Seki, Y. and Iida, H. : JAERI-M 8818 (1980)
(8) Drake, M.K. (edited) : BNL-50274 (T-601, TID-4500), ENDF 102 Vol. 1 (1970), Revised 1974
(9) Iida, H. and Igarashi, M. : JAERI-M 8019 (1978) (in Japanese)

X. DEVELOPMENT OF A LARGE TOKAMAK - JT-60

1. Introduction

Efforts made by the JT-60 Project was rewarded by the progress achieved in this year. The construction of its major components - tokamak machine, power supplies, and central control system - continued, resolving technical issues while upgrading its technical capability when considered worthwhile. The construction of JT-60 buildings and other facilities advanced as planned. The completion of JT-60 is expected in fall 1984.

Progress was significant in the development of plasma heating systems. The prototype neutral beam injector unit and klystron tubes are under fabrication and will be operated for test in fall 1981. The diagnostics development is now obtaining a substantial financial support. Hence, attentions were paid to solidify a programmatic foundation for future activities.

Anticipating the completion of JT-60 in a few years, more efforts were made in reviewing and reevaluating the experimental program and device operation program with an aim of enhancing productivity of the JT-60 Project.

2. Outline of the Progress of JT-60

The fiscal year of 1980 is characterized for JT-60 as the changing year from design phase to real construction phase.

The new site for JT-60 as shown in Fig. X.2-1, called "Mukouyama Area" of Tokai Research Establishment, is an westward town adjacent to Tokai-Mura. The layout of JT-60 facilities is shown in Fig. X.2-2. The construction of three major buildings, Experimentsl Building, Power Supplies Building and Control Building continued on schedule. In the same way, the construction of other facilities and buildings were started. The Engineering Development Building I and JT-60 Equipment Test Building were completed. Flat and cross sectional views of three major buildings are illustrated in Fig. X.2-3 to X.2-6.

Contract for all components of JT-60 (except diagnostic equipments, neutral beam injectors and radio-frequency heating system) have been concluded by the end of the fiscal year of 1980. Construction of JT-60

components have been on schedule. Fourteen toroidal field coils among nineteen ones were accomplished. The manufacture of the vacuum chamber, poloidal fields coils, the primary coolant system and the vacuum pumping system proceeded successfully. The construction of the poloidal field coil power supplies, the toroidal field coil power supplies and the central control system were on schedule, too. In Jan, 1981, contract of the secondary cooling system was conclude with Mitsubishi Electric Corporation. Contracts for the power distribution & emergency power supply system with Fuji Electric Corporation and the gas supply & preionization system with Sumitomo Shoji Ltd. were concluded in Mar, 1981, respectively.

The organization related to JT-60 program is shown in Fig. X.2-7. Division of Large Tokamak Development (DLTD) is directly responsible to development and construction of JT-60. DLTD has one adminstrative section and four project offices including a few technical groups respectively. JT-60 Project Office III was initiated from Jun, 1980, and take charge of the central control system and diagnostics equipments.

The master schedule of JT-60 program is shown in Fig. X.2-8. The completion of JT-60 is scheduled in Sep, 1984. The start of the heating experiment was delayed by three months owing to budget problems, but other milestones were kept unchanged. The major critical paths are the construction of the Experimental Building and the assembling and testing of the tokamak machine.

The engineering coordination of JT-60 was undertaken by Planning and Coordinating Group assisted by the JT-60 coordinating company, that is Hitachi Ltd.. The relationship among the work structures and the manufactures is shown schematically in Fig. X.2-9.

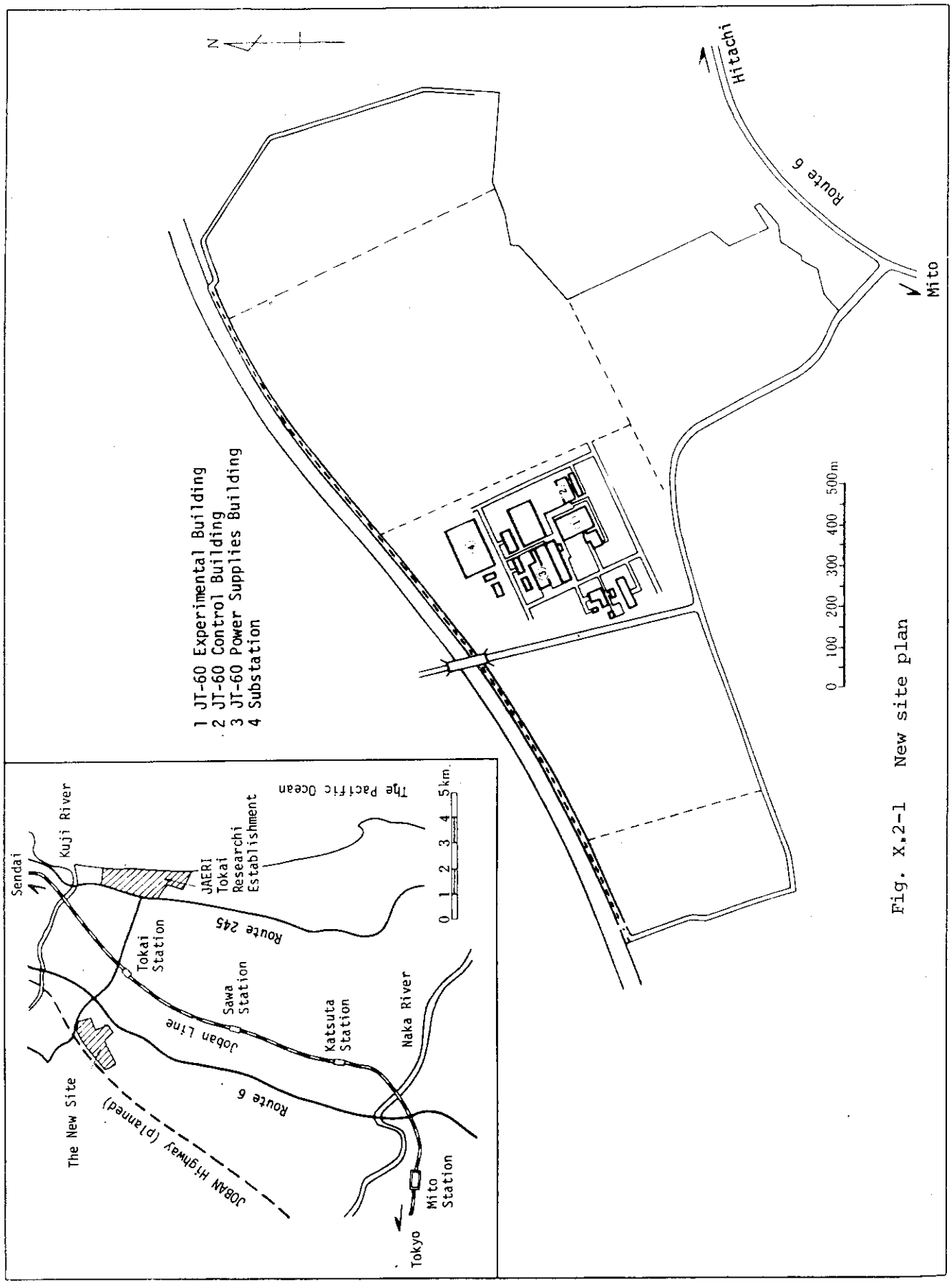

Fig. X.2-1 New site plan

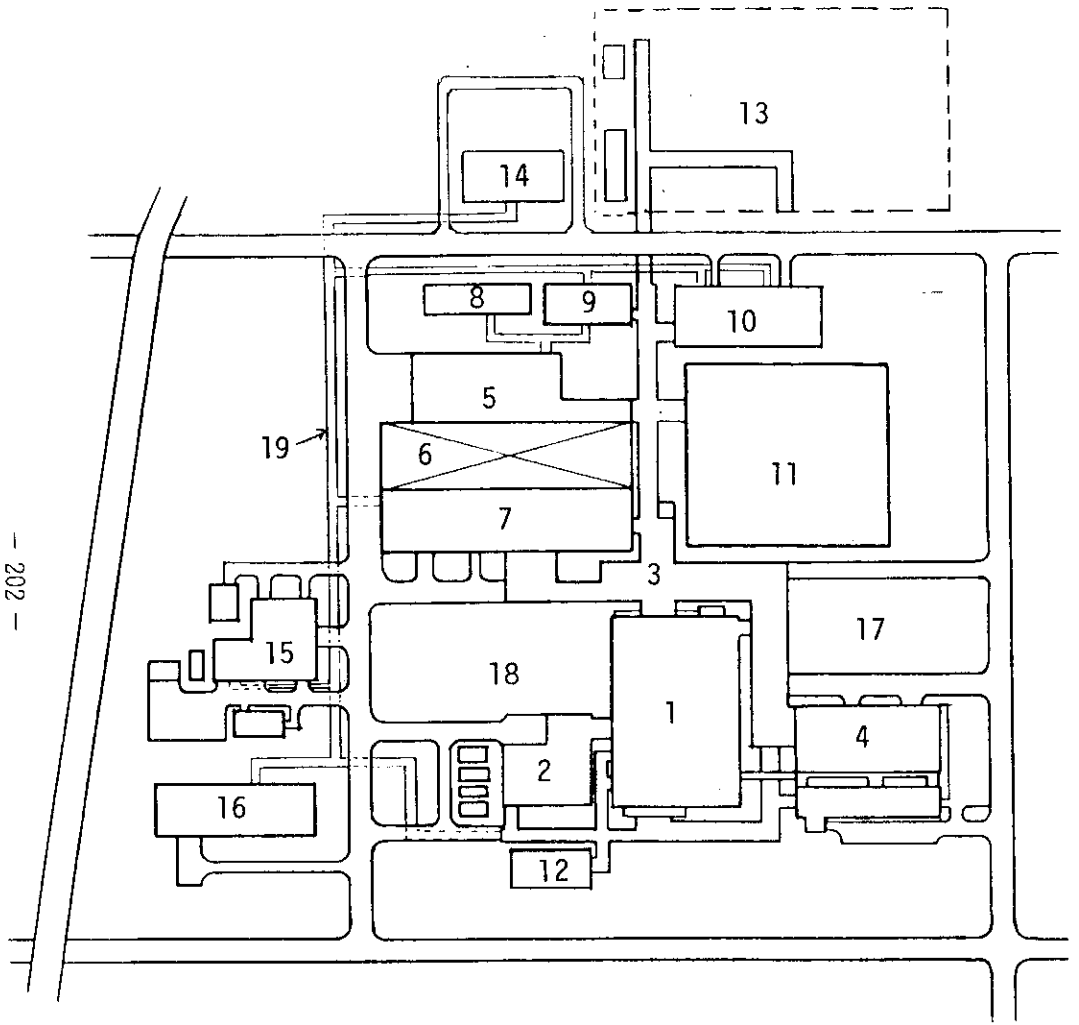

1. JT-60 Experimental Building
2. JT-60 Equipment Test Building
3. JT-60 Underground Ducts
4. JT-60 Control Building
5. JT-60 Power Supplies Building(Generator Building)
6. " (Transformer Yard)
7. " (Rectifier Building)
8. Secondary Cooling Towers
9. Secondary Cooling Pump House
10. Primary Cooling Pump House
11. NBI & RF Power Supplies Building
12. High Pressure Gas & Compressor Building
13. Substation
14. Utility Building
15. Engineering Development Building I
16. Auxiliary Experimental Building
17. Satelite Tokamak Experimental Building Area
18. JT-60 Experimental Building Expansion Area
19. Underground Ducts

Fig. X.2-2 Layout of JT-60 site

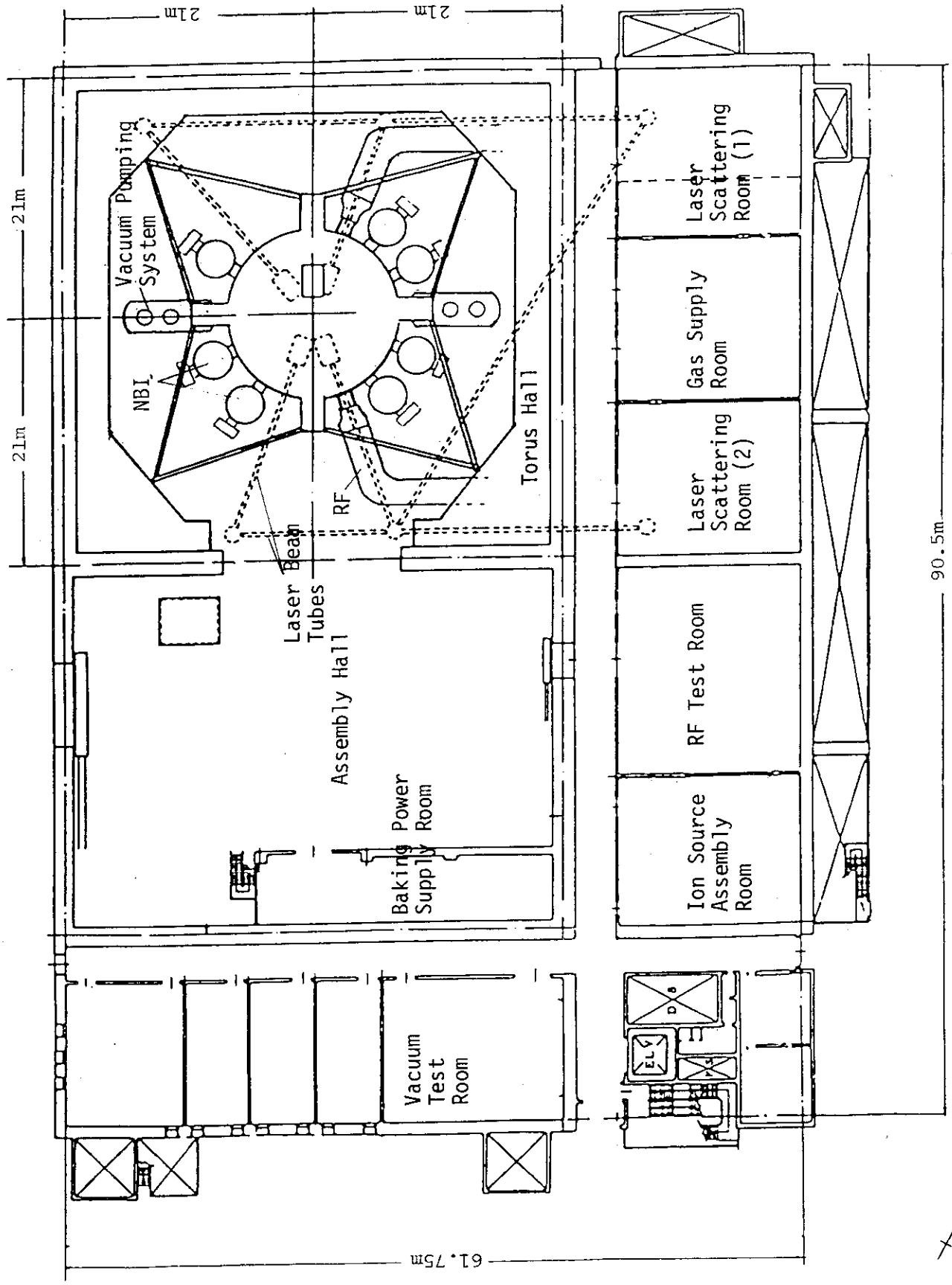

Fig. X.2-3 JT-60 Experimental Building 1F plane

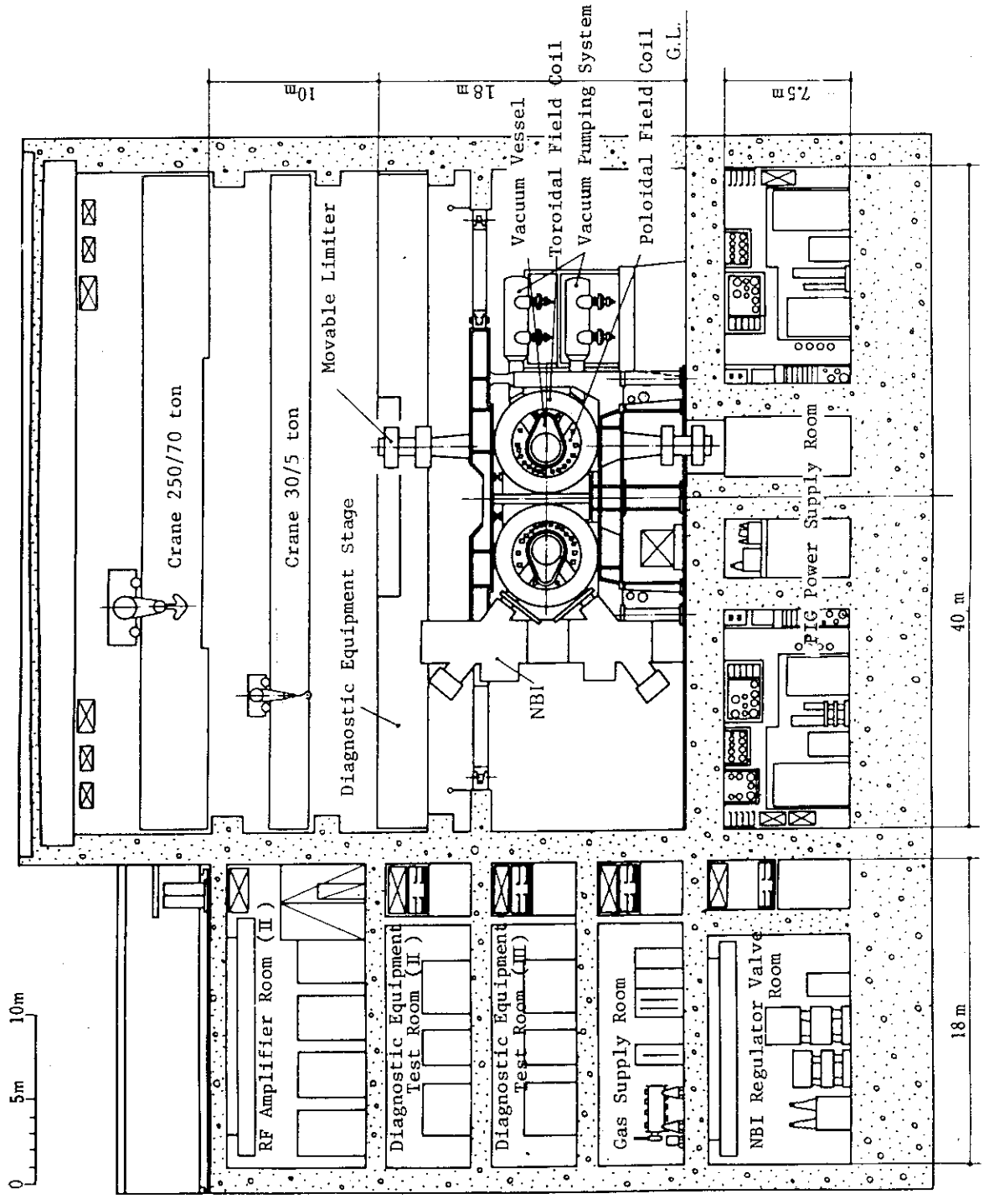

Fig. X.2-4 JT-60 Experimental Building cross section

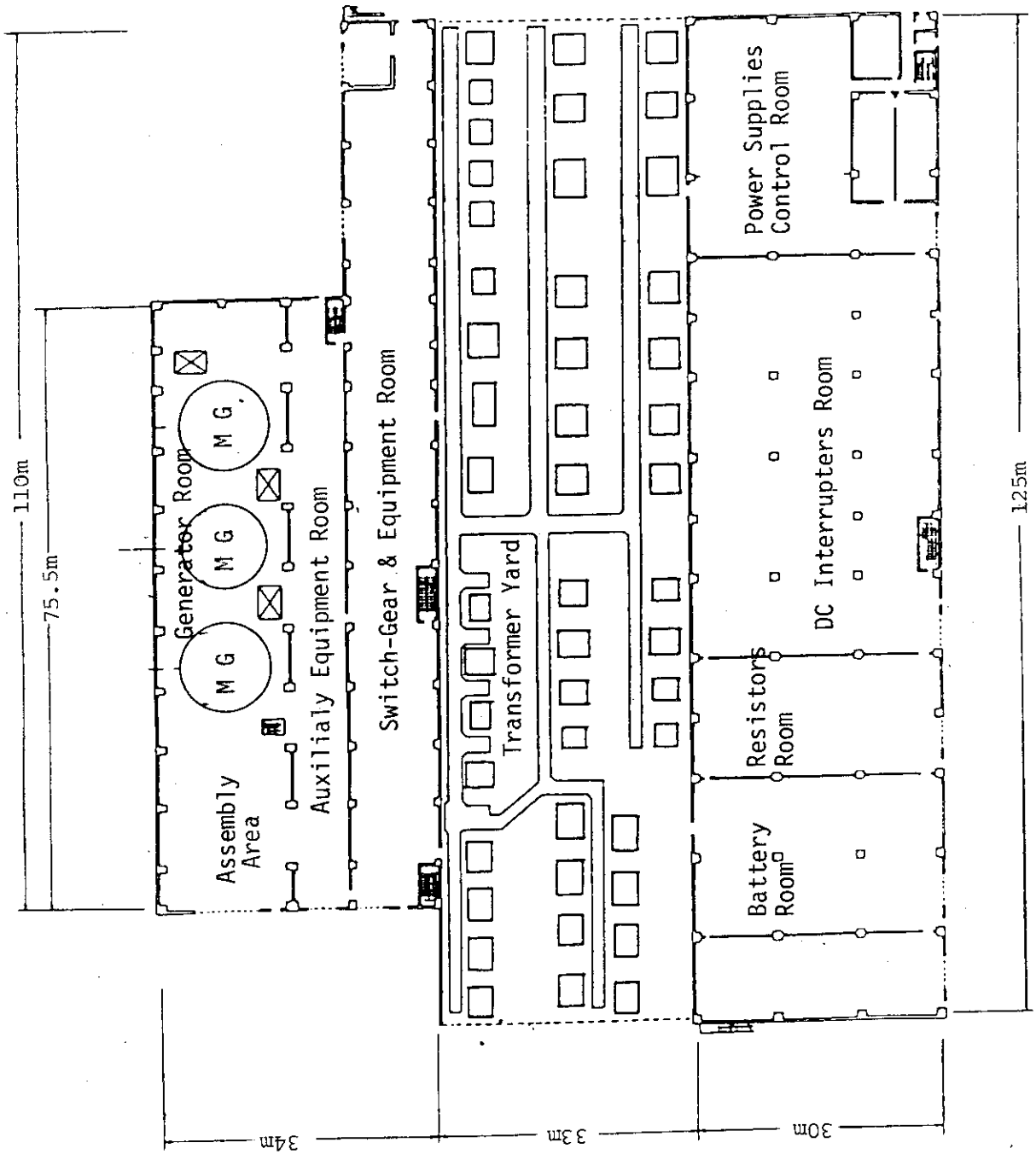

Fig. X.2-5 JT-60 Power Supplies Building 1F plan

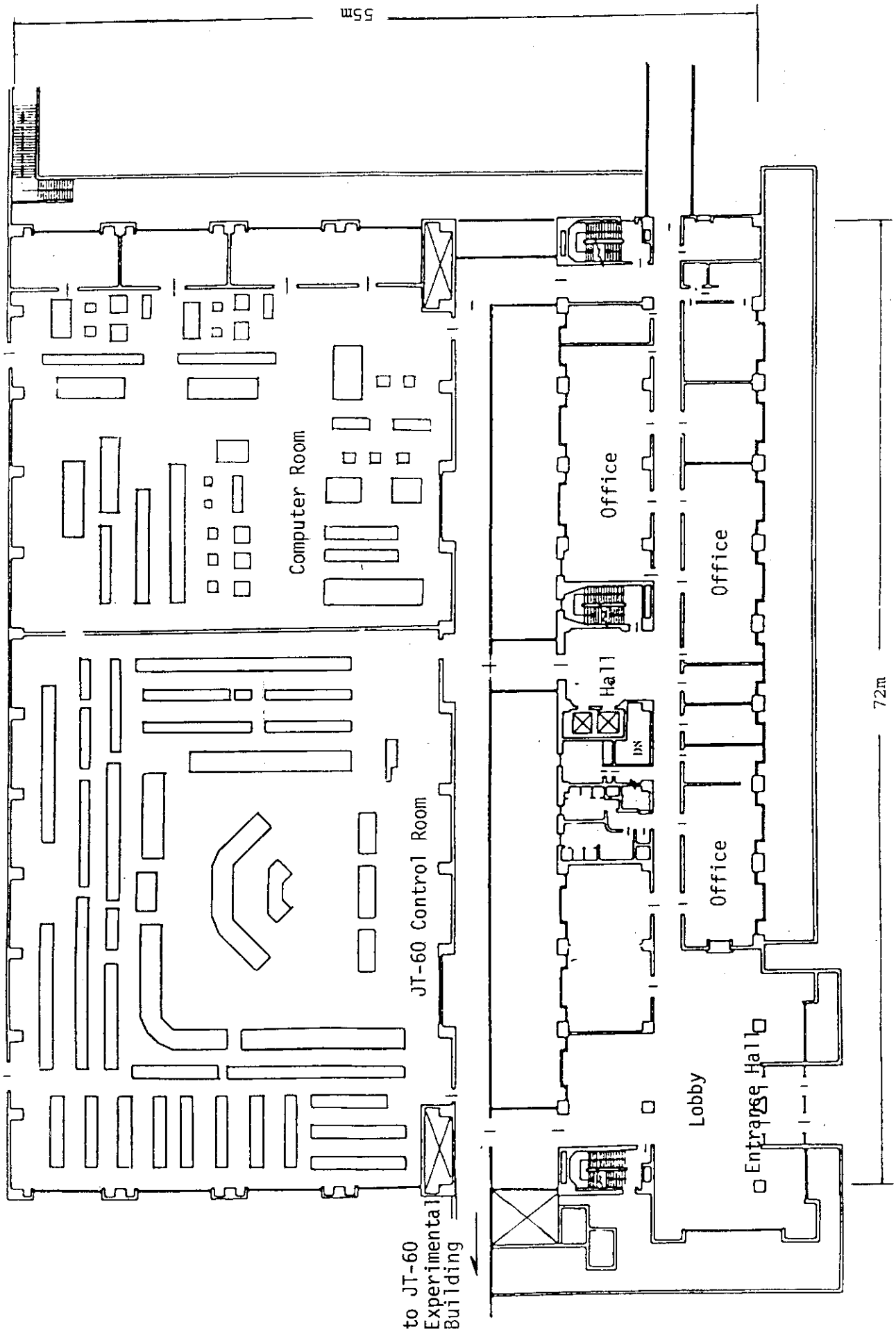

Fig. X.2-6 JT-60 Control Building 1F plan

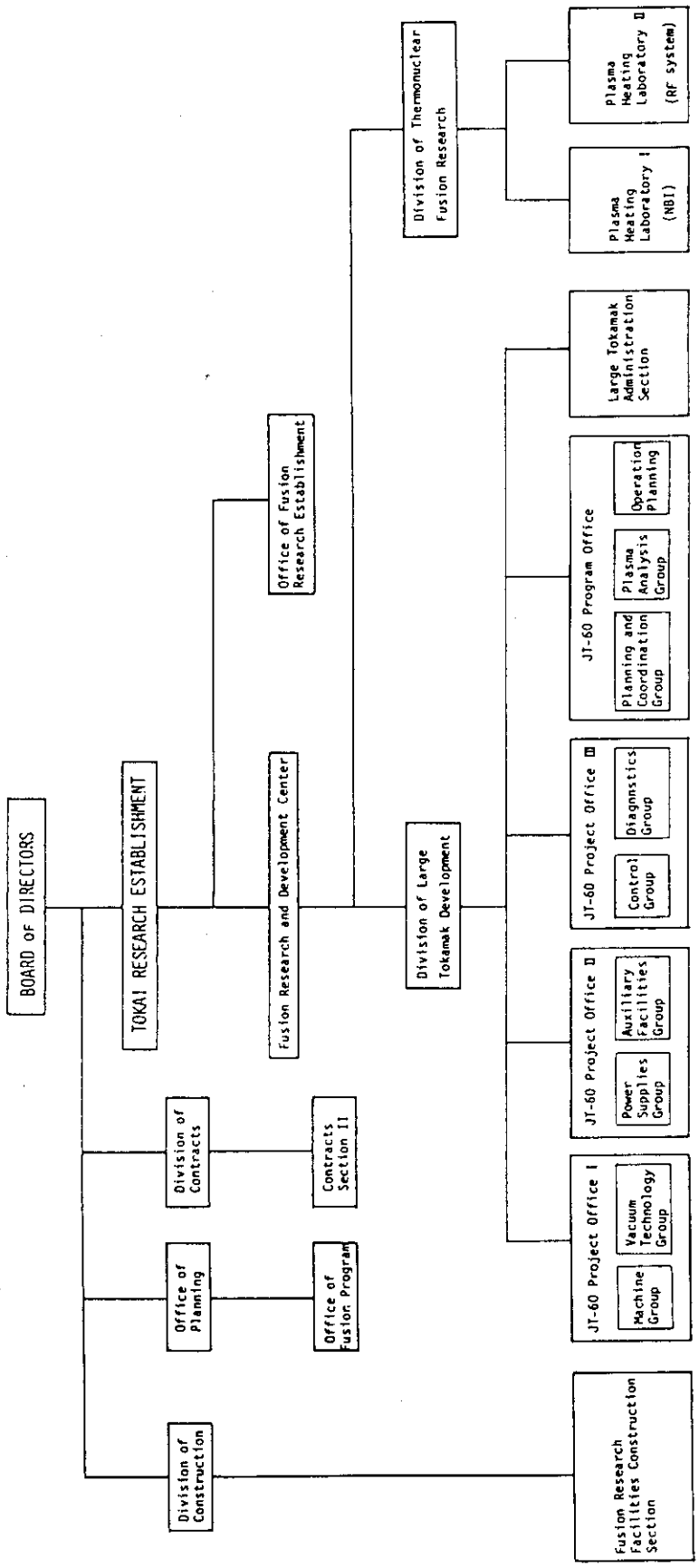

Fig. X.2-7 Organization related to JT-60 program

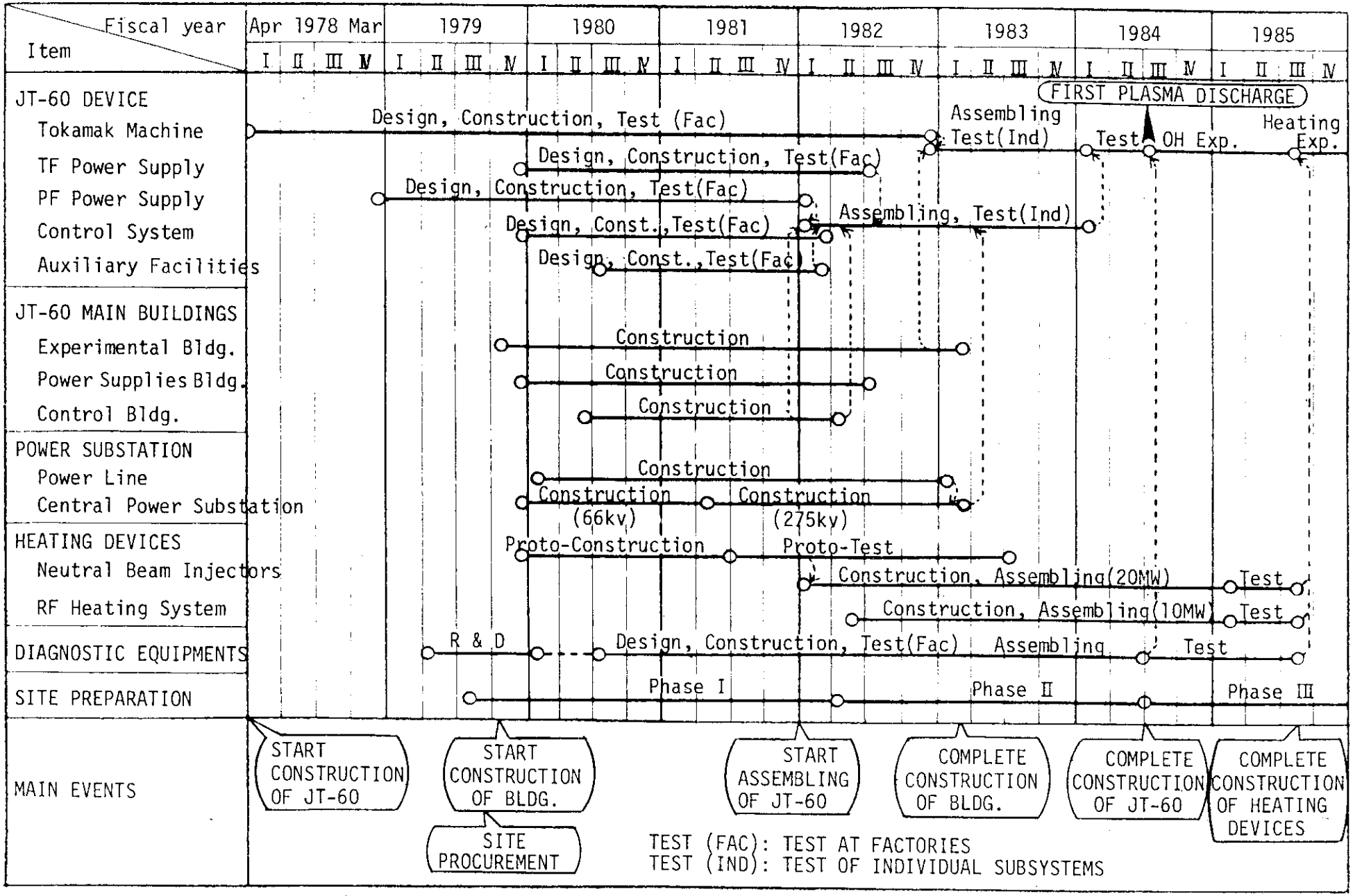

Fig. X.2-8 Master schedule of JT-60 program

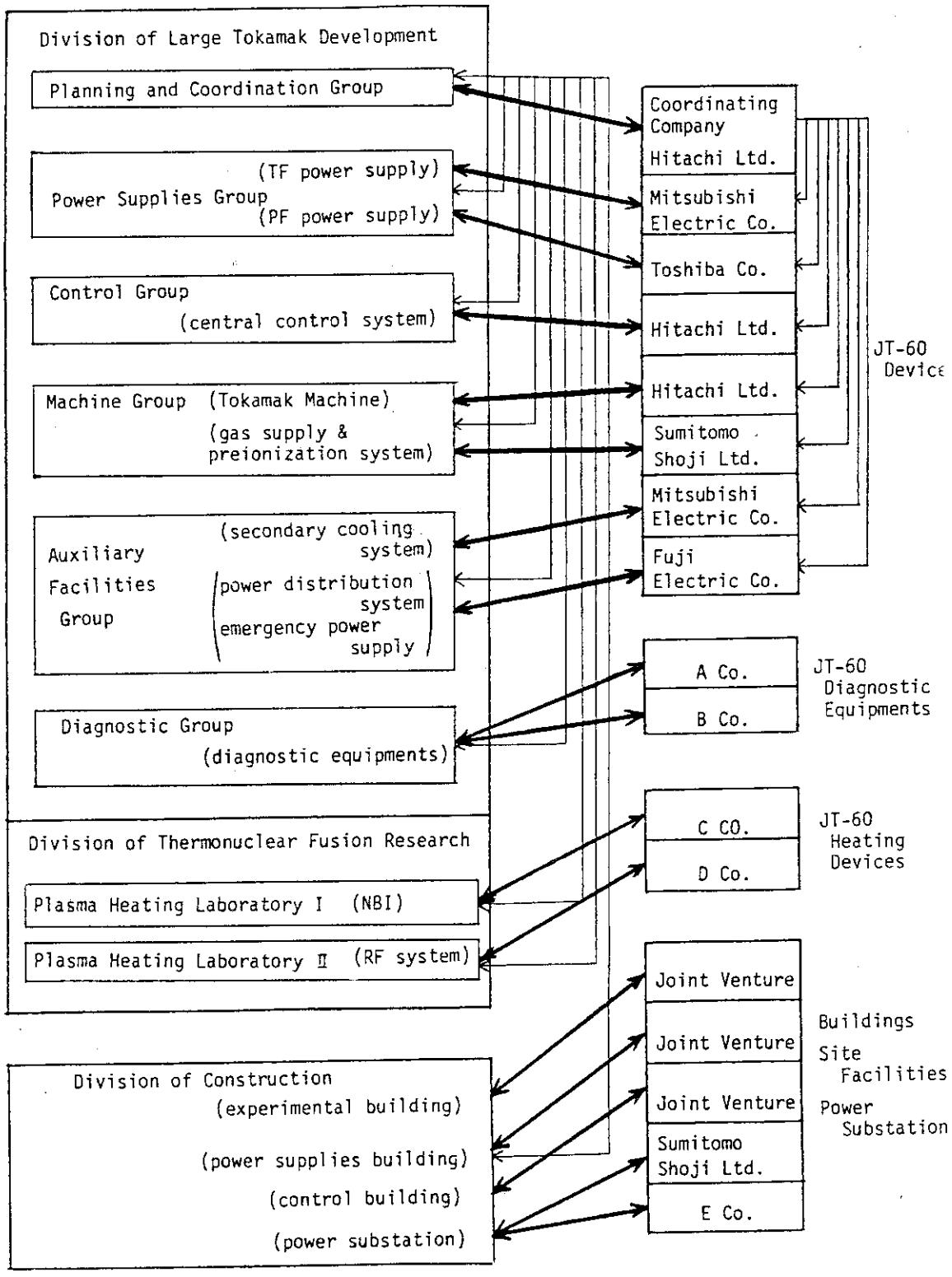

Fig. X.2-9 Organization structure

3. Status of Tokamak Machine

3.1 Major activity of tokamak machine

The tokamak machine of JT-60 is composed of a vacuum vessel, toroidal field coils, poloidal field coils, support structures, a primary cooling system, a vacuum pumping system, fast movable limiters, a preionization system, a gas-feed system, ajustable movable limiters, and a machine control system.

The contract of the construction of the tokamak machine except preionization and gas feed systems was made with Hitachi Ltd. in April 1978 and the design and fabrication of the machine components have been progressing favorably. The contract of the construction of the remained components was made with Sumitomo Heavy Isdustries Ltd. in March 1981 and their design has just started.

The present status of the machine is mentioned briefly as follows. All of the rigid ring plates of the vacuum vessel were pressed and welded with each other by electron beam welding into the sectorial rings with non-circular cross section. Some holes for various types of ports were cut off and some pads were welded to support first walls and magnetic limiter coils. The machining of them will be started early in the next fiscal year. The manufacture of eight U-shaped bellows is finished and the remained bellows will be delivered to Hitachi works from the bellows firm before July 1981. The fabrication of 14 toroidal field coils have been brought to completion and the remained 5 coils will be assembled by August 1981. The poloidal field coils are almost completely finished with design and is deeply into manufacturing. The manufacturing of the other components, which is not seen on the course of the critical path of JT-60 construction time schedule, poses no problems.

Some design changes have been made in the fields of a vacuum pumping system, a primary cooling system, a machine control system, amd first walls. The contract of the design change was made in March 1981. The time schedule of the machine itself is shown in Table X.3-1.

Related studies concerning the machine construction were also done successfully.

1) The effect of oxidation of copper metal seals at higher temperatures were examined through the experimental tests.

2) The reevaluation of mechanical strength of the welded connections of the vessel and the poloidal field coils was done by disccusing test and inspection methods, welding techniques, and accessibility at the assembly.
3) The computer codes to calculate stray fields produced by eddy currents and thermal convections around the machine were developed and their accuracy was examined through comparison with analytical results.

3.2 Status of machine components

3.2.1 Vacuum vessel

Following the basic design fixed in the last fiscal year, the fabrication design of the vacuum vessel was advanced and nearly completed in this fiscal year.

Fabrication of the vacuum vessel was advanced deeply in this fiscal year. Shaping and rough cutting of the large holes were completed for eight rigid rings with satisfactory dimensional deviation. And welding of the port boxes, pedestals of the first walls, support lugs and the other appendages of the inner and outer surfaces is now in progress. Fig. X.3-1 shows the 40°-sectorial rigid ring after shaping and welding the appendages.

Fabrication of eight bellows among eighteen (sixteen plus two spares) was also completed and fabricated ones, one of which is shown in Fig. X. 3-2, satisfied the required strict dimensional torelance.

The design of the diagnostic ports was changed drastically. In the former design welded bellows was to be installed at the root of the port to absorb the displacement of the rigid ring. However, as it has low reliability against twisting electromagnetic force and it seems hardly possible to access and repair it in case that it is damaged, it was taken away. And instead of it, shaped bellows is to be installed in the space inside the upper and lower support structures to absorb solely the vertical displacement of the rigid ring.

As the horizontal displacement of the rigid ring is absorbed by the deflection of the port, a large stress is afraid to be observed at the root of the port. Therefore, detailed structure design and stress analysis were carried out to reduce the stress concentration.

Together with the progress in the first wall design described in

3.2.2, efforts were concentrated on the design of the pedestals for the first walls and the other appendages which are attached on the inner and outer surfaces of the rigid ring. Geometrical arrangement of the electromagnetic diagnostic equipments was also taken into consideration for the pedestal design.

The control system of the temperature control equipment of the vacuum vessel was determined in consideration of safety, reliability and efficiency of the components and R&D is now in preparation to confirm its characteristics.

3.2.2 First wall

In this F.Y., the detailed analysis of electromagnetic forces have been done. Thermal analysis have been also performed under revised heat load concerning plasma behavior. As a result, the modifications of first wall design have been done[1].

(a) Liners; Since electromagnetic force at 1 msec major disruption is large, liner material has been changed. Liners in which large heat load of neutral beam shine-through deposits are molybdenum, 5 mm thick and cover ±60° in small major radius region as shown in Fig. X.3-3. The electromagnetic force induced on the liners around magnetic limiter coil can are large and heat load of scrape-off layer to the liner exceeds its permissible value. But, the liner design did not progress because its depend on the design of magnetic limiter coil can now in progress. Another part of liners are Inconel-625, 10-15 mm thick. Armor plates and bellows covering liners are attached without gaps to protect the vacuum vessel and bellows, respectively.

(b) Toroidal fixed limiters; Mechanical stress is not a serious problems. Thermal stress analysis is under way. Thermal snalysis was performed in the case of 10MW × 10 sec/10min deposition to all limiter lines and 3 limiter lines. All limiter lines case is permitted and 3 limiter lines case is not. In the latter case, thermal contacts between limiter and pedestral are necessary. Active cooling by N_2 gas of the limiter at outermost region has been adopted. To reduce large concentration of heat flux at the limiter edge, the edge was rounded off considering scrape-off plasma heat load.

(c) Poloidal fixed limiters; Poloidal fixed limiter, 20 mm thick

molybdenum plate, was attached in the outer region of 20°-50° to protect against orbit loss particle and to reduce heat load on the liners attached to sub-magnetic limiter coil cans.

(d) Magnetic limiter plates; Thermal analysis shows that 20 MW × 5 sec/10 min deposition is not permitted with radiation cooling. Therfore, the thermal contact between magnetic limiter plate and pedestral are necessary. To reduce electromagnetic force, each plate has a slit.

(e) Ripple loss protection plates; Design of ripple loss protection plates have been completed. Thermal cycle test to confirm its structure is under planning.

3.2.3 Toroidal field coils

Toroidal field coil (TF) coil system consists of eithteen unit coils and one spare unit coil. Till March 1981, fourteen TF coils have been fabricated as shown in Fig. X.3-4. These coils satisfied the criteria of all inspection tests. According to the ultrasonic inspection results for more than 2000 points of the brazed or welded joints, only eighteen defects of 6-10 mm in diameter and one defect of 10-15 mm in diameter were detected, and most of the joints had defects of less than 4 mm in diameter or no defects. Mechanical strength of these joints with above mentioned defects was calculated on the basis of fracture mechanics, and it became clear that all joints had sufficient mechanical strength. An error in measurement in winding conductor and casing process is less than 5 mm. This value is consistent with the assumption in error field calculation. Incidentally the last coil is to be fabricated not later than July, 1981. The fabricated unit coils must be kept in custody without worsening the property by February, 1983, start of JT-60 installation. The method of keeping the coils in custody is now under consideration.

3.2.4 Poloidal field coils

The poloidal field (PF) coils are composed of the ohmic heating coils (F coils), the vertical field coils(V coils), the quadrupole field coils (Q coils), the horizontal field coils (H coils) and the magnetic limiter coils (M coils). The design and manufacturing activities of the PF coils in FY 1980 are summarized as follows

A. Design

(1) The positions of the coils placed outside the vacuum vessel were slightly changed and the number of turns in the Q coils was reduced by 4 to enlarge the space for leading out the rewinding conductors. Following this, the coil support structure was also changed. Fig. X.3-5 shows the changed coil arrangement and the coil support. The revised specifications of the PF coils are listed in Table X.3-2.

(2) FEM stress analysis were made in detail for the turn-to-turn connecting conductor. The results show that the stresses appeared in the coils are very high, but these are acceptable. The mechnical tests of the F-13 mock-up coil are being performed to make sure the over all structural reliability of the coils. The F-13 coil and the test apparatus are shown in Fig. X.3-6

(3) Due to the high stress in the conductors, it was found to be necessary to develop an electrical insulation capable of withstanding a cyclic strain of about 0.3%. As a result of the screening tests, a combination system of epoxy semicured glass fiber-mica tape and epoxy semicured polyimid film was selected for the main insulation.

(4) FEM stress analyses of the coil support were also made. Results show that considerably high stresses arise on the corners of the coil bores at the inside of the support, but these are acceptable.

(5) The fatigue tests of full scale welded conductors were performed to confirm experimentally the allowable blow hole size. An evaluation from view point of fracture mechanics was also made.

(6) To reduce eddy currents induced in the copper conduit pipes for the supply of the cooling water, the material was changed to stainless steel.

(7) The optimization of the cooling paths were made in view of both the occupied space for the conduit pipes and the efficient heat removal. The path number of the M coil cooling system were reduced to half due to the limited space for taking out the coils from the vessel. The time dependent temperature rise of the welded joint of the M coils was calculated in detail coupled with the global thermal and hydraulic analysis by means of finite diference method.

(8) A change-over equipment of the M coil feeder is being designed for the independent operation of the main M coil.

(9) In considering the effect of the plasma beta on the flux change in the vicinity of the M coils on the occasion of plasma disruptions,

the reexamination of the eddy currents induced in the Inconel 625 jackets was made. Results show the larger value than that obtained so far. Hence, the thickness of the bellows was increased to 1.8 mm and Inconel 625 stopping rings and supporting rings were added to restrain the bellows deformation. Further, the ceramics which is inserted between supporting legs and the vacuum vessel were taken off to be capable of withstanding the increased mechanical load. Another feature is that the jacket is provided with the double wall protection plates as the thermal barriers against extraordinaly plasma heat unloads. One is the Inconel 625 cover plate which is welded to the support ring and the other the molybdenum liners which are bolt-jointed with the thick ring to face to the plasma. Fig. X.3-7 shows the cross-section of the M coil system.

(10) The research and development of the conductor connecting techniques of site has been continued. The fundamental structure of the conductor welded joint, the cooling pipe joint, the insulation system and the coil support assembling method have almost been determined. The pulse TIG welding method is thought to be most promising. The inside of the coil supports in this section were bent at several angles so that the insulation tape can be wrapped completely around the conductors.

B. Manufacturing

(1) The manufacturing of the conductors has been advanced without any trouble and by the end of March 1980 about 50% of the total PF coil conductors including the additionaly ordered ones has been produced.

(2) The manufacturing of non-magnetic steel plates for the coil support has been completed by the end of 1979.

(3) The preparations for purchasing Inconel 625 plates for the M coil jacket and molybdenum plates for the liners are now going forward.

(4) Through the trial fabrication of the F-13 coil, fabrication techniques and inspection methods of the individual coils have been established. The procedures of installing the coils in the coil supports were confirmed experimentally by use of the 1/6 wooden model shown in Fig. X.3-8. The fabrication of the individual coils were started from the innermost turn of the F coils. 25 turns of the F coils, which have total turns of 60, have been welded so far. The machining and the insulating process have begun. Electron beam welding method is to be adopted instead of MIG welding to improve efficiency of the work.

(5) Fabrication techniques and inspection methods of the coil supports have also been established.

(6) Manufacturing techniques of bellows for the M coils jacket have been established through the trial fabrication. Fabrication and assembling methods of the jackets as well as the coils are to be decided immediately.

3.2.5 Support structure

Fabrication design of the support structures was completed except minor adjustment.

All of the materials were delivered to works and fabrication is now in progress without any trouble. Foundation and central bases were already fabricated and are waiting for installation. Fig. X.3-9 shows the completed foundation base.

3.2.6 Vacuum pumping system

(1) Configuration

In order to fulfill the requirements for JT-60 vacuum pumping system turbomolecular pump system has selected. Its configuration is schematically shown in Fig. X.3-10.

This system has four identical sets each connected to a pumping port of vacuum vessel. One set consists of a manifold and three pumping subsystems. Total pumping speed of each subsystem is required as shown in Table X.3-3. The main pumping system has the pumping speed of 13,600 liters/sec for nitrogen and 29,000 liters/sec for hydrogen. This system used in the pressure range of less than 1.33Pa. Roughing pump system evacuates the vacuum vessel from atmospheric pressure to 1.33 Pa. Its average pumping speed is about 600 liters/sec. Maintenance pumping system keeps the vacuum vessel in high vacuum during suspension of operation. Its pumping speed is about 5,000 liters/sec.

In addition, peripheral subsystems such as compressed air supply system, cooling water supply system, dry nitrogen and/or dry air supply system, liquid nitrogen supply system, pressure measurement system and control system are provided in order to support each pumping system.

(2) Fabrication

Fabrication of roughing pumping system, maintenance pumping system

and the peripheral system exclusive of liquid nitrogen supply system has been started.

Turbomolecular pumps for main pumping system was imported and their acceptance tests are under way.

(3) Reliability tests

Two reliability tests are planned. One is 40-cm ID all metal gate valve and the other is for 53-cm ID ceramics insulation joint.

They will be accomplished by Dec. 1981.

3.2.7 Primary cooling system

The major part of fabrication design has been completed in F.Y. 1980. Fabrication of machine element was progressed satisfactorily. Heat exchanger and demineralizing system have been fabricated. Fabrication of filter and pump is now in progress to be completed in Aug. 1981.

3.2.8 Fast movable limiter

The problem of a mechanical strength of the adjustable mechanism had been solved by load tests using the actual size model. Because that most of fabrication design was completed, the manufacturing was started in Feb. 1981. Tests concerning vacuum characteristics and electrical insulations will be planned in coming June or July. The fabrication in work shop will be expected to be completed in Mar. 1982.

3.2.9 Adjustable movable limiter

Since the vibration problem of adjustable movable limiter due to the electromagnetic load on JT-60 vacuum vessel, a lot of careful design efforts have been made in last few months. The safety measure by the results of these analysis will confirm the operation of adjustable movable limiter with safety. Thus, the fabrication design is little behind the schedule, but the fabrication of adjustable movable limiter in work shop will be completed in Mar. 1982.

3.2.10 Gas feed and preionization system

Major efforts for construction of gas feed and preionization system were concentrated on the decision of their specification.

The contract of construction of their system was made with Sumitomo Heavy Industry at March, 1981. Two gas feed systems of fast electromagnetic valve and piezo-electric valve are connected with the vacuum vessel at four locations around the torus. The main features of gas feed system are shown in Table X.3-4. Preionization systems are composed of two type methods such as electron gun type and $J \times B$ plasma gun type.

3.2.11 Machine control system

Design change of the control system have been made, because microcomputerized CAMAC system was introduced for the interface between ZENKEI and machine control system. An actual CAMAC system is shown in Fig. X.3-11. The construction design of the control system, introducing CAMAC system, has been continued, and the final specification of CAMAC system was decided. Developed microcomputerised CAMAC crate controller is shown in Fig. X.3-12. The crate controller with microcomputer has a double width in order to provided the complete interface between H-08L(Hitachi Co.) computer and a CAMAC crate.

3.3 Related studies

(1) The eddy current analysis [2)]

Based on the finite element circuit theory, the analytical method of the eddy current on multi-shell torus system have been developed. Assuming an each conductive plate to be infinitely thin, the magnetic interaction between conductive surfaces is obtained by the enegy integration for the corresponding eigen mode of eddy current on the respective surface and a set of given circuit equations in this torus system is solved again by the method of eigen value expansion. Since the present method can provide the advanced results on eddy current problem in the actual tokamak divice composed of many component such as JT-60, it will be possible to discuss quantitatively the electromagnetic load and the effects of the eddy current field on the control of a plasma cross-section and its desired position according to the required accuracy. The computer program using this method is now developed to be completed in this autumn.

(2) Natural convection analysis

The thermal design of JT-60 showed some difficulties related to natural convection. When the vacuum vessel is baked up, the air flow heated at the surface of the thermal insulator covering the vacuum vessel makes trouble with diagnostics and electric insulator of poloidal magnetic field coils, located over and around the vacuum vessel. Therefore, it is necessary to analyze, in detail, the natural convection of air around the vacuum vessel, in order to determine the maximum allowable baking and operation temperature and to design heat removing equipments. For this purpose, two finite element codes are developed. One is a steady state analysis code with penalty function method [3]. The other is a transient analysis code with stream function and vorticity, instead of velocity, as basic variables. Both codes are tested by example problems, with good results. The technique for the stable computation of the problems with high Grashof number, such as the natural convection around JT-60 vacuum vessel, is to be investigated. Both codes will be compared with each other and the more suitable method will be chosen for further development of the code system.

(3) Reliability test of vacuum gasket under oxidation and deoxidation[4]

Oxidation and deoxidation treatments in the high temperature are adopted for cleaning of Mo first wall in JT-60.

Reliability test of vacuum gaskets were carried out under the condition of oxidation and deoxidation. Experimental conditions are shown in Table X.3-5. Vacuum gaskets are experienced five cycles. One cycle consists of oxidation and following deoxidation treatment. For Cu gaskets and stainless O-ring in Conflat flange, satisfactory vacuum seal (less than 1.3×10^{-11} Pa·m^3/s) was obtained. But, in the case of Cu gasket of ICF-253, peel is observed on the gasket surface and pinlike pieces made of gasket material are observed around the surface of flange. The pictures of gasket and pinlike pieces are shown in Fig. X.3-13.

These pieces may be the plasma impurities. But, Ag coating on Cu gasket may bear using in JT-60 because Ag resists the above mentioned chemical treatment.

Reference

1) Nakamura,H.,Masuda,M.,Miyauchi,Y.,Shimizu,M.,Yamamoto,M.,Ogiwara,N., Ohta,M., and Owada,K.:Proc. 11th Symposium on Fusion Technology, Oxford, UK, Sept. 15-19, 1980

2) Nakamura,Y., Ozeki,T.: JAERI-M 9612(1981) in japanese

3) Miyauchi,Y., et al.: to be published

4) Amano,S., Arai,T.: J.Vac.Soc.Japan Vol.24,No.2,pp 76-77(1981)

Table X.3-1 Time schedule of Tokamak system (JT-60).

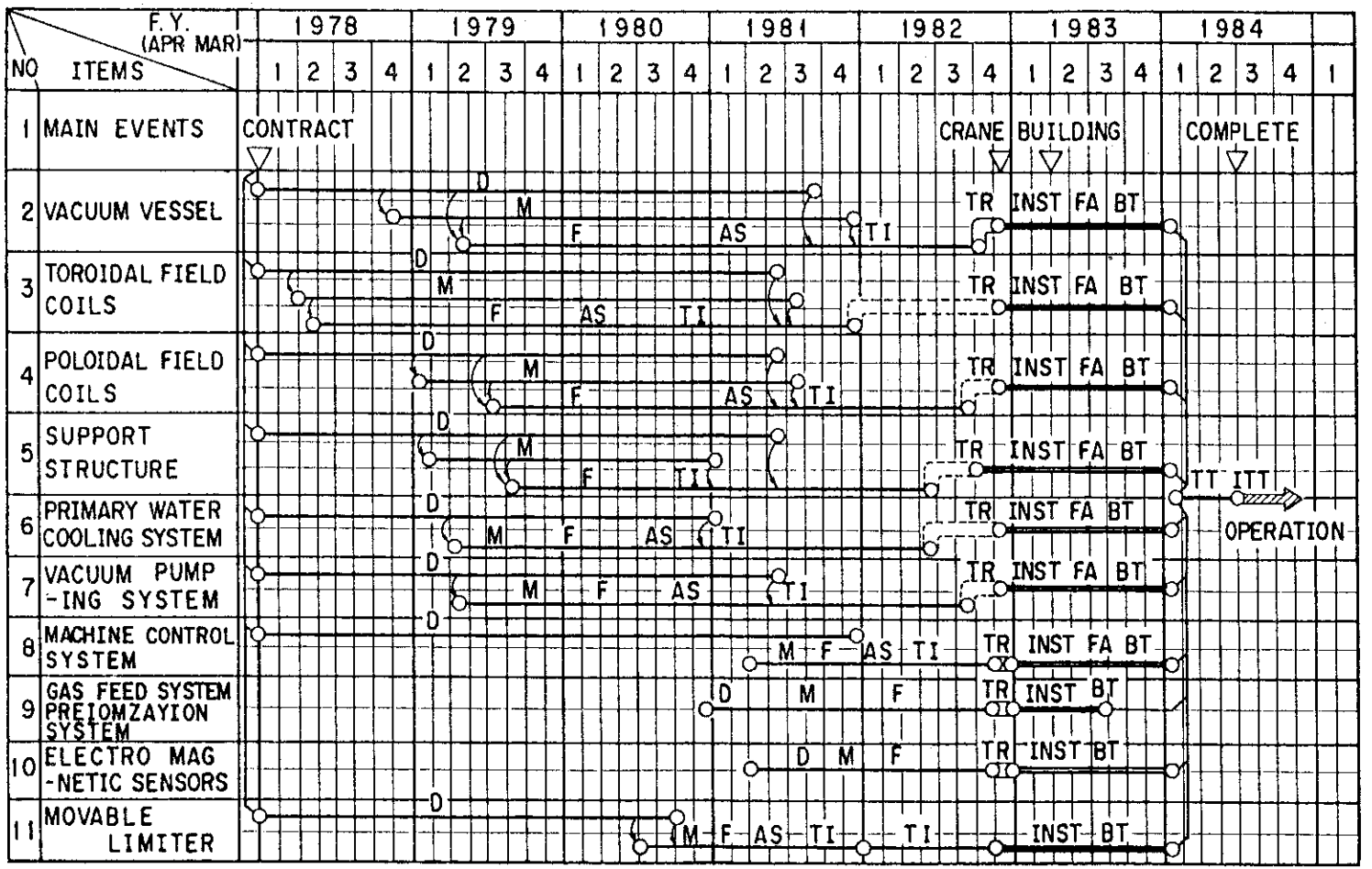

D : DESIGN
M : MATERIAL
F : FABRICATION
AS : ASSEMBLING
TI : TEST & INSPCTION
TR : TRNSPORTATION
INST : INSTALLATION
FA : FINAL ASSEMBLING
BT : BLOCK CHECK & TEST
TT : TOKAMAK SYSTEM CHECK & TEST
ITT : INTEGRATED TOKAMAK SYSTEM CHECK & TEST

Table X.3-2 Poloidal field coil specifications.

PARAMETER	F COILS	V COILS	H COILS	Q COILS	M COILS
AMPERE TURNS(MAT)	5.5	±1.84	±0.12	±0.45	±0.755
TOTAL TURNS	60	64	12	36	16
MAX. CURRENT(kA)	91.7	57.5	20	25	94.4
INDUCTANCE(mH)	8.3	9.7	0.44	2.2	0.87
RESISTANCE(mΩ)*1 (AT 75 °C)	4.6	11.9	4.1	13.0	3.2
TIME CONSTANT (SEC)	1.8	0.82	0.11	0.17	0.28
I^2R (MW)	38.7	39.3	1.6	8.1	28.5
$LI^2/2$ (MJ)	34.9	16.0	0.09	0.69	3.9
EQUIVALENT SQUARE WAVE PULSE LENGTH (SEC)	8	6	7	7	6

*1 NOT INCLUDING FEEDERS

Table X.3-3 Total pumping speed of each pumping system.

SYSTEM	PUMPING SPEED	PRESSURE RANGE
MAIN PUMPING SYSTEM	13,600 l/sec (N_2) 29,000 l/sec (H_2)	LESS THAN 1.33 Pa (10^{-2} Torr)
ROUGH PUMPING SYSTEM	120 ~ 1,400 l/sec	ATMOSPHERIC PRESSURE ~ 1.33 Pa (10^{-2} Torr)
MAINTENANCE PUMPING SYSTEM	5,300 l/sec (N_2) 10,000 l/sec (H_2)	

Table X.3-4 Specification of gas feed system.

	VALVE	Throughput (Torr-l/sec)	Injected Gas (Torr-l)
SUPPLY-I	FMV (H)	———	60
	PEV (H)	10-1600	3500
	PEV (L)	0.1-20	100
SUPPLY-II	FMV (L)	———	14
	PEV (H)	10-1600	3500
	PEV (L)	0.1-20	100
SUPPLY-III	PEV (L)	0.1-20	100
SUPPLY-IV	PEV (L)	0.1-20	100

FMV; Fast Electro-Magnetic Valve

PEV; Piezo Electric Valve

Table X.3-5 Experimental conditions of oxidation and deoxidation test.

Treatment	Oxygen treatment	Hydrogen treatment
Pressure (Pa)	133	367
Temperature (°C)	300	300
Time (hour)	4	20

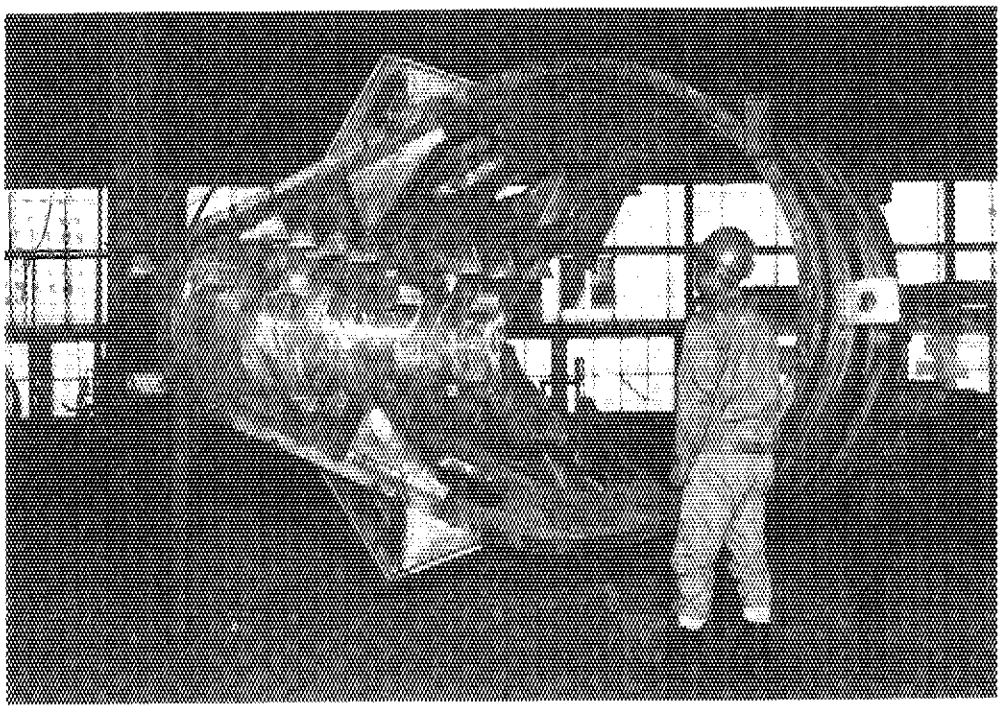

Fig. X.3-1 Shaped 40°-sectorial rigid ring before minute machining.

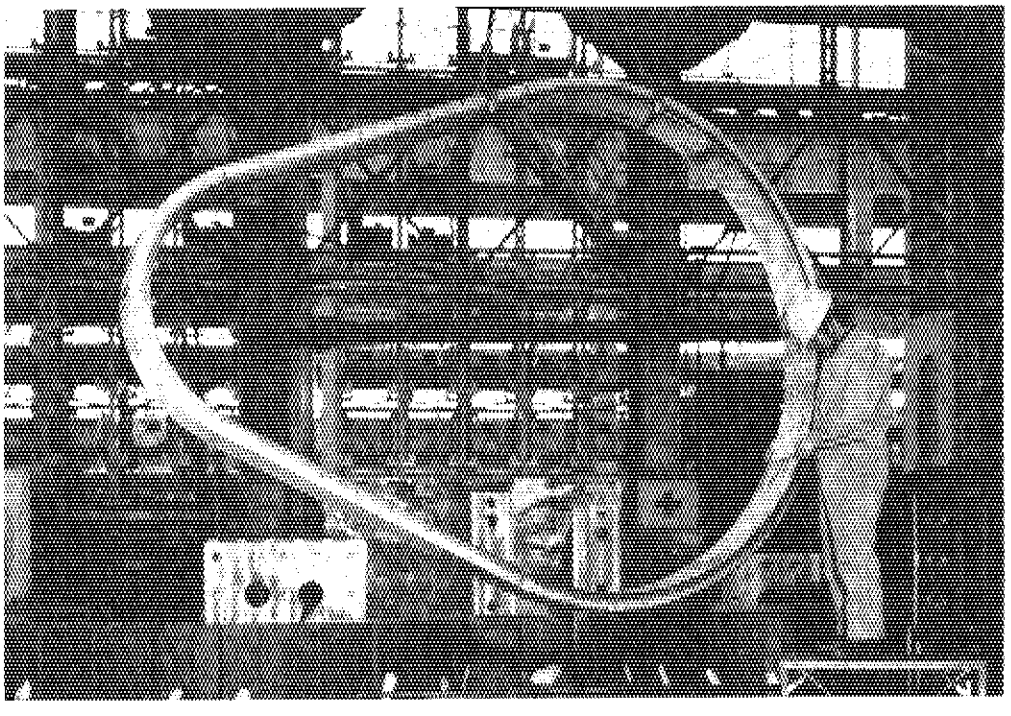

Fig. X.3-2 Fabricated U-shaped bellows.

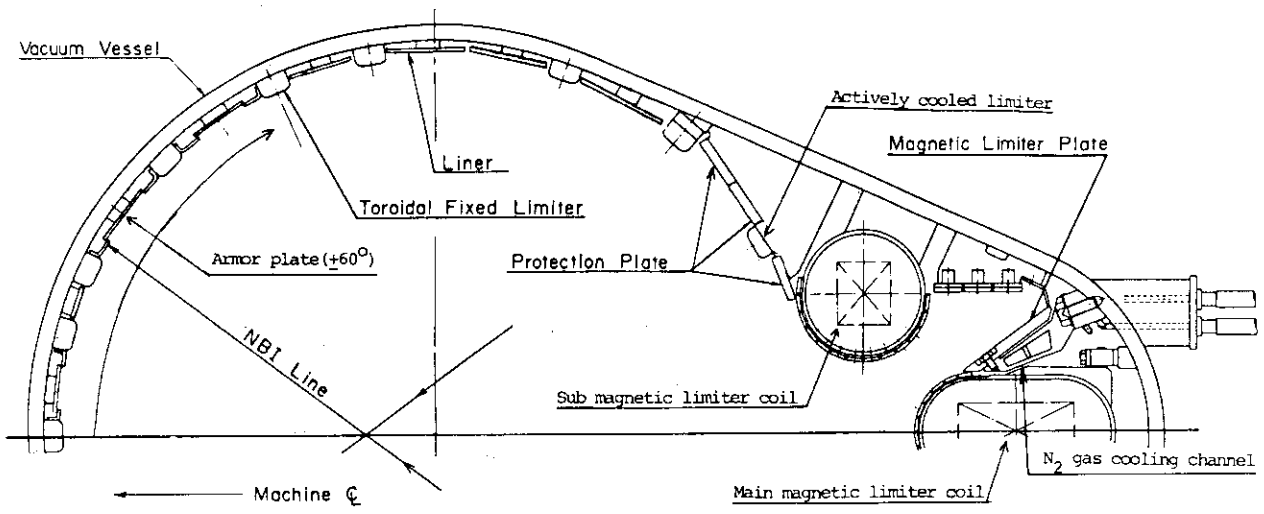

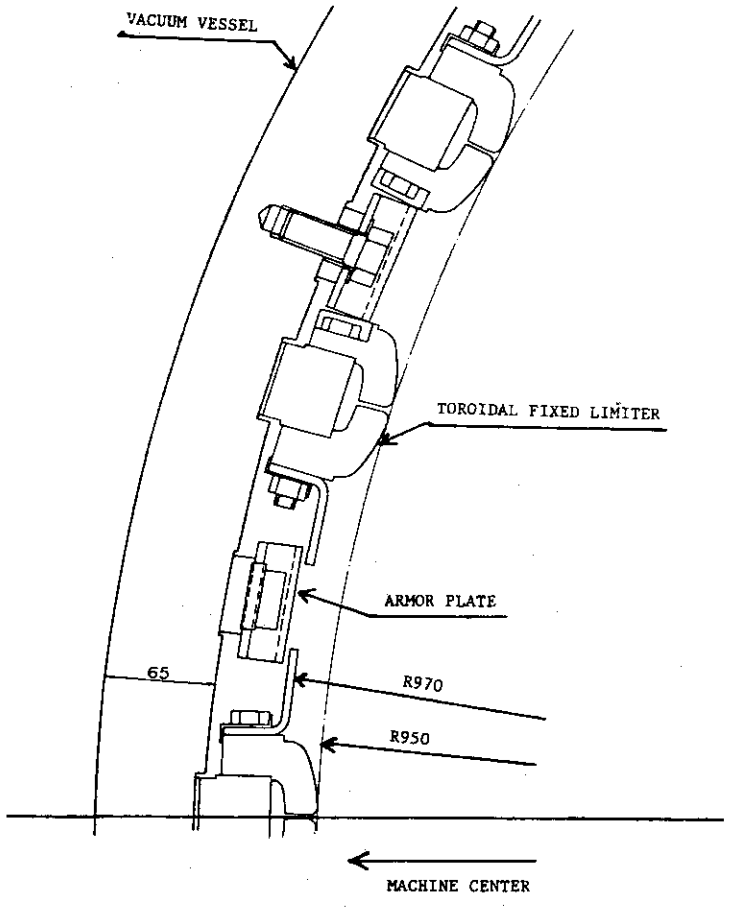

Fig. X.3-3 Arrangement of JT-60 first walls; Toroidal fixed limiter, Armor plate, Liner, Protection plate, Magnetic limiter plate. Lower figure is detailed structure of inner region.

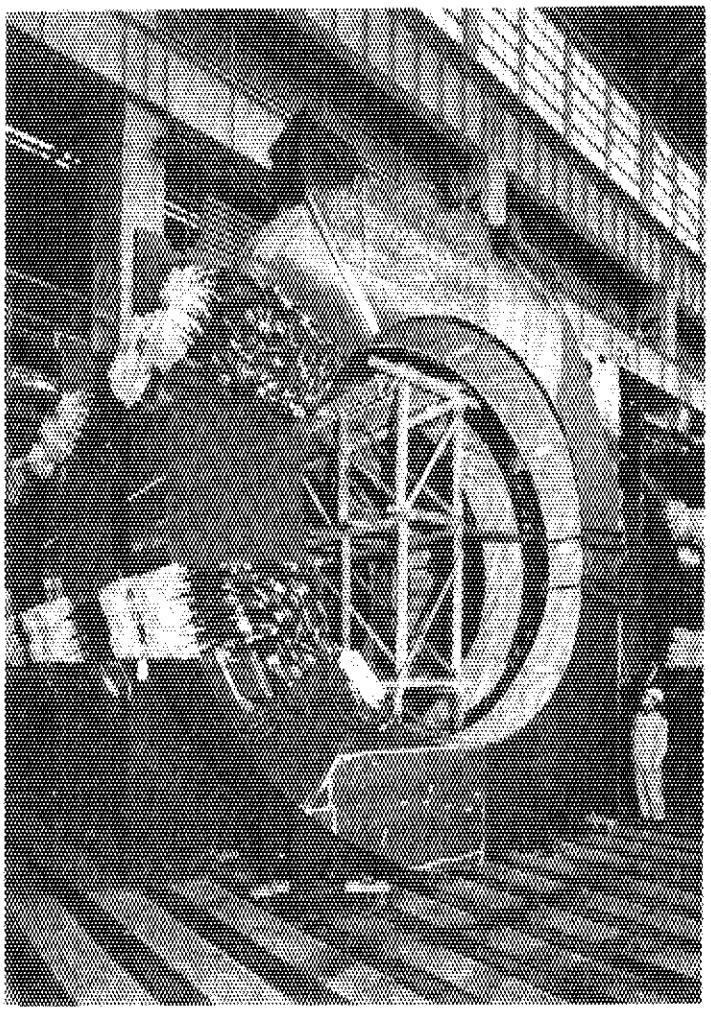

Fig. X.3-4 Fabricated Toroidal Field Coils.

Fig. X.3-6 F-13 mock-up coil being installed in the test apparatus.

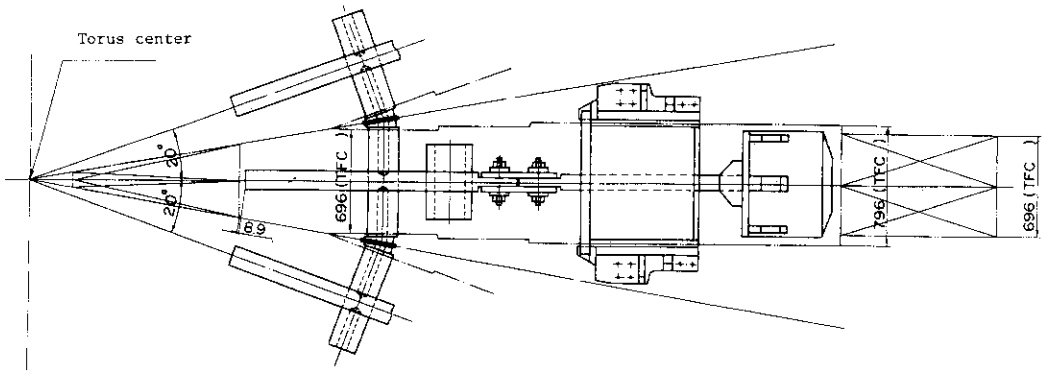

(a) Plane view of support structure

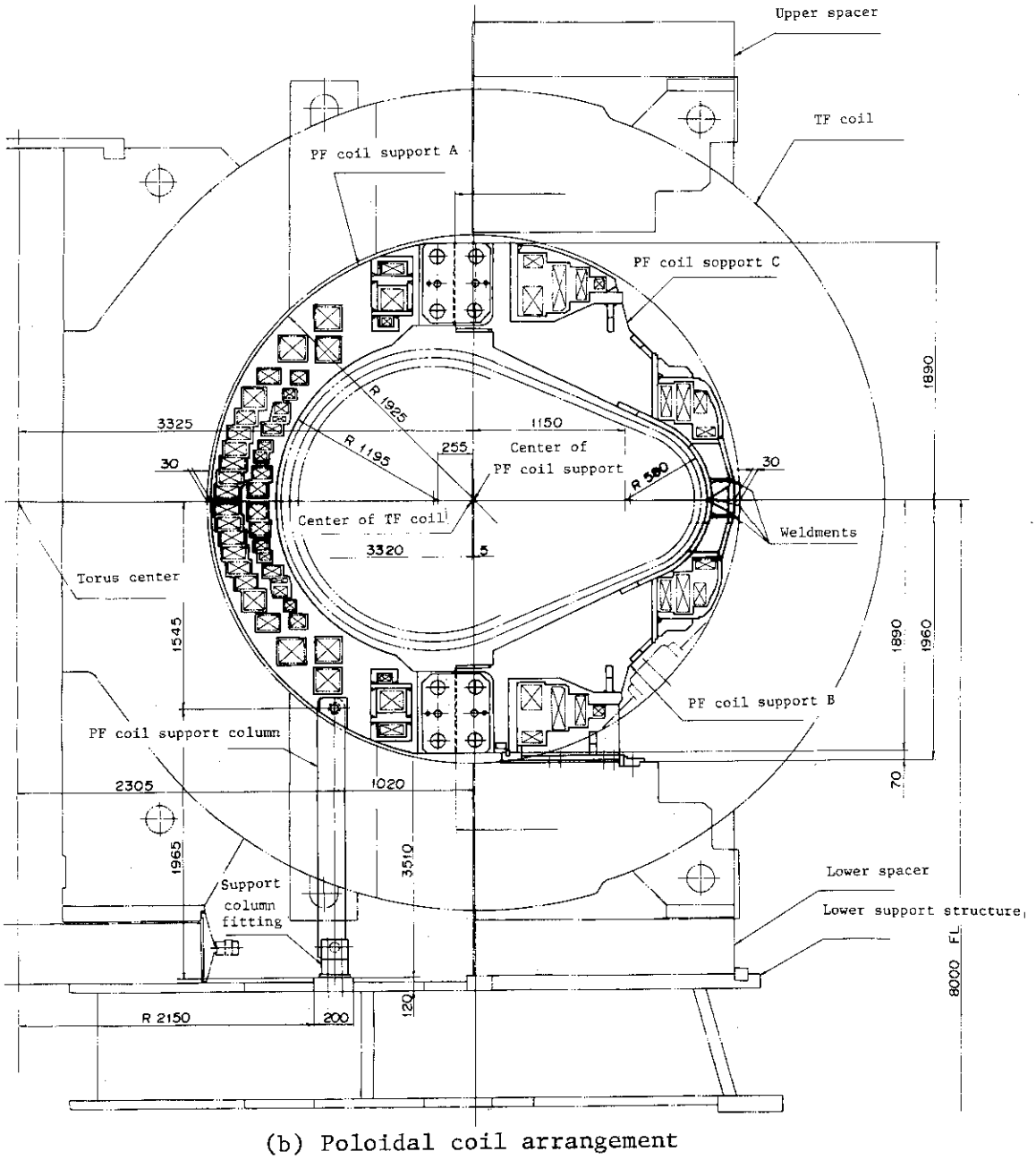

(b) Poloidal coil arrangement

Fig. X.3-5 Poloidal coil arrangement and support.

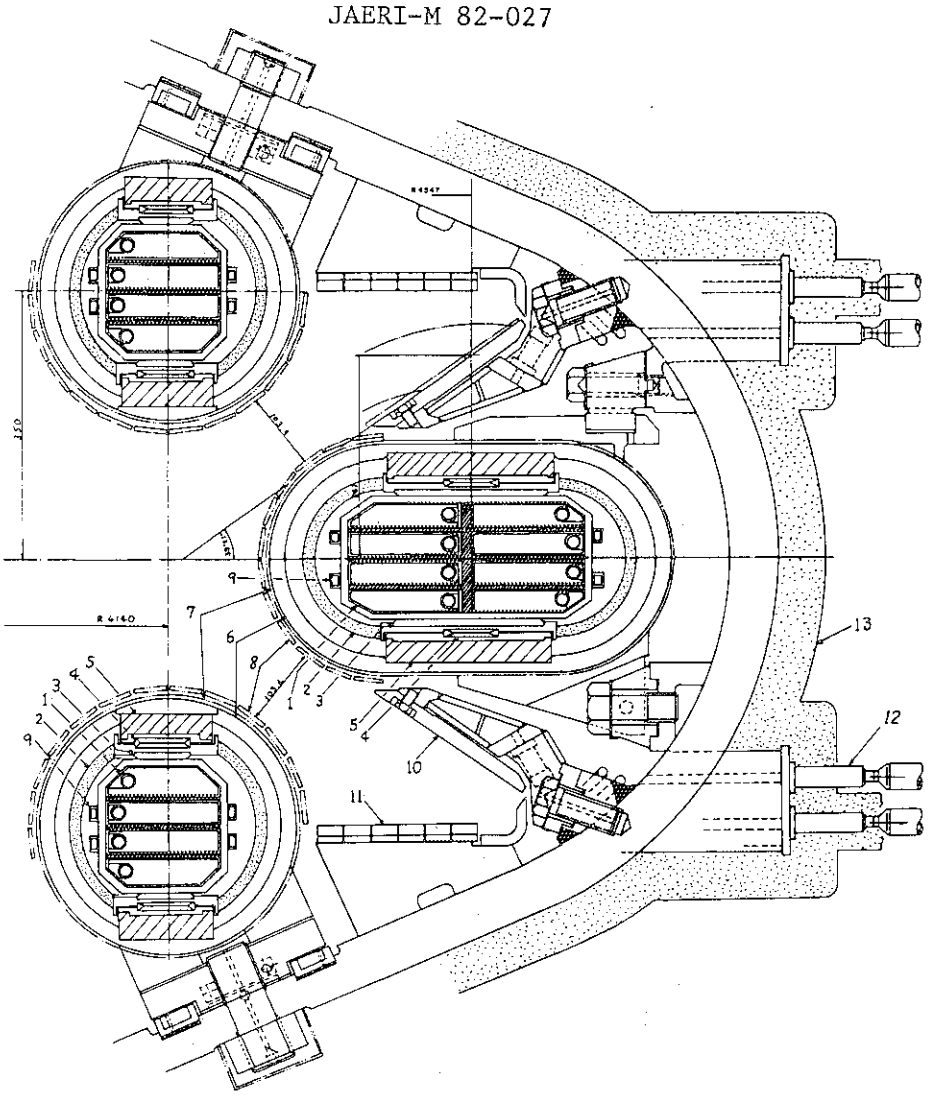

Fig. X.3-7 JT-60 magnetic limiter system

1 coil, 2 thermal insulation, 3 sliding plate, 4 coned disc springs, 5 ceramics, 6 thick ring, 7 support ring, 8 liner, 9 cooling pipe, 10 magnetic limiter plate, 11 liner, 12 cooling duct, 13 thermal insulation

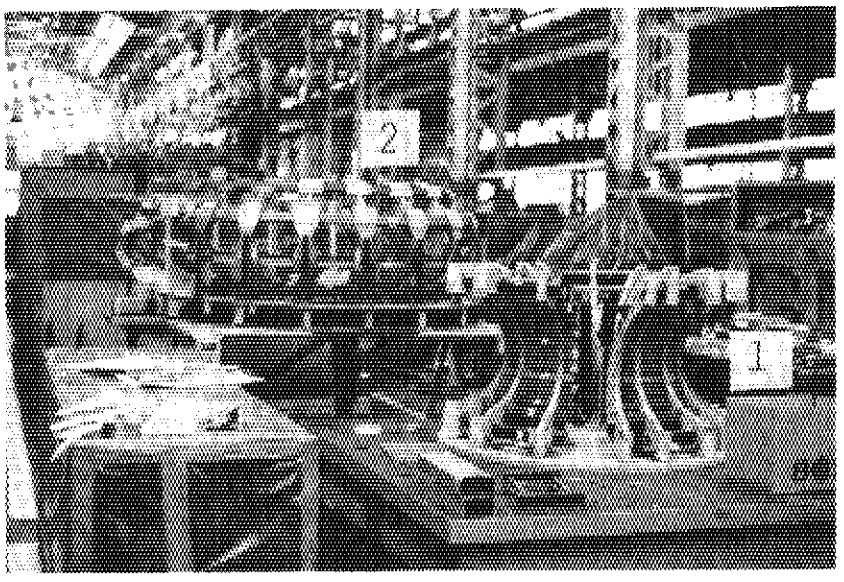

Fig. X.3-8 1/6 wooden model of the poloidal field coil assembly for the installation trainning.
1. inner assembly, 2. outer assembly

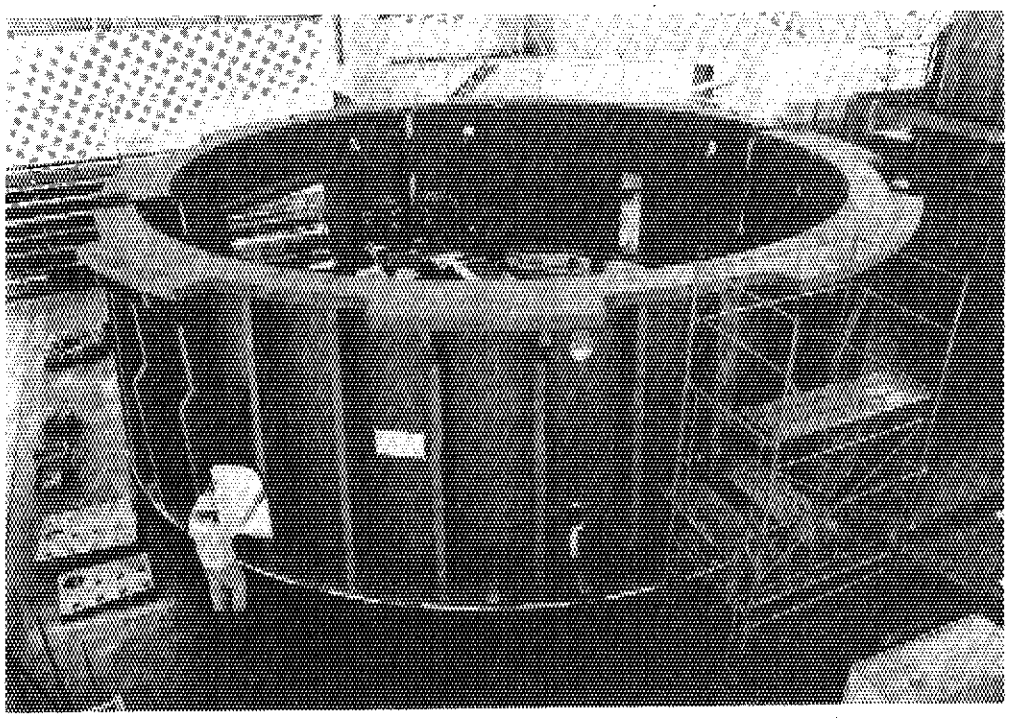

Fig. X.3-9 Lower support structure waiting for assembling.

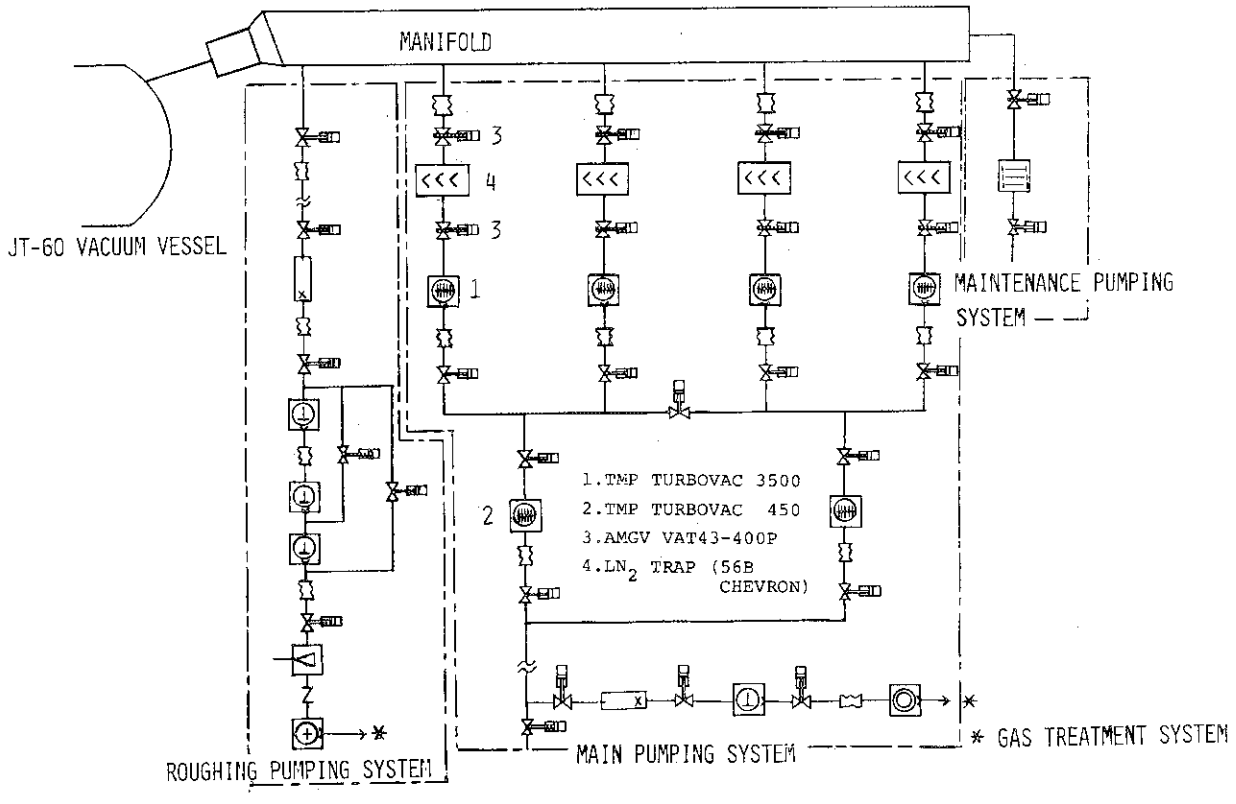

Fig. X.3-10 JT-60 vacuum pumping system configuration (1/4).

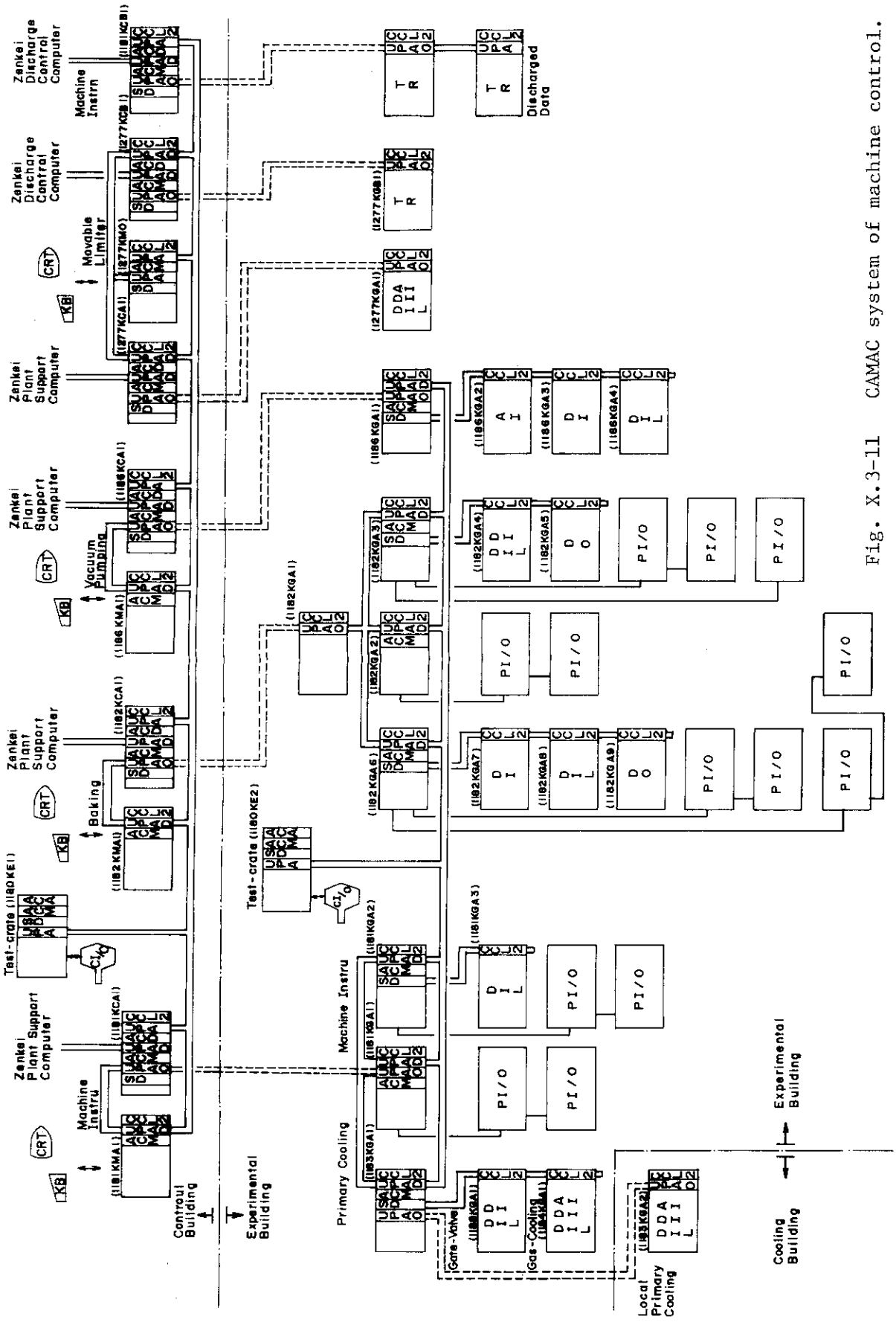

Fig. X.3-11 CAMAC system of machine control.

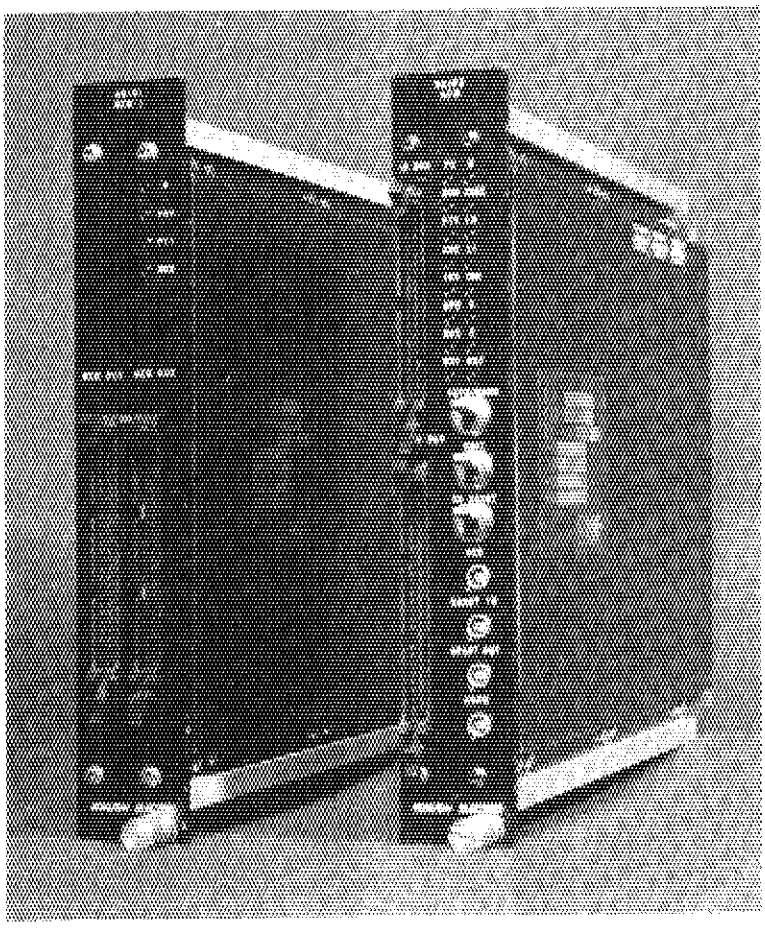

Fig. X.3-12 Microcomputerized CAMAC crate.

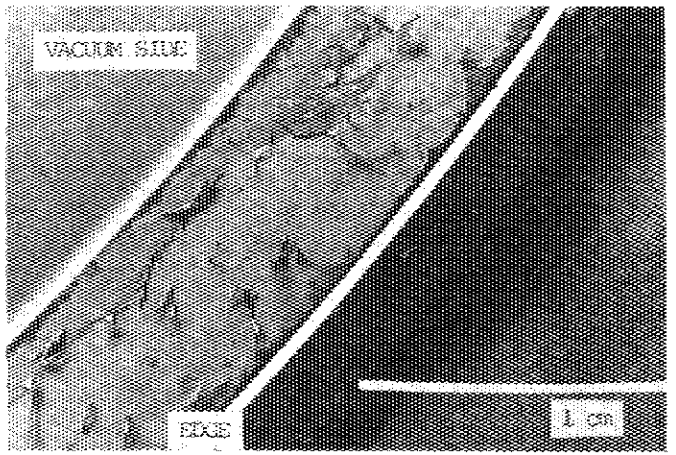

Surface change of ICF-253, Cu gasket. Peel is observed on the gasket surface.

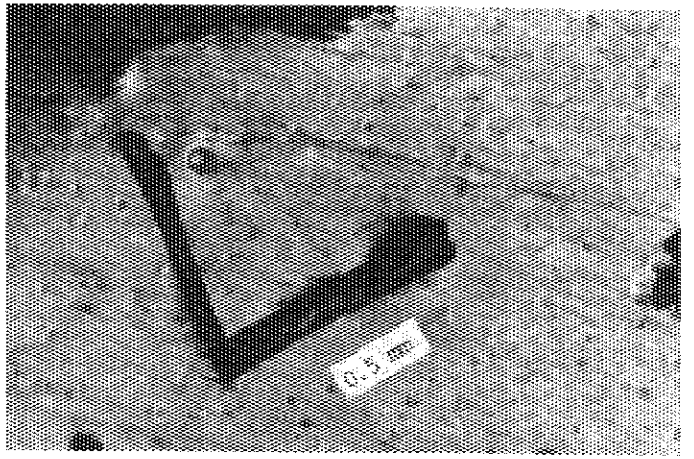

Microphotograph of peeled pinlike pieces about 0.5 mm length.

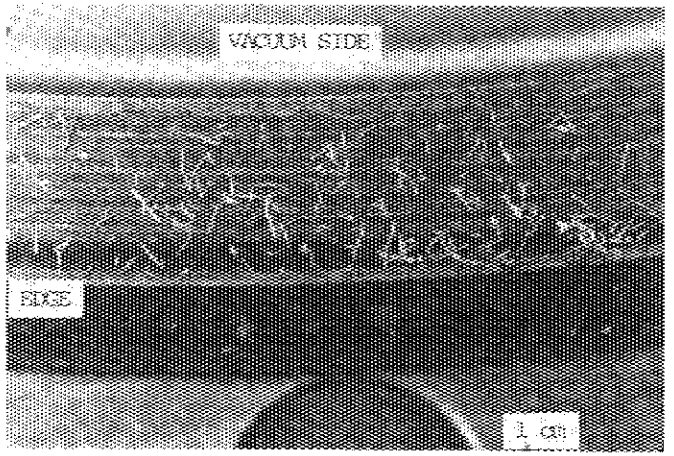

Pinlike pieces peeled from the gasket are observed around the edge of ICF-253, Cu gasket.

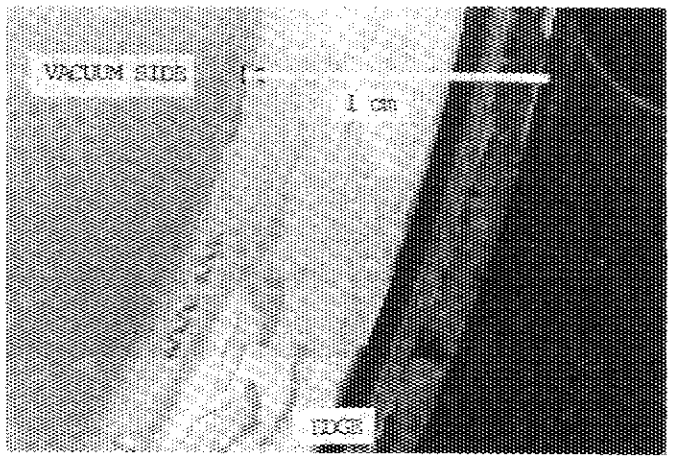

Surface change of ICF-152, Cu gasket (vacuum side is left-hand). Some swells are observed on the leftside of the gasket.

Fig. X.3-13 Pictures of gasket after oxidation and deoxidation test.

4. Status of JT-60 Power Supplies

The manufacture of the poloidal field power supply has been continued at Toshiba Corporation since April 1979. During this period, efforts were concentrated mainly on the manufacture of a 500 MVA motor generator. Along with this, performance tests of a prototype unit of thyristor convertors and some auxiliary equipment of the ohmic heating field power supply were carried out, and the final examination of their specification has been made by taking account of the results of the test. Shortly the manufacture of thyristor convertors systems will be started on a full scale. The systems design of the control system (CAMAC systems) has been completed, and preceding manufacturing, the detailed specification of hardware equipment is now being examined. Development of software for the control system is also going on. As a whole, the work of the poloidal field power supply has been in progress as scheduled.

The systems design and the layout plan of the toroidal field power supply have been finalized mostly. Following the final examination of specification, the manufacture of a 215 MVA-4000 MJ flywheel generator will be started shortly at Mitsubishi Electric Corporation. For the driving system of the generator, a static starter system using thyristors has been adopted in contrast with an induction motor for the poloidal field power supply. The progress of work of the toroidal field power supply is also going on favorably.

The construction work on the MG building in which three generators of the JT-60 electrical system are placed commenced in April 1980. The construction of the rectifiers building and the transformers yard will be started in October, 1981.

The construction of the JT-60 grounding system has progressed with the construction work on the JT-60 buildings and underground ducts for cabling and piping.

The design of the third generator for the JT-60 electrical system has been completed and the specifications are now being prepared. The generator is to supply electric power for both the neutral beam injection heating system and the radio-frequency heating system. The peak power required by the loads is about 400 MVA with a released energy of about 2600 MJ during a pulsed (10 sec) operation.

4.1 Poloidal field power supply

The poloidal field power supply of JT-60 is shown schematically in Fig. X.4-1 and the main characteristics of the major components are summarized in Table X.4-1. A motor generator supplies electric power for all the poloidal field coils with the peak apparent power of 500 MVA and the energy of 1.3 GJ. Each of the poloidal field coils is independently powered and controlled by respective thyristor banks to meet various operational requirements of the poloidal field system.

Detailed reexamination of the electrical and the mechanical design of the generator was completed, and the manufacture is now going on. (See Fig. X.4-2)

A check and review work on the design of the poloidal field power supply system has been made based on the discussions of reexamination meeting for JT-60 operational scenarios and plasma control. The quadrupole field coil power supply has been modified largely on the basis of the new scenario of plasma control, and its power rating has been changed to ±25 kA-±0.9 kV, approximately one-half of the original one. In the vertical field coil power supply, some improvements on the plasma controllability has been introduced. The magnetic limiter coil power supply has also been modified to meet a high-β plasma operation mode and some reconsideration about the new coil current form in the start-up phase was made.

The manufacture of a prototype unit of the ohmic heating coil power supply has been completed as mentioned above, and they were fully tested to obtain detailed information of their performances and accordingly to finalize the specifications for manufacture. Some optimization and improvement have been made on each prototype component. The brief descriptions of these components, thyristors, Hall DC-CT, trigger gaps and voltage dividers (See Fig. X.4-3) are as follows.

(1) Thyristor convertor PSF22 A

The outline of PSF2, which is build-up by 8 blocks of six-pulse thyristor bridge convertors, is shown in Fig. X.4-4. The specifications are the same as those used in PSF1. PSF2 is divided into two sections, the lower side (PSF21) and the upper side (PSF22) section, and each section consists of four six-pulse bridge convertors. The upper side and lower side section operate in 24-pulse mode individually. The PSF22 No.4 unit is the one of the four six-pulse convertors of PSF22. The

shift of firing timing among four banks in PSF22 is 15 degrees and the shift between the upper side and the lower side on the same branch, e.g. PSF22 No.4 and PSF21 No.4, is 30 degrees. The rating of the six-pulse convertor is shown in Table X.4-2.

The cross current limiting reactor is connected in series to the above six-pulse convertor and its rating was carefully determined considering the parallel operation of four convertors. The PSF22 No.4 unit consists of two sections. One is the thyristor convertor and the other is the DC reactor with DC current detector provided for protections. The thyristor convertor is composed of six modules that correspond to six arms of the six-pulse convertor. Each module consists of 2 series 7 parallel stacked thyristors.

The thyristors are fired by the gate pulse amplifier through the pulse transformer. The gate circuit is shown in Fig. X.4-5. The Direct-digital-control (DDC) system determines the firing timing, no analog control system or filter is used since it makes the response of convertor dull. Figure X.4-5 also shows the fault detection circuit to monitor the operation of this convertor and provide fault signals.

(2) Hall DC-CT

The DC current measurement is indispensable to control and protect the coil current and DC power supply. It is conventionally made by use of a shunt resistor or a DC-CT that would be a magnetic amplifier type, and sometimes a Logowsky coil with integrator is applied.

The poloidal field power supply requires difficult specifications to measure DC currents.

Concerning to the ohmic heating power supply of JT-60, the following specifications are required:

- rating current DC ± 100 KA
- accuracy (linearity) ±0.1 ∿ 0.5%
- response at least 1 kHz

The Hall DC-CT solves the problem and achieves the desired performance with measuring the magnetic field produced by the DC current by means of Hall device that converts the strength of magnetic field to voltages, called the Hall effect. As shown in Fig. X.4-6, the Hall DC-CT has four components.

When DC current flows in the bus, the iron core induces the magnetic

flux produced by the DC current. This magnetic flux is proportional to the DC current as far as the magnetic circuit remains in the linear region. The specifications are summarized in Table X.4-3.

(3) Trigger gaps for protection

Nitrogen gas gap with trigger electrode is connected to the protection switchgear in parallel as shown in Fig. X.4-3. It makes the on-delay time of this protection circuit to the order of micro-seconds. The rating of the trigger gap is shown in Table X.4-4 and the outline is shown in Fig. X.4-7. In case of the field distortion trigger type, the voltage region with the short delay time is in 0.9 $V_B \sim 0.3\ V_B$ of break-down voltage V_B. It is convenient to set the breakdown voltage at 50 kV ± 5 kV, while the operation voltage is 30 kV (0.6 V_B). The delay time from a start pulse is less than 10 μS.

(4) Voltage divider

The specifications of voltage divider used in the ohmic heating power supply as shown in Fig. X.4-3 are the rating voltage of 25 kV, accuracy of ± 1% and frequency response of DC ∿ 10 kHz. Requirement for the frequency response is determined considering the pulse voltages (50 μS rise) which may appear in the DC circuit breaker and/or thyristor convertors.

It requires the response of 10 kHz at high voltage level. As shown in Fig. X.4-8, the voltage divider has five series resistors and one resistor with a voltage convertor. The temperature characteristics of resistor must be about 100 PPN/°C to realize the accuracy of 0.5% within 50°C rise. The voltage convertor is a photo-decouple type amplifier from the viewpoint of noise protection.

The reduced output voltage by a known factor is converted two types of optical signals, analog signal line and pulse signal line.

•Analog signal line; The light intensity modulated by the input voltage directly transmits through the fiberoptic cable. This line is expected to be useful for the high frequency part of signals.

•Pulse signal line; The light pulse modulated by the V/F convertor transmits through another fiberoptic cable to the receiver that has an F/V convertor. The output voltage of F/V convertor is used to correct the static drift of analog line and improves the accuracy of the voltage measurements.

Table X.4-1 Specifications of Major Components of the Poloidal Field Power Supply.

Generator	Vertical shaft salient pole type	1	set
	pole	16	poles
	Capacity	500	MVA
	Voltage	18	KV
	Current	16	KA
	Frequency	78 - 54	HZ
	Xd, Xq	1.84, 1.18	p.u
	Xd"	0.24	p.u
	Power factor	more than 0.45	
	Flywheel effect	5,500	ton-m^2
	Revolution	585 - 405	RPM
	Energy yield	1.3	GJ
Induction motor	Wound rotor three-phase induction motor	1	set
	pole	10	pole
	Capacity	7.5	MW
	Voltage	11	KV
	Revolution	585 - 405	RPM
	Speed-up time	10	Min.
	Control	Stationary scherbius system and Water rheostat	
D.C. circuit breaker	Vacuum circuit breaker	2	sets
	Voltage	25,15	KV
	Current	92	KA
	Commutation capacity	1.0	mF
	di/dt, dv/dt	450A/μs, (mean)120A/μs(at zero) 300v/μs	
I.E.S. coil	Reactor of Iron core with air gaps	3	sets
	inductance	1.12 / 2.32 / 4.56	mH
	Connection	Series	
	Total inductance	8	mH
	Peak current	92	KA
	Resistance	7.5	mΩ
	R.M.S. current	92KA 2.9	sec
	Rated voltage	25	KV
Time constant controller	Resistance	0.072 - 1.0	Ω
	Variable	in 20 steps	
	Maximum energy dissipation	78	MJ
	Rated energy dissipation	50	MJ
	Allowable temperature rise	70	°C
Thyristor converter	OH coil and IES coil PSF1	SCR 24 pulse 101KA-2500V	
	PSF2	SCR 24 pulse 101KA-2500V	
	Vertical field coil PSVF1	SR 24 pulse 58.0KA-5KV	
	PSVF2	SCR 24 pulse* 58.0KA-5KV	
	PSVR	SCR 24 pulse* 8.6KA-5KV	
	Quadru-pole field coil PSQ	SCR 12 pulse* ±25KA-900V	
	Horizontal field coil PSH	SCR 12 pulse* ±22KA-500V	
	Magnetic limiter coil PSM	SCR 12 pulse 120KA-1000V	
		* bi-polar	

Table X.4-2 Specifications of Thyristor Convertor PSF22A.

PSF22 No. 4	Six-pulse thyristor bidge converter
Rating power	35 MW
Rating voltage	1,383 V
Current	25.3 KA
Thyristor	SF3000GX21 (4000V - 3000A)
Structure	2S-7P-6A

Table X.4-3 Specifications of Hall DC-CT.

Conditions	Temperature	-10 ∿ +40°C
	Humidity	max. 90%
	Magnetic field intensity	max. 100 Gauss
Ratings	Current	±100 KA (peak)
	output voltage	±10 V (max.)
	Output impedance	1 KΩ (min.)
	Overcurrent	1 MA - 1 sec
	Insulation	AC 50 KV
Characteristics	Error	±0.5% (±10 ∿ 100 KA)
		±10% (±DC 100 ∿ 200 KA)
	Step response	0.2 ms
	Frequency response	DC - 5 KH (-3 db)
	Temperature coefficient	0.02% / C°
	Magnetic field coefficient	±0.1% at 100 gauss

Table X.4-4 Ratings of Trigger gaps.

Ratings	Voltage	15 KV ∿ 25 KV
	Current	92 KA - 20 ms
	Over current	500 KA - 20 ms
	Insulation	AC 25 KV 1 minute
	Trigger delay time	Shorter than 10 μS
	Operation region	DC 15 KV ∿ 55 KV
	Operation times	10 filling N_2 gas is exchanged in every time

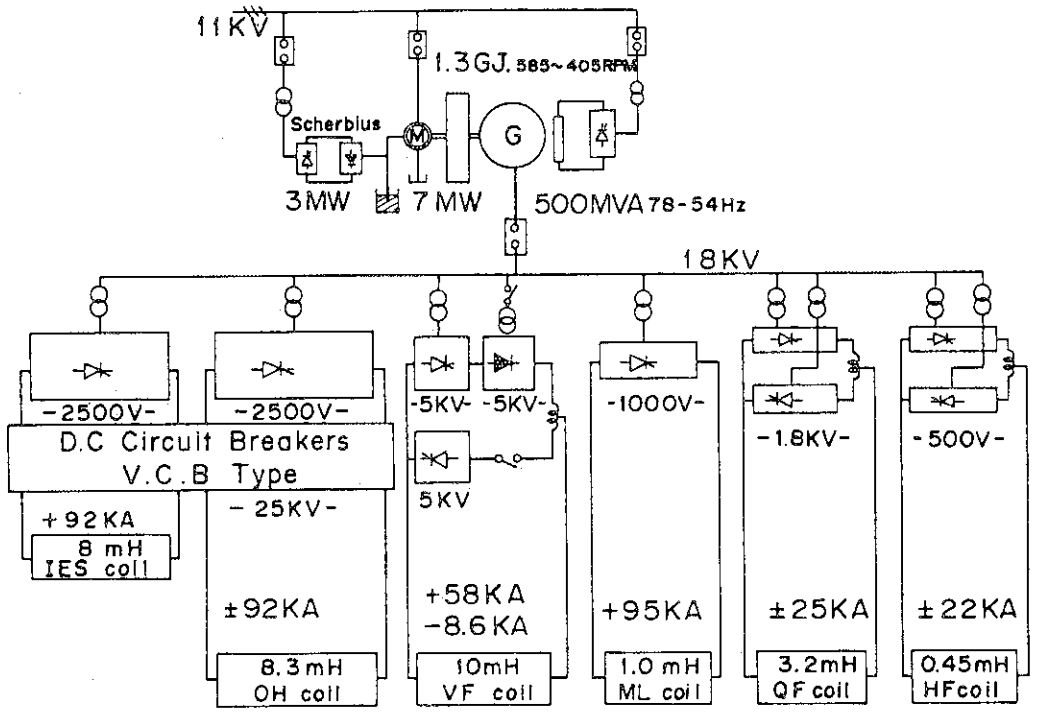

Fig. X.4-1 Schematic Diagram of the Poloidal Field Power Supply.

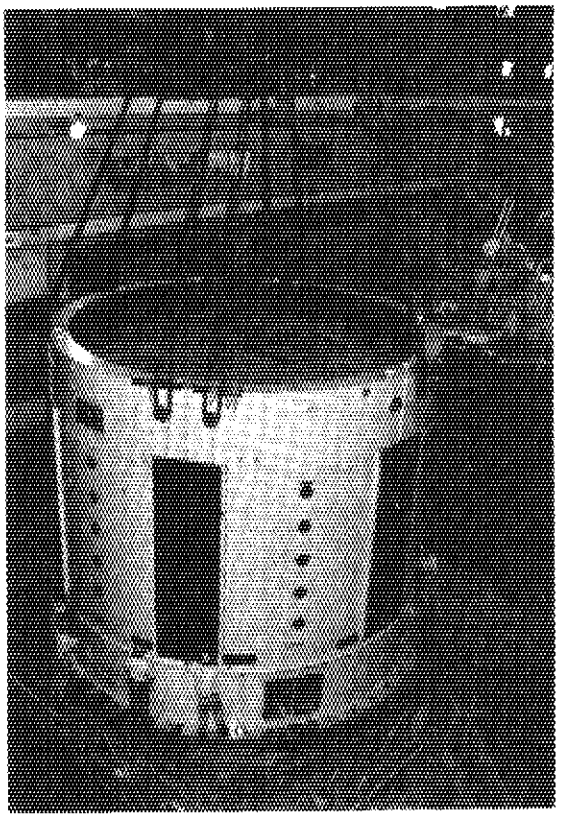

Fig. X.4-2 Stator Frame of Motor Generator.

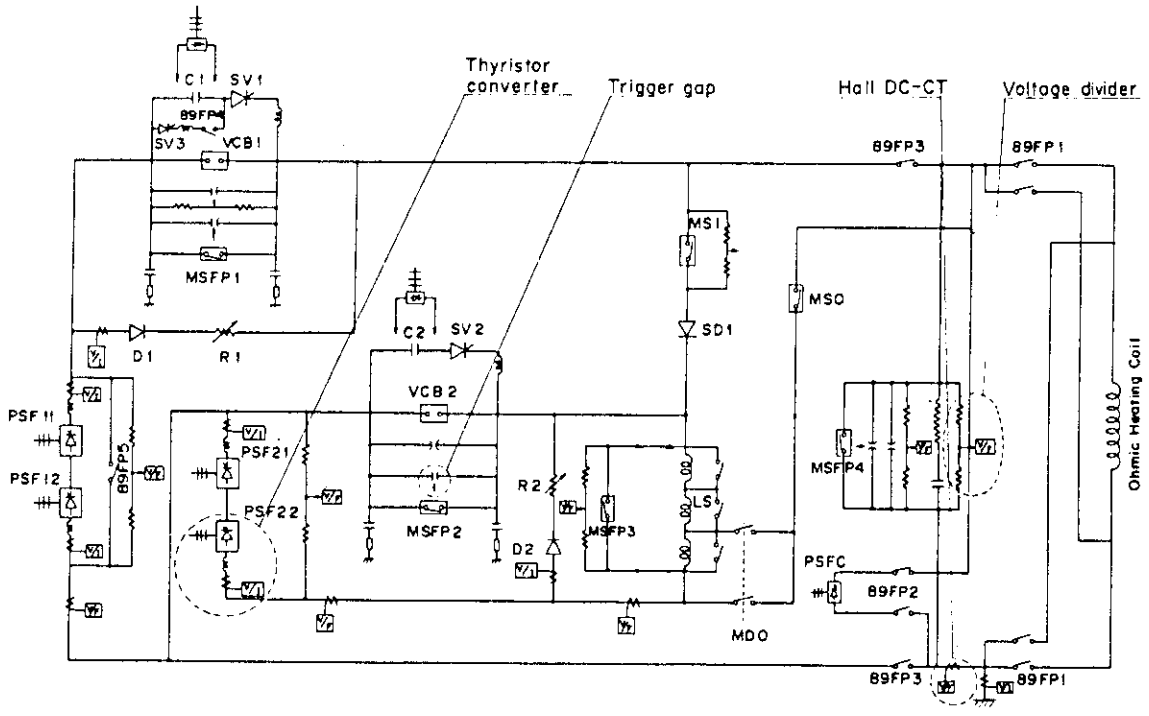

Fig. X.4-3 Ohmic Heating Circuit of JT-60.

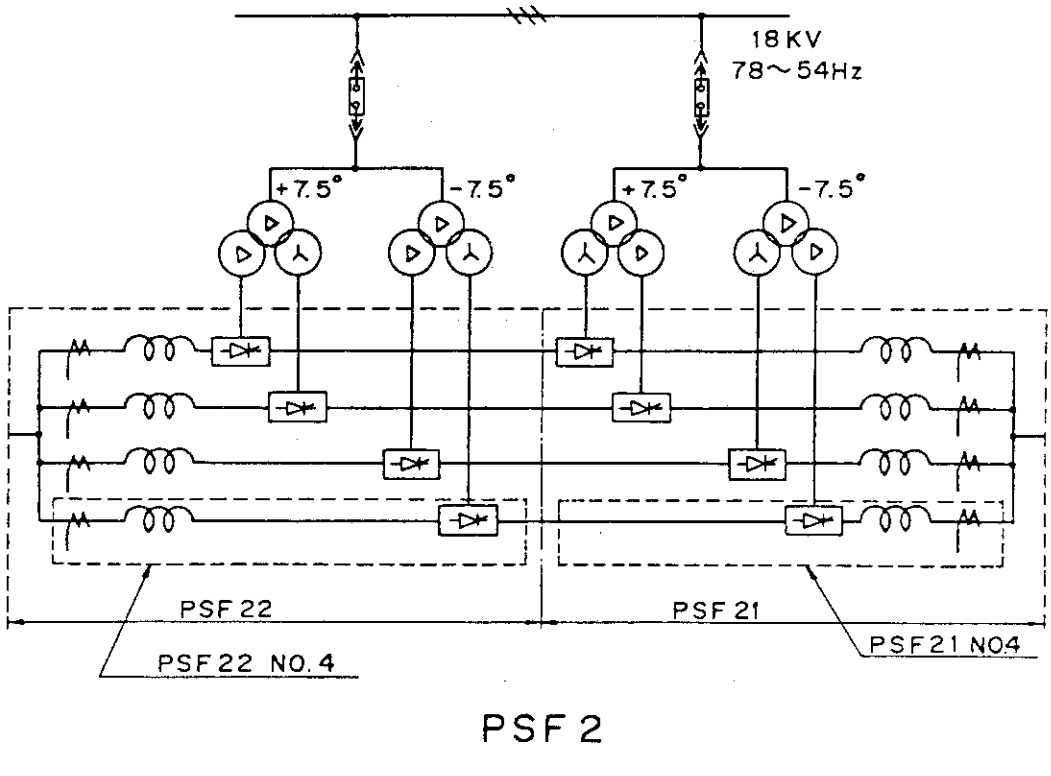

Fig. X.4-4 Structual Design of PSF-2.

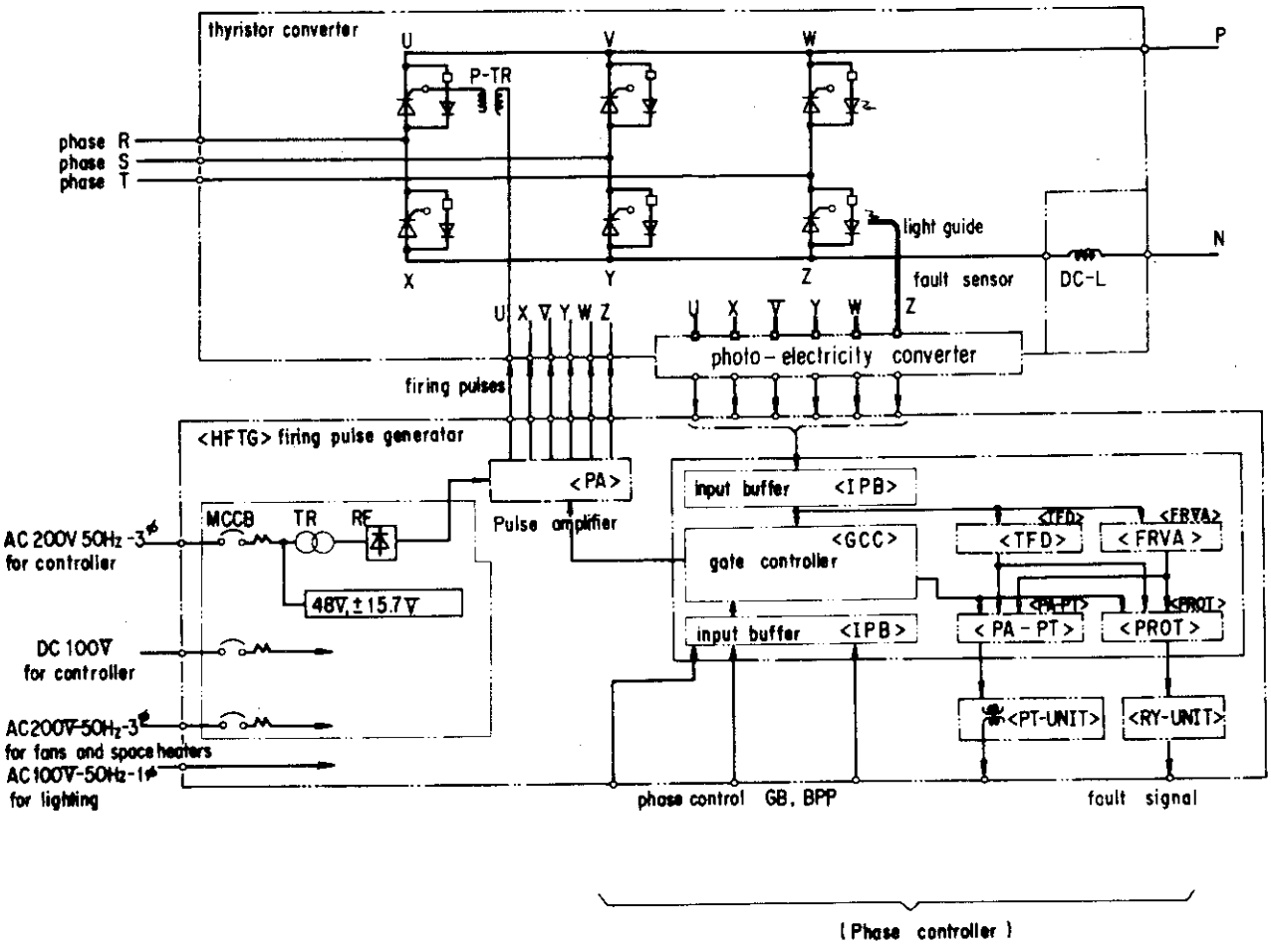

Fig. X.4-5 Thyristor Convertor Gate Control Circuit.

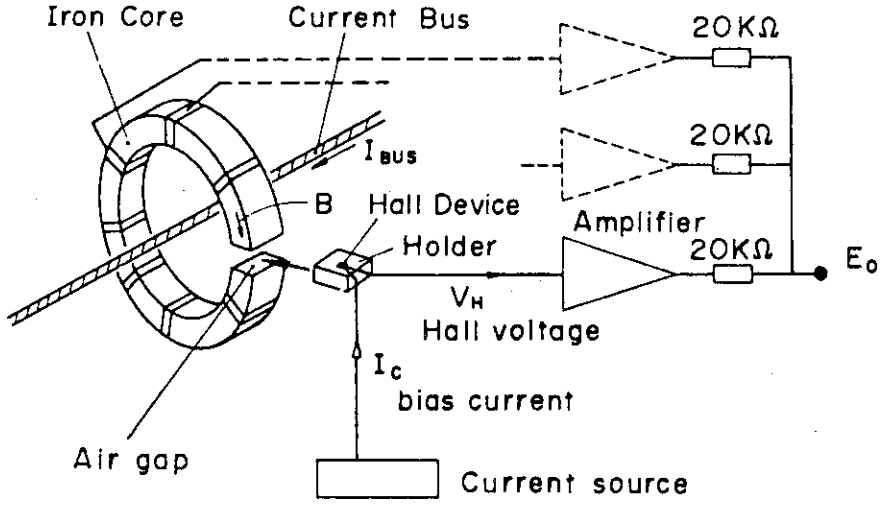

Fig. X.4-6 Schematic diagram of Hall DC-CT.

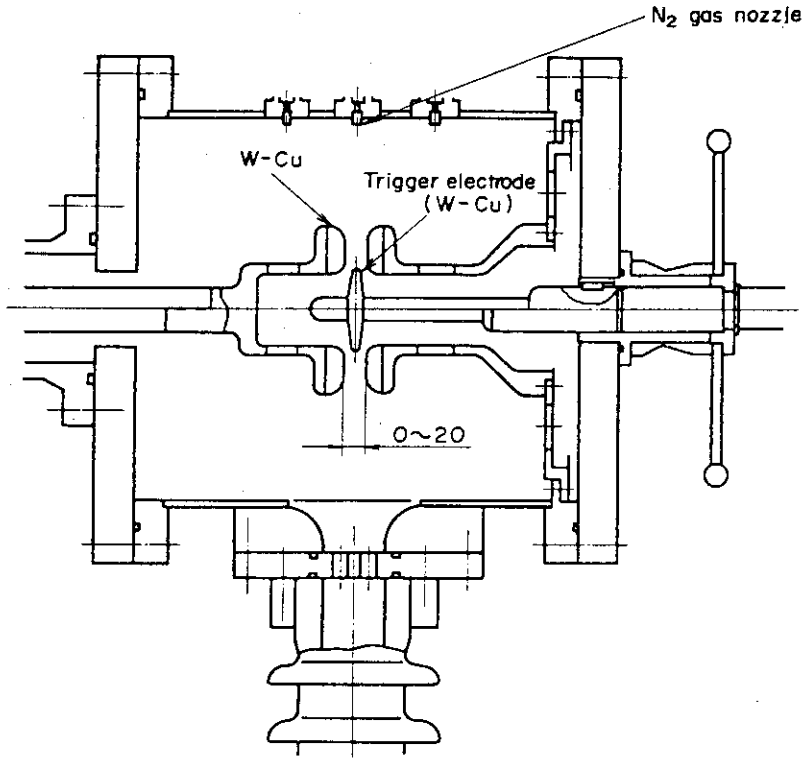

Fig. X.4-7 Electrode structure

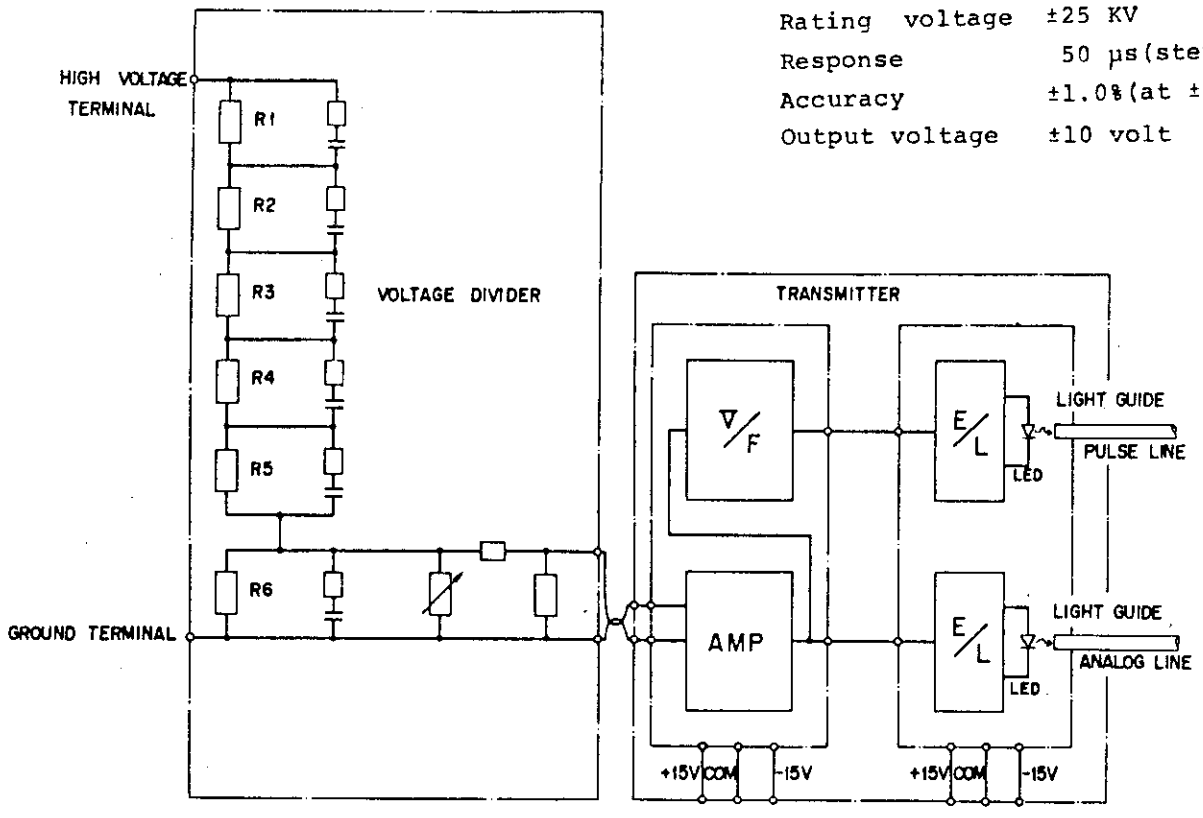

Rating voltage	±25 KV
Response	50 μs(step)
Accuracy	±1.0%(at ±100%)
Output voltage	±10 volt

Fig. X.4-8 Voltage Divider and Transmitter.

4.2 Toroidal field power supply

The diagram of the toroidal field power supply is shown in Fig. X.4-9. To excite the toroidal field coil, very large electric power (about 350MW: peak value) is necessary. To meet the power requirement, a combination system of the utility power network and an AC generator with flywheel has been adopted for the toroidal field power supply. The electric power is supplied to the coil through 24-pulse diode convertors.

After the contract was concluded with Mitsubishi Electric Corporation in March 1980, detailed reexaminations of the specification were made and have been nearly completed. Major items of the reexaminations are summarized below.

(i) The voltage regulation of 24-pulse diode convertors. The 24-pulse diode convertors are composed of 6-pulse diode convertors connected in series and parallel as shown in Fig. X.4-9. As the voltage regulation of the 24-pulse diode convertors is closely related with the electical design of other major components (transformers etc.), quantitative estimation of the voltage regulation is necessary to complete the system design. So the voltage regulation of the 24-pulse diode convertors was investigated theoretically and by computational simulation. The result obtained by the theoretical approach was in good agreement with the result of the computational simulation. The compensation for the voltage regulation by AVR and condenser(S.C.) was also studied.

(ii) The electrical design of major components. Based on the result of (i), the electrical design of major components, mainly the capacity and the GD^2 value of the generator, and the capacity and the transformation ratio of transformers for diode convertors, were reviewed. They are summarized in Tables X.4-5 and X.4-6.

(iii) The mechanical design of the generator with flywheel. The mechanical and thermal strength of the generator with flywheel was reexamined in detail, and the mechanical design has been determined. The cross-section of the generator is shown in Fig. X.4-10.

(iv) The specifications of other components. The electrical characteristics of the static starter and the thyristor exciter were examined according to the operation scenario of JT-60. The specification of the main transformer (198 MVA, 275kV/18kV) for the toroidal field power supply which receives electric power from the utility network has been finalized.

By the end of this period, the reexaminations of the specification have been almost completed, and the manufacture will be started early in the next fiscal year.

Table X.4-5 Specifications of the toroidal field power supply generator

Generator:	
Output Power(Peak Value)	215MVA
Output Voltage	18kV
Power Factor	0.85lagging
Pole Number	16poles
Output Frequency	80～56Hz
GD^2	1,400T-M^2
Flywheel:	
Weight	717 Tons
Diameter	6.6M
Length	2.6M
GD^2	14,600T-M^2

Table X.4-6 Specifications of the transformers for diode convertors

(i) TL1,2,3,4,5,6,7,8

Capacity : 28 MVA

Voltage : 18 kV/680 V(748 V)

(ii) TG1,2,3,4

Capacity : 60.2 MVA

Voltage : 18 kV/765 V(803.5 V)

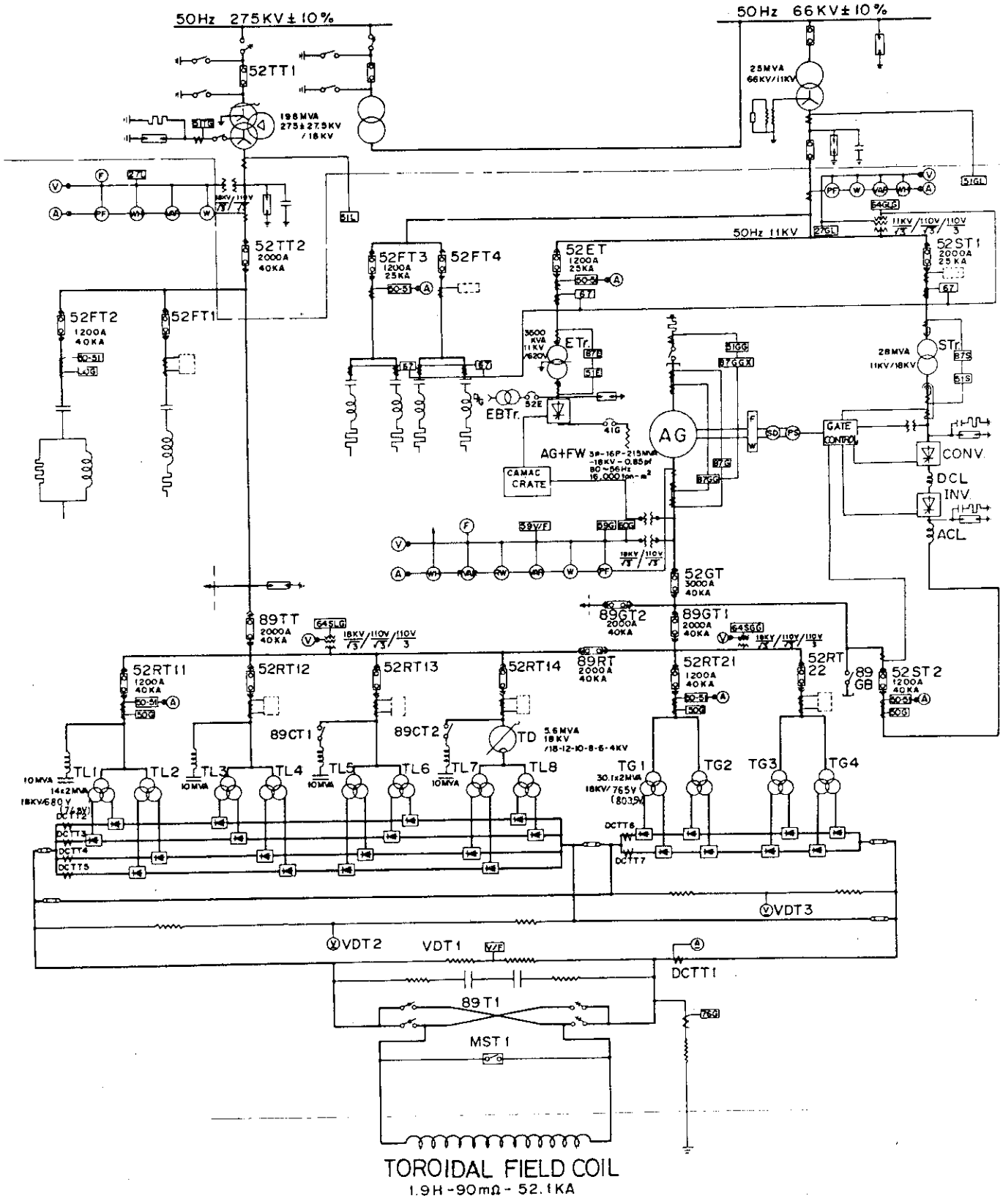

Fig. X.4-9 Diagram of the toroidal field power supply

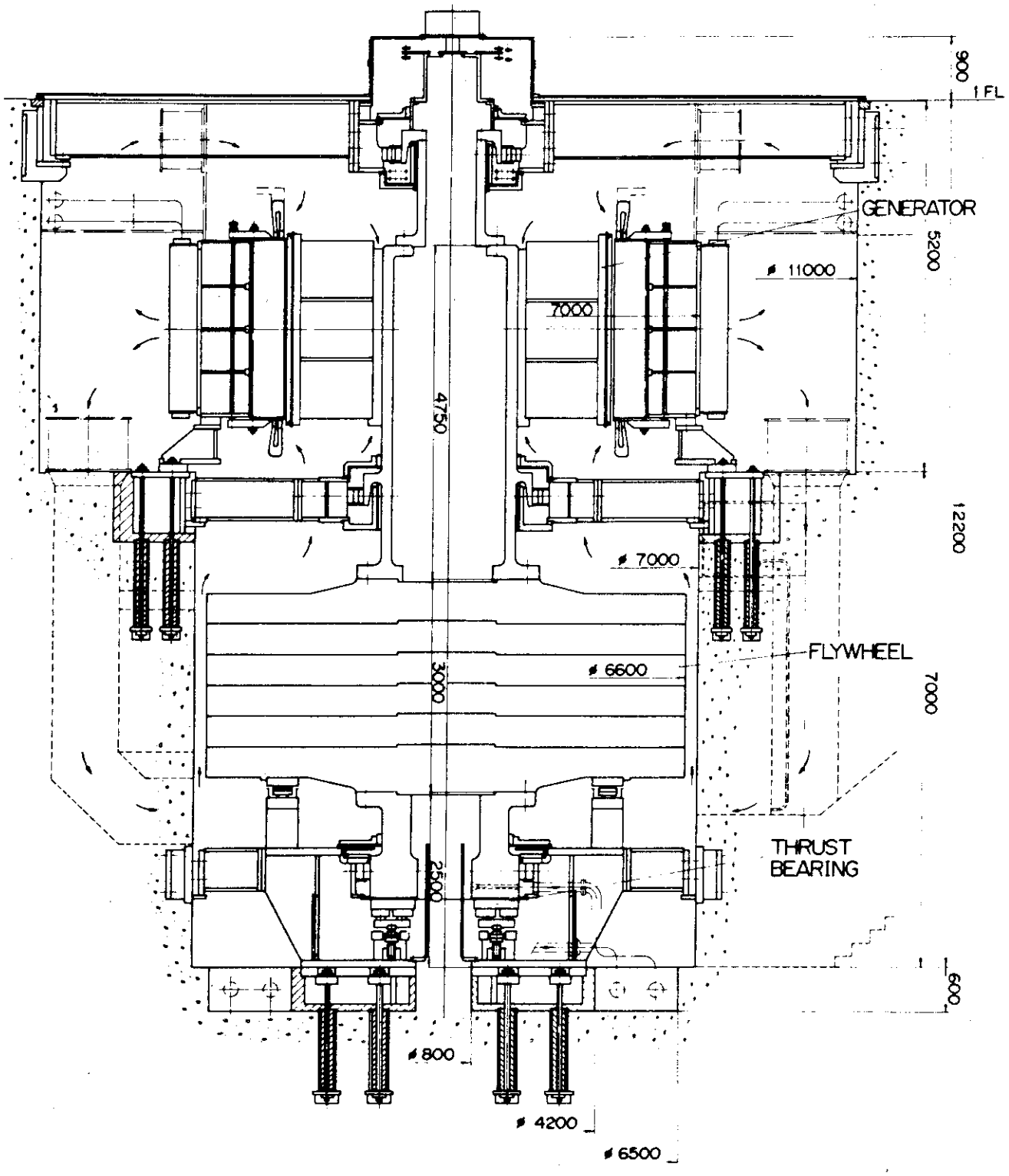

Fig. X.4-10 Cross section of the generator with flywheel

5. Status of Control and Diagnostic Systems

5.1 Major activities of control and diagnostic systems

The fabrication of JT-60 central controller, ZENKEI, was contracted with Hitachi Ltd. at the end of the last fiscal year (March, 1980). During the succeeding year, practical advance was made after many discussion with the industry on the manufacturing design, including some modification. The design work of plant support control part was almost completed and the discharge control part has been designed succeedingly in the relation with the control of the high-beta plasma.

As for the diagnostic systems, the executive plan for the whole diagnostic system has been made, considering the experimental plan of JT-60 and the fabrication status of JT-60 device. The developmental results which was obtained in the last year, was reflected on the ordering specifications and the contracts for the manufacturing parts of A-1 plasma density measuring, A-3 ion temperature measuring, A-4 impurity measuring and A-8 diagnostic support systems, were conducted with the industries, respectively.

5.2 Present design of control system

5.2.1 System design

The control system consists of ZENKEI and sub-control systems which locally control the Tokamak machine, the coil power supplies, NBI's and RF's and other devices which JT-60 is composed of. And, ZENKEI and the data processing system are tightly connected to each other. Among the sub-control systems, only those for NBI's and RF's have mini-computer systems as control intelligences, and other sub-control systems use micro-computers installed in CAMAC modules.

The hierarchical scheme of the control system is represented in Fig. X.5-1 the figure also represents the relation of ZENKEI to the power substation, the building and the satellite Tokamak device.

Main elements which constitute ZENKEI are the computer system, the CAMAC system, the timing system, the plasma monitor system, the safety interlock system and the control consoles.

5.2.2 Computer system

The ZENKEI computer system consists of seven CPU's (HIDIC 80E), and

is divided into the following sub-systems.

a. Plant support computer system which is used to watch the status of the over-all devices and to supervise them according to the flow of the operation modes, whose scheme is represented in Fig. X.5-2. (two CPU's)
b. Discharge control computer system which establishes the discharge condition, and controls plasma in real time. (two CPU's)
c. Feedback control computer system which, in combination with the discharge control computer system, controls the PF coil power supplies to perform feedback control of plasma current, position and profile. (two CPU's including one for back-up)
d. Off-line computer which is formerly supplied for off-line work to develop softwares, and for back-up of the plant support computer and the discharge control computer. Now, the purpose is being shifted to share the discharge control task functioning as a secondary discharge control computer, keeping a time margine to be used for off-line work.

Among the seven computers, only those of the feedback computer system are located in the JT-60 power supplies building, while the others in the JT-60 control building, connected to one another with shared memory.

5.2.3 CAMAC system

The above three computer systems have respective CAMAC systems of the sub-systems. Some of the sub-systems are linked to ZENKEI through more than one CAMAC high way. In that case, they have a test crate which supervise the CAMACs that are linked to different high ways. Fig. X.5-3 represents the linkage of the test crate to two CAMACs which belong to respective high ways. Here, "ACD" is the abbreviation of "Auxiliary Controller with D-port". The right two crates are controled by the micro-computer in the left crate and by the ZENKEI computers in shared-time through the ACD's or the type L2 crate controllers respectively. The ACD has a dual port memory, which is connected to the serial high way in one side and to the data way in another side.

5.2.4 Plasma control of JT-60

The experimental discharge and the discharge cleaning of JT-60 are performed according to the sequence that is controled by the discharge

computer system. The JT-60 control system has the ability that satisfies the rules of operation period;

(i) to make plasma shots in 10 minutes interval at the rated power.

(ii) the shot interval can be reduced to 3 minutes as the performances of the coil power supplies allow it.

(1) Discharge control of ZENKEI

The discharge control computer system has several functions such as discharge condition setting, pre-shot check, real-time discharge control, post-shot check and discharge data acquisition. The conceptions of these functions are represented in Table X.5-1.

a. Discharge condition setting

The items of the discharge condition are divided into three categories such as those of the device preparation condition, the global discharge condition and the devices whether to be used to discharge experiment or not. The operator sets the condition choosing the push buttons on the central console. The global discharge condition includes the selections of manual/auto, shot interval, number of shot repetitions, MG re-accellaration time, etc. These determine the discharge sequence which is controled by the discharge control computer, the device level discharge condition includes use/not use selections of the devices, their action timings, pre-programed values, control mode, control constants etc. The operator sets the global and the device level discharge conditions within the limits of the device preparation condition, following the setting guidance. The discharge control computer checks the given discharge conditions for inconsistency, and transfers them to the devices when no inconsistency is found.

These discharge conditions can be established and registered in the computer file at any time whatever the operation mode or the discharge time phase at the instant is.

b. Real time discharge control

The discharge control computer system supervises the discharge sequence to control the discharge operation. Fig. X.5-4 represents the structure of the sequence control.

(i) Control of global discharge sequence

Fig. X.5-5 represents the global discharge sequence of automatic operation, and Fig. X.5-6 represents the device operation sequence and the time phase.

(ii) Time-oriented control

In this case, the timing system is previously supplied with timing conditions and, during discharge, gives the timing signals according to the given conditions to the corresponding devices. Among the timing signals, some of them are controled under the conditions that are given by the states of the devices, the plasma condition etc. The discharge control computer system perceives the conditions in real-time, then decides whether the necessary condition is satisfied or not, and when it is satisfied, releases the inhibit states.

(iii) Event oriented control

In this case, the discharge control computer system has advantage over the timing system, and it wholely controles discharge operation preserving the progress of the discharge sequence, the states of the devices, the plasma condition etc, giving the control commands to the devices.

(iv) Feed-back control by discharge control computer

Beside the above functions, the discharge control computer system copes with abnormal events when the safety interlock system of the alarm system functions, or when something is wrong in ZENKEI itself, for instance, in the feed-back computer system or in the timing system.

(2) Feed-back control by the discharge control computer system

The discharge control computer executes the following tasks in the period of 10 msec.

(i) Data aquisition

Collects the plasma data, the coil currents, the coil voltages, states of NBI's, RF's and the gas supply system, information about abnormal events in the feed-back computer, or the timing system, and the safety interlock system if any.

(ii) Phase shift decision

Decides whether to stay in the phase or move to another phase.

(iii) Command outputs

Outputs the pre-programmed control objects and on/off commands. These are transfered to the feed-back control computer system (through which, to PF coil power supply DDC's), the gas

supply system, NBI heating system and RF heating system.

The computer system can still accept interruption to cope with occurrences of abnormal states that are informed from the feed-back control computer, the timing system or the safety interlock system.

(3) Function of feed-back control computer system

The feed-back control computer system is basically required to function as follows.

a. It executes program to control the plasma position and shape every 1 msec in linkage with the PF-coil power supply DDC's.
b. It receives the control objects of plasma current, position, shape and magnetic limiter coil current from the discharge control computer every 10 msec and following them, it executes the above program.
c. It copes with abnormal states of PF-coil power DDC's etc.

Under the above requirements, the feed-back control computer system, (i) received commands and data from the discharge control computer system, (ii) collects data from the electro-magnetic diagnostics about plasma current, tangential and normal magnetic field strength, (iii) calculates the plasma position and shape, and makes the control objects of V, H, Q-coil current (or voltage). The F, M-coil current (or voltage) ovjects are those given from the discharge control computer system. Fig. X.5-7 represents the discharge control loops with the discharge control computer system and the feed-back computer system.

Table X.5-1 Functions of discharge control.

Discharge Condition Setting	(1) Guidance for Setting
	(2) Consistency Check
	(3) File Control
	(4) Automatic Condition Changing
	(5) Pre-programming
	(6) Transfers of Conditions to Sub-systems
Pre-shot Check	(1) Check for Occurence of Abnormal Status (Safety Interlock System or Alarm System)
	(2) Check of Operation Status of Sub-systems
	(3) Check of Condition Settings at Sub-systems
	(4) Check of Commercial Line Input Condition
	(5) Prediction for Undesirable Event
Real-time Discharge Control	(1) Control of Global Discharge Sequence
	(2) Time-oriented Control
	(3) Event-oriented Control
	(4) Feed-back Control by Discharge Control Computer
	(5) Management of Abnormal Events Occurred
Post-shot Check	(1) Certification of Discharge Finish
	(2) Check of Condition of Electro-magnetic Diagnostics
	(3) Check of Commercial Line Input Condition
	(4) Check for Alarms Occurred during Discharge
Discharge Data Acquisition	(1) Acquisition and Filing
	(2) Engineering Data Conversion
	(3) Display and Record

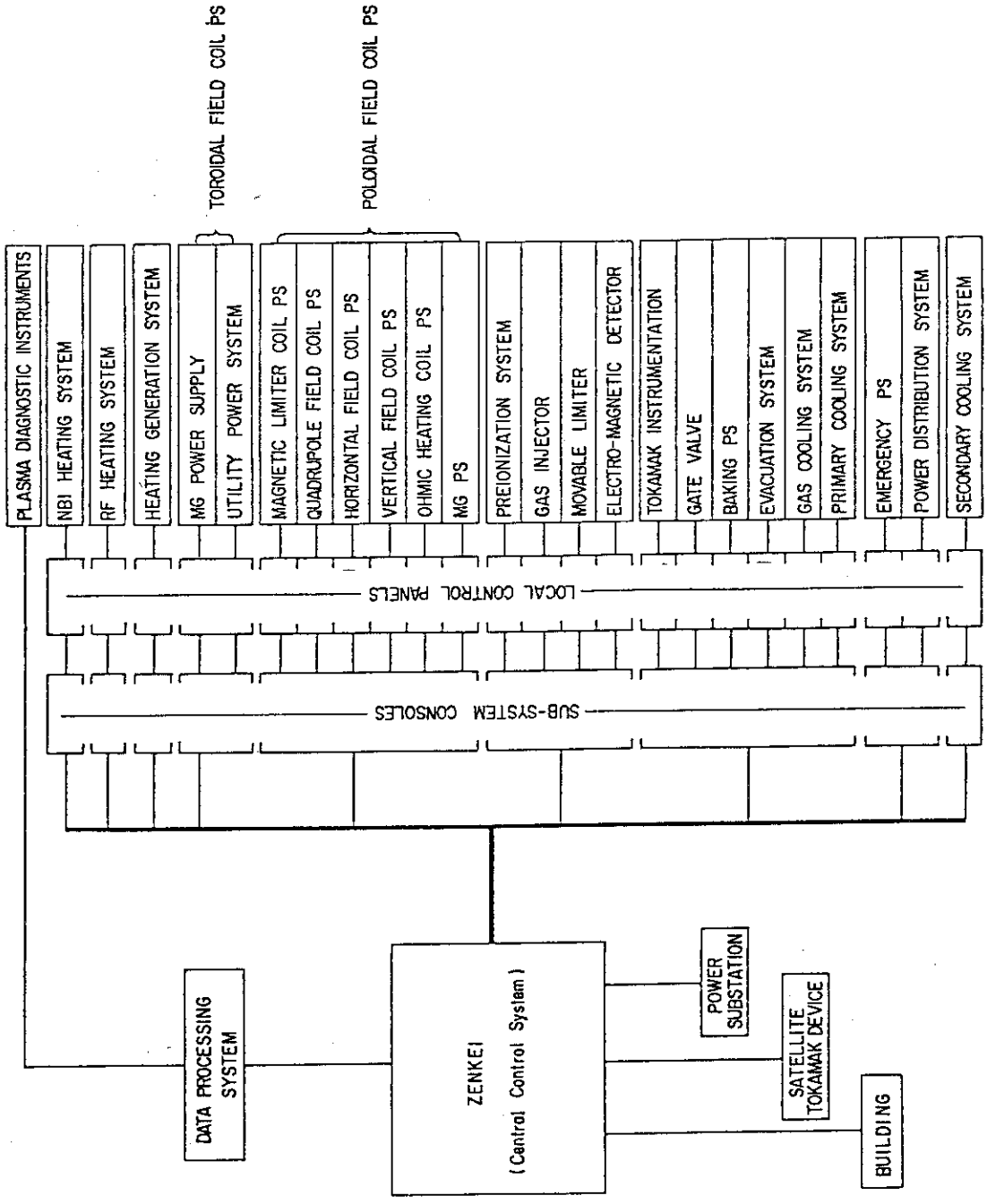

Fig.X.5-1 Configuration of JT-60 control system

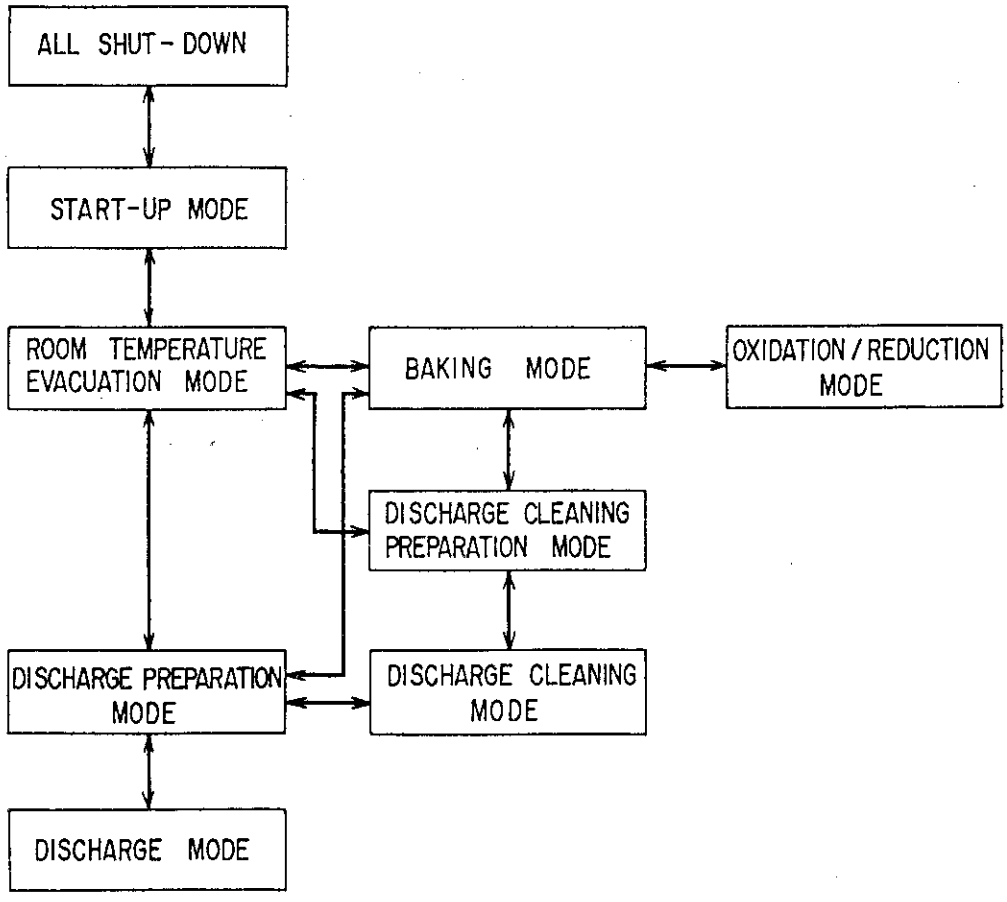

Fig.X.5-2 Operation mode scheme

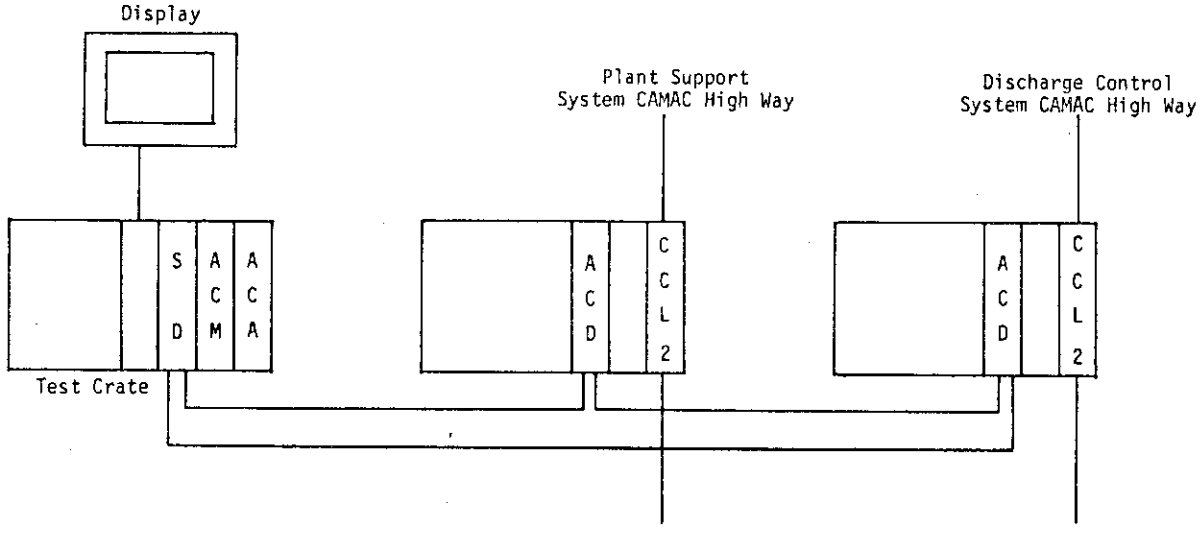

Fig.X.5-3 CAMAC network with test crate

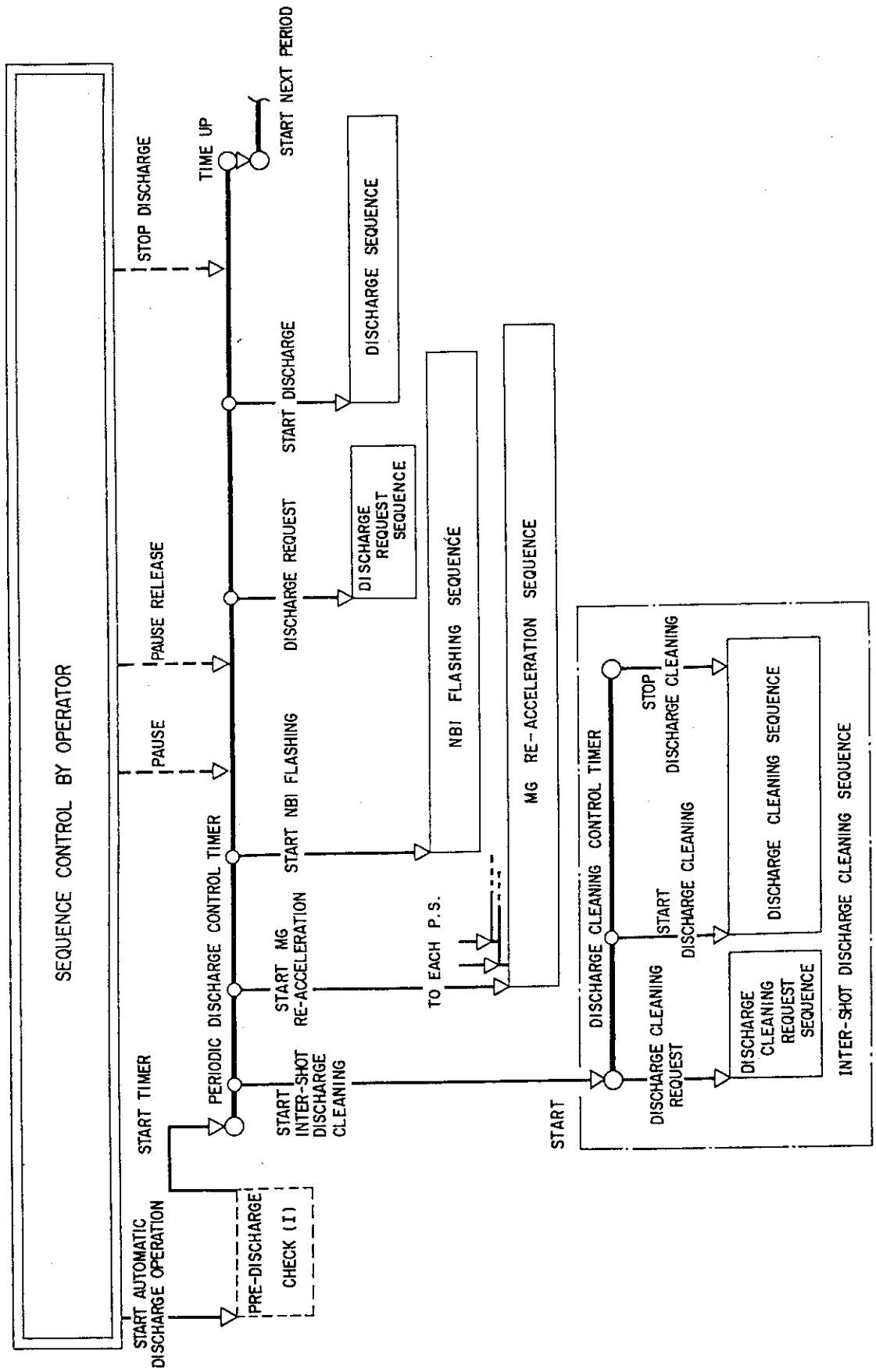

Fig.X.5-4 Structure of plasma discharge sequence (Automatic operation)

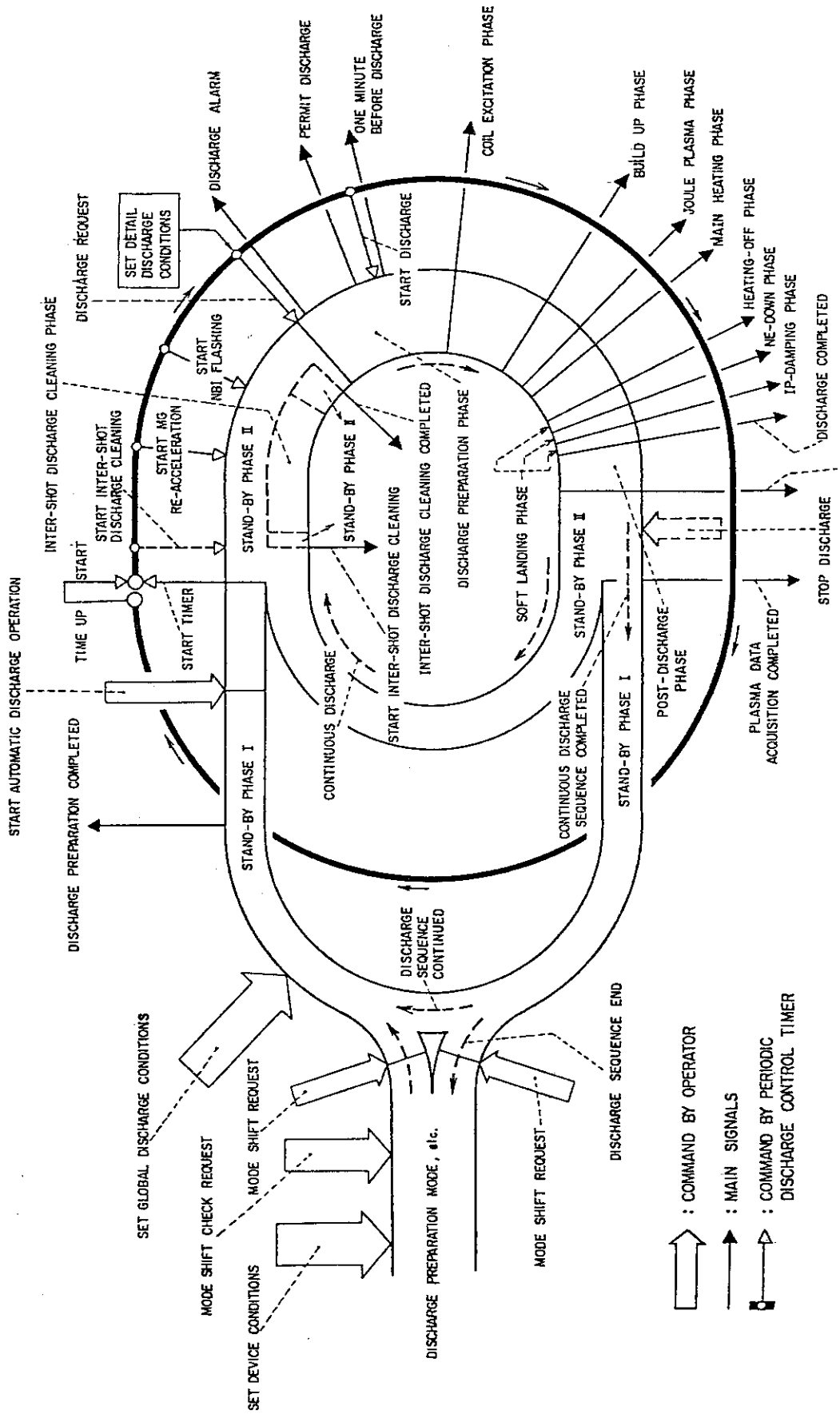

Fig.X.5-5 Phases of discharge sequence

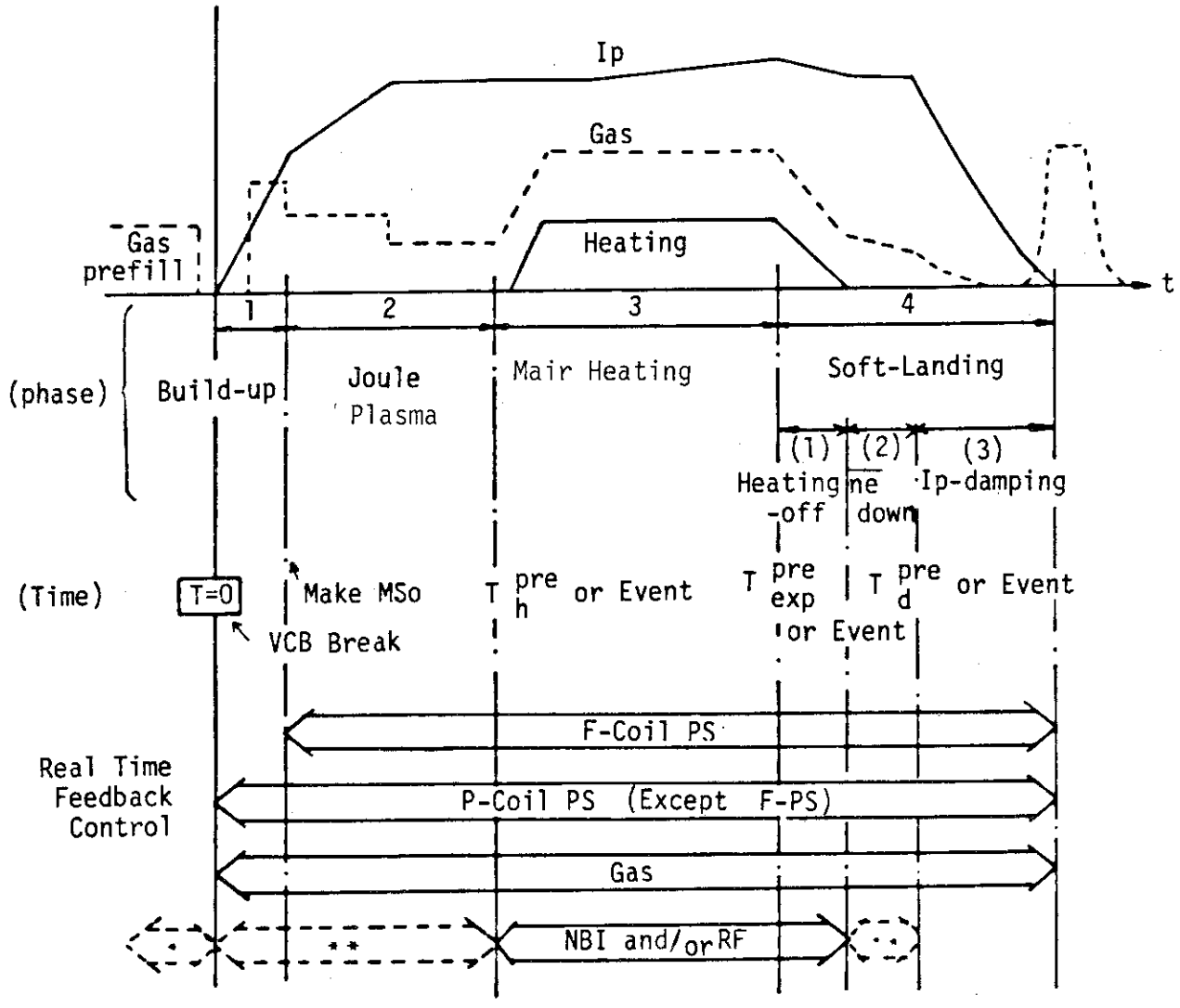

Time Chart of Feedback Control by Discharge Control Computer

T_h^{pre} : Heating Starting Time (preset)

T_{exp}^{pre} : End of Experiment Time (preset)

T_d^{pre} :Ip damping Start Time (preset)

Note

In Case of Joule Experiment, Phases 3 and 4-(1) are skipped

Fig.X.5-6 Device operations and time phases during discharge

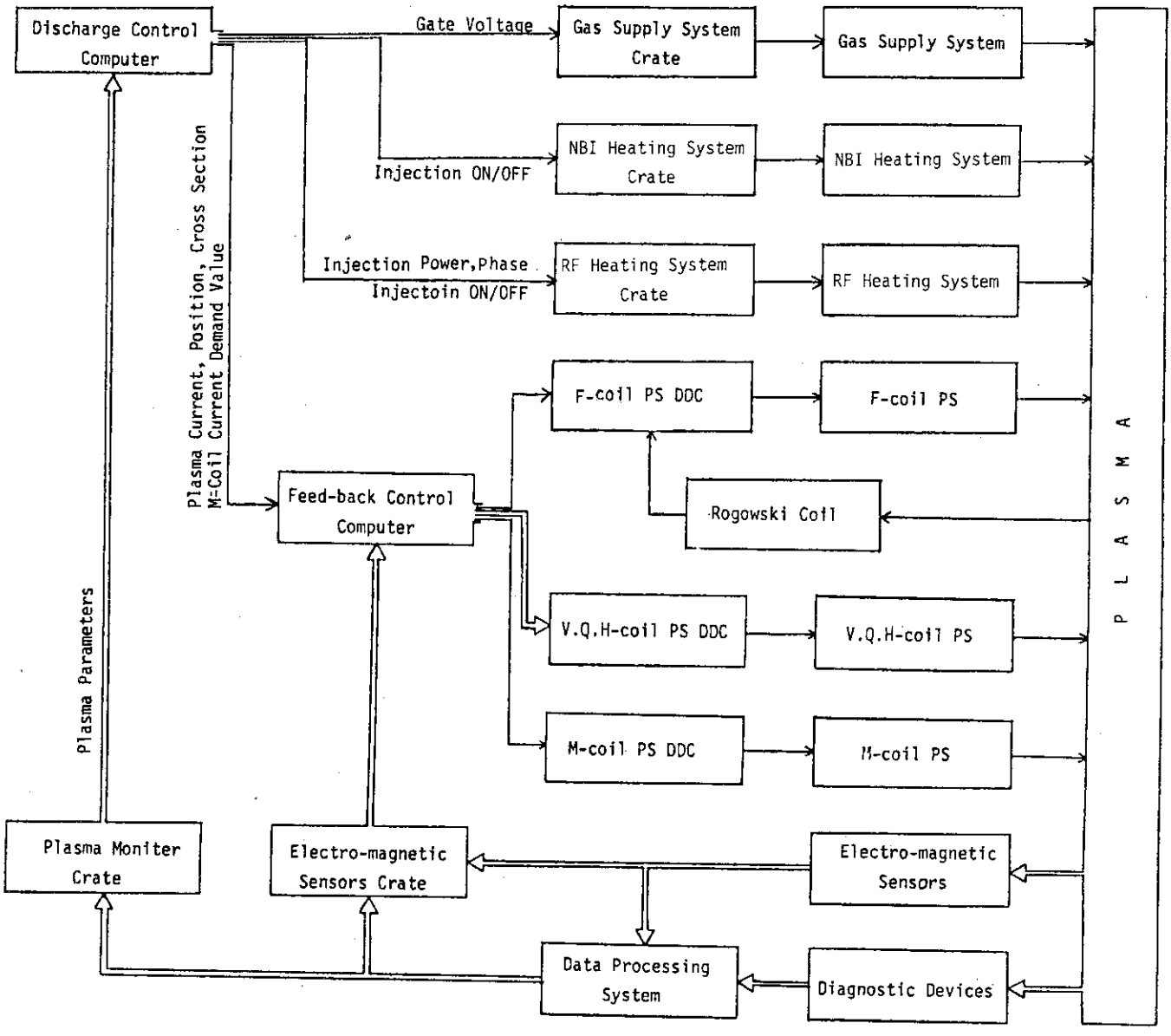

Fig.X.5-7 Real-time feed-back control loops

5.3 Present status of diagnostic system

5.3.1 System design

Diagnostic instruments for JT-60 are divided into two groups. One (Group A shown in Table X.5-2) is for the diagnostics of basic plasma parameters for control and the other (Group B shown in Table X.5-3) is for the diagnostics of detailed plasma parameters, which needs more advanced diagnostic techniques. Group A consists of a large number of diagnostic instruments in order to meet the above-mentioned requirements. Therefore, high accessibility to the tokamak torus is required. The greater part of efforts has been placed on the system design of Group A instruments in this fiscal year. To ensure the high accessibility, each instrument is required to be made in a compact size and standardized as possible. Such design was applied in particular to spectroscopic, bolometric and soft x-ray measuring units. This design feature also allows us to replace a certain unit with another one without any difficulty. Fig. X.5-8 shows an example of the arrangement of diagnostic instruments.

5.3.2 Electron density and temperature measuring systems (A-1 and A-2)

The electron density measuring system consists of mm and sub-mm wave interferometers. The sub-mm wave interferometer was chosen to provide the density measurement of a thick plasma to be produced in JT-60. The CH_3OH optically-pumped sub-mm wave (119 μm) laser is now under development aiming at high CW power capability of about 200mW to provide multi chord measurements by one laser oscillator. Because of its short wave length special attention must be paid to use the sub-mm wave interferometer against mechanical vibrations expected at JT-60 under operation. The optical passage length between mirrors set in the JT-60 will be monitored by a reference laser system and will be fed back to the sub-mm wave interferometer system to get the phase difference due to plasma. The prototype monitoring system was tested on the JIPP T-II device and proved to be successful.[1)]

The electron temperature measuring system consists of a Fourier spectrometer, a polychromator radiometer and a multipulse laser for Thomson scattering. The Fourier spectrometer will provide the power spectrum of cyclotron radiation from the JT-60 plasma and the profile of electron temperature with a time resolution of 10ms. The electron

temperature from the Fourier spectrometer will be normalized by the Thomson scattering measurement.

5.3.3 Ion temperature and impurity measuring systems (A-3 and A-4)

The ion temperature measuring system (A-3) consists of neutral particle analysers, an active beam probing apparatus and neutron counters. The prototype beam probing apparatus was tested on the JFT-2 device successfully, however, the influence of impurity ions on the scattered spectrum seems smaller than expected from Rutherford scattering. Detailed analysis is required for describing scattering process in a plasma.

The impurity measuring system (A-4) consists of specially developed spectrometers, standard spectrometers and Doppler broadening spectrometers. Spectrometers covering from 0.1 Å to 500 Å have been so designed to be made in compact units and observe the whole wavelength region with spatial resolution. This design feature allows us to get a lot of impurity line profiles with spatial resolution in one shot.

5.3.4 Radiation flux and peripheral plasma measuring systems (A-5 and A-6)

The radiation flux measuring system (A-5) consists of high counting rate PHA and X-ray wave measuring apparatus.

The peripheral plasma and wall surface measuring system (A-6) consists of probes, thermocouples, TV, gas analyzers and wall surface analyzers. IR-TV cameras will be designed to view the inner surface of the vacuum chamber during a shot, while visible-TV cameras will be designed to view the whole area of the inner surface with periscopes for maintenance purpose.

5.3.5 Data processing system (A-7)

Data processing system for JT-60 consists of an inter-shot processor, a real-time processor and a CAMAC system with a hierarchical structure of an upper and a lower levels. The system will have the structure shown in Fig. X.5-9. The inter-shot processor, which consists of two general purpose computers, governs the upper level CAMAC system during a shot-interval. On the other hand, the real-time processor[2] occupies the top level instead of the inter-shot processor during a shot. It consists of mini-computers and governs the lower level CAMAC system with

a real-time preprocessor. This design feature will provide capability of plasma control with a real-time data processing through each Group A diagnostics.

The inter-shot processor is designed to be placed in the computer room of the control building and operated through terminals placed in the control room of the same building. Several terminals are also distributed in the diagnostic rooms of the experimental building to provide an access to the inter-shot computer. The upper level CAMAC system with ACM is placed in the diagnostic room to provide a control of each diagnostic room to provide a control of each diagnostic instrument and data-acquisition through the lower level CAMAC system during a shot-interval. The lower level CAMAC system with the real-time preprocessor is placed near the torus for each Group A instrument.

References

1) A. Nagashima : 5th Int. Conf. IR and MM Waves Digest (1980) 199
2) A. Ogata, K. Kumahara, T. Matoba, A. Sawai and Y. Ohtake : Proc. 11th Symp. on Fusion Technology (Commission of the European Communities, 1980, 683)

Table X.5-2 JT-60 diagnostics (A group) (part 1)

System	Simbol	Diagnostics	Specification
A-1 Electron Density Measuring System	A-1-a	Sub-mm Wave Interferometer	Main Plasma $\Delta\bar{n}_e \geq 10^{12}cm^{-3}$, $\Delta t \sim \mu S$ Divertor Chamber $\Delta\bar{n}_e \geq 4\times10^{12}cm^{-3}$, $\Delta t \sim \mu S$
	A-1-b	1-mm Interferometer	$\Delta\bar{n}_e \geq 4\times10^{11}cm^{-3}$, $\Delta t \sim \mu S$
	A-1-c	2-mm Interferometer	$\Delta\bar{n}_e \geq 2\times10^{11}cm^{-3}$, $\Delta t \sim \mu S$
	A-1-d	4-mm Interferometer	$\Delta\bar{n}_e \geq 1\times10^{11}cm^{-3}$, $\Delta t \sim \mu S$
	A-1-e	Mechanical Vibration Monitoring Interferometer	$\Delta\bar{X}$ 1μm
A-2 Electron Temperature Measuring System	A-2-a	FIR Spectrometer	$\Delta t \sim 10mS$, ΔX:20/R
	A-2-b	Heterodyne Radiometer	$\Delta t \sim \mu S$, ΔX:10/R
	A-2-c	Multipulse Laser Scattering Apparatus	$\Delta t \sim 20/sec$, ΔX:20/R
A-3 Ion Temperature Measuring System	A-3-a	Neutral Particle Analyzer (E.S.)	$E = 0.1 - 30keV$, $\frac{\Delta E}{E} = 0.05 - 0.1$ $\Delta t = 10 - 100mS$
	A-3-b	Neutral Particle Analyzer (E.S., M.A.)	$E = 0.1 \sim 30keV$, D & H, $\Delta E/E = 0.1$: electrostatic with mass analyzer $\Delta t = 50 - 500mS$
	A-3-c	Neutral Particle Analyzer Array	E:10 - 200keV, $\Delta E/E = 0.1 - 0.3$ $\Delta t = 1 - 100mS$, ΔX:20/R
	A-3-d	Neutral Particle Detector (PHA, M.A.)	$E = 10 - 200keV$, H,D & He, $\Delta E/E = 0.1$, $\Delta t = 10 - 100mS$
	A-3-e	Active Beam Probing Apparatus	see "A-3-d"
	A-3-f	Neutral Beam Source	$E_b = 30 - 200keV$, H,D & He (<0.1A) beam pulse: 10sec, choppable ~ μS
	A-3-g	Neutron Counter	$E_n = E_{th} \sim 2.45MeV$ $\Delta t = 1 \sim 100mS$

Table X.5-2 JT-60 diagnostics (A group) (part 2)

System	Simbol	Diagnostics	Specification
A-4 Impurity Measuring System	A-4-a	Light Impurity Spectrometer (Spatial Resolution)	λ = 10 - 500Å, ΔX:20 points/R Δt : ~1ms
	A-4-b	Light Impurity Spectrometer (Doppler)	λ = 1000 - 3000Å, Grating Δt : ~1ms
	A-4-c	Heavy Impurity Spectrometer (Spatial Resolution)	λ = 0.1 - 10Å, ΔX:20/R Δt : ~1ms
	A-4-d	Heavy Impurity Spectrometer (Doppler)	λ = 0.1 - 10Å Δt : ~1ms
	A-4-e	Spectrometer for Periphery	λ = 1000 - 3000Å, Δt : ~1ms ΔX: several points/periphery Grating
	A-4-f	see "A-4-e"	see "A-e-e"
	A-4-g	Spectrometer for Divertor	λ = 20 - 300Å, near X points Grating Δt : ~1ms
	A-4-h	Visible Spectrometer (Spatial Resolution)	λ = 2000 - 8000Å, ΔX:20/R Grating Δt : ~1ms
	A-4-i	Visible Spectrometer (Standard)	λ = 2000 - 8000Å
	A-4-j	Grazing Incidence Spectrometer (Standard)	λ = 10 - 1300Å
A-5 Radiation Flux Measuring System	A-5-a	High Counting Rate PHA	Si(Li) or Ge(I), E = 1~200keV Δt ~ 1ms, ΔX:3/R
	A-5-b	High Counting Rate PHA Array (Spatial Resolution)	Si(Li) or Ge(I), E = 1~200keV Δt ~ 1ms, ΔX:10 - 20/R
	A-5-c	PIN Diode Arrays	PIN Diode or SSD Δt ~ μs, ΔX:20/R
	A-5-d	Bolometer Arrays	Δt ~ 1ms, ΔX:20/R
	A-5-e	Hard X-ray Monitor	Hard X-ray, Δt:1ms
	A-5-f	Runaway Monitor	see "A-5-f"

Table X.5-2 T-60 diagnostics (A group) (part 3)

System	Simbol	Diagnostics	Specification
A-6 Peripheral Plasma and Wall Surface Measuring System	A-6-a	Moving Prove	Speed 1m/s { Langmure Probe { Directional Double Probe { Katsumata Probe
	A-6-b	Probe	{ Faraday Cup { Magnetic Probe { Target Probe
	A-6-c	Visible TV	
	A-6-d	IR-TV	
A-7 Electro-Magnetic Probing System		(1) Magnetic probes (2) Rogowski coils (3) One turn coils (4) Diamagnetic loops	
A-8 Data Processing System		(1) Inter-shot data processor (2) Real time data processor (3) CAMAC systems	
A-9 Diagnostic Support System		(1) Diagnostic stages (2) Carriers (3) Cabling and piping (4) Vacuum connecting instruments (5) Shielding cases ∘ Magnetic shield ∘ Radiation shield	

Table X.5-3 JT-60 diagnostics (B group).

DIAGNOSTIC SYSTEM	DIAGNOSTIC INSTRUMENTS
B-1 Neutron Measuring System	(1) Energy analysis
B-2 Ion Density Measuring System	(1) Beam probing
B-3 FIR Scattering System	(1) Ion temperature (2) Fluctuation
B-4 Current Density Profile Measuring System	(1) FIR polarimeter
B-5 Resonance Scattering System	

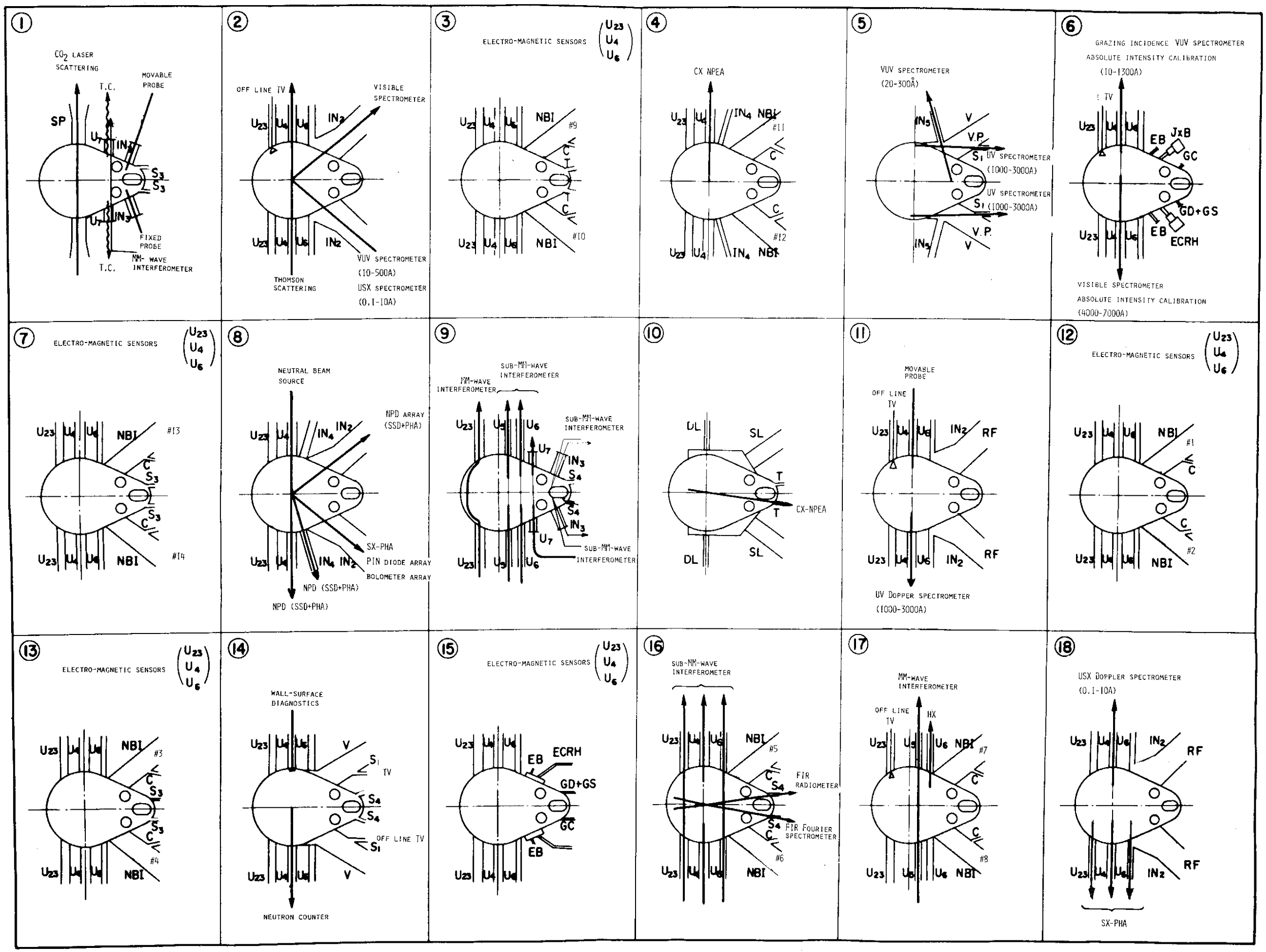

Fig. X.5-8 Allocation of diagnostics.

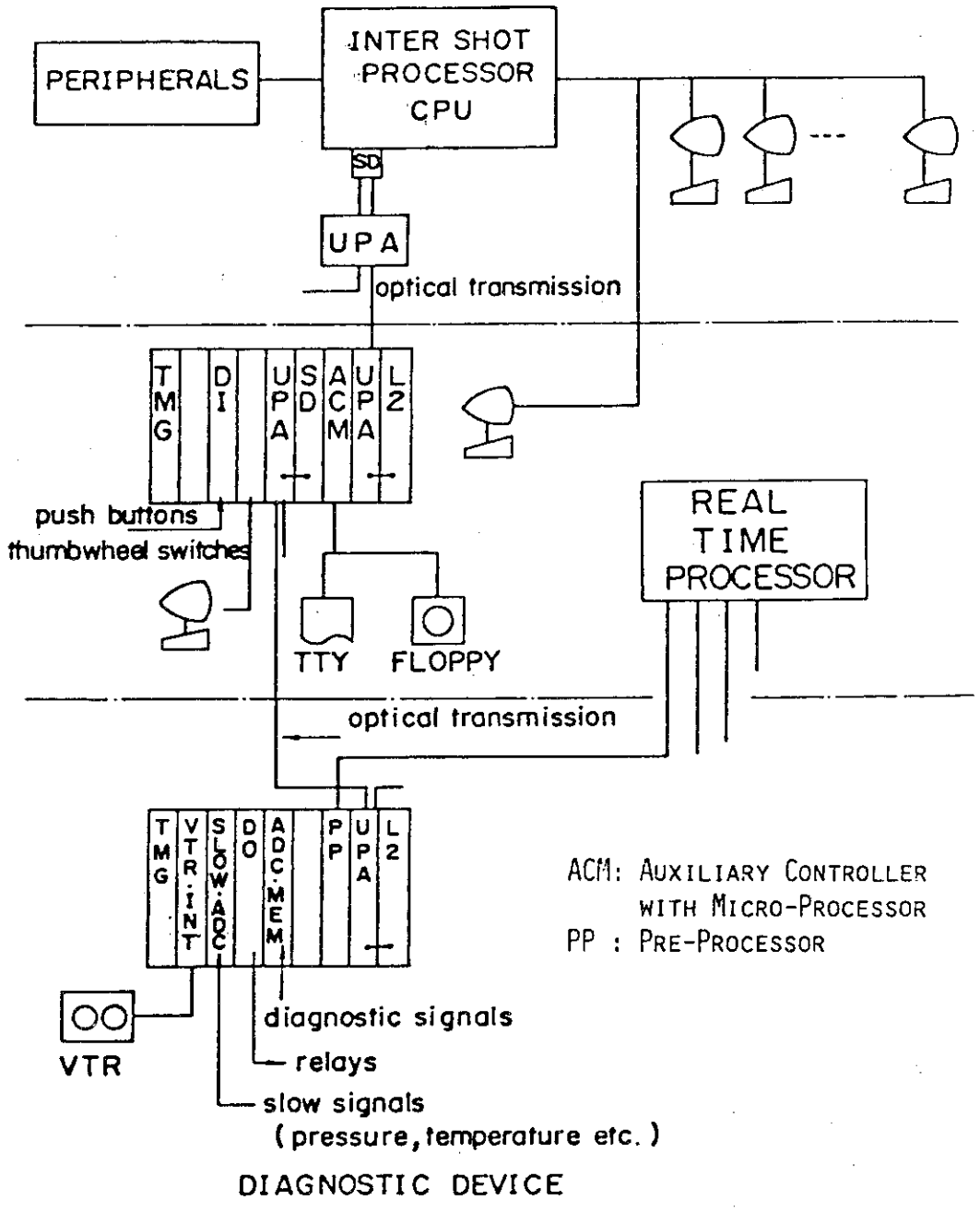

Fig. X.5-9 Detailed structure of the data processing system.

6. Status of Auxiliary Systems

6.1 Secondary cooling system

Secondary cooling system consists of the cooling tower, the pumps and other equipments for the purpose of the transfer and removing heat to air which is generated in the respective systems or equipments of JT-60. These cooling systems are mainly for the primary cooling of tokamak machine, the poloidal and toloidal field power supply, the supplementary heating power supply and the primary cooling of NBI and RF heating.

The contract for the manufacturing and construction for this system was made on January 1981 and the detailed specifications are under examination at present. The specifications are as follows.

(1) Cooling tower consists of six cells and these cells can be operated respectively and intentionally according to the heat load condition by pushing buttons in the control room at local or in the central control building.

Moreover, the speed of fans in cooling tower is changeable in two stages and shall be able to make full use of this performance according to environmental condition.

(2) The pair of pumps for the respective line systems are to run normally during the ordinary time. As for the secondary tokamak cooling line and power supply cooling line, the third pump is designed as the back up pump and shall be also driven by emergency power automatically at emergency.

The pump of auxiliary equipment cooling system is to maintain running all the time and pumps of other flow lines are operated in cycle accompaning with Tokamak machine.

(3) Water treatment system has the facililies for enriched concentration (coefficient N = 4 or 5) of cooling water in order to save the make-up water and drain, which includes the recirculating filter system, corrosion-proof devices, scale-proof devices and slime-proof devices.

(4) The arrangement of piping, pumps and other equipment in the pump house and around the cooling tower is almost completed. At present, the detailed specification of hardware and software of process equipments are being examined.

(5) The locations for operation and control are the central control room in JT-60 control building at normal, the field control room in the secondary cooling pump house for the individual operation and the field box near the equipment for maintenance.

The erection work is scheduled to be begun about the end of this year from the cooling tower at first.

The flow diagram of this system is shown below in Fig. X.6-1.

Essential characteristic specification was covered in the latest ANNUAL REPORT, JAERI-M 9421, issued on March 1981.

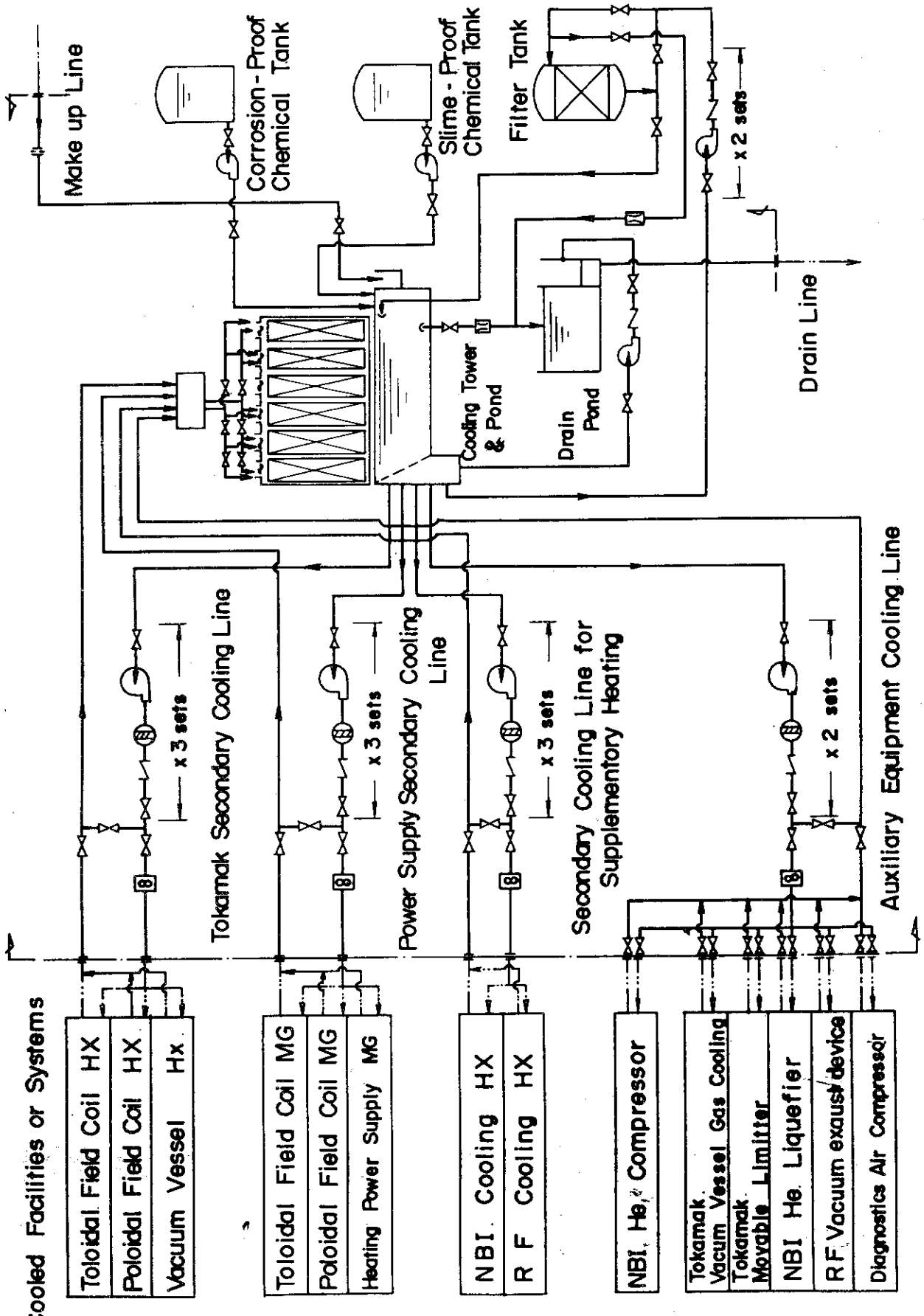

Fig. X. 6-1 Secondary Cooling Flow Diagram.

6.2 The system of power distribution and emergency power supply for operation.

The system of power distribution for operation is the facility which receives electric power at 6.6kV from the central substation and supplies the auxilliary system of JT-60 with this transformed power at appropriate voltages.

Main equipments of the auxilliary system to be supplied are the tokamak primary cooling pumps, the secondary cooling pumps, the power supply facilities for the respective auxiliary equipments and the power supply for baking and vacuum pumping system.

The emergency power supply system, which consists of the systems of emergency diesel generator and no break power system, is the facility for suppling the respective equipments of JT-60 with the indispensable power for those protection and safety at the power failure.

At the utility power failure, emergency diesel generator system receives the power from the emergency diesel generator installed in the central substation and supplies the respective equipments. In addition, the emergency diesel generator shall start immeadiately at the utility power failure and gain the required voltage in 20 seconds. It is impermissible for no-break power to break even the very moment in order to maintain the power of the control system of Zenkei and respective equipments. These operation and monitoring shall be made in the central control room and also possible in the local control panel.

The wiring diagram of this power distribution and emergency power supply system is shown in Fig. X.6-2.

Power Capacity Specification

(1) The power distribution system for operation.	13 MVA	
(2) The emergency power supply system.	8.3 MVA	
(3) The A.C. no break power supply.		
∘ Static type Invertor	450 KVA	4 Sets
∘ Battery	2500 AH	2 Sets
(4) The D.C. no break power supply.		
∘ Rectifier Device	2 Sets	
∘ Battery	800 AH	2 Sets

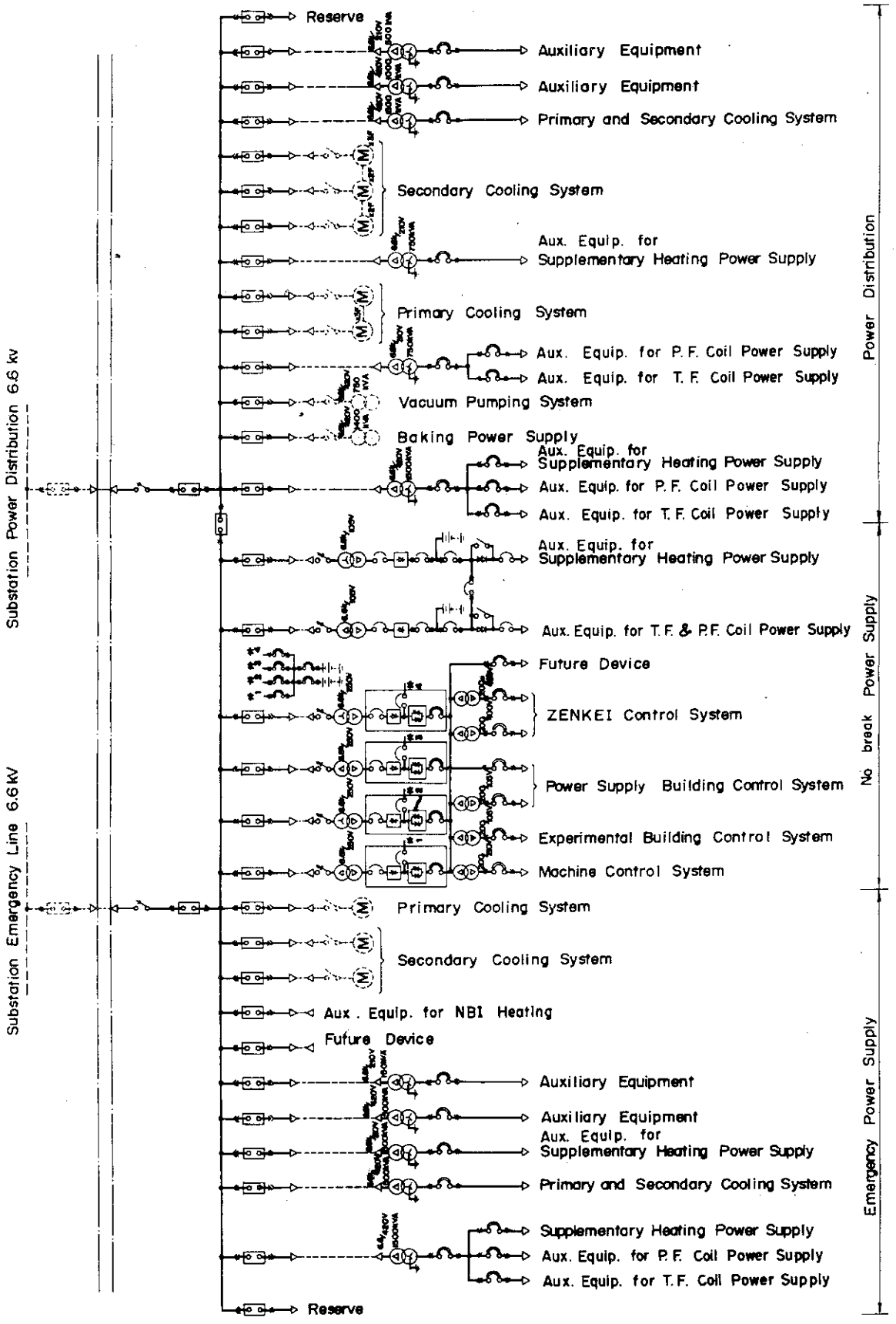

Fig.X.6-2 Wiring Digram of Power Distribution and Emergency Power Supply System

7. Vacuum Technological Development for JT-60

7.1 Introduction

In June 1979 Vacuum Technology Group was started in the Division of Large Tokamak Development. This group has the responsibility for vacuum and surface technology development for the JT-60 construction and experiment.

The construction of a JAERI Vacuum experiment facility (JVX) was started in FY 1979, and completed in May 1981. Experiments with JVX will become active in FY 1981 at the new site. Development of low-Z surface coatings is going on to take advantage of these materials in reducing the undesirable effect of wall material impurity in JT-60. In FY 1980 performance tests were made on small samples to screen coating materials. For the procurement of metal-sealed gate valves for diagnostic ports, performance tests were continued in cooperation with Hitachi, Ltd.

7.2 Construction of JVX

This facility consists of JVX-I and JVX-II.

JVX-I is intended to use mainly for the optimization of in-situ coatings of low-Z materials and for the demonstration of surface cleaning procedures including high temperature bakeout and RF glow discharge cleaning. The main features of JVX-I are as follows:

i) Vacuum chamber
- material: Inconel 625
- dimensions: 0.36 m^{ϕ} × 1.5 m
- max. baking temperature: 550 °C

ii) Liner
- material: molybdenum and Inconel 625 (as a substrate)
- dimensions: 0.32 m^{ϕ} × 1.4 m × 0.5 mm^{t}

iii) Pumping system
two turbo-molecular pumps (450 and 220 liter/sec) and a cryo-pump (20 K)

iv) RF power supplies
- frequency: 200, 400 kHz; 1, 13.56, 27 MHz; 2.45 GHz

- power — max. 10 kW (5 kW for 2.45 GHz)

v) In-situ coating devices

cylindrical magnetron sputtering source, and titanium evaporation source

vi) Atomic hydrogen production device

tungsten hot filaments

vii) Diagnostics

monochrometer (0.17 - 1.5 μm)

surface monitor station with AES, SIMS and SEM

JVX-II is intended to use mainly for the development of a leak location system and for the testing of vacuum components such as gate valves and vacuum seals. For JT-60 leak location would be done by detecting a gas influx from the inside of the vacuum vessel. In this case a small pressure sensor must be moved in the vessel by using a skilful manipulator. The main features of JVX-II are as follows:

i) Vacuum chamber

- material — 304 stainless steel
- dimensions — 1.0 m^{ϕ} × 1.5 m
- max. baking temperature — 500°C (200°C for manipulator operation)

ii) Pumping system

turbo-molecular pump (500 liter/sec)

iii) Leak location system

3-dimensional manipulator with unidirectional pressure sensor

Figure X.7-1 shows the panoramic view of JVX installed at the new site.

7.3 Development of low-Z surface coatings

A preliminary estimate of low-Z coating requirements was made in FY 1979 and a coating development program was started in FY 1980. In Fig. X.7-2 are shown the time schedule and major milestones for the development. For the precoating, a decision will be made in 1982 on the most desirable coating-substrate combination for the first phase experiment of JT-60. Development of in-situ coating techniques for low-Z materials is also planned. In FY 1981 a preliminary experiment will be completed by using JVX-I, and scaling to JT-60 will be considered in FY 1982.

Evaluation of low-Z surface coatings (precoating) with small samples was made in FY 1980. Coating materials and methods tested are summarized in Table X.7-1. The coated film thickness was about 20 μm. The small samples of 10mm × 10mm × 0.5mm were subjected to two types of heat loads. The thermal cycle test by infra-red heat irradiation was made under a high vacuum by using a conventional infra-red lamp furnace. For the thermal shock test, a neutral beam apparatus, ITS-2, was operated at a power density of 2 kW/cm^2. Total sputtering yield and chemical sputtering yield measurements were made on some of low-Z surface coatings. Experiments on blistering were also done by using a Cockcroft-Walton accelerator, HSP. (see Chapter VI)

The main results are as follows:

(1) The carbon on both substrates showed partial peeling off after one cycle of the infra-red heat irradiation.

(2) In the TiC and TiN films on molybdenum cracks grew with the thermal cycles, but the films never peeling off even after the maximum number of heat cycles of 3000.

(3) The thermal shock test showed that, in the case of TiC (CVD) on molybdenum, there was no evidence of failures until the melting of the substrate under the coating.

(4) In the case of TiN (CVD) on molybdenum, there was no evidence of exfoliation or spalling until the melting of the substrate, but the film was decomposed at high temperatures.

From these results, it is seen that TiC is the most promising coating material for JT-60.

Table X. 7-1 Materials and coating methods examined.

Coating Materials	Coated Film Thickness (μm)	Substrate Materials	Coating Methods
C	20	Mo	DVD
C	20	Inconel	DVD
TiC	20	Mo	RIP
TiC	20	Inconel	RIP
TiC	20	Mo	CVD
TiN	20	Mo	CVD
TiN	20	Inconel	CVD

DVD: Discharge vapor deposition
RIP: Reactive ion plating
CVD: Chemical vapor deposition

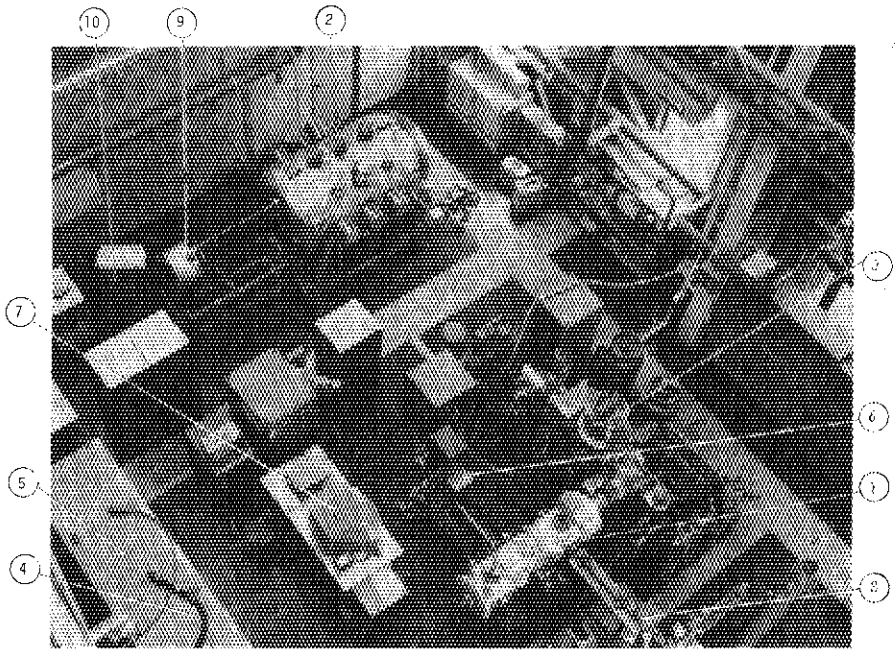

① vacuum chamber (JVX-I)
② vacuum chamber (JVX-II)
③ pumping system (JVX-I)
④ RF power supply (2.45 GHz)
⑤ power supplies
⑥ in-situ coating device
⑦ monochrometer
⑧ surface monitor station (AES, SIMS, SEM)
⑨ vacuum manipulator
⑩ manipulator operating panel

Fig. X. 7-1 Panoramic view of JVX installed at the new site.

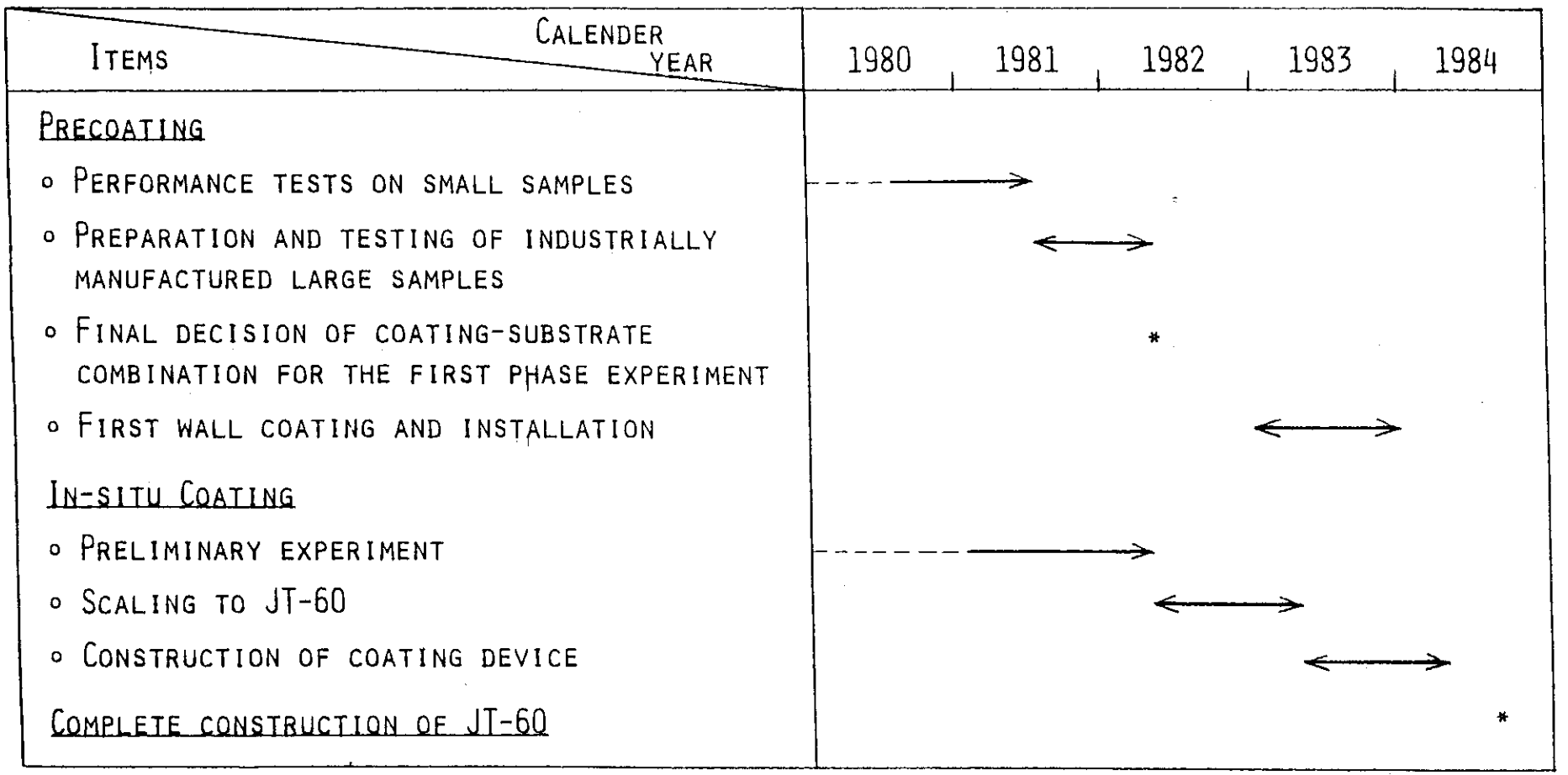

Fig. X. 7-2 Time schedule and major milestones for the low-Z surface coating development.

8. JT-60 Experimental Planning and Plasma Consideration

8.1 Experimental program and schedule

The research objective, experimental program and schedule were not changed and are briefly discussed in this section.

The objective of JT-60 is the study of a reactor grade plasma including plasma-machine interface. In other words, technology to generate and maintain a reactor grade plasma has to be researched and it is necessary to show how we can obtain and control a reactor core with realistic methods. The scheduled experimental programs are summarized in Fig. X.8-1 and are briefly discussed below.

1) Preliminary experiment

In the first phase of this experiment, plasmas only with ohmic heating are studied. A suitable target plasma for additional heating has to be obtained with and without the divertor. Discharges, however, will not be intensively studied in a wide range of plasma parameters because installation and/or test of heating devices, diagnostics and the real time control system will be more important. A $Q^* = 1$ plasma will be easily obtained with 20 $\sim$ 30 MW heating because the plasma will have been obtained in the other large Tokamak devices. The main objective in this phase is to confirm the results in the other projects and to prepare the following experiments.

2) Basic experiment

In this experiment, the standard operation with 30 MW and 5 $\sim$ 10 sec heating is investigated with following items.

(i) Build-up phase of $Q^* \simeq 1$ plasmas

Clean and stable current raising by using the poloidal divertor, control coils, dynamic limiter, gas puff and/or heating devices is investigated. Heating experiment with 20 MW NBI and 10 MW RF with and without the poloidal divertor will be done. 14 injectors and 4 sets of RF devices are independently operated. It will be necessary to control the scrape-off layer plasma as well as the main plasma.

(ii) Confinement characteristics of reactor grade plasmas

Detailed parameter study with and without the poloidal divertor is made.

(iii) Steady state operation

Control of a long pulse plasmas by the real time control system is studied. Not only the plasma position and shape but also the major plasma parameters are controlled by employing various actuators with and without the poloidal divertor. Current drive by RF of 23 MW be also tested.

(iv) High β operation

The maximum β value will be obtained with the maximum toroidal field of 4.5 T and high β plasmas are maintained during 5 ∿ 10 sec. Build-up process will be intensively investigated as well as characteristics of the high β plasma with and without the poloidal divertor. Very-low-q operations are also investigated.

(v) First wall and impurity experiment

In order to obtain first wall data for a reactor, various kinds of wall materials including low-z, medium-z and high-z materials are tested as the first wall. The first wall material to be used in a reactor will be intensively investigated with various wall temperature up to 500°C. Impurity control by controling the scrape-off layer plasma is investigated as well as by using the poloidal divertor.

(vi) Plasma operation to mitigate engineering difficulty

The following items will be studied: Disruption control; slow current raise and shut down; slow heating; reducing the heat flux density by using swinging divertor; edge cooling and/or vibrating the plasma column; conventional wall material; impurity control without the poloidal divertor; systematic study of stress of coils, vacuum chamber and so on; easy cleaning method; simulation of easy ash exhaust system such as the simple poloidal divertor and/or mechanical divertor; high efficient RF heating; very-low-q operation free from disruption.

(vii) High efficiency heating

The maximum RF power into the torus is 23 MW. If the scrape-off layer plasma can be controlled, the heating efficiency can be increased.

(viii) Development of a control system for a reactor core

It is necessary to develop a reliable real time control system, especially simple sensors for controlling parameters including temperature, density, β, impurity, heat flux and heating. This problem is also planned to be studied.

3) Advanced experiment

It is considered to raise the heating power in the advanced experiments. After increasing NBI power up to 30 MW and RF heating efficiency, the total heating power will be 40 ∿ 50 MW. A $Q^* \simeq 3$ plasma will be obtained, which is very similar to the reactor core plasma. The each experiment listed in 2) will be also done with this condition. Extremely long pulse operation will be also studied if it is required.

4) Modification

When the design of the next generation reactor is established, JT-60 is planned to be modified so as to complement its program. Among options considered, one is to conduct simulation or exploratory experiments in hydrogen plasmas to support the program (Proto ETR experiment).

In order to do these experiments, JT-60 has following characteristics.

1) hydrogen machine
2) large plasma volume (60 m^3),
3) long pulse operation with additional heating (30 ∿ 50 MW, 10 sec),
4) high-β plasma with B_t=4.5 T (4%, 5 ∿ 10 sec),
5) poloidal divertor with a short and wide throat,
6) easy exchangeability of the first wall material, and
7) real time data processing and real time control system.

A brief description of the each characteristics are shown below.

1) Hydrogen machine

It is important to demonstrate D-T burning, to study α-particle heating and burn control, and to investigate neutronics in a D-T machine. The studies, however, cannot be done in a wet wood burning device, i.e. $Q^* \lesssim 5$. Therefore, these studies cannot be done even with a full D-T operations in JT-60. From this point of view, no D-T operation is planned in JT-60 and various other important studies can be done in detail because of no activation.

2) Plasma volume (60 m^3)

It is reasonable to consider that the size of JT-60 is similar to that of a reactor from plasma engineering point of view.

3) Long pulse operation with additional heating (30 ∿ 40 MW, 10 sec)

The duration 10 sec is enough long to study a heating phase, a steady state and plasma control by using a real time control system with

a reactor like conditions. Heating power is also enough to obtain a reactor grade plasma.

4) High-β plasma with B_t = 4.5 T

In JT-60, behaviors of a reactor like circular plasma near critical β will be examined in detail. Combining the experiment in JT-60 and the experiment in a D-shape device, e.g. JFT-2M or D-III, it is easy to picturize a reactor core plasma.

5) Poloidal divertor with a short and wide throat

In a reactor, it is expected that a magnetic divertor is not required. However it is not clear whether a magnetic divertor is necessary or not. A simplified poloidal divertor with a short and wide divertor throat is the most reliable divertor concept in a reactor. From this point of view, it is very important to study the simplified poloidal divertor in JT-60.

6) Easy exchangeability of the first wall material

By this time, it is impossible to decide the first wall material of a reactor. Therefore it is very important to study various kinds of wall materials in a large device. Neutron effects have to be studied in another program. The first wall of JT-60 is easily demounted.

8.2 Plasma control

In a large tokamak, a careful plasma control is essential not only for production of a high quality plasma but also for safety and protection. From this point of view, the real time control system is employed not only for the position and shape but also for other important quantities or behaviors, e.g. separatrix configuration, heating power, gas influx and disruption, in JT-60. The all diagnostic instruments can be used as sensors for the real time control system and the major actuators are the poloidal coil system, divertor coils, hydrogen and impurity gas supply system, 14 NBI injectors and 4 units of RF systems. Disruption control and soft plasma termination will be intensively investigated as well as control of conventional plasma parameters. In this subsection, consideration results on plasma control are described.

8.2.1 Plasma position detection by magnetic probes

A dozen of probes set on the inner surface of the vacuum vessel

shown in Fig. X.8-2 are used as magnetic sensors for detecting a plasma position. Two calculating methods, i.e. the conventional method[1] and the multipole moment method,[2~3] are investigated. The major results are summarized as follows:

1) The two methods, especially the multipole moment method, give an accurate plasma position with a small value of $\beta_p + \frac{\ell i}{2}$, e.g. ~ 0.5, (Figs. X.8-3 and X.8-4) and are useful in an ohmically heated plasma experiment.

2) The conventional method is still valuable with a rather large value of $\beta_p + \frac{\ell i}{2}$ and gives an accurate plasma position near the machine centre (Fig. X.8-3). Therefore the conventional method is always useful to set the plasma centre near the machine centre even with the high power heating. If we need other plasma operations, e.g. an adiabatic compression, the minor radius should be obtained by another measurement in order to obtain an accurate plasma position.

3) The multipole moment method does not give a correct position with a rather large value of $\beta_p + \frac{\ell i}{2}$ (Fig. X.8-4). If we know the value of $\beta_p + \frac{\ell i}{2}$, we can obtain the correct position after some numerical corrections (Fig. X.8-5). The value, however, can not be accurately obtained from the magnetic probe measurement and the multipole moment method is not useful in the heating experiment.

4) The external coil currents do not affect the measurement. Induced currents on the divertor coil cans and vacuum vessel affect to the measurement only during the very early phase of the current rising.

The above mentioned results show that the conventional method is very useful in a wide range of plasma parameters in JT-60. In special operations, other sensors are necessary and are under investigation.

8.2.2 Magnetic divertor configuration

The conventional magnetic method is still useful for detection of a plasma position with the divertor but numerical corrections are necessary. The other important control item is the position of the separatrix magnetic surface especially near the divertor throat and the neutralizer plate. Figures X.8-6, X.8-7(a) and X.8-7(b) show relations between B_ρ/B_ω δ and x where B_ρ/B_ω are poloidal field intensity ratio shown in Fig. X.8-2, the distance between the outer surface of the main divertor coil can and the separatrix magnetic surface, and the distance between

the centre of the neutralizer plate and the separatrix magnetic surface, respectively. These figures show that the position of the separatrix magnetic surface can be easily obtained by the simple magnetic measurement set at a suitable position in the divertor chamber. The overall configuration, however, cannot be detected by these magnetic probes and other measurements such as the diverted heat or particle flux profile measurement will be necessary. The heat deposition profile on the neutralizer plate is also important for the real time divertor control. These advance scheme is also under investigation.

8.3 Plasma consideration

Plasma operation scenarios, main plasma parameters, NBI and RF heating, impurities, scrape-off layer plasmas, plasma-wall interactions and so on have been numerically studied. The major results were reported in the previous annual report. In this subsection, some additional studies are described.

8.3.1 1-D tokamak transport code

In a tokamak transport code, it is particularly important to calculate impurity transport and impurity radiation loss. From this point of view, the following two efforts have been done.

1) Formulating self consistent boundary conditions for a 1-D tokamak transport code.
2) Developing a solving method to calculate impurity behaviors consistently during a reasonable time scale.

Concerning the later effort, there are serious problems on the numerical calculation of impurity continuous equations. The diffusion and atomic terms, which are included in the continuous equations, should be treated simultaneously and a time step required for computation should be $10^{-6} \sim 10^{-7}$ sec which is the fastest ionization characteristic time. Therefore, it is impossible to investigate impurity evolution for a realistic duration, i.e. $10^{-1} \sim 10$ sec. Previous work of M. OKAMOTO and T. AMANO[4] has settled up these numerical problems with a splitting and fractional step method for noncommutative operators. This method gives accurate results with the time step up to 10^{-4} sec. The time step 10^{-4} sec, however, is still too small to analyze JT-60 plasma.

An alternative method for solving impurity continuous equations has

been developed and a new unsteady impurity analysis code which treats both power balance and impurity radiation simultaneously and consistently is developed. The impurity continuous equations are refered as a stiff equation. It is generally known that a full implicit method ensures numerical stability for a stiff equation. In the new impurity analysis code, a diffusion term is solved by the traditional Crank-Nicholson scheme and an atomic term by the full implicit method. Since impurity neutral, which is generally calculated from the diffusive impurity ion fluxes, is the nonlinear boundary condition for the continuous equations, a careful treatment of impurity neutral particle is also required. An equation binding impurity neutral is linked with the continuous equations and impurity neutral is consistently solved with impurity ions. The conbined numerical method and the restriction equation get the time step stably extended to a order of confinement time of a plasma, for example $\sim 5 \times 10^{-2}$ sec for PLT. This impurity code has the characteristic as follow:

1 The code calculates one specie of carbon, oxygen or iron, in which atomic processes are calculated by the steady impurity analysis code developed by T. Tazima, Y. Nakamura and K. Inoue[5].
2 The expression of impurity particle flux is sum of anomalous and Samain's collisional neoclassical one.
3 The impurities in the plasma scrape-off region are calculated as well as the ones in the main plasma region.

8.3.2 Ripple diffusion

We have investigated the heat conductivity of ions by using the orbit-following Monte-Carlo code. Some results are shown in Fig. X.8-8. Here the neoclassical contribution to ion heat conduction without ripple χ_i^{NC} agrees fairly with the theoretical predicition[6]. Numerical results of χ_i^{RP} also show a good agreement with the theoretical ones for the high collision frequency. On the other hand, χ_i^{RP} is found to decrease in the collisionless side and the transition from the collisional regime to the collisionless one occurs at the collision frequency ν_i much larger than the prediction from the simple arguments[7]. This behavior of χ_i^{RP} results in a significant reduction of the value of χ_i^{RP} in the collisionless regime. It is considered for the reason of this result that most of ions are trapped weakly by ripple in a collisionless plasma and thereby

are detrapped out of ripple within a time interval much shorter than δ/ν_i. The collisionless ripple detrapping also contributes to a decrease of the radial walk step.

Other detailed results of NBI heating analysis were reported in the previous annual report.

8.3.3 Radio frequency heating

RF heating is very attractive as the further heating method of a plasma in a tokamak reactor, since it is engineeringly simple compared with NBI heating. Therefore LHRF heating with 10 MW of RF power will be done in JT-60. Recently, many experimental results which demonstrated the effectiveness of RF heating in tokamaks have been reported[8∿10]. As for the lower hybrid range of frequencies (LHRF) heating, though some harmful nonlinear effects like parametric instabilities and ion tail formation near the plasma edge have been reported, they will be reduced in a hot dense plasma in future large tokamak, since the ratio of the RF power density and plasma energy density $R_N = S^{RF}/nT$ will be a few hundredths of that of the present experiments.

Results in the JFT-2 and possible Alcator A showed good heating efficiency[9]. Moreover, LHRF have shown several experimental success in a current drive[11]. There are many other experimental results which support the feasibility of the LHRF heating in tokamaks. These results encourages the LHRF heating plan with 10 MW in the JT-60.

ICRF heating with 2-3 MW power is also in scope of JT-60 program together with the LHRF. The ICRF has shown an excellent heating efficiencies in several experiments. But it is often pointed out that loop antenna is not applicable in a reactor environment. Therefore, the aim of the ICRF experiment in JT-60 is to testify the waveguide coupling mentioned in the section V.3.1.1 as well as the loop antenna which has a possibility to be applied to a reactor.

(1) Ion heating

Numerical studies of the LHRF heating in JT-60 were described in the last report[12]. An appropriate frequency for JT-60 is 2.0 GHz. A phased array of 32 waveguides, each of which has the size of 35 mm × 115 mm, is adopted. The power spectrum of this launcher ranges mainly from $N_z = 1.6$ to $N_z = 2.4$ with phase difference $\Delta\phi = 180°$.

Here, the results of the numerical simulation of the LHRF heating

in a large tokamak is described as an example of the time behavior of the plasma parameters during the RF pulse. Details of the simulation code is explained in refs. 13) and 14). The time evolutions of ion temperature in both linear heating and nonlinear stochastic heating theories are shown in Figs. X.8-9 (a) and (b), respectively. In this simulation, RF power, phase difference and frequency are all constant during the pulse. Therefore, the ion temperature near the center, at first, increases rapidly but it saturates soon in the case of the linear heating. The final ion temperature is about 5 keV. But in the case of the nonlinear heating model, the ion temperature gradually increases up to 20 keV, since the deposition profile of the RF power is kept almost constantly well automatically due to the nonlinear penetration of wave. This feature is figuratively explained in Fig. X.8-10, where the time change of the radial profiles of ion temperature is shown in both cases. The outshift of the deposition is clearly seen in the (a). The results of the simulations indicate that it is extremely important to have a measure to optimise the deposition profile of the RF power during the heating pulse in the absence of the nonlinear penetration, which has not been clarified yet in the present time.

Real time feed back control of RF power, phase difference and, if possible, frequency is planned in JT-60 experiment to cope with the deposition outshift, as described in the section V.3.2.

(2) Current drive

Recent success in a current drive in tokamaks gives a hope to operate a tokamak reactor in steady state[11]. Therefore, current drive experiment is also in scope of the JT-60 program. The possibility to drive currents without the change of the present design of the LHRF heating system os JT-60 has been investigated. In a current drive experiment, unidirectional wave whose phase velocity is greater than three times of the electron thermal velocity is required. Accessibility condition for the penetration of the wave into the core plasma is given with $N_z \geq 1.2$ in the low density plasma aimed at the current drive. From the above two limitations, the range of N_z which enables to drive currents is from 1.2 to 1.7. Spectra obtainable with the present launcher having various $\Delta\phi$ are shown in Fig. X.8-11. Asymmetry of the spectrum with $\Delta\phi = 120° - 150°$ provides unidirectional wave of necessary range of N_z, though the effective power to drive currents is less than

half.

Current driving efficiency of the lower hybrid wave is estimated as follows[15].

$$I_{RF}/P_{RF} = 2 \times 10^{-3} \left(\frac{T}{R\ n} \right) \left(J/P_D \right) , \qquad (1)$$

where T is ion temperature in keV, R is the major radius in m, n is the plasma density in m^{-3} and J/P_D is the key parameter of the RF current drive which is determined by the wave property and is the order of 10. In JT-60, these parameters are R = 3, T = 10, n = 0.5 and J/P_D = 15. They give the efficiency of $\sim$0.2 A/W. Effective power for current drive is about 50% of the whole power, as mentioned before, It will be expected that currents of $\sim$1 MA is driven by the 10 MW injection. Here, it must be noted that these estimation is preliminal. One must consider the effect of nonlinear saturation to get a more exact calculation.

References

1) Ninomiya, H. et al.: (to be published in JJAP)
2) Zakharov, L.F. and Shafranov, V.D.; Soviet Phys. Tech. Phys. 18 (1973) 151
3) Aikawa, H., Ogata, A. and Suzuki, Y.; JJAP 15 (1976) 2031
4) Okamoto, M. and Amano, T.; J. Comp. Phys. 26 (1978) 80
5) Tazima, T., Nakamura, Y. and Inoue, K.; Nucl. Fusion 17 (1977) 419
6) Galeev, A.A. and Sagdleev, R.Z.; Sov. Phys. JETP 26 (1968) 233
7) Stringer, T.E.; Nucl. Fusion 12 (1972) 689
8) Hosea, J.C. et al., in Proc. of 8th Int. Conf., Brussels (1980) IAEA-CN38/D5-1. : Kimura, H. et al., ibid, IAEA-CN38/D5-2. : Equipe TFR, ibid, IAEA-CN38-D3
9) Imai, T. et al., in Proc. of 4th Top. Conf. on RF Plasma Heaging, Austin (1981) C2. : Shuss, J.J. et al.; Nuclear Fusion 21 (1981) 427
10) Gilgenbach, R.M. et al., Phys. Rev. Lett. 44 (1980) 647 : Moeller, G.P. in Proc. of 4th Top. Conf. on RF Plasma Heating, Austin (1981) D1
11) Yamamoto, T. et al.; Phys Rev. Lett. 45 (1980) 716 : Luckhardt, S.C. et al., in Proc. of 4th Top. Conf. on RF Plasma Heating, Austin (1981) B6

12) Annual Report of the Fusion Research and Development Center for the Period of April 1, 1979 to March 31, 1980, JAERI-M 9421 (1981)
13) Imai, T. et al.; J. Phys. Soc. Japan 50 (1981) 647
14) Amano, T. and Okamoto, M.; Japan Atomic Energy Research Institute Report, JAERI-M 8420 (1979)
15) Fish, N.J. and Boozer, H.; Phys. Rev. Lett. 45 (1980) 720

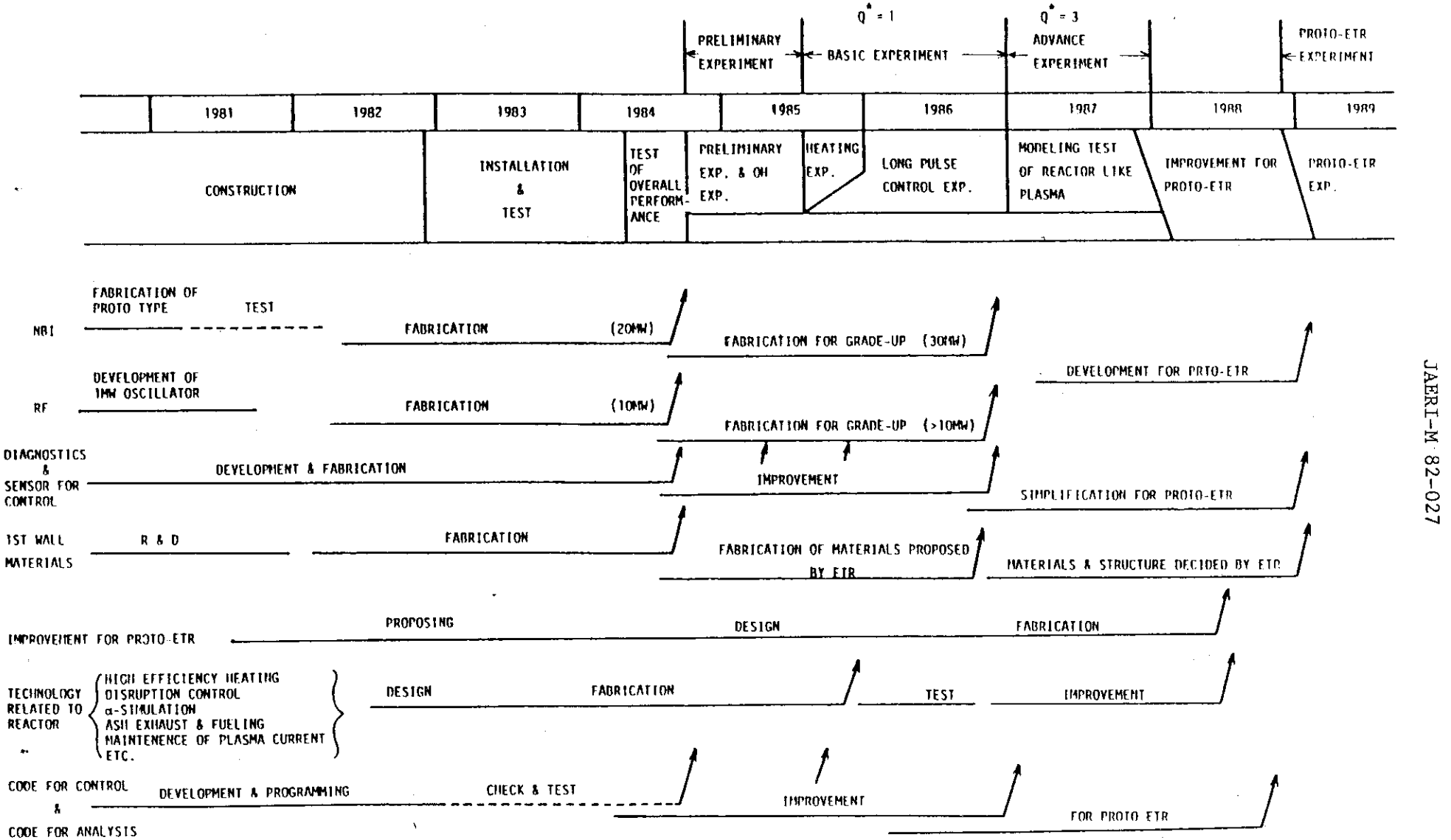

Fig. X.8-1 Experimental programm and schedule of JT-60.

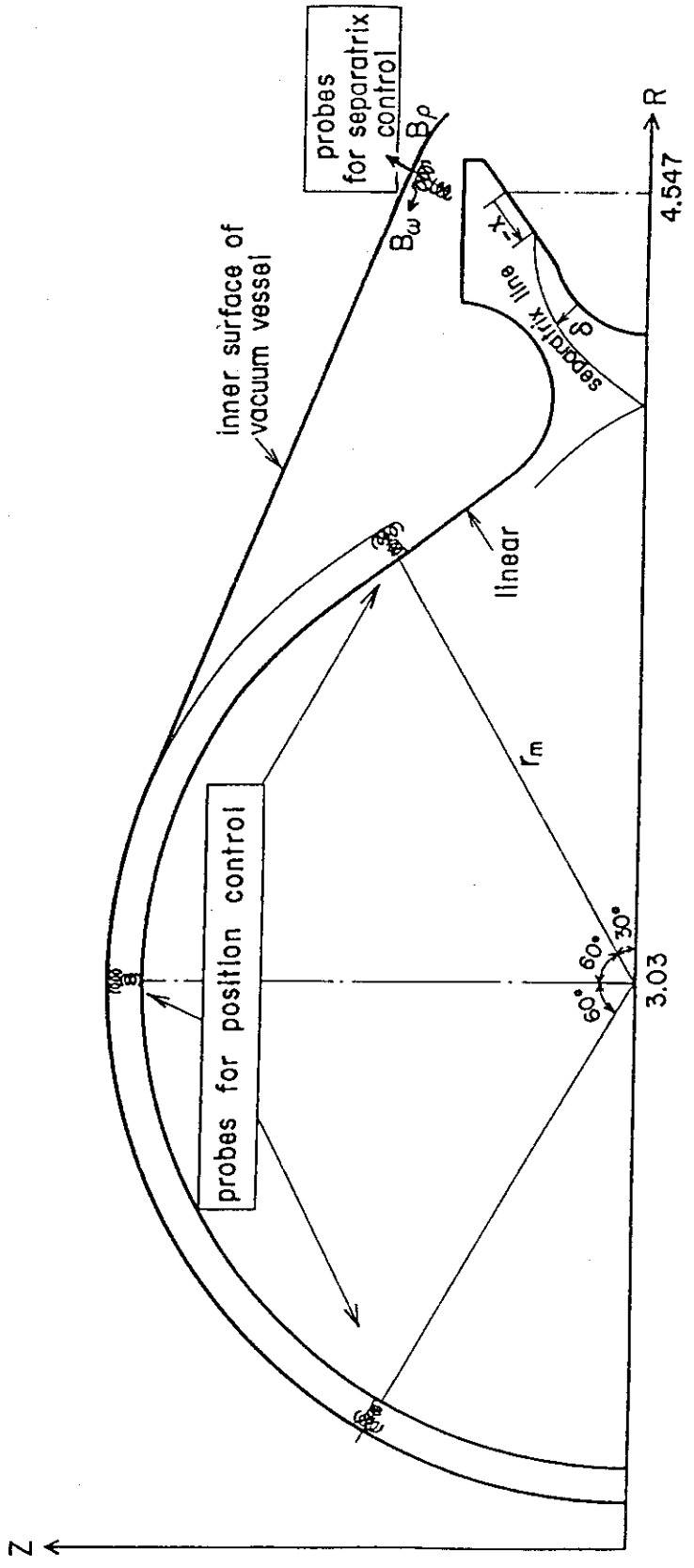

Fig. X.8-2 Schematic drawing of magnetic probes.

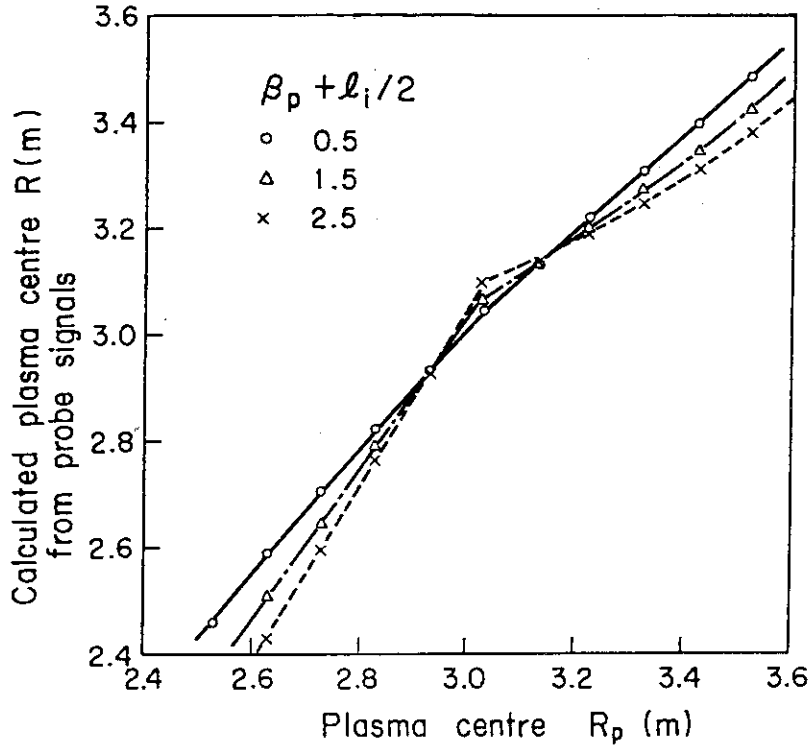

Fig. X.8-3 Given plasma positions (R_p) v.s. calculated plasma positions (R) by using the conventional method[1] and assumming a_p = 85 cm.

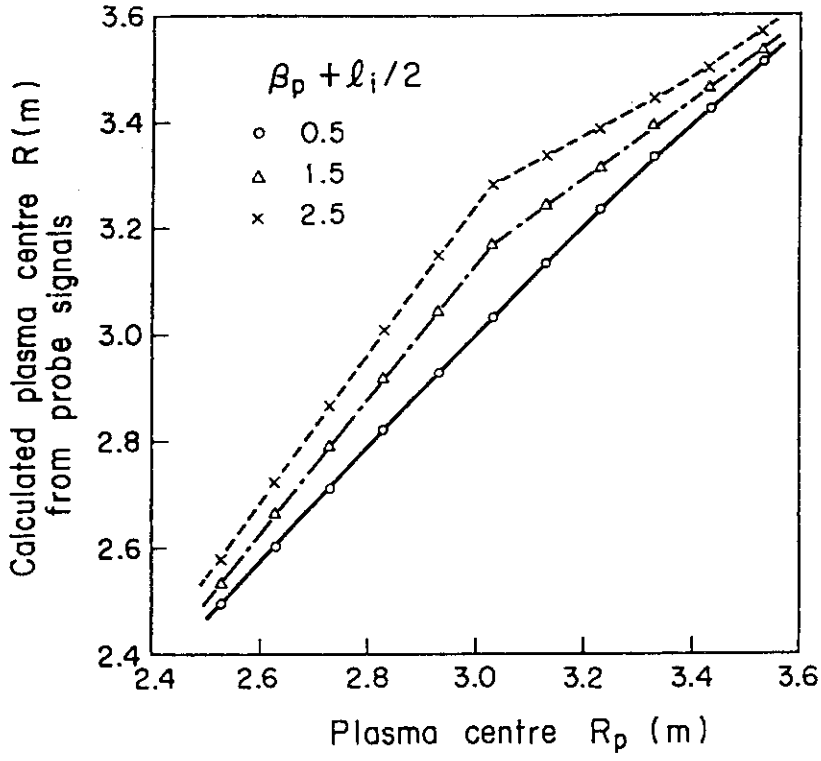

Fig. X.8-4 Given plasma positions (R_p) v.s. calculated plasma positions (R) by using the multipole moment method[2)~3)].

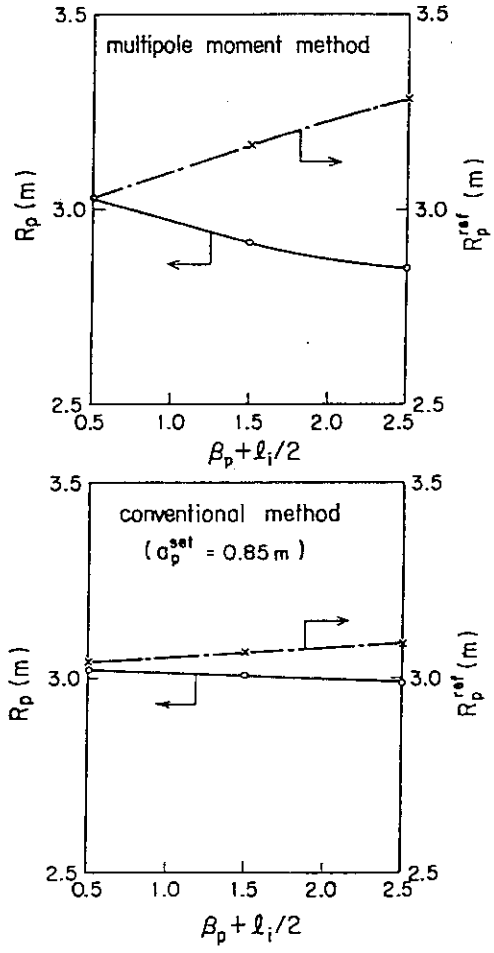

Fig. X.8-5 Expecting plasma centre positions R_p with fixing the reference value of the major radius at 3.03m and the necessary reference values to fix the major radius at 3.03m.

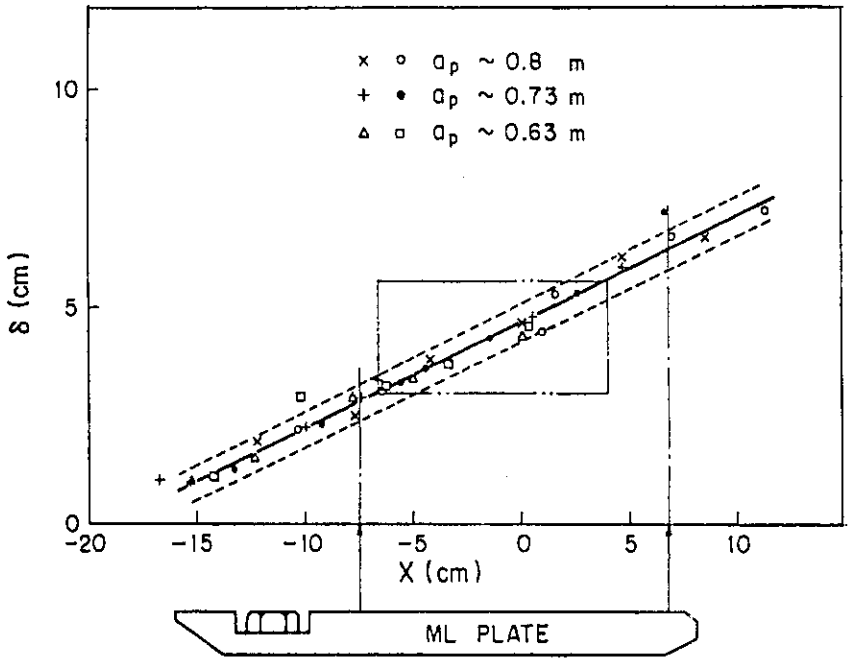

Fig. X.8-6 δ v.s. x. δ and x are shown in Fig. X.8-2.

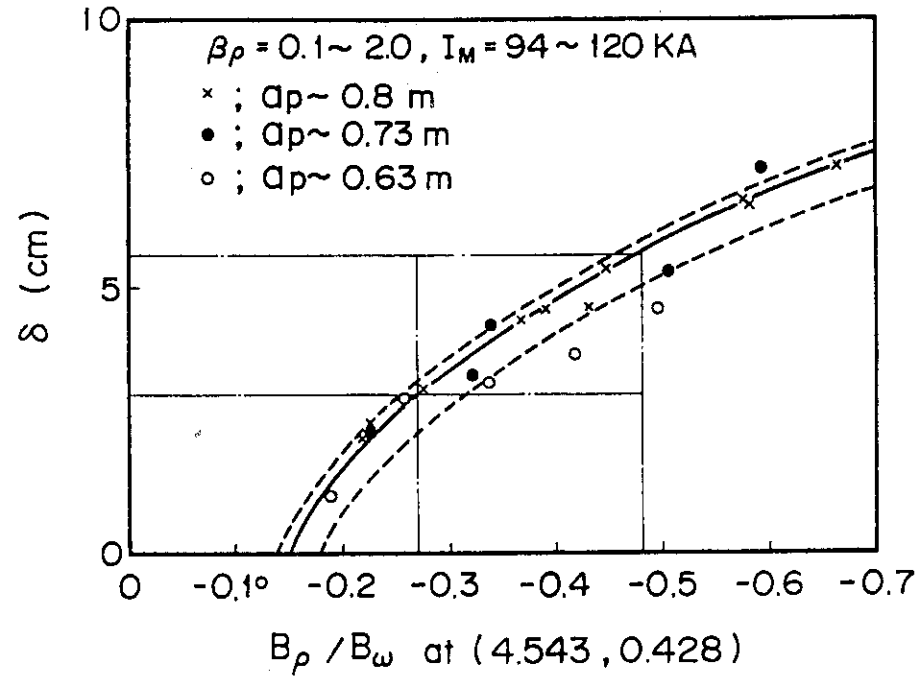

Fig. X.8-7(a) δ v.s. B_ρ/B_ω. δ and B_ρ/B_ω are shown in Fig. X.8-2.

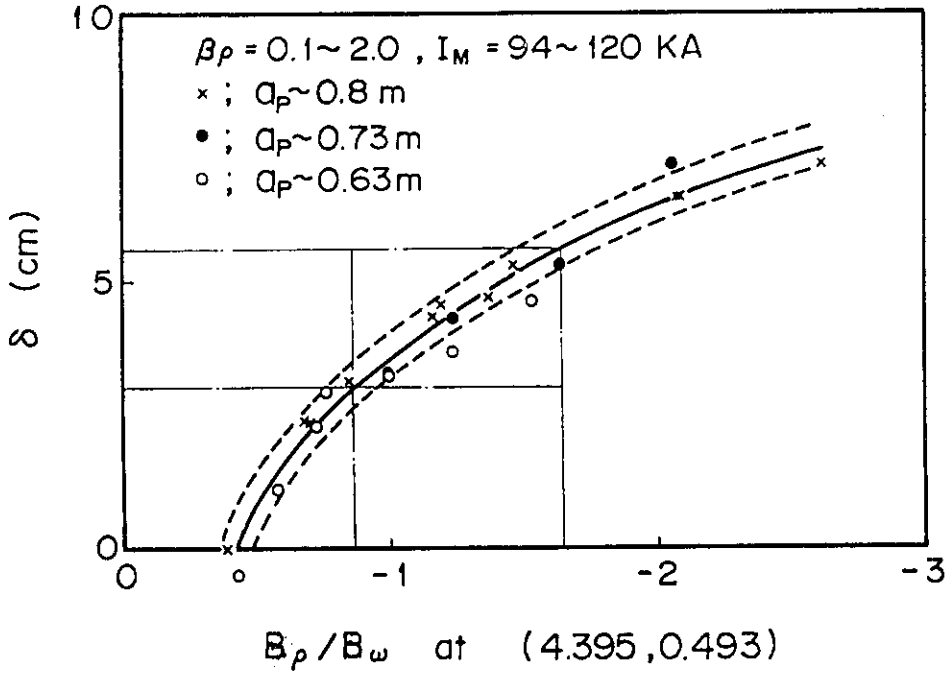

Fig. X.8-7(b) δ v.s. B_ρ/B_ω. δ and B_ρ/B_ω are shown in Fig. X.8-2.

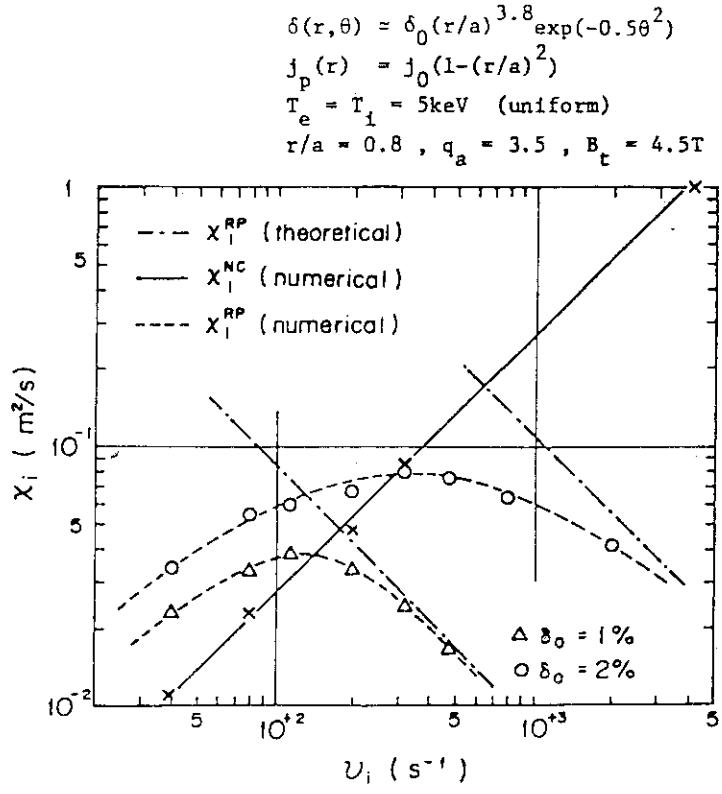

Fig. X.8-8 Thermal conduction coefficient with ripple.

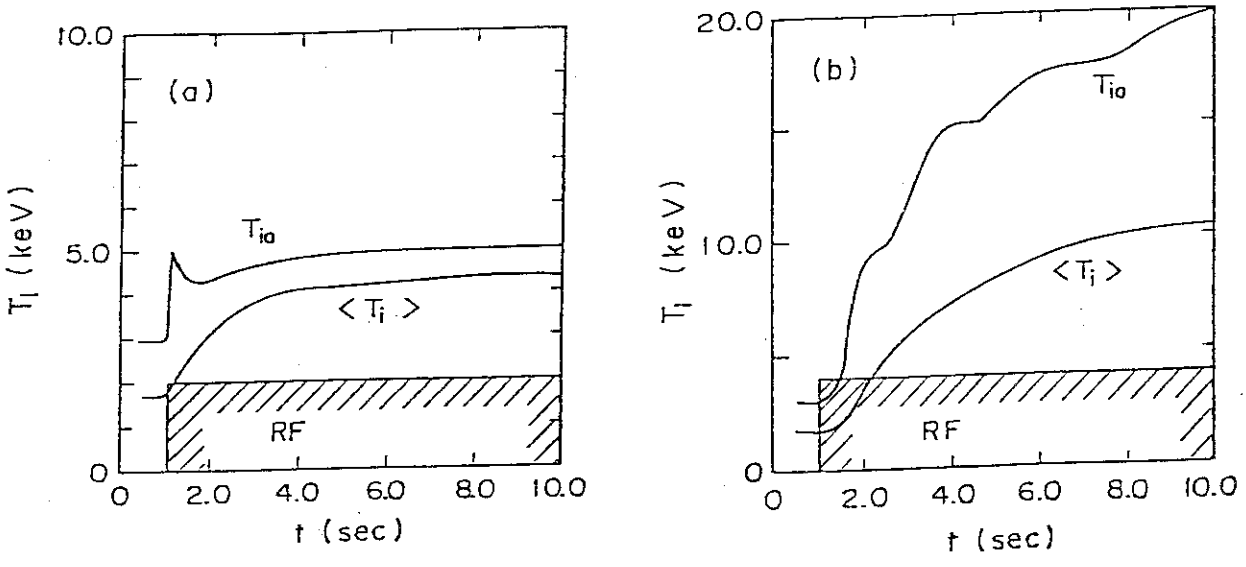

Fig. X.8-9 Time evolutions of the ion temperature during the RF pulse in a large tokamak plasma in the cases of (a) linear model and (b) nonlinear stochastic model.

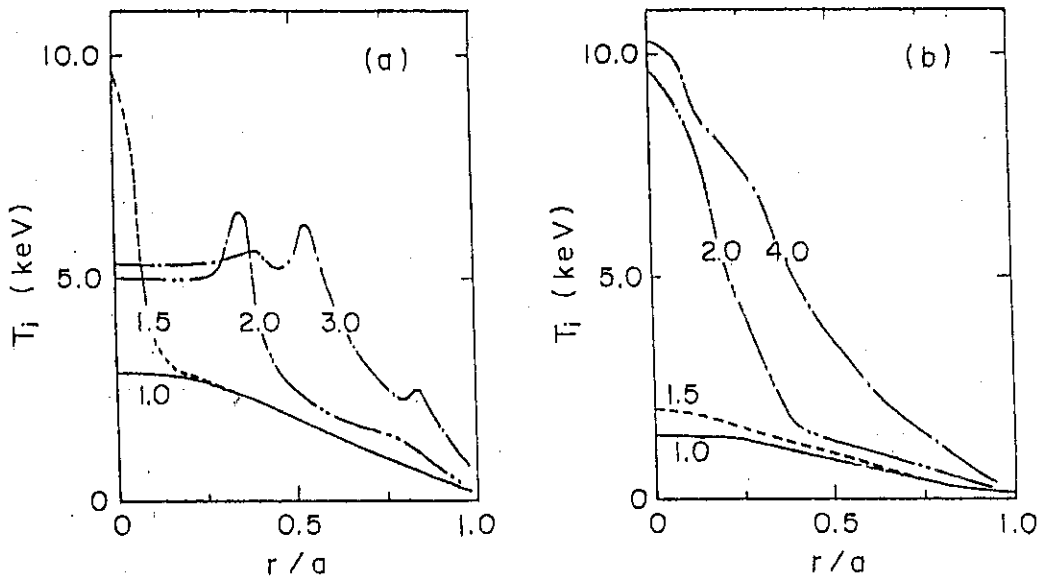

Fig. X.8-10 Time changes of the profile of ion temperature. (a) linear and (b) nonlinear stochastic model.

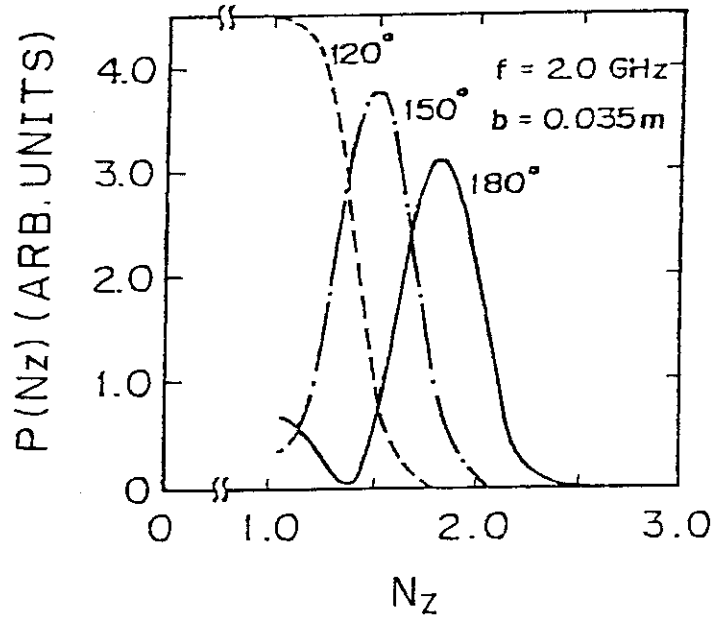

Fig. X.8-11 Power spectrum of the radiated wave from the same launcher aimed at the ion heating.

9. JT-60 Operation Program

The basic scheme of operation and maintenance has been investigated to achieve efficient operation of JT-60 in safety. The standard cycle of JT-60 operation was set as a period of two weeks. Startup and shutdown processes of major components through one cycle is illustrated in Fig. X.9-1. Execution of operation would be done along the short-term schedules determined basing on the long-term JT-60 experimental and operational programs.

It was recognized that preventive maintenance should be essential to sustain the JT-60 plant conditions. Periodic inspection and maintenance might be effective; daily, cyclic, quarterly and yearly.

A few of JT-60 components would be accepted by the end of October, 1983 and be operated steadily then after. The performance test of the other major components is scheduled to start in 1983. Education and trainning of the early-accepted components and the trial run during the performance test.

Organization and manpower for the operation and maintenance of JT-60 are the key factor of the operational and experimental programs. Some tentative proposals were examined and presented.

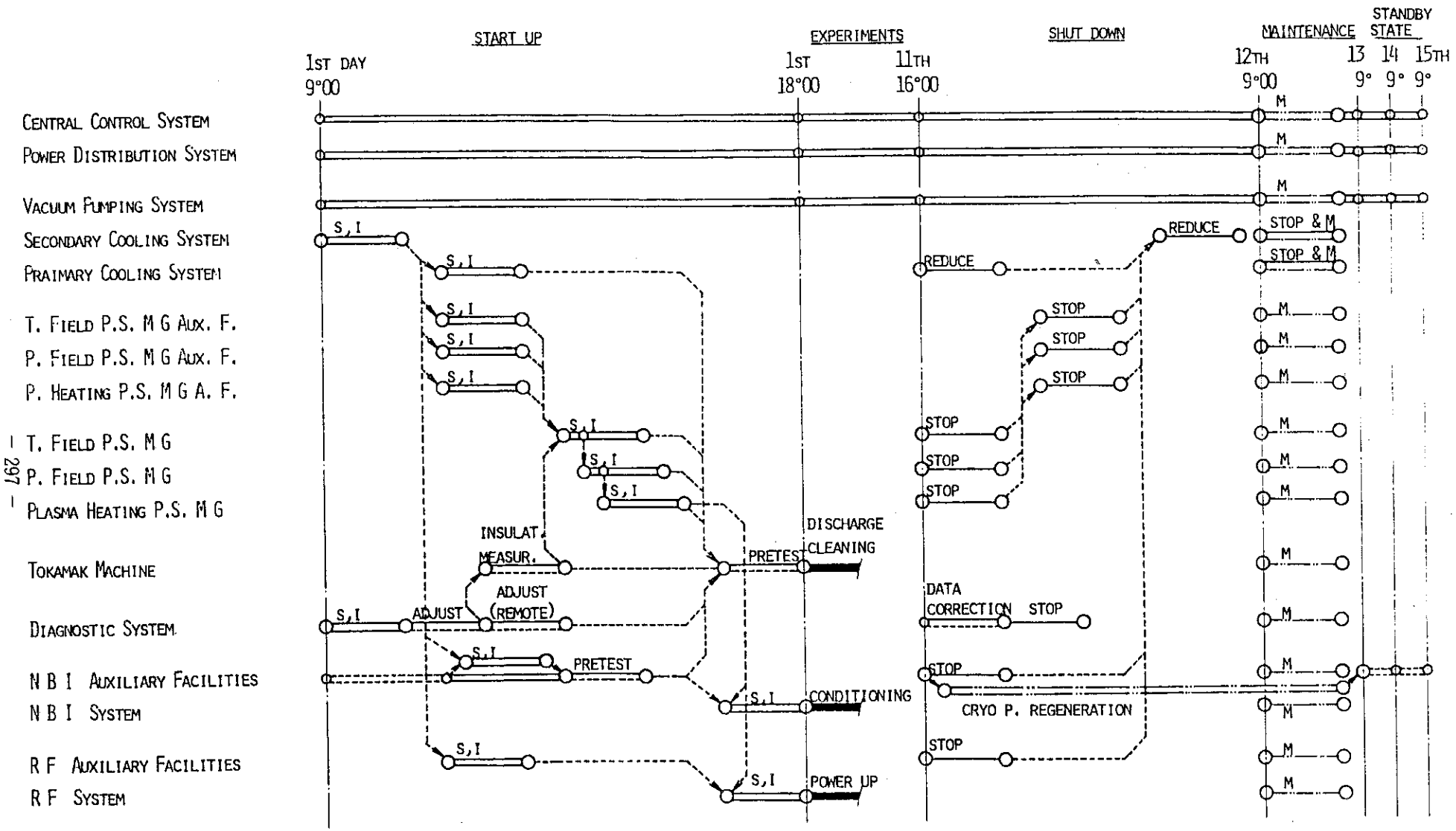

S,I : START UP & INSPECTION

M : PREVENTIVE MAINTENANCE

Fig. X.9-1 Startup and shutdown of JT-60 components.

XI. DEVELOPMENT OF THE NEXT LARGE TOKAMAK MACHINE

1. Introduction

The design studies of the next generation tokamak have been performed by Fusion Research and Development Center in cooperation with Divisions of Nuclear Fuel, Reactor Engineering, Health Physics. Three major activities performed in this fiscal year are:

1) Physical investigation of reactor plasma and plasma design of the next generation tokamaks,
2) Analysis of reactor systems, and
3) Design studies of next generation tokamaks.

The mechanical designs of the next generation tokamaks have been carried out by the contracts with industries, Toshiba Corporation, Hitachi Ltd, Mitsubishi Electric Corporation, Kawasaki Heavy Industries, Ltd. and Sumitomo Heavy Industries, Ltd.

2. Plasma Design Study

2.1 Plasma major parameters

Choice in a working point of the reactor core (i.e. density, temperature, major and minor radii, magnetic field, etc.) strongly depends on the missions to be performed in the machine. The major requirements for the plasma of the next machine have been selected as follows;

(1) self-ignition of a D-T plasma,

(2) long burn pulse (e.g. more than 100s),

(3) appropriate neutron wall loading (e.g. 1 MW/m^2).

In addition to these conditions, the severe restraint imposed on the plasma beta value has to be taken into consideration in the plasma design. It is well known that the large beta value leads to the compact and economical machine. The maximal beta value estimated theoretically, however, is not so large. Moreover, the maximum magnetic field is also limited from its technical point, therefore, the beta value limit gives a great impact on the plasma design in the next machine. The maximum beta depends on a shape of the plasma cross-section, a safety tactor, and an aspect ratio. Then, the D-shaped plasma adopted for the next machine has its maximum beta of 3 ~ 4%.[1]

In determining the major parameters of the plasma, crucial is what should be optimized (e.g. cost, size, power, etc.). Moreover, the above all conditions can not always be satisfied at the same time. When one of them is favored to meet the special mission, some of the remainders must be somewhat sacrificed. The severity in attaining the large beta value has been described in the above. It is reasonable for the next device to choose the condition where the beta has its minimum, which corresponds to about 10 keV in the temperature.

The toroidal magnetic field of 5.0 - 5.5 T was adopted, which was the maximum, judging from the present coil technique. Taking into account of the wall loading condition, we can obtain the major parameters in Table XI.2-1.

2.2 Operational considerations of discharges [1]

Steady operation of a tokamak discharge would be essentially feasible. Judging from the state of the art in driving discharge currents, however, a quasi-steady operation is forced to be adopted for the next large device. A pulse of a discharge, therefore, can be split into four phases, i.e., start-up, burn, shut-down, and dwell phase.

2.2.1 Start-up phase

The start-up phase contains the ionization of gases, the ohmic heating along with the rise of the discharge current, and the additional heating to ignition. The following items have been studied; the initial loop voltage required for the ionization and the current initiation, the volt-second consumed in this period, the scenario of the poloidal coil currents from low to high beta plasma, the necessary heating power and its loss due to the toroidal field ripple.

The initial loop voltage of 50-70 V is judged to be sufficient for the ionization. The some uncertainty, if the discharge can pass through the intial low tenperature phase, will be taken away by an introduction of the supplementary additional heating, which also helps in reduction of the consumed resistive volt-second. The necessary volt-second for this start-up phase is estimated to amount to about 100 V.s., which may account for 80 ~ 90% of the total flux.

The beta value of the plasma varies from small value to 4 ~ 5% during the start-up phase, like the discharge current. The time behavior of the poloidal coil currents has been calculated, which maintains the

elongated D-shaped plasma. The total ampere-turn through the coils amounts to ~100 MAT, which needs the large power supply. The further study will be continued to reduce the power.

Simulation studies indicate that the heating power of 60-80 MW will be required for the additional heating to ignition. The loss of the NBI power induced by the toroidal field ripple has been investigated. It is concluded that the field ripple value at the outer plasma edge has to be less than 0.7 ~ 0.8 % to suppress the loss within about 10 ~ 20 %.

2.2.2 Burn phase

During the burn phase, various discharge parameters, such as equilibrium, stability, burn temperature and impurity content, have to be controlled.

Considerable progress has been made in the analysis on the burn temperature control by means of the toroidal field ripple, which induces the ion thermal transport loss expected to have a favorable temperature dependence ($T^{7/2}$) for burn control. Recent studies, however, do not confirm that the ion thermal conductivity has such a strong temperature dependence for the parameters of the next device. Therefore, it is doubtful whether stable burn can be achieved by this scheme. Simple calculations show that a smooth burn control without an excessive temperature overshoot, which may be dangerous from the beta restriction, requires the ripple control with a relatively fast response time of a few second even if a strong temperature dependence is assumed.[2] Further studies are needed to assess the potential of using the field ripple for the burn temperature control.

Poloidal divertors have been adopted for the impurity control, which means both the suppression of impurities below an allowable level and the helium ash exhaustion in the next device. The single-null type

and the double-null type poloidal divertor, as shown in Fig.XI.2-1, were selected for INTOR and the domestic next large device, respectively. It is evident that the distance between the adjacent magnetic surfaces at the inside is by three times as large as at the outside. The single-null divertor, therefore, requires broader space at the inboard than the double-null case, because of the connection of magnetic field lines between the inside and the outside scrape-off layers. On the other hand, it is needless to say that the double-null case needs more rooms at the top or bottom region compared with the single-null.

Studies on the behavior of particles in the divertor region and the helium ash exhaustion have progressed steadily. Results obtained from the Monte-Corlo simulation show that the helium ash can be evacuated through a pumping duct installed by the divertor collector plates with a pump of a reasonable speed, e.g. 10^5 ℓ/s. They also suggest that the high density plasma would be produced in front of the divertor plate.

2.2.3 Shut-down phase

The reduction of the shut-down time has been studied to increase a duty cycle. During the cooling period of the plasma, it is important to decrease the density along with the temperature. The forced current ramp-down, after cooling the plasma, has to be realized by some methods to reduce the shut-down time.

3. Analysis of Reactor System

3.1 Reactor structure, neutronics and safety

The following issues of reactor structure, neutronics and safety related to the design study of INTOR and the next generation tokamaks were investigated.

(1) Reactor Structure
   a) Effects of toroidal field ripple on the loss of energetic injected ions and the toroidal coil[3]
   b) Structure of high heat flux divertor[4]
   c) Structure of Pb-Li_2O breeding blanket[5]
   d) Tritium inventory in blanket

(2) Neutronics
   a) Tritium breeding and shield
   b) Improvement of neutron-gamma coupled cross section file

(3) Safety and Environment
   a) Tritium system
   b) Tritium release from stack
   c) Magnetic exposure
   d) Skyshine
   e) Accident analysis

3.2 Development of a calculational system for fuel producing blanket

A calculational system of a nuclear fuel producing blanket utilizing a fusion reactor has been developed and tested.

A one dimensional discrete ordinates radiation transport code called ANISN-SP was developed to reduce the computation time required in obtaining the neutron flux distribution in a nuclear fuel producing blanket of a fusion reactor. This code employs the separation method proposed by Youssef and Conn[6] which solves separately, the distribution of the neutrons coming directly from the plasma and that of the neutrons resulting from the fission reactions. This code is made by modifying the original ANISN code[7] and uses the coupled neutron-gamma ray cross section GICX40[8]. A preliminary test of the code resulted in the reduction of 30 - 50% computation time without loosing the accuracy of calculated

neutron flux when compared with the direct calculations.

A library of cross sections for the burn-up calculations including the (n,γ), (n,f), (n,2n) and (n,3n) reactions for heavy nuclides is produced mainly from the ENDF/B-4 file[9]. This library also includes cross sections of lumped (n,γ) reactions of ^{232}Th, ^{233}U, ^{235}U, ^{238}U and ^{239}Pu made from the FP nuclides file of Japan Nuclear Data Committee. In addition, the decay chain data for the burn-up calculations are compiled in the form compatible with the induced activation calculation code system THIDA[10].

4. Design Studies of the Next Generation Tokamak Machines

4.1 INTOR

The conceptual design of International Tokamak Reactor (INTOR) has been promoted by EC, Japan, USA and USSR under IAEA as Phase 1 activity (February, 1980 - June, 1981) following Phase 0. Each of four contries or opganization has performed its own design following the general specifications as a reactor with the single null divertor settled by INTOR Workshop and they are unified as a single reference design. The major parameters of INTOR are shown in Table XI.2-1. The bird's view of INTOR is shown in Fig. XI.4-1.

JAERI's proposal of INTOR is shown in Fig. XI.4-2. Other than the reference design, the alternative of INTOR with the double null divertor has been also conceptually designed. The lithium oxide breeding blanket is proposed to INTOR Workshop and it is also employed as a major alternative to the lithium silicate blanket. JAERI made a lot of contributions to the INTOR reference design such as solid breeding blanket concept and divertor concept of tungsten blazed to copper heat sink.

4.2 Domestic next generation tokamak machines

Conceptual designs of Fusion Experimental Reactor (FER) have been carried out as the next generation tokamak to JT-60. The major objectives of FER is to achieve self-ignition, to aim the breeding ratio larger than unity and to perform reactor engineering tests, which meet to those defined by Long Term Strategy Review Sub-Committee of Fusion Council.

FER has a double null poloidal divertor and the blanket covering

the whole inner surface of the torus. Emphases at the conceptual designs have been put on reduction of the reactor size. Major parameters of FER are also shown in Table XI.2-1.

Two concepts of FER are proposed, the conventional type and the swimming pool type. Their reactor sizes are almost same.

4.2.1 Conventional type FER

The conventional type FER has been designed so as to suppress the radiation level during the reactor shut-down by solid shield, considering the essential human accessibility for daily inspection, maintenance of the reactor and auxiliary facilities and instruments.

The many detail analysis such as electromagnetic force analysis and seismic dynamics have been performed. Its cross sectional view is shown in Fig. XI.4-3.

The issues as a conventional type reactor, such as disassembly, have been investigated. The design of the penetration shield has been remained for future work.

4.2.2 Swimming pool type FER[11]

The swimming type FER has been proposed last year in order to reduce the complexity of the reactor structure and the reactor size. The reactor is submerged in the water pool as shown in Fig. XI.4-4. This type can eliminate the heavy solid shield. The exchange of the vacuum vessel can be done relatively easily and it meets the required flexibility as an experimental reactor.

REFERENCES

(1) "INTOR Zero Phase Report", IAEA, 1980.
(2) M. Sugihara, M. Kasai, T. Tazima, T. Tone, K. Maki, Plasma Burning Control by Variable Toroidal Field Ripple in Tokamak Reactors, J. Nucl. Sci. Tech., 17 (1980), 729-736.
(3) T. Tone, et al., JAERI-M 8938 (1980).
(4) T. Iida, et al., JAERI-M 8944 (1980).
(5) T. Iida, et al., JAERI-M 9520 (1980).
(6) M. Z. Youssef and R.W. Conn, Nucl. Sci. Eng., 74 (1980), 130.
(7) W. W. Engle, Jr., K-1893, Computing Technology Center, Union Carbide Corporation (1963).
(8) Y. Seki and H. Iida, JAERI-M 8818 (1980).
(9) M. K. Drake (edited), BNL-50274 (T-601, TLD-4500), ENDF 102, Vol. 1 (1970), Revised 1974.
(10) H. Iida and M. Igarashi, JAERI-M 8019 (1978),in Japanese.
(11) K. Sako, et al., JAERI-M 9050 (1980), in Japanese.

Table XI.2-1 Major Parameters of INTOR and FER

	INTOR (Phase 1)	FER (1980)
plasma major radius (m)	5.3	5.3
plasma minor radius (m)	1.2	1.1
plasma elongation	1.6	1.5
plasma volume (m^3)	240	200
axial toroidal field (T)	5.5	5.2
plasma current (MA)	6.4	3.9
average ion temperature (KeV)	10	10
average ion density ($10^{20}/m^3$)	1.4	1.1
average beta (%)	5.6	4(fuel purticles)
Q value	ignition	ignition
peak fusion power (MW)	620	400
burn time (sec)	200	100
duty cycle (%) / availability (%)	80/50	50/25
neutron wall load (MW/m^2)	1.3	1.0
toroidal magnetic field coil	superconducting	superconducting
poloidal magnetic field coil	superconducting, Cu	superconducting
diverter	yes	divertor
tritium consumption (kg/year)	7	3
initial tritium inventory (kg)	∿4	up to 1
tritium breeding ratio	0.65	∿1

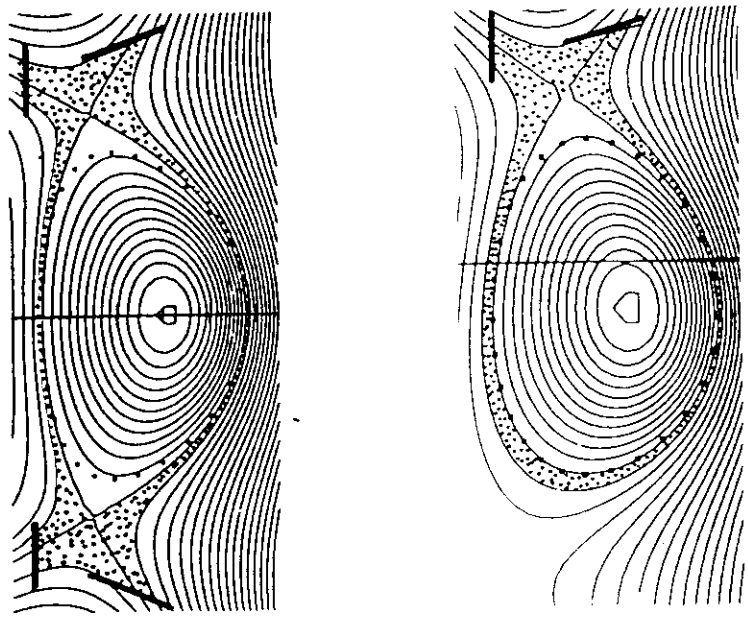

(a) (b)

Fig. XI. 2-1 Magnetic configurations of (a) double-null type and (b) single-null type poloidal divertors.

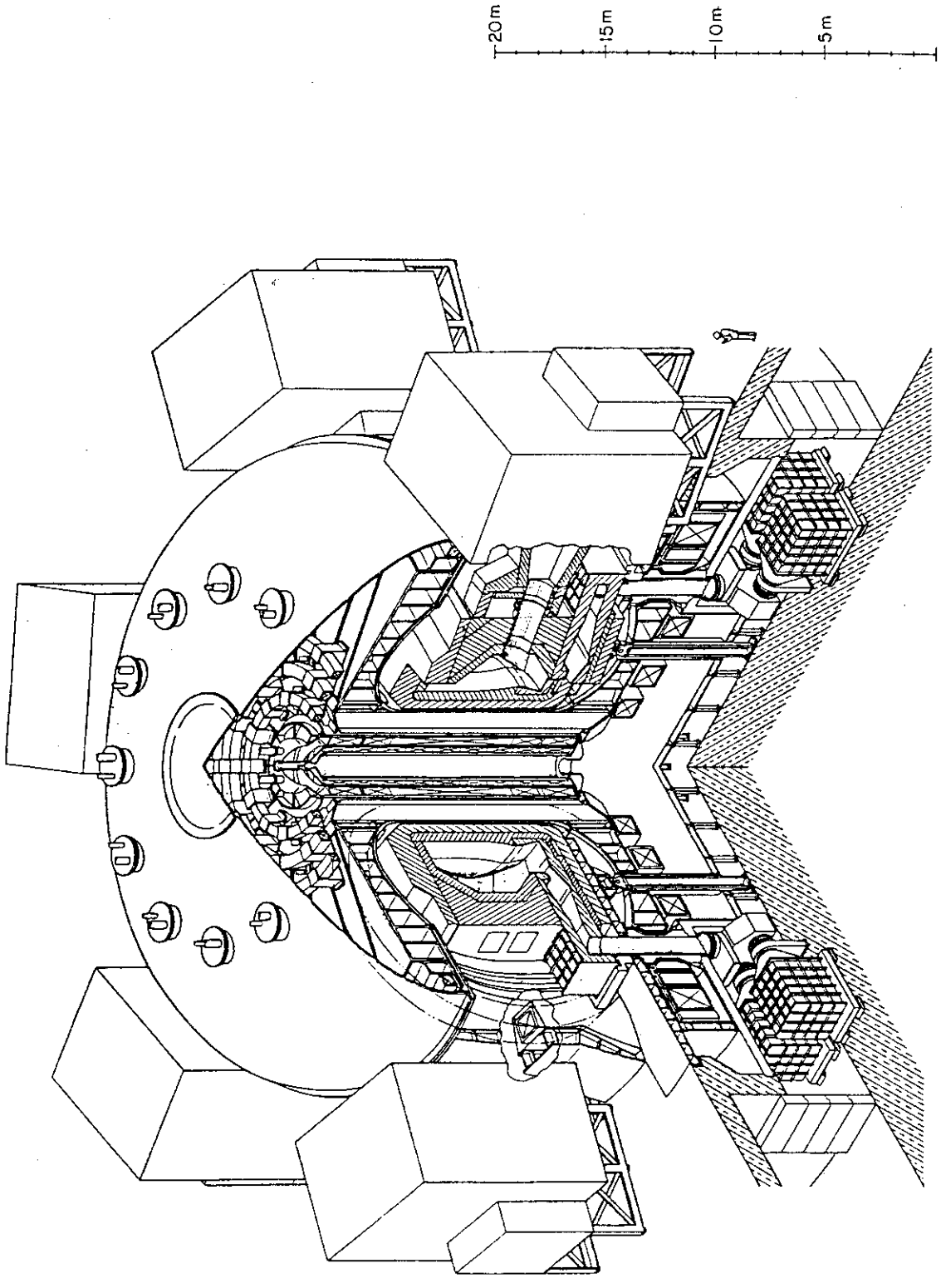

Fig. XI. 4-1 Bird's view of the INTOR reference design.

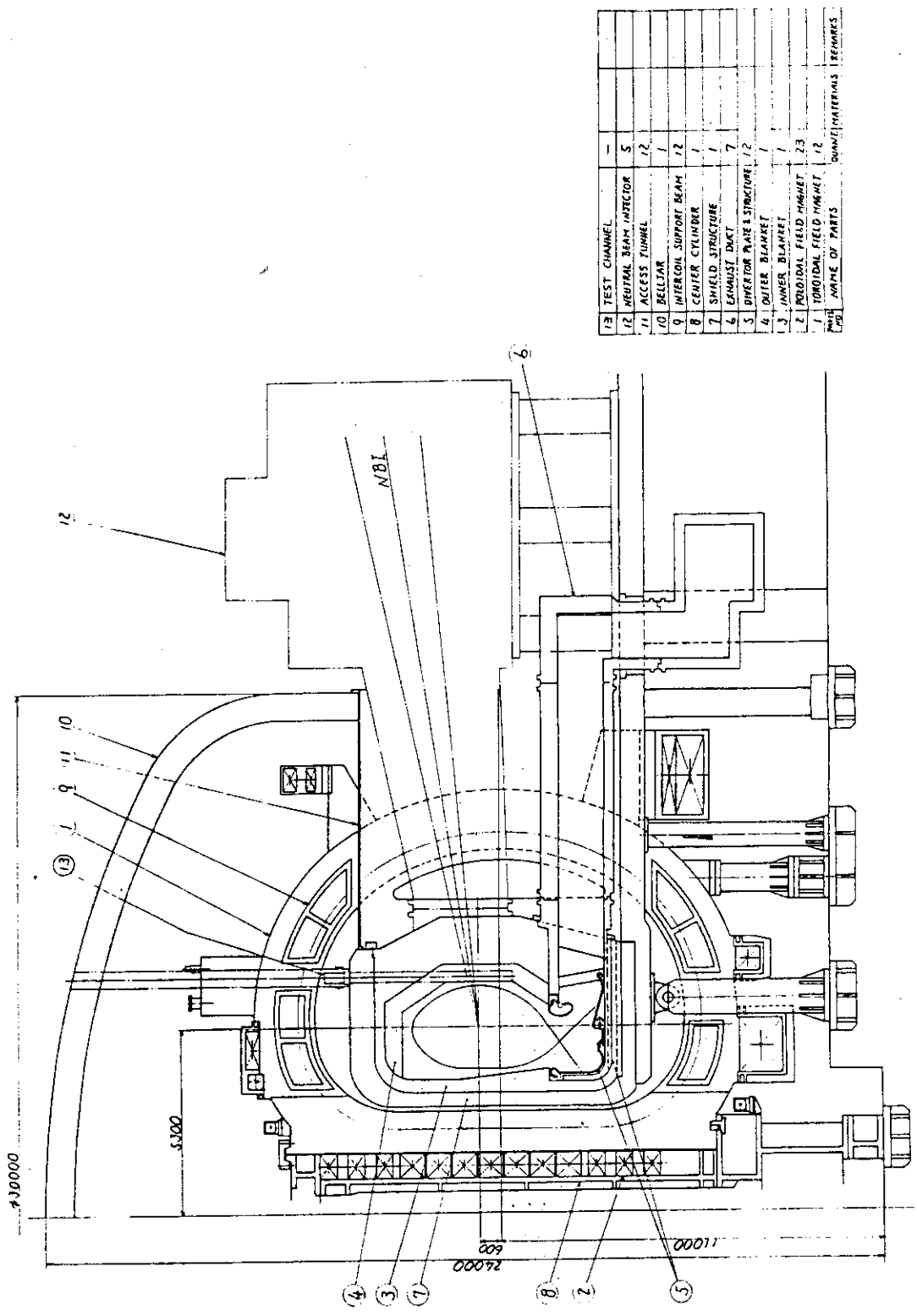

No.	NAME OF PARTS	QUANTITY/MATERIALS	REMARKS
13	TEST CHANNEL	—	
12	NEUTRAL BEAM INJECTOR	5	
11	ACCESS TUNNEL	12	
10	BELLJAR	1	
9	INTERCOIL SUPPORT BEAM	12	
8	CENTER CYLINDER	1	
7	SHIELD STRUCTURE	1	
6	EXHAUST DUCT	7	
5	DIVERTOR PLATE & STRUCTURE	12	
4	OUTER BLANKET	1	
3	INNER BLANKET	1	
2	POLOIDAL FIELD MAGNET	23	
1	TOROIDAL FIELD MAGNET	12	

Fig. XI. 4-2 Vertical cross sectional view of INTOR (JAERI's proposal).

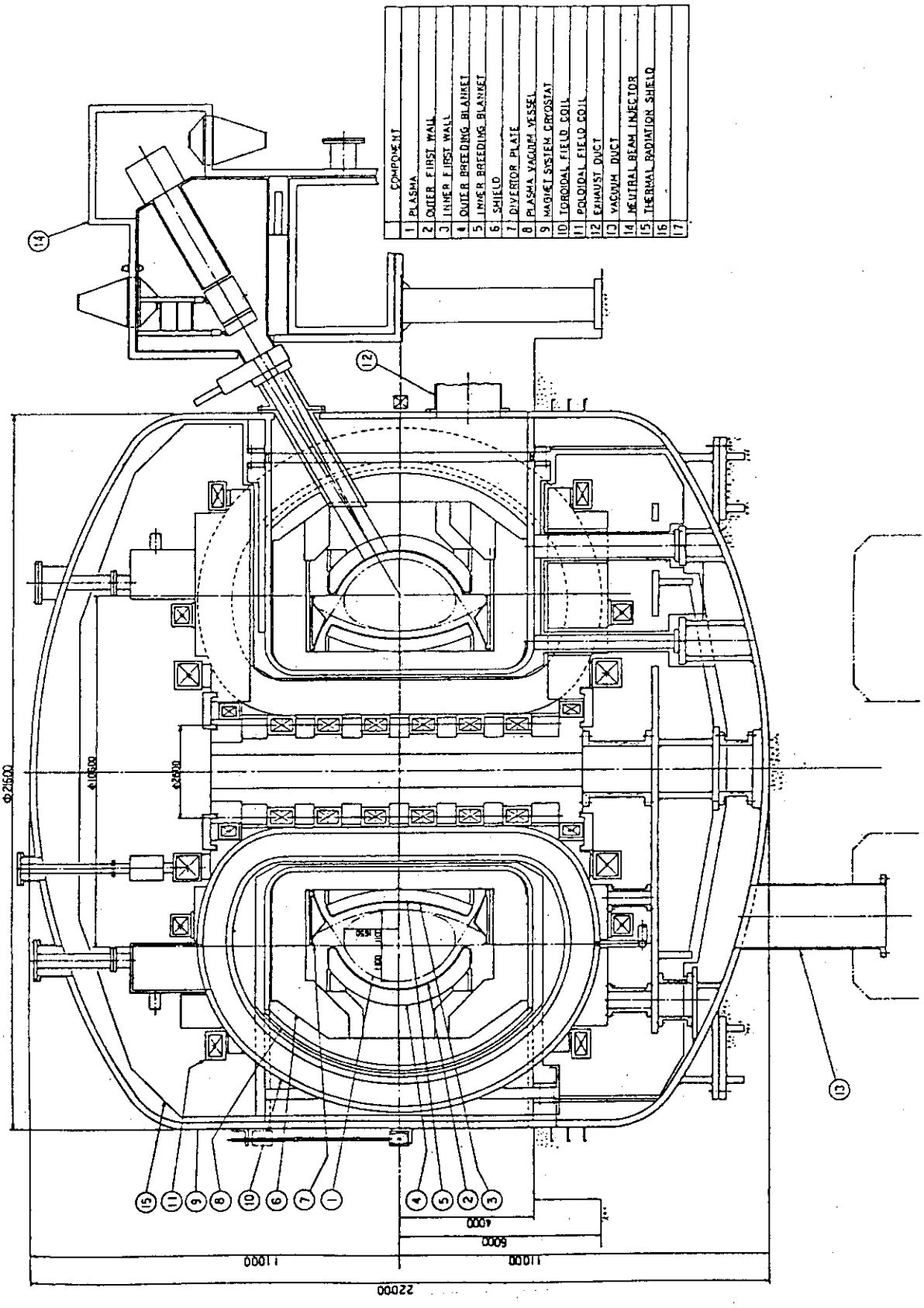

Fig. XI. 4-3 Vertical cross sectional view of FER (Conventional Type).

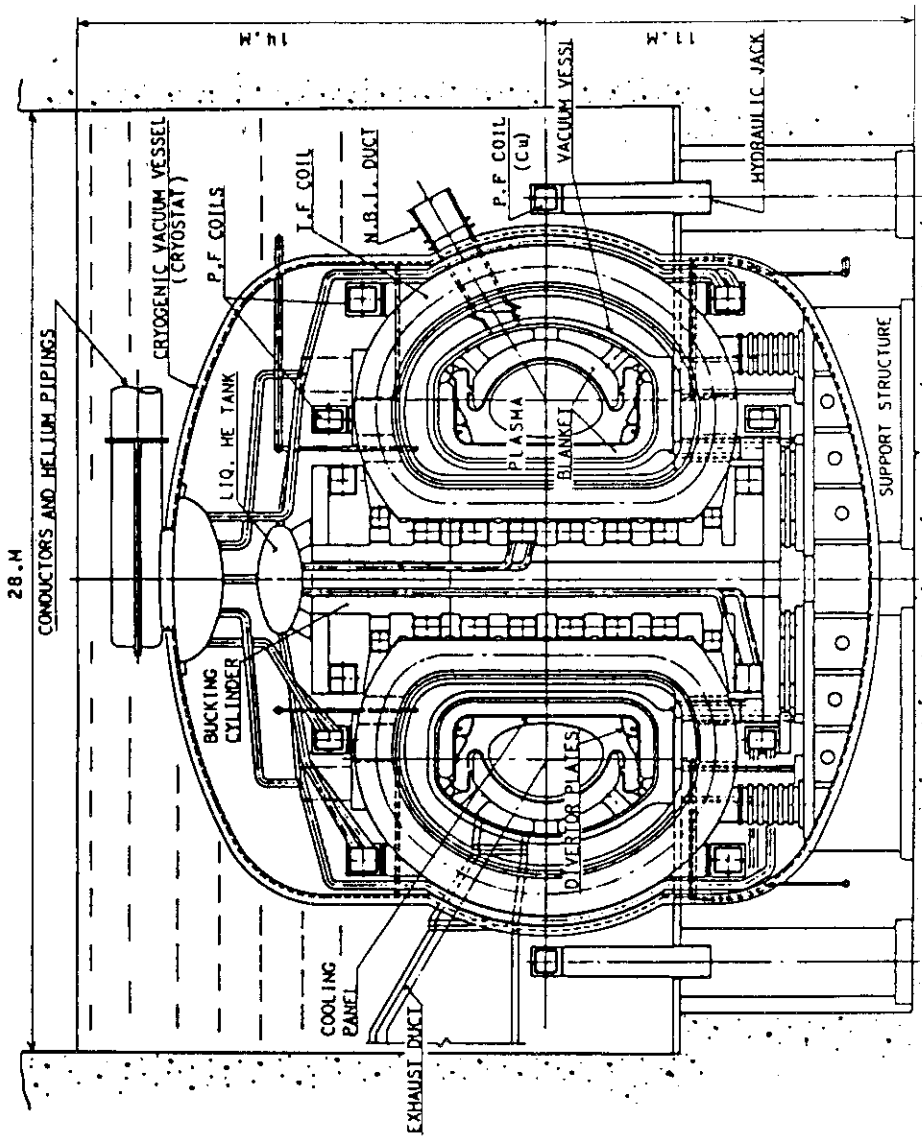

Fig. XI. 4-4 Vertical cross sectional view of FER (Swimming Pool Type).

APPENDIXES

A.1 Publication List

A.1.1 List of JAERI-M Report

1) Kamoto S[*6]., Shoji T., Tanaka Y., and Yoshida K.: "Effects of Iron Core in JFT-2M", JAERI-M 8725 (March 1980) (in Japanese)
2) Arakawa Y., Akiba M., Araki M., Horiike M., Itoh T., Kawai M., Kuriyama M., Matsuda S., Matsuoka M., Mizutani Y[*8]., Ohara Y., Ohga T., Okumura Y., Sakuraba J., Shibata T., Shirakata H. and Tanaka S.: "The Present Status of Ion Source Development at JAERI", JAERI-M 8869 (May 1980) (in Japanese)
3) Kimura H., "Power Balance in the Divertor-tokamak DIVA", JAERI-M 8890 (June 1980)
4) Itoh K. and Inoue S[**6].: "Kinetic Theory of Kink-Like Instabilities", JAERI-M 8975 (July 1980) (in Japanese)
5) Shibanuma K., Kuriyama M. and Okumura Y.: "Estimation of Effective Elastic Constants for Grid Plate", JAERI-M 8923 (July 1980) (in Japanese)
6) Shibata T., Horiike H., Kuriyama M., Matsuda S., Sakuraba J. and Shirakata H.: "Estimation of Heat Loads to the Cryopanels and Temperature Rise of Panel Surface of the Cryopump for JT-60 Neutral Beam Injector", JAERI-M 8935 (July 1980) (in Japanese)
7) Sakuraba J., Matsuda S. and Shibata T.: "A Code to Calculate Transmission Probability of Cryostron Radiation through a Neutral Beam Injector Port", JAERI-M 8936 (July 1980) (in Japanese)
8) Tanaka Y.[**11], Matsuura T.[**11], Takeda T., Azumi M., Tokuda S., Tsunematsu T., Kurita G. and Takizuka T.: "MHD Stability Analysis Code ERATO-J — User's Manual of JAERI version ERATO —", JAERI-M 9040 (Aug. 1980) (in Japanese)
9) Kuriyama M., Horiike H., Matsuda S. and Morita H.[*7] : "Design of calorimeter for JT-60 NBI", JAERI-M 8988 (Aug. 1980)
10) Tanaka M. and Murakami Y. (Editors) : "Proceedings of the US/Japan Workshop on Divertors, First Wall Materials, and Impurity Control", JAERI-M 8791 (Aug. 1980)

11) Shimomura Y., Suzuki N., Yamamoto S., Maeno M., Ohasa K., Konoshima S., Odajima K., Yamauchi T., Yamamoto T., Takeuchi H., Matsuda T., Sugie T., Kimura H., Kumagai K., Matsumoto H., Sengoku S., Kawakami T., Ohtsuka H., Katagiri M., Hoshino K., Funahashi A., Fujisawa N., Anno K., Shibata T., Matsuzaki Y., Isaka M., Azumi M., Kurita G., Amano T.[**2], Okamoto M.[**2], Arakawa Y., Akiba M., Matsuda S., Kurihara K., Nagashima A., Shiho M., Nishitani T. and Neyatani Y.: "High-β Study in JFT-2", JAERI-M 9065 (Sep. 1980)

12) Kinoshita M. and Naruse Y.: "Computer Analysis on Separation Characteristics of Falling Liquid Film Condenser for Separation of Helium and Hydrogen Isotopes", JAERI-M 9103 (Sep. 1980)

13) Takeda T., Tsunematsu T. and Okada T.[*13] : "Supervisive Code of TRITON, HARMONIA-F75", JAERI-M 9096 (Oct. 1980) (in Japanese)

14) Horiike H., Kondoh U.[*8], Morita H.[*7] and Tanaka S.: "Heat Removal from the Simulation Electrode of a High Power Long Pulse Ion Source", JAERI-M 9004 (Oct. 1980)

15) Tanaka S.: "Calculation of Temperature Distribution of Tangusten Filament Cathode in Gaseous Discharge — in the case of constant heater current —", JAERI-M 9152 (Oct. 1980)

16) Odajima K., Kimura H., Matsumoto H., Yamamoto T. and Iizuka S.[**5] : "Design of Antenna and Impedance Matching Network for JFT-2 1MW ICRF Experiment", JAERI-M 9217 (Nov. 1980)

17) Araki M., Horiike H., Kuriyama M., Matsuda S., Morita H.[*7] and Ohara Y.: "Design of Pulsed Heat Load Removal System for JT-60 Neutral Beam Injectors", JAERI-M 9198 (Nov. 1980)

18) Shibata T., Mizutani Y.[*8], Okumura Y., Sakakibara J.[*9] and Shibanuma K.: "Experiment of Long Pulse Beam Injection into Cryopump", JAERI-M 9213 (Nov. 1980) (in Japanese)

19) Tuda T., Itoh K. and Itoh S.[**6] : "Troidal Drift Wave", JAERI-M 9234 (Dec. 1980) (in Japanese)

20) Itoh T., Horiike H., Matsuoka M., Matsuda S., Ohara Y. and Tanaka S.: "A Computer Simulation Code of Heat Input due to Incidence of Fast Ion Beam", JAERI-M 9226 (Dec. 1980) (in Japanese)

21) Kinoshita M. and Naruse Y.: "Effects of Thermodynamic Properties of Hydrogen Isotopes on Separation Characteristics of Cryogenic Distillation Columns", JAERI-M 9238 (Dec. 1980)

22) Takizuka T., Tsunematsu T., Tokuda S., Azumi M., Kurita G., Tuda T., Itoh K., Tanaka Y.[*13], Matsuura T.[*13] and Takeda T.: "Computational Studies of Tokamak Plasmas", JAERI-M 9354 (Feb. 1981)

23) Division of Thermonuclear Fusion Research : "Proceedings of the US/Japan Workshop on Fusion Fuel Handling", JAERI-M 9390 (Mar. 1981)

24) Sano K.[*14], Sugie T. and Funahashi A.: "Spectrograms of the JFT-2 Plasmas in the Vacuum Ultraviolet Region I (Wavelength Region 7Å-600Å)", JAERI-M 9510 (May 1981) (in Japanese)

25) Kanamori T.[*3], Matoba T., Funahashi A., Suzuki Y.: "Spectrum Analysis of Far-Infrared Laser Scattering for a High Temperature Plasma", JAERI-M 8777 (Mar. 1980) (in Japanese)

26) Nishio S., Ohkubo M., and Sasajima H.[*3] : "Evaluation of Mechanical Strength of the Joints in JT-60 Toroidal Field Coil Conductors", JAERI-M 8822 (April 1980) (in Japanese)

27) Seki Y., and Iida H.: "Coupled 42-Group Neutron and 21-Group Gamma Ray Cross Section Sets for Fusion Reactor Calculations", JAERI-M 8818 (Apr. 1980)

28) Oyama Y., Seki Y., Maekawa H., and Nakamura T.: "Cross Section Sensitivity Analysis of ^{235}U and ^{238}U Fission Rates in a Graphite Reflected Lithium Oxide Assembly", JAERI-M 8870 (May, 1980) (in Japanese)

29) Iida H., and Seki Y.: "Studies on Increasing Tritium Breeding Ratios of JXFR and INTOR-J Blankets", JAERI-M 8896 (May 1980) (in Japanese)

30) Tone T., Yamamoto T., Tani K., Sugihara M., and Kasai M.[*5] : "Some Considerations of Design Issues on Toroidal Field Ripple", JAERI-M 8938 (June 1980)

31) Iida H., Minato A.[*4], Sakamoto H.[*7] and Sako K.: "Design Problems of High Heat Flux Divertor Structure", JAERI-M 8944 (July 1980)

32) Fujisawa N., Nagami M., Yokomizo H., Shimada M., Konoshima S., Seki S., Sugawara T.[*11], Ohara Y., Ioki K.[*5], Jahns G.[*16], Brooks N.H.[*16], Groebner R.[*16], Kitsunezaki A.: "Impurity Status of Dee-Shaped Discharges in Doublet III with Inconel Wall and Limiters —— with and without Titanium Gettering ——", JAERI-M 9181 (Nov. 1980)

33) Nagami M., Fujisawa N., Ioki K.[*5], Kitsunezaki A., Konoshima S., Ohara Y., Seki S., Shimada M., Sugawara T.[*11], Yokomizo H., Brooks N.H.[*16], Groebner R.[*16], Seraydarian R.[*16] : "A Single Null Poloidal Divertor Experiment in Doublet III", JAERI-M 8983 (Aug. 1980)

34) Fusion Reactor System Laboratory: "Preliminary Study of Swimming Pool Type Tokamak Reactor (SPTR)", JAERI-M 8944 (Aug. 1980) (in Japanese)

35) Nakamura H.: "Proc. the U.S/Japan workshop on divertors, first wall materials and impurity control", JAERI-M 8971 (Aug. 1980)

36) Ninomiya H., Kameari A.[*5] and Shinya K.[*11] : "A Toroidal Plasma MHD Equilibrium Code EQUCIR version 1", JAERI-M 9127 (Oct. 1980) (in Japanese)

37) Fujisawa N., Konoshima S., Nagami M., Seki S., Yokomizo H., Shimada M., Jahns G.[*16], Ejima S.[*16], Groebner R.[*16], Brooks N.H.[*16], Kitsunezaki A.: "Accumulation and Elimination of Metal Impurities near the Center of Dee Plasmas in Doublet III", JAERI-M 9179 (Nov. 1980)

38) Sugawara T.[*11], Fujisawa N., Shimada M., Jahns G.[*16], Yokomizo H., Nagami M., Ioki K.[*5], Kitsunezaki A.: "A Study of Helical Modulation in the Doublet III Plasma Column", JAERI-M 9180 (Nov. 1980)

39) Tone T., Maki K.[*3], Kasai M.[*5] and Nishida H.[*10] : "A One-Dimensional Transport Code for the Simulation of D-T Burning Plasma POISE1", JAERI-M 9167 (Nov. 1980) (in Japanese)

40) Iida H. et al.: "Structural Design Study of Tritium Breeding Blanket with a Lead Layer as a Neutron Multiplier", JAERI-M 9250 (Dec. 1980)

41) Takatsu H., Shimizu M., Ohta M., Imai K.[*21], Ono S.[*21], Minami M.[*21]: "Detailed Analysis of the Dynamic Response of the JT-60 Vacuum Vessel Under the Saddle-like Electro-magnetic Forces", JAERI-M 9242 (Dec. 1980)

42) Ogata A.: "Physics Programmes and Goal of Large Tokamak Experiments", JAERI-M 9228 (Dec. 1980)

43) Shinya K.[*11] and Ninomiya H.: "A MHD Equilibrium Code EQUCIR version 2 Applicable to Up-Down Asymmetric Toroidal Plasma", JAERI-M 9278 (Jan. 1981) (in Japanese)

A.1.2 List of Papers Published in Journals

1) Tsunematsu T., Takeda T., Matsuura T.[*13], Kurita G. and Azumi M.: "Convergence of Solutions of the MHD Stability Code ERATO", Computer Phys. Commun. 19 (1980) 179
2) Itoh K. and Inoue S.[**6] : "Comments on 'Resistive Drift Alfven Waves in Sheared Magnetic Field'", Phys. Fluids 23 (1980) 847
3) Tokuda S., Kamimura T.[**2] and Itoh H.[**9] : "Anomalous Plasma Transport due to Electron Temperature Gradient Instability", J. Phys. Soc. Japan 48 (1980) 1722
4) Inoue S.[**6], Itoh K. and Yoshikawa S.[**8] : "Electrostatic Drift Instability of Tokamak Plasma", J. Phys. Soc. Japan 49 (1980) 367
5) Itoh S.I.[**6] and Itoh K.: "Kinetic Theory of Helical Instabilities in Cylindrical Tokamak", Nucl. Fusion 21 (1981) 3
6) Itoh K. and Itoh S.I.[**6] : "Kinetic Theory of Collisionless Tearing Instability", Physics Letters 82 (1981) 85
7) Itoh K., Itoh S.I.[**6] and Tuda T.: "Kinetic Theory of Nonlocal High-n Ballooning Mode", J. Phys. Soc. Japan 50 (1981) 655
8) Sengoku S. and Ohtsuka H.: "Experimental Results on Boundary Plasmas, Resulting Surface Interactions and Extrapolation to Large Fusion Devices", J. Nucl. Mater. 93/94 (1980) 75
9) Ohtsuka H., Ogiwara N. and Maeno M.: "Unipolar Arcs in JFT-2 Tokamak", J. Nucl. Mater. 93/94 (1980) 161
10) Sengoku S., Matsuda T., Matsumoto H., Abe T., Ohtsuka H., Arai T., Ohasa K., Yamamoto S., Odajima K., Kimura H., Kasai S., Kumagai K., Takahashi K. and Shimomura Y.: "Carbon Wall Experiment in DIVA", J. Nucl. Mater. 93/94 (1980) 178
11) Sakamoto Y.[**11], Ishibe Y.[**11], Yano K.[**11], Ohyama H.[**11], Tanaka Y., Fujisawa N., Matsuzaki Y., Suzuki N., Maeno M., Yamamoto T. and Yokokura K.: "Electron Cyclotron Resonance Discharge Cleaning of JFT-2 Tokamak", J. Ncl. Mater. 93/94 (1980) 333
12) Funahashi A. and Yamamoto S.: "Data Needs from the Present JAERI Tokamak Experiments", Physica Scripta. 23 (1981) 87
13) Yamamoto S., Sengoku S., Matsuda T., Matsumoto H., Ohasa K., Odajima K., Kimura H., Yamauchi T., Kumagai K., Sugie T., Kasai S., Maeda H. and Shimomura Y.: "Observation of Non-Circular Cross-Section for q=1 Magnetic Surface in Very Low-q Discharge ($q_a \lesssim 2$) of DIVA Tokamak", Jpn. J. Appl. Phys. 19 (1980) L 413

14) Maeno M. and Katagiri M.: "An Application of a Germanium Film Bolometer to Radiation Loss Measurement in JFT-2 Tokamak", Jpn. J. Appl. Phys. 19 (1980) 1433

15) Maeno M., Suzuki N., Yamamoto T. and Fujisawa N.: "Metal Impurity Reduction by Working Gas Injection in a Tokamak", Jpn. J. Appl. Phys. 19 (1980) 1509

16) Yamauchi T., Nagami M. and Sengoku S.: "Metal Impurity Injection into DIVA Plasma with a Q-Switched Laser Beam", Jpn. J. Appl. Phys. 19 (1980) 1737

17) Yamamoto S., Shimomura Y., Ohasa K., Kimura H., Sengoku S., Odajima K., Matsuda T., Matsumoto H., Ohtsuka H. and Maeda H.: "Role of Runaway Electrons in the Formation of Arcing on the Electrically Isolated Target in Tokamak", J. Phys. Soc. Jpn. 48 (1980) 1053

18) Yamamoto T., Imai T., Shimada M., Takeuchi H., Uehara K., Konoshima S., Suzuki N., Hirayama T., Maeno M., Fujii T., Yoshida H., Nagashima T. and Fujisawa N.: "Parametric Heating by Radio-Frequency near the Lower Hybrid Frequency in the JFT-2 Tokamak", J. Phys. Soc. Jpn. 48 (1980) 1349

19) Shimada M., Fujii T., Yamamoto T., Imai T., Konoshima S., Suzuki N., Shoji T., Takeuchi H., Nagashima A., Uehara K., Maeno M., Nagashima T. and Fujisawa N.: "Loss Mechanism of Energic Ions Produced during the Lower Hybrid Heating of JFT-2 Tokamak", J. Phys. Soc. Jpn. 49 (1980) 1643

20) Maeno M., Ohtsuka H., Yamamoto S., Ogiwara N., Yamamoto T., Suzuki N. and Fujisawa N.: "On the Origin of Arcing in a Tokamak", J. Phys. Soc. Jpn. 48 (1980) 2177

21) Seki Y., Shimomura Y., Maki K.*3, Azumi M. and Takizuka T.: "Numerical Calculations of Helium Ash Enrichment and Exhaust by a Simple Divertor", Nucl. Fusion 20 (1980) 1213

22) Odajima K., Kimura H., Iizuka S.**5, Sugie T., Takahashi K., Takeuchi H., Azumi M., Hirayama T., Yamauchi T., Kumagai K., Sengoku S., Matsumoto H., Matsuda T., Yamamoto S., Ohasa K. and Shimomura Y.: "High-Efficiency ICRF Heating in DIVA", Nucl. Fusion 20 (1980) 1330

23) Yamauchi T., Shoji T., Funahashi A. and Kumagai K.: "Electron Heat Conduction Coefficient in Low-q DIVA Plasmas", Nucl. Fusion 20 (1980) 1381

24) Maeno M., Ohtsuka H., Yamamoto S., Yamamoto T., Suzuki N. and Fujisawa N.: "Mechanism of Unipolar Arcs in Tokamaks", Nucl. Fusion 20 (1980) 1415

25) Yamamoto T., Imai T., Shimada M., Suzuki N., Maeno M., Konoshima S., Fujii T., Uehara K., Nagashima T., Funahashi A. and Fujisawa N.: "Experimental Observation of the rf-Driven Current by the Lower-Hybrid Wave in a Tokamak", Phys. Rev. Lett. 45 (1980) 716

26) Iizuka S.[**5], Odajima K., Kimura H., Sengoku S., Matsumoto H., Sugie T., Takahashi K., Yamauchi T., Kumagai K., Kawakami T., Takeuchi H., Matsuda T., Ohasa K., Nagami M., Yamamoto S., Nagashima T., Maeda H. and Shimomura Y.: "Propagation and Absorption of the Fast Magnetosonic Wave in the Ion-Cyclotron Range of Frequencies in the DIVA Tokamak", Phys. Rev. Lett. 45 (1980) 1256

27) Nagami M., Shimada M., Yokomizo H., Seki S., Konoshima S., Fujisawa N., Ohara Y., Sugawara T.[*11], Brooks N.H.[*16], Groebner R.[*16], Seraydarian R.[*16], Kitsunezaki A.: "Information of Dee-Shaped Plasmas with Single-Null Poloidal Divertor in Doublet III", Nuclear Fusion 20 (1980) 1325

28) JAERI team at Doublet III (Konoshima S., Fujisawa N., Kitsunezaki A., Nagami M., Seki S., Shimada M., Toyama T.[**4], Yokomizo H.: "Ohmically Heated Dee-Shaped Plasmas in Doublet III", Nuclear Fusion 20 (1980) 1455

29) GA D-III Groups, JAERI team: "Status of Impurity Studies in Doublet III", J. Nucl. Material 93 & 94 (1980) 259

30) Groebner R.[*16], Brooks N.H.[*16], Shimada M.: "Spectroscopic Observations of OVII and OVIII Near 20 Nanometers with Aluminum and Polypropylene Filters", GA-A16248 (Jan. 1981)

31) Shimada M., Fujii T., et al.: "Loss Mechanism of Energetic Ions Produced during the Lower Hybrid Heating of JFT-2 Tokamak", J. Phys. Soc. Japan, 49 (1980) 1643

32) Okumura, Mizutani[*8] and Ohara : "Experimental Study of Ion Beamlet Steering by Aperture Displacement in Two-stage Accelerator", Rev. Sci. Instrum. 51 (1980) 471

33) Okumura, Matsuda, Mizutani[*8], Ohara and Ohga : "Quasi-dc Extraction of 70 keV 5A Ion Beam", Rev. Sci. Instrum. 51 (1980) 728

34) Y. Ohara, Akiba, Arakawa, Okumura and J. Sakuraba[*9] : "Electron Backstream to the Source Plasma Region in an Ion Source", J. Appl. Phys. 51 (1980) 3614

35) S. Tanaka, Morita[*7] and J. Sakuraba[*9] : "Use of a Hollow Cathode in a DuoPIGatron Hydrogen Ion Source", Japan J. Appl. Phys. 19 (1980) 1703

36) Horiike, Akiba, Arakawa, S. Matsuda and J. Sakuraba[*9] : "Design and Development of the Coaxial DuoPIGatron Ion Source", Rev. Sci. Instrum. 51 (1980) 1463

37) Okumura, Mizutani[*8], Y. Ohara and T. Shibata : "Measurement of Impurities in a Long-pulse, Multiampere Hydrogen Beam", Rev. Sci. Instrum. 52 (1981) 1

38) Shirakata H.: "Power Supply for Plasma Heating System", J. IEEE of Japan, 100 (1980) 805 (in Japanese)

39) Matsuda S. and Shimomura Y.: "Present Status of the Neutral Beam Injector Development", J. Atomic Energy Soc. Japan. 22 (1980) 703 (in Japanese)

40) Shibata T. and Matsuda S.: "Cryopump of Neutral Beam Injector for Plasma Heating Experiment — Research and Development at JAERI —", J. Vac. Soc. Japan, 29 (1981) 130 (in Japanese)

41) Uehara K., Fujisawa N., Yamamoto T., Imai T., Nagashima T.: "Particle and Heat Transport during Lower Hybrid in JFT-2 Tokamak", J. Phys. Soc. Jpn. 48 (1980) 1333

42) Uehara K., Takeuchi H., Imai T., Yamamoto T., Fujii T., Nagashima T.: "Parametric Absorption of Lower Hybrid Wave in the Boundary Plasma of JFT-2 Tokamak", J. Phys. Soc. Jpn. 49 (1980) 2364

43) Imai T., Okamoto M.[**2], Nagashima T.: "Numerical Study of LHRF Heating in a Tokamak", J. Phys. Soc. Jpn. 50 (1981) 647

44) Nagashima T.: "Status of Development of RF Plasma Heating System", J. Atomic Energy Soc. Jpn. 23 (1981) No.3 (in Japanese)

45) Uehara K., et al.: "Energy Transport during LHRF in JFT-2 Tokamak", Kakuyugo-Kenkyu 44, Suppl. 5 (1980) 97 (in Japanese)

46) Imai T., et al.: "LHRF Heating Experiment on JFT-2", Kakuyugo-Kenkyu 44, Suppl. 5 (1980) 103 (in Japanese)

47) Okamoto M.[**2], Imai T., Nagashima T.: "Estimation of LHRF-Heating in JFT-2 Tokamak by Numerical Simulation", Kakuyugo-Kenkyu 44, Suppl. 5 (1980) 109 (in Japanese)

48) Yamada R., Sone K., Saidoh M. and Nakamura K.: "Measurement of Chemical Sputtering Yield of Various Types of Carbon", J. Nucl. Materials 95 (1980) 278

49) Saidoh M., Sone K., Yamada R. and Nakamura K.: "Continuous Observation of Surface Erosion of Polycrystalline Molybdenum Implanted with Helium Ions with Different Energies", J. Nucl. Materials 96 (1981) 358

50) Suzuki N., Ohtsuka H., Sugie T., Ogiwara N., Kasai S., Fujisawa N., Maeno M., Yamamoto T., et al.: "Plasma Surface Interaction during RF Heating on JFT-2 Tokamak", J. Nucl. Materials 93 & 94 (1980) 282

51) Obata Y., Tanaka K. and Naruse Y.: "Present Status and Future Prospect of Fusion Reactor Fuel Technology", Nuclear Engineering, 26, No.9 (1980) 38 (in Japanese)

52) Seki Y. and Iida H.: "Monte Carlo Simuration of First wall Neutron Flux in Tokamak Fusion Reactor", J. Nucl. Sci. Technol., 17(4) (1980) 301

53) Iida H. and Seki Y.: "Simple method of Eliminating Infinite Variance in Point Detector Problem of Monte Carlo Calculation", J. Nucl. Sci. Technol., 17(4) (1980) 315

54) Iida H. and Seki Y.: "Reduction of Computational Time for Point Detector Estimator in Monte Carlo Transport Code", Nucl. sci. Eng., 74(3) (1980) 213

55) Seki Y., Shimomura Y., Maki K.*3, Azumi M. and Takizuka T.: "Numerical Calculations of Helium Ash Enrichment and Exhaust by a Simple Divertor", Nucl. Fusion, 20(10) (1980) 1213

56) Iida H. and Seki Y.: "A Point Detector Scoring Method Compatible with Monte Carlo Transport Calculations of Specularly Reflected Particles", Nucl. Sci. Eng., 76 (1980) 302

57) Horie T.**4, Masuda M., Yagawa G.**4, and Ando Y.**4 : "Finite Element Analysis of Thermo-Fluid-Mechanical Behaviors of Lithium Cooled Blanket of Fusion Reactor UWMAK-III", J. At. Energy Soc. Japan, Vol.22, No.5, (1980) 335-342 (in Japanese)

58) Takatsu H., Shimizu M.: "Dynamic Analysis Method for a large Complicated Structure and Application to a Fusion Device", Nucl. Eng. Des. 60 (1980) 297-309

59) Amano S.*12, Arai T.: "Reliability Test of Vacuum Gasket under Oxidation and Deoxidation", Vacuum 24 (1981) 76 (in Japanese)

60) Shimada R., Tani K., and Tamura S.: "Excitation of Plasma Current in Tokamak Devices by Inductive Energy Storages", Electrical Engineering in Japan, Scripta Electronica Japonica I 99 (1979) 14

61) Ogata A. and Yuasa K.*23 : "The Number of Computers in a Non-Hierarchical System for Tokamak Data Processing", Computer Physics Communications 19 (1980) 35

62) Suzuki Y., Kondo I., Ogata A., Kumahara T., Hatakeyama H.[*3], Mrai K.[*3] and Iba D.[*3] : "System Design of Zenkei, the Central Control System for JT-60", Proce-dings of the Eleventh Symposium of Fusion Technology 2 (1980) 757

63) Ogata A. and Kumahara T.: "Real-Time Processor for a Tokamak", ibid. 681

64) Fukunishi K.[*3], Saito S.[*3], Ogata A. and Ninomiya H.: "Equilibrium Plasma Position Control for a Large Tokamak Using Modern Control Theory", Jpn. J. Appl. Phys. 19 No.9 (1980) 1729

65) Ogata A. and Andó T.: "Large Tokamak Experiments", Nucl. Fusion 20 (1980) 1471

66) Kumahara T., Ogata A., Matoba T., Kondo I. and Suzuki Y.: "A CAMAC System for the Large Tokamak JT-60", Nucl. Science NS-27 (1980) 637

67) Sugihara M., Kasai M.[*5], Tazima T., Tone T., Maki K.[*3] : "Plasma Burning Control by Variable Toroidal Field Ripple in Tokamak Reactors", J. Nucl. Sci. Tech. 17 (1980) 729-736

68) Shinya K.[*11], Sugihara M.: "Tokamak Fusion Reactor Design and Related Physics", Ohyo-butsuri 50 (1981) 255-262

69) Mori S., Sako K., Hiraoka T., Tazima T.: "IAEA INTOR Workshop", J. Atomic Energy Soc. Jap. 22 (1980) 456-461

70) Mori S., Sako K., Hiraoka T., Tazima T.: "INTOR Zero Phase Report", IAEA 1980

71) Hiraoka T.: "Report on the 8th Int. Conf., Brussels 1980", Nucl. Fusion 20 (1980) 1617

A.1.3 List of Papers Published in Conference Proceedings

1) Inoue S.[**6], Itoh K. and Terashima Y.[**2] : "An Improved Energy Principle", Proc. International Conference on Plasma Physics (Nagoya, April 1980) p.47
2) Itoh K., Inoue S.[**6] and Tuda T.: "Kinetic Ballooning Mode and Critical Beta Value", ibid p.80
3) Tokuda S.: "New Spectral Analysis Method for the Plasma Simulation", ibid p.198
4) Tuda T., Itoh K. and Inoue S.[**6] : "Spatial Structure of Drift Instability", ibid p.256
5) Inoue S.[**6] and Itoh K. :"Kinetic Theory of Kink-Like Mode", ibid p.299
6) Tuda T.: "Toroidal Drift Mode", Proc. Workshop on Optimization of Toroidal Confinement (Hiroshima, April 1980) HIFT-25 (May 1980) p.3
7) Itoh K.: "Kinetic Theory of Helical and Toroidal Instability", ibid p.10
8) Azumi M., Tsunematsu T., Itoh K., Tsuda T., Kurita G., Takeda T., Takizuka T., Tokuda S., Matsuura T.[*13], Tanaka Y.[*13], Inoue S.[**6] and Tanaka M.: "Evolution of Stable High Beta Tokamak Equilibria", Proc. 8th International Conf. on Plasma Physics and Nuclear Fusion Research (Brussels, 1980) IAEA-C-38/K-1-1
9) Takizuka T., Azumi M., Seki Y., Sengoku S., Maki K.[*3], Shinya K.[*11], Sugihara M., Yamamoto S., Odajima K., Kimura H., Ohasa K., Nagami M., Sugie T., Kasai T., Maeda H., Funahashi A. and Shimomura Y.: "Poloidal Divertor Study in Tokamaks", ibid IAEA-C-38/X-3
10) Inoue S.[**6] and Itoh K.: "Improvement of Plasma Confinement by Radio Frequency Flux Control", ibid IAEA-C-38/Z-2
11) Takizuka T., Tsunematsu T., Tokuda S., Azumi M., Kurita G., Tuda T., Itoh K., Tanaka Y.[*13], Matsuura T.[*13] and Takeda T.: "Monte Carlo Simulation of Divertor", US-Japan Workshop on Computational Theory (Nagoya, Oct. 1980) in press
12) Takeda T., Takizuka T., Tsunematsu T., Tokuda S., Azumi M., Kurita G., Tuda T., Itoh K., Tanaka Y.[*13] and Matsuura T.[*13] : "Linear MHD Stability Analysis", ibid
13) Kurita G., Takizuka T., Tsunematsu T., Tokuda S., Azumi M., Tuda T., Itoh K., Tanaka Y.[*13], Matsuura T.[*13] and Takeda T.: "Nonlinear MHD Stability Analysis of Tokamak", ibid

14) Kimura H., Odajima K., Iizuka S.[**5], Sengoku S., Sugie T., Takahashi K., Takeuchi H., Yamauchi T., Kumagai K., Matsumoto H., Matsuda T., Ohasa K., Yamamoto S., Anno K., Shibata T., Sunaoshi H., Hiratsuka H., Yokoyama K., Funahashi A., Nagashima T., Maeda H. and Shimomura Y.: "High Efficiency ICRF Heating Experiment in DIVA", 8th International Conference on Plasma Physics and Controlled Nuclear Fusion Research (Brussels) 1980, IAEA-CN-38/D-5-2

15) Suzuki N., Imai T., Fujisawa N., Maeno M., Yamamoto T., Fujii T., Uehara K., Iizuka S.[**5], Yoshida H., Nagashima T., Takeuchi H., Sugie T., Kasai S., Kumagai K., Shoji T., Kawakami T., Yamauchi T., Funahashi A., Ohtsuka H., Konoshima S., Shimada M., Hirayama T., Matsuzaki Y., Shiina T., Tani T., Yokokura K., Anno K., Shibata T., Sunaoshi H., Katagiri M., Yamamoto S., Ohasa K., Odajima K., Matsuda T., Kimura H., Matsumoto H., Sengoku S., Hoshino K., Azumi M., Amano T.[**2], Okamoto M.[**2], Matsuda S., Arakawa Y., Akiba M. and Shimomura Y.: "Recent Results on the Modified JFT-2 Tokamak", 8th International Conference on Plasma Physics and Controlled Nuclear Fusion Research (Brussels) 1980, IAEA-CN-38/T-2-3

16) Kimura H. and Yamamoto S.: "JFT-2 High Power Heating Experiment", US-Japan Workshop on Tokamak Results (Oak Ridge, 1980)

17) Anno K., Ohara K., Shimomura Y., Matsuda K.[*11], Ohsaki O.[*11], Yamamoto K.[*11], Watanabe M.[*11], Tanabe Y.[*11], Gotoh M.[*11] and Ioka S.[*11] : "Beam Line System of Neutral Beam Injection for JFT-2", Proceeding of 11th Symp. on Fusion Technology (Oxford, 1980)

18) Matsuda S., Shibata T., Shimomura Y., Yamamoto S., Nagamura H.[*11], Higa O.[*11], Yoshizawa S.[*11], Fujiwara N.[*11] and Ioka S.[*11] : " Power Supply of Neutral Beam Injection for JFT-2", Proceeding of 11th Symp. on Fusion Technology (Oxford, 1980)

19) DIVA Group : "ICRF Heating Experiment in DIVA", International Conference on Plasma Physics (Nagoya) 1980

20) Iizuka S.[**5], Odajima K., Kimura H., Sengoku S., Sugie T. and Takeuchi H. : "Propergation and Absorption of Fast Magnetosonic Wave at Two-Ion Hybrid Resonance Layer in DIVA-ICRF Heating", International Conference on Plasma Physics (Nagoya) 1980

21) Suzuki N., Ohtsuka H., Sugie T., Ogiwara N., Kasai S., Fujisawa N., Maeno M., Yamamoto T., Nagashima T., Imai T., Fujii T., Uehara K., Yoshida H., Funahashi A., Takeuchi H., Shoji T., Kumagai K., Kawakami T. and Yamauchi T.: "Plasma Surface Interaction during RF

Heating on JFT-2 Tokamak", 4th International Conference on Plasma Surface Interactions in Controlled Fusion Devices (Germish-Partenkirchen) 1980

22) Yamamoto T., Suzuki N., Funahashi A., Fujisawa N., Hoshino K., Iizuka S.[**5], Kawakami T., Kumagai K., Maeno M., Roh T.[**4], Shoji T., Sugie T., Takeuchi H., Toyama H.[**4], Yamauchi T., Moeller C.[*16] and LaHaye R.[*16] : "Electron Cyclotron Heating Experiments on the JFT-2 Tokamak", Joint Workshop on ECE and ECRH (Oxford) 1980

23) Kitsunezaki A., Fujisawa N., Ioki K.[*5], Konoshima S., Nagami M., Ohara Y., Ozaki N., Seki S., Shimada M., Sugawara T., Toyama T.[**4], Yokomizo H., Ga D-III Division : "First Results of Dee Experiments in Doublet III", 8th IAEA Conf. IAEA-CN-38/N-3 (Brussels, July 1980)

24) Nagami M., Fujisawa N., Ioki K.[*5], Kitsunezaki A., Konoshima S., Ohara Y., Seki S., Shimada M., Sugawara T.[*11], Yokomizo H., GA D-III Divisions : "Simplified Poloidal Divertor Experiment in Doublet III", 8th IAEA Conf. IAEA-CNB-38/02 (Brussels, July 1980)

25) Stambaugh R.[*16], Seki S., Shimada M., Yokomizo H.: "Plasma Equilibrium Control in Doublet III", 11th SOFT Conf. (Oxford, UK, Sept. 1980)

26) Kitsunezaki A.: "Dee-Shaped Plasma and Single Null Poloidal Divertor Experiments in Doublet III", APS 22nd Annual Meeting (San Diego, USA 1980)

27) Yokomizo H., Jujisawa N., Ioki K.[*5], Kitsunezaki A., Konoshima S., Nagami M., Ohara Y., Ozaki N.[*3], Seki S., Shimada M., Sugawara T.[*11], Toyama H.[**4] : "Shaping and Control of Dee-Shaped Plasmas with and without Divertor in Doublet III", APS 22nd Annual Meeting (San Diego, USA 1980)

28) Kitsunezaki A., Nagami M., Yokomizo H., Shimada M., Fujisawa N., Konoshima S., Seki S., Ohara Y., Sugawara T.[*11], Ioki K.[*5] : "A Single Null Poloidal Divertor Experiment in Doublet III", APS 22nd Annual Meeting (San Diego, USA 1980)

29) Nagami M., Kitsunezaki A., Fujisawa N., Ioki K.[*5], Konoshima S., Ohara Y., Ozaki N.[*3], Seki S., Shimaa M., Sugawara T.[*11], Toyama H.[**4], Yokomizo H.: "Energy Confinement Study on Ohmically Heated Dee Plasmas in Doublet III", APS 22nd Annual Meeting (San Diego, USA 1980)

30) Shimada M., Nagami M., Yokomizo H., Fujisawa N., Ioki K.[*5], Izumi S.[*3], Konoshima S., Maeno M., Ohara Y., Seki S., Sugawara T.[*11], Yoshida H., Kitsunezaki A.: "Radiation Loss and Impurity Transport

in Doublet III", APS 22nd Annual Meeting (San Diego, USA 1980)

31) Ioki K.[*5], Fujisawa N., Kitsunezaki A., Maeno M., Nagami M., Ohara Y., Shimada M., Yokomizo H.: "Limiter Heat Load Measurement in Doublet III", APS 22nd Annual Meeting (San Diego, USA 1980)

32) Kitsunezaki A., Nagami M.: "Divertor Experiment in D-III", DOE Review Meeting (Washington, USA 1980)

33) Nagami M.: "Low-q Experiments in DIVA", DOE Disruption Workshop (San Diego, USA 1980)

34) Kitsunezaki A.: "Dee Plasma Experiments in D-III", DOE Energy Research Advisory Board Meeting (San Diego, USA 1980)

35) Nagami M.: "Single-Null Divertor Experiments in D-III", DOE Divertor Workshop (Boston, USA 1980)

36) Shimada M.: "Remote Radiative Cooling by a Diverted Plasma in D-III", DOE Non-divertor Impurity Control Workshop (Boston, USA 1980)

37) Nagami M.: "Confinement of Dee Plasmas in Doublet III and Low-q Experiments in DIVA", FED Task Team Meeting (San Diego, USA 1980)

38) Yokomizo H.: "Elongation Limit of Stable Dee Plasmas in Doublet III", Japan/US Joint Workshop (Oak Ridge, USA 1980)

39) Nagami M.: "Confinement Studies in D-Shaped Plasmas in Doublet III", Japan/US Joint Workshop (Oak Ridge, USA 1980)

40) Nagami M., JAERI team: "Dee-Shaped Plasma Experiments in Doublet III (Diverted and Low-q)", Japan/US Joint Workshop (Princeton, USA 1981)

41) Shimada M., JAERI team: "Helium Exhaust by Poloidal Divertor", Japan/US Joint Workshop (Princeton, USA 1981)

42) Ioki K.[*5], JAERI team: "Heat Load Measurement and Energy Balance of Diverted Plasmas in Doublet III", Japan/US Joint Workshop (Princeton, USA 1981)

43) Stambaugh R.[*16], Seki S., Shimada M., Yokomizo H.: "Plasma Equilibrium Control in Doublet III", JET/US Plasma Control Workshop (Princeton, USA 1981)

44) Yokomizo H., JAERI team: "Shaping and Control of Highly Elongated Dee Plasmas", JET/US Plasma Control Workshop (Princeton, USA 1981)

45) Kitsunezaki A., JAERI team: "Experimental Results of the JAERI team", DOE Review Meeting (Washington, USA 1981)

46) Nagashima T.: "The JAERI heating activities tokamak experiments and R&D works", 2nd Joint Greonoble-Varenna Int. Symp. on Heating in Toroidal Plasma, Como, Italy (1980) 3m2

47) Imai T., Suzuki N., Fujii T., Fujisawa N., Funahashi A., et al.: "Energy balance of the LHRF heating experiments on the JFT-2 tokamak", 2nd Joint Greonoble-Varenna Int. Symp. on Heating in Toroidal Plasma, Como, Italy (1980) 10 a 111

48) Imai T., Yamamoto T., Suzuki N., Uehara K., Fujii T., et al.: "LHRF Heating Experiment in JFT-2", Proc. of 4th Topical Conf. on RF Plasma Heating, Austin, Texas (Feb. 1981) C2

49) Okamoto M.[**2], Imai T., Nagashima T.: "Estimation of LHRF-Heating in JFT-2 Tokamak by Numerical Simulation", Proc. of the work shop on Physics of High Power RF Heating, Kyoto, Japan (1980) 9

50) Imai T., Nahashima T., Suzuki N., Fujii T., Fujisawa N., et al.: LHRF Heating Experiments on the JFT-2 Tokamak", Proc. of the work shop on Physics of High Power RF Heating, Kyoto, Japan (1980) 19

51) Shimamoto S., Ando T., Hiyama T., Tsuji H., Tada E., Nishi M., Yoshida K., Okuno K., Koizumi K., Takahashi Y., Kato T., Oka K.[*2], Ibaraki Y.[*15], Sanada Y.[*11], Yasukochi K.: "Construction and Operation of Cluster Test Facility", Proc. of 1980 Applied Superconductivity Conference, IEEE Trans. MAG-17 (1981) No.1, p.494

52) Tsuji H., Okuno K., Takahashi Y., Ando T., Shimamoto S., Ogasawara T.[**3] : "Pulsed Field Loss Characteristics of Japanese Test Coil for Large Coil Task", Proc. of 1980 Applied Superconductivity Conference, IEEA Trans. MAG-17 (1981) No.1, p.42

53) Yoshida K., Tada E., Koizumi K., Hiyama T., Shimamoto S.: "Mechanical Study on the Japanese Test Coil for the Large Coil Task", Proc. of 1980 Applied Superconductivity Conference, IEEE Trans. MAG-17 (1981) No.1, p.203

54) Nishi M., Ando T., Yoshida K., Koizumi K., Shimamoto S., Yasukouchi K.: "Roughened Surface Study on Japanese Test Coil for the Large Coil Task", Proc. of 1980 Applied Superconductivity Conference, IEEE Trans. MAG-17 (1981) No.1, p.904

55) Tada E., Hiyama T., Koizumi K., Yoshida K., Nishi M., Okuno K., Tsuji H., Ando T., Shimamoto S., Yasukouchi K.: "Construction of Cryogenic System of the Cluster Test Facility", Emerging Technology Conference (ASME division), San Francisco, August 1981

56) Yoshida K., Tada E., Koizumi K., Ando T., Shimamoto S., Tada N.[*3], Mori T.[*3], Yasukouchi K.: "Mechanical Study for the Japanese LCT Coil", NBC-DOE Workshop Materials at Low Temperatures, Vail Colorado, October 7-9 1980

57) Shimamoto S., Ando T., Hiyama T., Tsuji H., Takahashi Y., Yoshida K., Tada E., Nishi M., Okuno K., Koizumi K., Kato T., Yasukouchi K., Kensley R.S.[**10], Oka K.[*2], Shimada M.[*17], Sanada Y.[*11], Ibaraki Y.[*15] : "Evolution of the Japanese Test Coil Wark for the Large Coil Task", 7th International Conference on Magnet Technology, Karlsruhe, March 1981

58) Shimamoto S., Ando T., Hiyama T., Tsuji H., Takahashi Y., Yoshida K., Tada E., Nishi M., Okuno K., Koizumi K., Kato T., Yasukouchi K., Kensley R.S.[**10], Oka K.[*2], Shimada M.[*17], Sanada Y.[*11], Ibaraki Y.[*15] : "Test Result and Perspectives of the Cluster Test Program", 7th International Conference on Magnet Technology, Karlsruhe, March 1981

59) Naruse Y., Tanaka K., Tachikawa K., Matsuda Y., Kinoshita M. and Obata Y.: "A Comceptual Design of Tritium Handling Facility", ANS National Topical Meeting on Tritium Technology in Fission, Fusion and Isotopic Applications (Dayton, 1980)

60) Abe T., Yamaguchi K., Kudo H., Tanase M., Shikata E., Umei H., Tachikawa K. and Tanaka K.: "Development of Tritium Production Technology in Nuclear Fusion Research Program of JAERI", ibid

61) Obata Y.: "Tritium Research Program and Present Status of Tritium Technology in JAERI" US/Japan Workshop of Fusion Fuel Handling

62) Tanaka K., Naruse Y., Tachikawa K., Matsuda Y. and Obata Y.: " A Conceptual Design of Tritium Handling Facility", ibid

63) Naruse Y. and Matsuda Y.: "An Analysis of Tritium Containment System", ibid

64) Yoshida H.: "Permeability of Hydrogen Isotopes through Pd-Ag Membrane", ibid

65) Kinoshita M.: "Computor Simulation Study of Hydrogen Isotope System by Cryogenic Distillation", ibid

66) Udoguchi T.[**1], Takatsu H., Shimizu M., Minami M.[**21], and Uchino K.[*22] : "Dynamic Response Analysis of the Vacuum Vessel of JT-60 Against the Saddle-like Electromagnetic Forces", 11th Symposium on Fusion Technol., Oxford, 15-19 September, 1980

67) Nakamura H., Masuda M., Miyauchi Y., Shimizu M., Ogiwara N., Yamamoto M., Ohta M., and Ohwada K.[*22], ibid.

68) Ohkubo M., Nishio S., Ohta M., Itou Y.[*3], Takizawa T.[*3], Furuyama M.[*3], Saito R.[*3], Matunobe K.[*3], Takane F.[*3], "A Reliability Test on a Toroidal Field Coil by Imposing Force and Heat Simulating the Actual Load", ibid.

69) Horie T.[**4], Yagawa G.[**4], Ando Y.[**4] : "Fracture Mechanics Analysis Related to Electro Magnetic Force", Transactions of 6th International Conference on Structural Mechanics in Reactor Technology, Vol.N PN 6/6

70) Miya N., Shimada R., Aoyagi T. and Tamura S.: "JT-60 Ohmic Heating Power Supply", Proc. 11th Symp. on Fusion Technology (Oxford, 1980)

71) Takahashi I.[**9], Nabae A.[**9], and Shimada R.: "High Speed Thyristor Power Amplifier Control for the JT-60 Poloidal Field", Proc. 11th Symp. on Fusion Technology (Oxford, 1980)

72) Kumahara T., Ogata A., Matoba T. and Suzuki Y.: "A CAMAC System for the Large Tokamak JT-60", Proc. of the first european symposium (Berlin 1979) 339

73) Nagashima A.: "FIR Laser Interferometric Ayatem for the Density Measurement of JT-60", Proc. of the Fifth International Conference on Infrared and Millimeters Waves (Würzburg, 1980)

74) Tani K., Kishimoto H. and Tamura S.: "Toroidal Ripple Effects on Fast Ion Behavior and Burn Control in Tokamak", Proc. of 8th Int. Conf. on Plasma Physics and Controlled Nuclear Fusion Research, Brussels, 1-10 July (1980), Paper CN-38/W-2-2

75) Shimomura Y.: "Objectives and Experimental Programme of JT-60", Report on the Physics Session of Fourth IAEA Technical Committee Meeting on Large Tokamak Experiments, Tokyo, 14-18 April, (1980) (JAERI-M 9228)

A.2 Personnel of the Center

A.2.1 Number of the staff of the Division

	FY 1979	FY 1980	FY 1981
Regular Staff*1	162	169	172
Staff on loan	20	20	32*2
Guest scientist	3	3	5*3
Scholarship fellow	5	5	1

*1 Including scientists, technicians, and secretaries.

*2 Four from Hitachi Ltd.
One from Hitachi Cable Co.
Two from Fuji Electric Co., Ltd.
One from Kawasaki Heavy Ind. Ltd.
Two from Mitsubishi Atomic Power Ind. Inc.
Three from Mitsubishi Electric Co., Ltd.
One from Mitsubishi Heavy Ind. Ltd.
One from Touyou Information System Co., Ltd.
Eleven from Tokyo Shibaura Electric Co., Ltd.
Two from ULVAC Co.
One from Nippon Kogaku K.K.
One from Teisan K.K.
One from Kobe Steel Ltd.
Two from Nippon Electric Co., Ltd.
One from Osaka Vacuum Ltd.
One from Nissei Sangyo Co., Ltd.
One from FB-National Magnet Laboratory

*3 One from Nihon University
One fron Nagoya University
One from Ochanomizu University
Two from the University of Tokyo

A.2.2 List of Scientific Staffs and Officers during FY 1980

Fusion Research and Development Center

MORI Sigeru (Center Director) (~July 1980)

ISO Yasuhiko (Center Director) (July 1980~)

(A) Division of Thermonuclear Fusion Research

OBATA Yukio (Head)

TANAKA Masatoshi (Deputy Head)

HAYASHI Takashi (Administrative Manager)

Plasma Theory Laboratory

AZUMI Masafumi

ITOH Kimitake

KURITA Gen-ichi

TAKEDA Tatsuoki (Chief, June 1980-)

TAKIZUKA Tomonori

TANAKA Masatoshi (Chief), (- May 1980)

TOKUDA Shinji

TSUNEMATSU Toshihide

TUDA Takashi

Experimental Plasma Physics Laboratory

TANAKA Yuji (chief)

* JFT-2

FUJISAWA Noboru (Senior Scientist)

HOSHINO Katsumichi

MAENO Masaki

SUZUKI Norio

YAMAMOTO Takumi

* NBI/ICRF

KIMURA Haruyuki

MAEDA Hikosuke (Senior Scientist)

MATSUDA Toshiaki

MATSUMOTO Hiroshi

ODAJIMA Kazuo

OHASA Kazumi

SENGOKU Seio

SHIMOMURA Yasuo (Senior Scientist)

YAMAMOTO Shin

* Diagonostics

FUNAHASHI Akimasa (Senior Scientist)

KASAI Satoshi

KAWAKAMI Tomohide

KUMAGAI Katsuaki

SUGIE Tatsuo

TAKEUCHI Hiroshi

YAMAUCHI Toshihiro

SANO Kazuo *14

* JFT-2M

SHOJI Teruaki

KAMOTO Satoru *6

Facility Operation and Engineering Section

ANNO Katsuto

HASEGAWA Kouichi

ISAKA Masayoshi

KAZAWA Minoru

KIKUCHI Kazuo

KUNIEDA Shunsuke (Chief)

MATSUZAKI Yoshimi

OKANO Fuminori

SHIBATA Takatoshi

SHIINA Tomio

SUNAOSHI Hidenori

SUZUKI Kihachiro (Deputy Chief)

TANI Takashi

TAJIMA Yoshihiro

YOKOKURA Kenji

YOKOYAMA Kenji

Plasma Heating Laboratory I

SHIRAKATA Hirofumi (Chief)

AKIBA Masato

ARAKI Masanori

HORIIKE Hiroshi

ITOH Takao

KAWAI Mikito

KASAHARA Takeo*5

KURIYAMA Masaaki

MATSUDA Shinzaburo (Senior Scientist)

MATSUOKA Mamoru

MUKAIDA Hidetoshi*11

OHARA Yoshihiro

OHGA Tokumichi

OKUMURA Yoshikazu

OTSUKI Hiroshi*3

SHIBANUMA Kiyoshi

SHIBATA Takemasa

TANAKA Shigeru

Plasma Heating Laboratory II

FUJII Tuneyuki

HONDA Masao

IMAI Tsuyoshi

KAMAKURA Akira*18

NAGASHIMA Takashi (Senior Scientist)

NAKAMURA Tetsurou*11

TANAKA Masatoshi (Chief)

UEHARA Kazuya

Fusion Reactor System Laboratory

IIDA Hiromasa

MINATO Akio*4

NISHIDA Hidetsugu*10

SAKO Kiyoshi (Chief)

SEKI Yasushi (Senior Scientist)

TONE Tatsuzo (Senior Scientist)

YAMAMOTO Takashi*1

KITAMURA Kazunori*11

Plasma Engineering Laboratory

MURAKAMI Yoshio (Chief)
NAKAMURA Kazuyuki
OHTSUKA Hidewo
SAIDO Masahiro
SONE Kazuho
YAMADA Raiji

Superconducting Magnet Laboratory

ANDO Toshinari
HIYAMA Tadao
IBARAKI Yoshihiro*15
KATO Takashi
KENSLY Richard**10
KOIZUMI Kouichi
NISHI Masataka
OKA Kouichi*2
OKUNO Kiyoshi
SANADA Yoshinao*11
SHIMADA Masao*17
SHIMAMOTO Susumu (Chief)
TADA Eisuke
TAKAHASHI Yoshikazu
TOKUCHI Akira (Schoolarship fellow)
TSUJI Hiroshi
YOSHIDA Kiyoshi

Tritium Engineering Laboratory

KINOSHITA Masahiro
MATSUDA Yuji
NARUSE Yuji (Chief)
OKUNO Kenji
TACHIKAWA Katsuhiro
TANAKA Kichizo (Senior Scientist)
YOSHIDA Hiroshi

(B) Division of Large Tokamak Development

TOMABECHI Ken (Head)

YOSHIKAWA Masaji (Deputy Head)

Large Tokamak Administration Section

SAITO Jo (Chief)

YOSHIZAWA Kiyoshi (Deputy Chief) (- May 1980)

JT-60 Program Office

HIRAOKA Toru (Chief)

KISHIMOTO Hiroshi (Deputy Chief)

KODAMA Kozo

* Planning and Coordinating Group

KASAHARA Yuko

SUZUKI Kunihiro

TOKUTAKE Toshikuni

* Plasma Analysis Group

HIRAYAMA Toshio

NINOMIYA Hiromasa

SEKI Shogo

TANI Keiji

* Doublet-III Experiment Group

IOKI Kimihiro*5

IZUKI Shigeru*3

KONOSHIMA Shigeru

KITSUNEZAKI Akio (Senior Scientist)

NAGAMI Masayuki

SHIMADA Michiya

SHINYA Kichiro*11

SUGAWARA Toru*11

YOKOMIZO Hideaki

YOSHIDA Hidetoshi

* Next Large Tokamak Design Group

FUJISAWA Noboru (Senior Scientist)

SAKAMOTO Hiroki*7

SUGIHARA Masayoshi

UEDA Koju*6

JT-60 Project Office I

IIJIMA Tsutomu (Chief)

TOMIOKA Hideo (Deputy Chief)

* Machine Group

AMANO Shigeru*12

ANDO Toshiro

ARAI Takashi

HIRATSUKA Hajime

KAWAMOTO Nobunari

KAWASAKI Kozo

MASUDA Michio

MIYAUCHI Yasuyuki

NAKAMURA Hiroo

NAKAMURA Yukiharu

NISHIO Satoshi

NISHIYAMA Takeji*3

OGIWARA Norio

OHKUBO Minoru

OHTA Mitsuru (Senior Scientist)

OZEKI Takahisa

SATO Osamu

SEIMIYA Munetaka

SHIMIZU Masatsugu

TAKATSU Hideyuki

TOYOSHIMA Noboru

TSURUMI Satoshi*3

YAMAMOTO Masahiro

* Vacuum Technology Group

ABE Tetsuya

KUROKI Tetsuzan

OBARA Kenjiro

JT-60 Project Office II

TAMURA Sanae (Chief)

* Power Supplies Group

AOYAGI Tetsuo

ARAKAWA Kiyotsugu

MATSUKAWA Tatsuya

MIYA Naoyuki

SHIINA Minoru

SHIMADA Ryuichi

TAKAHASHI Shunji

TSUNEOKA Masaki

YOSHIDA Yasuo*6

* Auxiliary Facilities Group

AKAO Yohichiro

HIRUTA Kazuharu

HOSODA Ryujiro

IKAWA Ken*1

OIKAWA Akira

JT-60 Project Office III

SUZUKI Yasuo (Chief)

KONDO Ikuro (Deputy Chief)

NISHITANI Takeo

OGATA Atsushi (Senior Scientist)

TOYOKAWA Ryoji

* Control Group

AIKAWA Hiroshi

HOSOGANE Nobuyuki

KIMURA Toyoaki

KURIHARA Kenichi

YONEKAWA Izuru

YOSHINO Ryuji

* Diagnostics Group

INOUE Akihiko*18

KIMURA Hironobu*11

MATOBA Tohru (Senior Scientist)

MORIMOTO Jiro*12

NAGASHIMA Akira

NEYATANI Yuzuru

OIKAWA Hisashi*19

OHSATO Yukio*20

SHIHO Makoto

Guest Scientists

IWATA Giiti (Ochanomizu University)

AMANO Tsuneo (Nagoya University)

YASUKOCHI Ko (Nihon University)

YAMAMURA Sakae (The University of Tokyo)

MIYAMOTO Goro (The University of Tokyo)

On leave from

*1 Fuji Electric Co., Ltd.
*2 Hitachi Cable Co.
*3 Hitachi Ltd.
*4 Kawasaki Heavy Ind. Ltd.
*5 Mitsubishi Atomic Power Ind. Inc.
*6 Mitsubishi Electric Co., Ltd.
*7 Mitsubishi Heavy Ind. Ltd.
*8 Nissin Electric Co., Ltd.
*9 Sumitomo Heavy Ind. Ltd.
*10 Touyou Information System Co., Ltd.
*11 Tokyo Shibaura Electric Co., Ltd.
*12 ULVAC Co.
*13 Fujitsu Ltd.
*14 Nippon Kogaku K.K.
*15 Teisan K.K.
*16 General Atomic Co.
*17 Kobe Steel Ltd.
*18 Nippon Electric Co., Ltd.
*19 Osaka Vacuum Ltd.
*20 Nissei Sangyo Co., Ltd.
*21 Mitsubishi Engineering and Shipbuilding Co., Ltd.
*22 Ishikawajima-Harima Heavy Ind. Ltd.
*23 Oki Electric Co., Ltd.

**1 Chiba University
**2 Nagoya University
**3 Nihon University
**4 The University of Tokyo
**5 Tohoku University
**6 Hiroshima University
**7 Kyoto University
**8 Princeton University
**9 Osaka University
**10 FB-National Magnetic Laboratory
**11 The Institute of Physical and Chemical Research

A.3 Budget of the Center

(unit: Million¥)

	FY[*1] 1979	FY[*1] 1980	FY[*1] 1981
Scientific program (excluding Staff & administrative cost)	22,751.2[*2] (25,558.7)	28,813.9[*2] (24,147.0[*3])	35,468.3[*2] (30,910.4[*3])
Building	16,900.1	19,968.7	23,943.0
Site	1,723.0	2,520.3	4,100.7

*1 From April to March

*2 Including cashing of the financial obligation in each FY.

*3 The total financial obligation from FY 1980 to FY 1983 for the construction of part of the components of JT-60 and for the development of plasma heating system and superconducting magnet.